



Norwegian University of  
Science and Technology

# Sustainability Assessment of Additive Manufacturing Processes

**Vincenzo Lunetto**

Master's Thesis

Submission date: July 2017

Supervisor: Knut Sørby, MTP

Norwegian University of Science and Technology  
Department of Mechanical and Industrial Engineering



# Table of contents

Abstract

Acknowledgements

Glossary of terms

Table of contents

Chapter 1: Introduction

Chapter 2: Human safety risks due to different routes of exposure to metal powders

2.1 Human safety risks

2.1.1 Animal experiments

2.1.2 Case studies of human exposure

2.2 explosions, fires, protection, safety rules

Chapter 3: Process phenomena models

3.1 Cost estimation and energy demand models

3.2 Footprints emission models

3.3 Safety indexes

Chapter 4: Case study

4.1 Topology optimization study

4.2 Experimental study

4.3 Application of the models

4.3 Considerations on the obtained results

Appendix A: Respiratory protection for some metal substances exposed on Chapter 2

Reference list

## Abstract

Additive Manufacturing (AM) processes were developed in the 1980s to reduce the time for the realization of prototypes. Nowadays, AM processes are considered as real manufacturing techniques suitable to build end-use products. As for any new technology, research efforts aiming to process planning and optimization within a sustainable development framework are needed. In particular, the application of the sustainable manufacturing principles requires the creation of products that use processes that minimize negative environmental impacts, conserve energy and natural resources, are safe for employees, communities, and consumers, and are economically sound. In this work, the three aspects of sustainability, namely environmental, economic and social sustainability are critically analyzed for AM. For each topic, an analysis of models that can evaluate the consumption of energy and CO<sub>2</sub> emissions, costs and the impact on workers' health is carried on. The functional redesign of a mechanical object, with the aim of reducing its mass and trying to keep unchanged the constraint conditions imposed is accounted for. A critical analysis of the impacts on workers' health focusing on the hazardous aspects related to the animal and human exposure to metal powders is presented. Considerations on body weight, cancer, cardiovascular, dermal, endocrine, gastrointestinal, hematological, hepatic, musculoskeletal, neurological, ocular, rheumatologic, renal, reproductive, respiratory effects are reported for different elements as Cobalt, Chrome, Nickel, Titanium and for each kind of exposure (inhalation, oral, dermal). Methods for the comparison and evaluation of an inventory's dissimilar pollution loads have been proposed and are critically analyzed. Considerations on the possible workplace maintenance techniques to be followed for handling metal powders (such as those according to ASTM, NFPA and OSHA standards) are also evaluated. Whatsoever, it is possible to consolidate a new technology in the industrial scenario only if it is economically sustainable and profitable. A critical study of the evolution of the main economic models is reported. In addition, approaches that can take into account also the pre-process and post-process phases as well as the production of different objects in the same built are presented. Moreover, in this work, several examples and comparisons of the sustainable performance of different AM techniques are discussed. A critical study of models that can evaluate the amount of CO<sub>2</sub> emissions during the production of part via AM techniques is studied. A model for the calculation of CO<sub>2</sub> emissions from the consumption of electricity is also detailed. The above mentioned models have been applied to selected case studies before and after the redesign phase. NX and ANSYS software were used to perform the geometrical optimization. An experimental study was then conducted to validate the results.

## Acknowledgements

When I received my Bachelor's degree after studying in the Università degli Studi di Palermo, I decided to move to Turin in order to continue my master studies. I had different feelings about that experience: I was certainly excited about living in a multicultural context, but at the same time aware that I left behind the place where I had lived until then, my home Sicily.

Since my arrival at the Politecnico di Torino, I found a dynamic and enriching reality. I immediately realized how much this would have helped me and I tried to work hard to take advantage from this new life. In Prof. Luca Settineri and in Dr. Paolo C. Priarone, I found two guides who accompanied me in my studies, until to become my supervisors for my master's thesis. They have been teaching me so much about overcoming various problems in my university path. I want to thank them for the opportunities they have been giving me, but above all for their ever-present availability, even when it had not to be, which went beyond the simple student-supervisors relationship.

I developed my thesis at the Norges Teknisk-Naturvitenskapelige Universitet, through the Erasmus program. In this way, I had the opportunity to live in Norway, a country rich of culture and amazing landscapes. I was immediately welcomed by the people of the place, but moreover I found in the person of my Prof. Knut Sørby, a warm welcome and a great guide for my work. I admit that I often asked for more than how much I should have received, but my Supervisor has always been available and patient in helping me.

Finally, I do thank my parents, Gioacchino and Anna, and my dearest friends. Both gave me the ambition and the desire to improve always myself, the tenacity to work hard, the patience to overcome obstacles.

Vincenzo Lunetto

Trondheim, 07th of July 2017

## Glossary of terms

AHP - Analytical Hierarchy Process	HMILD - Hard Metal Interstitial Lung Disease
AM - Additive manufacturing	HPDC - High Pressure Die Casting
BAL - Broncho-Alveolar Lavage	HRCT - High Resolution Computed Tomography
CDC - Centers for Disease Control	HTP - Human Toxicity Potential
CERs - Cost-Estimation Relationships	IM - Injection Moulding
CES - Carbon Emission Signature	LCA - Life Cycle Assessment
CF - Cutting Fluid	LDH - Lactate Dehydrogenase
CI - Confidence Interval	LOAEL - Lowest Observed Adverse Effect Level
COD - Chemical Oxygen Demand	LS - Laser Sintering
CM - Conventional Manufacturing	MCV - Mean Connectivity Value
DFE - Design For Environment	MDHS - Methods for the Determination of Hazardous Substances
DMLS - Direct Metal Laser Sintering	MIPS - Material Input Per Service-unit
EBM - Electron Beam Melting	MIT – Minimum Ignition Temperature
EIM - Emissions Inventory Module	MMAD - Mass Median Aerodynamic Diameter
ELU - Environmental Load Unit	MMEF - Maximum Midexpiratory Flow
EMCL - Emulsion Mist Cooling/Lubrication	MQL - Minimum Quantity Lubrication
EPS - Environmental Priority System	MRL - Minimal Risk Level
FDM - Fused Deposition Modelling	MRR - Mean Reciprocal Rank
FEV1 - Forced expiratory volume in the 1st second	MSDS - Material Safety Data Sheet
FM - Finish Machining	MTD - Maximum Tolerable Dose
FVC - Forced Vital Capacity	NEL - No-Effect Level
GDP - Gross Domestic Product	NOAEL - No Observed Adverse Effect Level
GHG - Greenhouse Gas	OR - Odds Ratio
GIP - Giant Cell Interstitial Pneumonitis	PEF - Peak Expiratory Flow Rate
GM - Geometric Mean	PEL - Permissible exposure limit
GSD - Geometric Standard Deviation	RM - Rapid Manufacturing
GWP - Global Warming Potential	
HIP - Hot Isostatic Pressing	
HHS - Health Hazard Score	

RP - Rapid Prototyping

RTECS - Registry of Toxic Effects of  
Chemical Substances

SEP - Swiss Eco-Point

SGOT - Serum Glutamic Oxaloacetic  
Transaminase

SGPT - Serum Glutamic Pyruvic  
Transaminase

SL - Stereolithography

SLM - Selective Laser Melting

SLS - Selective Laser Sintering

SMR - Standardized Mortality Ratio

SMs - Subtractive Methods

SPI - Sustainable Process Index

STL - Stereolithography

TM - Toxicity Measure

UPLCI - Unit Process Life Cycle Inventory

## Chapter 1: Introduction

Early additive manufacturing equipment and materials were developed in the 1980s. In 1984, Chuck Hull of 3D Systems Corporation developed a prototype system based on a process known as stereolithography (STL), in which layers are added by curing photopolymers with ultraviolet light lasers. Hull defined the process as a "system for generating three-dimensional objects by creating a cross-sectional pattern of the object to be formed". Hull's contribution is the design of the STL file format widely accepted by 3D printing software as well as the digital slicing and infill strategies common to many processes today. Additive manufacturing processes (AM) were created to reduce the time for the realization of prototypes and for many years have assumed the name of "rapid prototyping techniques". Depending on which stage of product development is interested, it is possible to distinguish the following types of prototypes: conceptual, functional, technical, pre-series; the goals of each are obviously different as well as the material and the manufacturing technology used for the construction. Subsequently it was recognized the potential of this technology, and today AM processes are considered as real manufacturing techniques that are able to build end-use products. Moreover additive technologies can also be effectively used for rapid tooling and rapid casting operations. Figure 1 presents a possible classification of AM processes, according to the type of the raw material used.

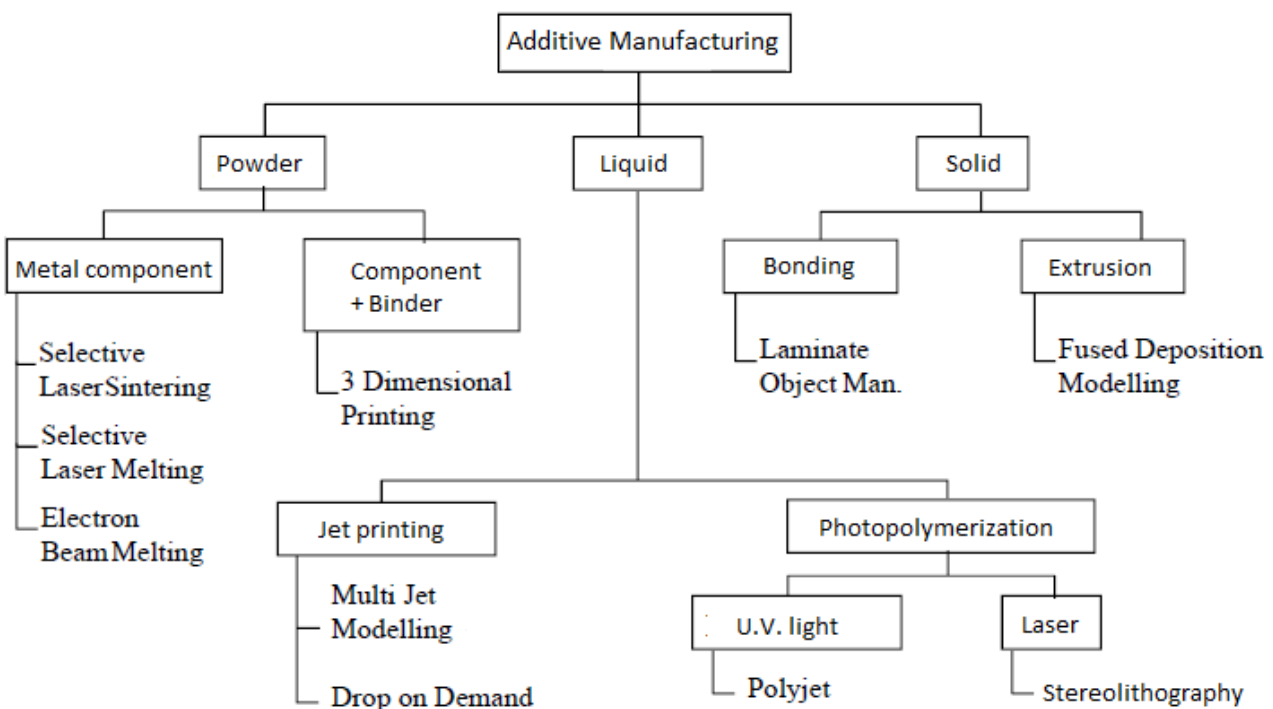


Figure 1: Classification of Additive techniques according to the used chemical material state.

At the current state of the art, technologies that work powders are the only ones that are able to realize metal products. Selective Laser Sintering (SLS) is an AM technique that uses a laser as the power source to sinter powdered material (typically metal), aiming the laser automatically at points in space defined by a 3D model, binding the material together to create a solid structure. It is similar to Direct Metal Laser Sintering (DMLS); the two are instantiations of the same concept but differ in technical details. Selective Laser Melting (SLM) uses a comparable concept, but in SLM the material is fully melted rather than sintered, allowing different properties (crystal structure, porosity, and so on). Electron Beam Melting (EBM) is an AM technique where metal powders can be consolidated into a solid mass using an electron beam as the heat source. EBM technology manufactures parts by melting



metal powder layer by layer under vacuum, which makes it suited to manufacture parts in reactive materials with a high affinity for oxygen, e.g. titanium. Compared to SLM and DMLS, EBM has a generally superior build rate because of its higher energy density and scanning method. All these processes work by fusing a powder bed in each scan cycle, with a thickness of a few hundreds of micrometers.

Some advantages of additive techniques are the ability to make objects of complex shape, in order to have less assembly problems, less spare parts in stock, less complexity in business because of less parts to manage. There is also the advantage that no production of tools is necessary. However, compared to other manufacturing technologies the available software is a limiting factor, machines need a high calibration effort, a rework of parts is often necessary, often it is necessary to design the support structures, the building time depends on the height of the part in the building chamber (Lindemann et al., 2012). It is possible to understand the peculiarities of this technique by comparing it with other manufacturing techniques. Additive techniques realize the final product by progressive addition of material, on the contrary machining operations are subtractive techniques. AD products have lower density with equal volume, because of the internal porosity. It is also possible a functional redesign of the part by minimizing the weight where loads are minor, maintaining the overall mechanical properties comparable to the ones of the pieces made for machining; one example of this new approach is the production of lightweight structural parts for robotic applications reported in Manfredi et al., (2013). The achieved surface quality is not usually adequate to meet the strict requirements of the aerospace and automotive industry (Priarone et al., 2012). Comparative studies present some differences between a traditional manufacturing route (injection moulding) with layer manufacturing processes (stereolithography, fused deposition modelling and laser sintering) in terms of the unit cost for parts made in various quantities. Figure 2 illustrates the breakeven analysis comparing conventional High Pressure Die Casting (HPDC) technique with SLS for the selected landing gear structure. Especially the breakeven point is estimated for a production of about 42 assembly components made of aluminum alloy (21 aircraft models). SLS of aluminum landing gear structures appears economically convenient for this application. But the convenience is more than economical; landing gears are produced within about 2.5 days from the availability of the 3D CAD model, while time to produce moulds for impression die forging and to get started the production is on the order of weeks (Atzemi et al., 2012).

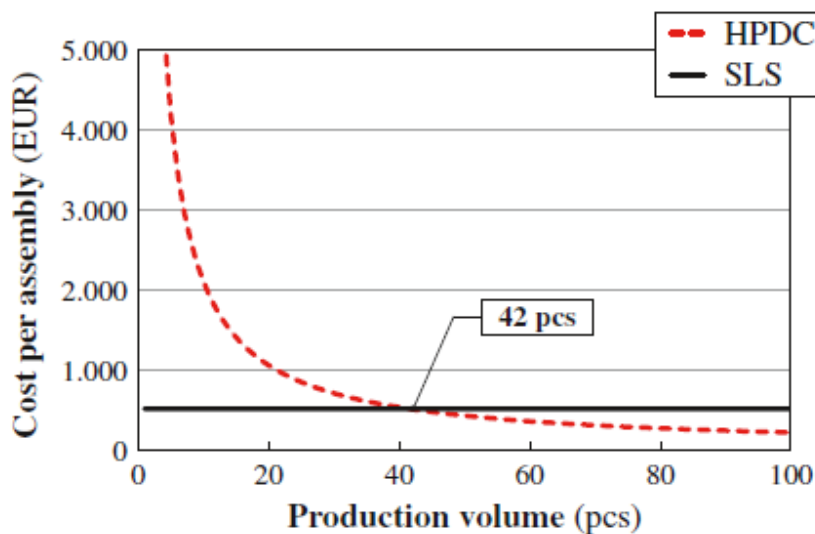


Figure 2: Breakeven analysis comparing conventional highpressure die-casting HPDC process with SLS technique (Atzemi et al., 2012).

This shows how AM techniques are able to create niche objects belonging to the biomedical sector and particular products realized in small-scale to be used in the automotive and aerospace industry. Additive manufacturing techniques are spreading thanks to their potentialities, however like any new technology, it is necessary to study them in order to be able to structure and optimize these processes. There are several critical issues in these processes, especially with regard to topics such as toxicity, safety and environmental problems. Among the additive fabrication processes that ones that use metal powders as raw materials are particularly sensitive to these issues and the first part of this work is a literature review focused on the hazard aspect concern this kind of AM processes. Laser sintering and melting technologies normally use fine particle size distribution powders (10-45  $\mu\text{m}$ ) that offer good flowability and purity, instead Electron Beam Melting technology requires coarser powders (45-106  $\mu\text{m}$ ) with exceptional flowability. In any case the size of the powders are very small and it is very easy for workers to be exposed to them by inhalation. Obviously an oral and dermal exposures is also possible. Because this technology is relatively new, in literature there are a few experiments only on animals according to different routes of exposure, but there are not enough documents on workers in these areas. However, the possible routes of exposure and the type of materials used suggest that the effects on human health could be similar to those of workers in the metallurgical industries such as production of alloys and powders, workers subject to fumes from welding and electrolysis processes. It is therefore necessary to use appropriate equipment for the cleaning operations of the work areas and to carry out the operations of adduction of the new powder in the machine stock. Other problems are connected to the high possibility of fire related to the use of sensitive powders to combustions reactions such as aluminum and titanium powders. Because of the very small size of these powders, the ratio between the exposure surface to the entire volume is very high and the reactions may occur in a very violent manner such as to generate powerful explosions. That is why many organizations are working to standardize the safety rules to be followed and provide the threshold parameters of exposures for the workers in these manufacturing sectors. It is possible to consolidate a new technology in the industrial scenario if it is economically sustainable and profitable. This is one of the challenges that the additive processes have to win, and there are many studies in the literature about cost models to better characterize these processes. Continuing the comparison between additive processes and subtractive processes it can be observed as when complex-geometries have to be manufactured, the additive manufacturing approach could be the best strategy, if it enables a larger amount of material savings than conventional machining. Vice versa, when a small amount of material has to be machined-off, the high energy intensity of an AM process has a negative effect on the performance of the process. The same authors consider the environmental impact of the additive and subtractive manufacturing approach, focusing their attention to the whole life cycle of their case study product. Although AM and SM offer several unique advantages, there are technological limitations such as tolerance and surface finish requirements; tooling and fixturing, etc. that cannot be met by a single type of manufacturing. Some authors are going to study economic models for a new hybrid method where additive manufacturing and subtractive methods are integrated through composite process planning in order to be able to obtain the best advantages from each one of the two techniques (Manogharan et al., 2015).

## Chapter 2: Human safety risks due to different routes of exposure to metal powders

### 2.1 Human safety risks

Workers of production sectors that used metals and in particular metal powders, can come into contact with them in various ways, such as Inhalation Exposure, Exposure Oral, and Dermal Exposure. It is useful to study each of these routes of exposure in order to properly regulate the safety rules in these working environments. However, a systematic study of the effects caused by any single metal element according to a given route of exposure is not enough, it is necessary to study the cumulative effects caused by different routes of exposure, and the combined effects of contact with metal powders of different elements. To this study must also be add considerations on genotoxicity and toxicokinetics of these phenomena. In genetics, genotoxicity describes the property of chemical agents that damages the genetic information within a cell causing mutations, which may lead to cancer. While genotoxicity is often confused with mutagenicity, all mutagens are genotoxic, whereas not all genotoxic substances are mutagenic. The alteration can have direct or indirect effects on the DNA. To assay for genotoxic molecules, researchers assay for DNA damage in cells exposed to the toxic substrates. This DNA damage can be in the form of single- and double-strand breaks, loss of excision repair, cross-linking, alkali-labile sites, point mutations, and structural and numerical chromosomal aberrations. The compromised integrity of the genetic material has been known to cause cancer. As a consequence, many sophisticated techniques including Ames test, in vitro and in vivo Toxicology Tests, and Comet Assay have been developed to assess the chemical potential to cause DNA damage that may lead to cancer. Toxicokinetics is the description of what rate a chemical will enter the body and what happens to it once it is in the body. It is an application of pharmacokinetics to determine the relationship between the systemic exposure of a compound in experimental animals and its toxicity. It is used primarily for establishing relationships between exposures in toxicology experiments in animals and the corresponding exposures in humans. However, it can also be used in environmental risk assessments in order to determine the potential effects of releasing chemicals into the environment. In order to quantify toxic effects toxicokinetics can be combined with toxicodynamics. However, about these studies it is necessary to remember that the effects on workers could not be unique, but they can be very different depending on the physical condition of the individual person. It is therefore necessary to carry out the experiments with statistical studies on a large number of laboratory animals. It is also important for the studies on workers, try to take a sample of volunteers the most optimal possible.

#### 2.1.1 Animal experiments

Rats and other rodents are exposed by inhalation to identify agents that might present hazards for lung cancer in humans exposed by inhalation. In some cases, the results are used in attempts to develop quantitative estimates of human lung cancer risk. However, rats differ from mice and nonhuman primates in both the pattern of particle retention in the lung and alveolar epithelial hyperplastic responses to chronic particle exposure. Present evidence warrants caution in extrapolation from the lung tumor response of rats to inhaled particles to human lung cancer hazard, and there is considerable uncertainty in estimating unit risks for humans from rat data. It seems appropriate to continue using rats in inhalation carcinogenesis assays of inhaled particles, but the upper limit of exposure concentrations must be set carefully to avoid false positive results. A positive finding in both rats and mice would give greater confidence that an agent presents a carcinogenic hazard to man, and both rats and mice should be used if the agent is a gas or vapor. Aluminium

The following pages report considerations derived from the toxicological profile for aluminum (2008) written from U.S. DEPARTMENT OF HEALTH AND HUMAN SERVICES, Public Health Service Agency for Toxic Substances and Disease Registry.

### *Inhalation Exposure*

*Respiratory Effects.* An increase in the number of alveolar macrophages and granulomatous lesions in the lungs and peribronchial lymph nodes were also observed in rats and guinea pigs exposed to 0.61 or 6.1 mg Al/m<sup>3</sup> aluminum chlorhydrate for 6 hours/day, 5 days/week for 6 months (Steinhagen et al. 1978); the severity of the alterations was concentration-related. In addition, statistically significant increases in absolute and relative lung weight were observed in the rats exposed to 6.1 mg Al/m<sup>3</sup>; the authors noted that pulmonary edema was not observed in these rats. Alveolar proteinosis was observed in rats, guinea pigs, and hamsters exposed to  $\geq 15$ , 20, or 30 mg/m<sup>3</sup> of several types of aluminum flake powders; the particle sizes ranged from 2.5 to 4.8  $\mu\text{m}$  (Gross et al. 1973). The investigators noted that aluminum powders did not induce pulmonary fibrosis in the guinea pigs or hamsters; in rats, foci of lipid pneumonitis were observed. A similar exposure to aluminum oxide did not result in alveolar proteinosis, pulmonary fibrosis, or pneumonitis; effects were limited to foci consisting of alveoli filled with macrophages; the particle size of the aluminum oxide dust was much smaller (0.8  $\mu\text{m}$ ) than the aluminum flake powders. Increases in relative lung weights (21–274%) have been observed in rats and guinea pigs exposed to 5.1 mg Al/m<sup>3</sup> aluminum chlorhydrate for 6 hours/day, 5 days/week for approximately 2 years (Stone et al. 1979).

*Cardiovascular Effects.* No histological alterations were observed in the hearts of Fischer 344 rats or Hartley guinea pigs exposed by inhalation (6 hours/day, 5 days/week) to 6.1 mg Al/m<sup>3</sup> as aluminum chlorhydrate for 6 months (Steinhagen et al. 1978).

*Gastrointestinal, Musculoskeletal, Hepatic, Renal, Endocrine, Dermal, Ocular, Reproductive Effects.* No histological changes were observed in the gastrointestinal tissues, muscle or bone, livers, kidneys, adrenal or thyroid or pituitary glands, skin, eyes, reproductive tissues of Fischer 344 rats or Hartley guinea pigs exposed by inhalation (6 hours/day, 5 days/week) to 6.1 mg Al/m<sup>3</sup> as aluminum chlorhydrate for 6 months (Steinhagen et al. 1978).

*Hematological Effects.* No hematological effects were observed in Fischer 344 rats or Hartley guinea pigs exposed by inhalation (6 hours/day, 5 days/week) to 6.1 mg Al/m<sup>3</sup> as aluminum chlorhydrate for 6–24 months (Steinhagen et al. 1978; Stone et al. 1979).

*Body Weight Effects.* Unspecified body weight decreases were reported for male Golden Syrian hamsters acutely exposed via whole-body inhalation to 3, 10, or 33 mg Al/m<sup>3</sup> as alchlor, a common component of antiperspirants (Drew et al. 1974).

*Neurological Effects.* No brain weight or histological changes were observed in Fischer 344 rats or Hartley guinea pigs exposed by inhalation to up to 6.1 mg Al/m<sup>3</sup> as aluminum chlorhydrate for 6 months (Steinhagen et al. 1978).

*Cancer.* An increase in cancer was not observed in male and female Wistar rats exposed via whole-body inhalation to atmospheres containing 2.18–2.45 mg Al/m<sup>3</sup> as alumina fibers ( $\approx 96\%$  aluminum oxide) for 86 weeks (Pigott et al. 1981).

### *Oral Exposure*

*Cardiovascular, Gastrointestinal Effects.* No organ weight or histological changes were found in the hearts, gastrointestinal tissues of female Sprague-Dawley rats that ingested 133 or 284 mg Al/kg/day as aluminum nitrate in drinking water and base diet for up to 1 month (Gomez et al. 1986).

*Hematological Effects.* No alterations in hemoglobin, hematocrit, and/or erythrocyte osmotic fragility were observed in rats exposed to 133 mg Al/kg/day as aluminum nitrate in drinking water for 1 month (Gomez et al. 1986), rats exposed to 284 mg Al/kg/day as aluminum nitrate in drinking water for 100 days (Domingo et al. 1987b). Hyperemia in the red pulp of the spleen was reported in rats exposed to 79 mg Al/kg/day as aluminum nitrate in drinking water for 1 month (Gomez et al. 1986); this may be indicative of erythrocyte damage.

*Hepatic Effects.* Hyperemia and periportal monocytic infiltrate were observed in the livers of female Sprague-Dawley rats given 133 mg Al/kg/day as aluminum nitrate in drinking water for 1 month (Gomez et al. 1986).

*Renal Effects.* No alterations in kidney histopathology were observed in rats exposed to 284 mg Al/kg/day as aluminum nitrate in drinking water for 100 days (Domingo et al. 1987b).

*Dermal, Ocular Effects.* No histologic changes of the skin, eyes were observed in Fischer 344 rats or Hartley guinea pigs exposed by inhalation to 6.1 mg Al/m<sup>3</sup> as aluminum chlorhydrate for 6 months (Steinhagen et al. 1978).

*Body Weight Effects.* Of the studies reporting reductions of body weight gain, many involved gestational and/or lactational exposure; significant decreases in body weight gain were observed in rats administered via gavage 38 mg Al/kg/day as aluminum nitrate on gestation days 6–14 (Paternain et al. 1988).

*Neurological Effects.* Decreases in spontaneous motor activity have also been observed in rats exposed to aluminum chloride in the diet for 7 weeks or 11 months (Commissaris et al. 1982); the amounts of aluminum added to the diet were 184 and 66 mg Al/kg/day, respectively. A chronic-duration study (Roig et al. 2006) found no significant alterations in the total distance traveled or the total number of rearings in rats exposed to 103 mg Al/kg/day as aluminum nitrate in drinking water (citric acid added) from gestation day 1 through 2 years of age. Decreases in thermal sensitivity were observed following chronic exposure of mice to 100 mg Al/kg/day as aluminum lactate in the diet (Golub et al. 2000). Decreased responses to auditory and/or air puff stimuli were observed in mice exposed to 195 mg Al/kg/day as aluminum lactate in the diet for 5–7 weeks (Oteiza et al. 1993) or 90 days (Golub et al. 1992b). In Morris water maze tests, impaired learning and memory was observed following gavage doses of 500 mg Al/kg/day of an unreported aluminum compound for 90 days (Jing et al. 2004). In contrast, no significant alterations in performance on the water maze test were found in rats exposed to 103 mg Al/kg/day as aluminum nitrate in the drinking water for a chronic duration (Roig et al. 2006). Abd El-Rahman (2003) reported spongiform changes in the neurons of the hippocampus, nuclear deformity, neurofibrillary degeneration, and foci of demyelination in rats receiving gavage doses of 85.9 mg Al/kg/day as aluminum sulfate (aluminum content of the diet was not reported).

*Reproductive Effects.* In a study of female reproductive system development (Agarwal et al. 1996), offspring of rats that were gavaged with aluminum lactate on gestation days 5–15 showed a transient irregularity of the estrus cycle (increased number of abnormal cycle lengths) at 250 mg Al/kg/day; doses as high as 1,000 mg Al/kg/day did not affect other end points (gonad weights, anogenital distance, time to puberty, duration of induced pseudopregnancy, or numbers of superovulated

oocytes). The inconsistent findings summarized above may reflect differences in susceptibility among different strains/species of animals or compound differences in toxicity or bioavailability. An intermediate-duration oral study in male rats found that sperm count was decreased following exposure to 2.5 mg Al/kg/day as aluminum chloride for 6–12 months (Krasovskii et al. 1979).

*Cancer.* Animal bioassays have found no conclusive evidence for carcinogenicity of aluminum.

### *Dermal Exposure*

*Dermal Effects.* Skin damage has been observed in female TF1 Carworth mice, New Zealand rabbits, and Large White pigs following the application of 10% aluminum chloride (0.005–0.1 g Al) or aluminum nitrate (0.006–0.013 g Al) for 5 days; but not from aluminum sulfate, hydroxide, acetate, or chlorhydrate (Lansdown 1973). The damage consisted of hyperplasia, microabscess formation, dermal inflammatory cell infiltration, and occasional ulceration. These results suggest that the development of adverse dermal effects from exposure to aluminum depends upon its chemical form.

### Chrome

The following pages report considerations derived from the toxicological profile for chrome (2002) written from U.S. DEPARTMENT OF HEALTH AND HUMAN SERVICES, Public Health Service Agency for Toxic Substances and Disease Registry.

### *Inhalation Exposure*

*Respiratory Effects.* The respiratory effects of chromium(III) compounds were investigated in male and female CDF rats exposed to insoluble chromic oxide or soluble basic chromium sulfate by nose-only inhalation at 3, 10, or 30 mg chromium(III)/m<sup>3</sup> for 6 hours/day, 5 days/week for 13 weeks (Derelanko et al. 1999). After 5 days of exposure, BAL was conducted on a subgroup of animals. In rats treated with chromic oxide, a yellow crystalline material was observed in the cytoplasm of mononuclear cells of all exposure groups; however, it is not clear if this observation represents an adverse effect. In rats exposed to chromic oxide for 13 weeks, absolute and relative lung weights were increased by 12 and 13%, respectively, in males exposed to 30 mg chromium(III)/m<sup>3</sup> as chromic oxide; no change was observed in females. Histopathological examination of respiratory tissues showed pigmented macrophages containing a dense black substance, presumably the test substance, throughout the terminal bronchioles and alveolar spaces in rats from all treatment groups; this finding is consistent with normal physiological clearance mechanisms for particulates deposited in the lung and is not considered to be adverse. At concentrations of 10 and 30 mg chromium(III)/m<sup>3</sup>, trace to mild chronic interstitial inflammation, characterized by inflammatory cell infiltrates, and septal cell hyperplasia was observed. No lesions were observed in the nasal cavity. Following a 13-week recovery period, microscopic examination of respiratory tissues of rats treated with chromic oxide showed pigmented macrophages and black pigment in peribronchial tissues and the mediastinal lymph node in all treatment groups and septal cell hyperplasia and chronic interstitial inflammation of the lung, both trace-to-mild in severity, in males of all treatment groups and in females exposed to 10 and 30 mg chromium(III)/m<sup>3</sup>. Data from the Derelanko et al. (1999) study was used as the basis for intermediate-duration inhalation Minimal Risk Levels (MRLs) for chromium(III) compounds. Since soluble and insoluble chromium(III) compounds exhibited different effects in the respiratory tract, distinct intermediate-duration MRLs were derived for insoluble and soluble trivalent chromium particulates. For insoluble chromium(III) compounds (chromic oxide), the minimal Lowest Observed Adverse Effect Level (LOAEL) of 3 mg chromium(III)/m<sup>3</sup> was used to calculate an intermediate-duration inhalation MRL of 0.005 mg chromium(III)/m<sup>3</sup> for exposure to trivalent chromium

particulates. For soluble chromium(III) (basic chromium sulfate) compounds, the LOAEL of 3 mg chromium(III)/m<sup>3</sup> was used to calculate an intermediate-duration inhalation MRL of 0.0001 mg chromium(III)/m<sup>3</sup> for exposure to trivalent chromium particulates. Pulmonary fluid from hamsters exposed to 0.9 or 25 mg chromium(III)/m<sup>3</sup> as chromium trichloride for 30 minutes revealed sporadic changes in activities of acid phosphatase and alkaline phosphatase in the lavage fluid at 25 mg chromium(III)/m<sup>3</sup>. In the lung tissue, a 75% increase in the acid phosphatase activity was found at 0.9 mg chromium(III)/m<sup>3</sup>. Histological examination revealed alterations representing mild nonspecific irritation but no morphological damage (Henderson et al. 1979). In rabbits exposed to 0.6 mg chromium(III)/m<sup>3</sup> as chromium nitrate intermittently for 4–6 weeks, changes in the lungs were confined to nodular accumulations of macrophages in the lungs. Macrophage morphology demonstrated black inclusions and large lysosomes. These changes represent normal physiological responses of the macrophages to the chromium particle. Mice exposed to 4.3 mg chromium(VI)/m<sup>3</sup> as calcium chromate dust intermittently for 18 months had epithelialization of alveoli. Histopathology revealed epithelial necrosis and marked hyperplasia of the large and medium bronchi, with numerous openings in the bronchiolar walls (Nettesheim and Szakal 1972). Significantly increased incidences of pulmonary lesions (lung abscesses, bronchopneumonia, giant cells, and granulomata) were found in rats exposed chronically to a finely ground, mixed chromium roast material that resulted in airborne concentrations of 1.6–2.1 mg chromium(VI)/m<sup>3</sup> compared with controls.

*Cardiovascular Effects.* For intermediate-duration exposures, no histopathological changes to the heart were observed in male Sprague-Dawley rats exposed to 1.15 mg chromium(VI)/m<sup>3</sup> as chromium trioxide (Kim et al. 2004) or in male and female CDF rats exposed to 30 mg chromium(III)/m<sup>3</sup> as chromic oxide or basic chromium sulfate for 3 months (Derelanko et al. 1999). No histopathological lesions were found in the hearts of rats exposed chronically to chromium dioxide at 15.5 mg chromium(IV)/m<sup>3</sup> (Lee et al. 1989).

*Gastrointestinal Effects.* For intermediate-duration exposures, no histopathological changes to gastrointestinal tissues in male and female CDF rats exposed to 30 mg chromium(III)/m<sup>3</sup> as chromic oxide or basic chromium sulfate for 3 months, (Derelanko et al. 1999).

*Hematological Effects.* Hematological effects were observed in male Sprague-Dawley rats exposed to chromium trioxide mist for 90 days; changes included significant decreases in hematocrit (at 0.23 and 1.15, but not 0.49 mg chromium(VI)/m<sup>3</sup>), hemoglobin (at 0.49 and 1.15 mg chromium(VI)/m<sup>3</sup>) and erythrocyte count (at 1.15 mg chromium(VI)/m<sup>3</sup>) (Kim et al. 2004). Rats exposed to 0.1 mg chromium/m<sup>3</sup> as a 3:2 mixture of chromium(VI) trioxide and chromium(III) oxide for 18 months had increased red and white blood cell counts, hemoglobin content, and hematocrit (Glaser et al. 1986, 1988).

*Hepatic Effects.* The hepatic effects observed in animals after inhalation exposure to chromium or its compounds were minimal and not considered to be adverse.

*Renal Effects.* Exposure of rats to sodium dichromate at ≤0.4 mg chromium(VI)/m<sup>3</sup> for ≤90 days did not cause abnormalities, as indicated by histopathological examination of the kidneys. Serum levels of creatinine and urea and urine levels of protein were also normal (Glaser et al. 1985, 1990). Rats exposed to 15.5 mg chromium(IV)/m<sup>3</sup> as chromium dioxide for 2 years showed no histological evidence of kidney damage or impairment of kidney function, as measured by routine urinalysis. Serum levels of blood urea nitrogen, creatinine, and bilirubin were also normal (Lee et al. 1989).

*Endocrine Effects.* For intermediate-duration exposures, no histopathological changes to the endocrine tissues were observed in male Sprague-Dawley rats exposed to 1.15 mg chromium(VI)/m<sup>3</sup>

as chromium trioxide (Kim et al. 2004) or in male and female CDF rats exposed to 30 mg chromium(III)/m<sup>3</sup> as chromic oxide or basic chromium sulfate for 3 months (Derelanko et al. 1999).

*Ocular Effects.* Histopathologic examination of rats exposed to 15.5 mg chromium(IV)/m<sup>3</sup> as chromium dioxide for 2 years revealed normal morphology of the ocular tissue (Lee et al. 1989).

*Body Weight Effects.* In rats exposed to an aerosol of sodium dichromate for 30 or 90 days or for 90 days followed by an additional 30 days of non-exposure, body weight gain was significantly decreased at 0.2 and 0.4 mg chromium(VI)/m<sup>3</sup> for 30 days (p<0.001), at 0.4 mg chromium(VI)/m<sup>3</sup> for 90 days (p<0.05), and at 0.2 (p<0.01) and 0.4 mg chromium(VI)/m<sup>3</sup> (p<0.05) in the recovery group (Glaser et al. 1990). However, exposure of male and female rats to 30 mg chromium(III)/m<sup>3</sup> as basic chromium sulfate for 13 weeks did not produce body weight changes (Derelanko et al. 1999). Similarly, there was no effect on body weight gain in rats exposed to 15.5 mg chromium(IV)/m<sup>3</sup> as chromium dioxide for 2 years (Lee et al. 1989).

*Neurological Effects.* No histopathological lesions were found in the brain of male Sprague-Dawley rats exposed to 1.15 mg chromium(VI)/m<sup>3</sup> as chromium trioxide for 3 months or in male and female CDF rats exposed to 30 mg chromium(III)/m<sup>3</sup> as chromic oxide or basic chromium sulfate for 3 months (Derelanko et al. 1999; Kim et al. 2004) or in the brain, spinal cord, or nerve tissues of rats exposed to 15.5 mg chromium(IV)/m<sup>3</sup> as chromium dioxide for 2 years (Lee et al. 1989).

*Reproductive Effects.* Histopathological examination of the testes of rats exposed to 0.2 mg chromium(VI)/m<sup>3</sup> as sodium dichromate for 28 or 90 days (Glaser et al. 1985), to 0.1 mg chromium(VI)/m<sup>3</sup> as sodium dichromate for 18 months, or to 0.1 mg chromium/m<sup>3</sup> as a 3:2 mixture of chromium(VI) trioxide and chromium(III) oxide for 18 months (Glaser et al. 1986, 1988) revealed no abnormalities. For intermediate-duration exposures to chromium(III) compounds, no histopathological changes to the reproductive tissues in male and female CDF rats exposed to 30 mg chromium(III)/m<sup>3</sup> as chromic oxide or basic chromium sulfate

for 3 months; treatment also had no effect on sperm count, motility, or morphology (Derelanko et al. 1999). No histopathological lesions were observed in the prostate, seminal vesicle, testes, or epididymis of male rats or in the uterus, mammary gland, or ovaries of female rats exposed to 15.5 mg chromium(IV)/m<sup>3</sup> as chromium dioxide for 2 years (Lee et al. 1989).

*Cancer.* Chronic inhalation studies provide evidence that chromium(VI) is carcinogenic in animals. Mice exposed to 4.3 mg chromium(VI)/m<sup>3</sup> as calcium chromate had a 2.8-fold greater incidence of lung tumors, compared to controls (Nettesheim et al. 1971). Lung tumors were observed in 3/19 rats exposed to 0.1 mg chromium(VI)/m<sup>3</sup> as sodium dichromate for 18 months, followed by 12 months of observation. The tumors included two adenomas and one adenocarcinoma. No lung tumors were observed in 37 controls or the rats exposed to ≤0.05 mg chromium(VI)/m<sup>3</sup> (Glaser et al. 1986, 1988). Several chronic animal studies reported no carcinogenic effects in rats, rabbits, or guinea pigs exposed to ≈1.6 mg chromium(VI)/m<sup>3</sup> as potassium dichromate or chromium dust 4 hours/day, 5 days/week (Baetjer et al. 1959b; Steffee and Baetjer 1965). Rats exposed to ≤15.5 mg chromium(IV)/m<sup>3</sup> as chromium dioxide for 2 years had no statistically significant increased incidence of tumors (Lee et al. 1989).

#### *Oral Exposure*

*Gastrointestinal Effects.* No histopathological changes to the stomach or small intestine were observed in mice and rats exposed to oral chromium(III) (as chromium nicotinate, chromium oxide,



and chromium picolinate) for 3 months or 2 years (Ivankovic and Preussmann 1975; NTP 2008b; Rhodes et al. 2005; Shara et al. 2005, 2007).

*Hematological Effects.* Microcytic, hypochromic anemia, characterized by decreased mean cell volume (MCV), mean corpuscular hemoglobin (MCH), hematocrit (HCT), and hemoglobin (HGB), was observed in F344/N rats and B6C3F1 mice exposed to chromium(III) compounds in drinking water for exposure durations ranging from 4 days to 1 year (NTP 2007, 2008a). Severity was dose-dependent. After exposure for 3 months to 1 year, microcytic, hypochromic anemia in rats and mice was less severe than that observed after 22 or 23 days (NTP 2007, 2008a). For intermediate duration exposure, no hematological effects were observed in rats exposed to chromic oxide in the diet at doses up to 1,806 chromium(III)/kg/day for 3 months (Ivankovic and Preussmann 1975).

*Hepatic Effects.* In male and female F344/N rats exposed to 4.0 and 4.1 mg chromium(VI)/kg/day, respectively, as disodium dichromate in drinking water for 5 days, serum alanine aminotransferase (ALT) activity was increased by 15 and 30%, respectively (NTP 2007). In females, morphological changes to the liver included cellular histiocyte infiltration and chronic focal inflammation at doses of 3.5 and 20.9 mg chromium(VI)/kg/day, respectively. For intermediate-duration exposures, no morphological changes were observed in rats exposed to 1,806 mg chromium(III)/kg/day as chromium oxide in the diet 5 days/week for 90 days (Ivankovic and Preussmann 1975), rats exposed to 9 mg chromium(III)/kg/day as chromium chloride or chromium picolinate in the diet for 20 weeks (Anderson et al. 1997b), rats exposed to 506 mg chromium(III)/kg/day and mice exposed to 1,415 mg chromium(III)/kg/day as chromium picolinate in the diet for 14 weeks (NTP 2008b; Rhodes et al. 2005). For chronic-duration exposures, histological examination revealed no morphological changes in the livers of rats exposed to chromium oxide in the diet 5 days/week at 2,040 mg chromium(III)/kg/day for 2 years (Ivankovic and Preussmann 1975).

*Renal Effects.* Renal effects have been observed in animals following oral exposure to chromium(VI), but not chromium(III), compounds. Rats treated by gavage with 13.5 mg chromium(VI)/kg/day for 20 days had increased accumulation of lipids and accumulated triglycerides and phospholipids in different regions of the kidney than controls (Kumar and Rana 1982). Exposure of mice and rats to chromium(III) compounds (chromium acetate, chromium nicotinate, chromium oxide, chromium picolinate, and chromium trichloride) in food or drinking water for up to 2 years did not result in renal damage, based on histopathological examination of kidneys (Anderson et al. 1997b; Ivankovic and Preussmann 1975; MacKenzie et al. 1958; NTP 2008b; Schroeder et al. 1965; Shara et al. 2005, 2007).

*Body Weight Effects.* Significant decreases in body weight have been reported in several intermediate-duration oral chromium(VI) studies in animals (Bataineh et al. 1997; Chowdhury and Mitra 1995; De Flora et al. 2006; Elbetieha and Al-Hamood 1997; NTP 1996a, 1996b, 2007; Quinteros et al. 2007; Yousef et al. 2006). However, it should be noted that high concentrations of chromium in drinking water decrease palatability of water, resulting in decreased water consumption; thus, decreased body weight may, in part, be due to decreased water consumption, in addition to other causes. An acute exposure (9 days) resulted in 8 and 24% decreases in body weight gain in pregnant mice exposed to 101 or 152 mg chromium(VI)/kg/day, respectively (Junaid et al. 1996b).

*Neurological Effects.* Histopathological examination of the brain and nervous system tissues has been evaluated in rats and mice exposed to oral chromium(VI) (as sodium dichromate dihydrate) and chromium(III) (as chromium nicotinate, chromium oxide, and chromium picolinate) for durations of

3 months to 2 years, with no abnormalities observed (Ivankovic and Preussmann 1975; NTP 2007, 2008a, 2008b; Shara et al. 2005, 2007).

*Reproductive Effects.* A number of studies have reported reproductive effects in animals orally exposed to chromium(VI). After exposure for 2 months, significant decreases in sperm count (by 13%) and motility (by 12%) were observed only in monkeys treated with 8.3 mg chromium(VI)/kg/day, whereas after 6 months, dose-dependent decreases in sperm count and motility were observed at doses of  $\geq 2.1$  mg chromium(VI)/kg/day. Histopathological assessment of testes showed decreased diameter of seminiferous tubules and germ cell rearrangement within the tubules. Effects of chromium(VI) on the female reproductive system have been reported in rats and mice. Murthy et al. (1996) reported a number of reproductive effects in female Swiss albino mice exposed to potassium dichromate in drinking water for 20 days. The observed effects included a significant reduction in the number of follicles at different stages of maturation at  $\geq 60$  mg chromium(VI)/kg/day, reduction in the number of ova/mice at  $\geq 120$  mg chromium(VI)/kg/day, significant increase in estrus cycle duration at 180 mg chromium(VI)/kg/day, and histological alterations in the ovaries (e.g., proliferated, dilated, and congested blood vessels, pyknotic nuclei in follicular cells, and atretic follicles) at  $\geq 120$  mg chromium(VI)/kg/day.

*Cancer.* Groups of 50 male and 50 female F344/N rats were exposed to drinking water containing 0, 14.3, 57.3, 172, or 516 mg/L sodium dichromate dihydrate for 2 years. NTP (2008a) calculated 2-year mean daily doses of 0, 0.6, 2.2, 6, or 17 mg sodium dichromate dihydrate/kg/day (equivalent to 0, 0.21, 0.77, 2.1 or 5.9 mg chromium(VI)/kg/day) in male rats and, 0, 0.7, 2.7, 7, or 20 mg sodium dichromate dihydrate/kg/day (equivalent to 0, 0.24, 0.94, 2.4, and 7.0 mg chromium(VI)/kg/day) in female rats. Incidences of squamous epithelial neoplasms of the oral mucosa and tongue were elevated in rats exposed to sodium dichromate compared to controls, with significant increased mortality-adjusted incidence in males at the 5.9 mg chromium(VI)/kg/day dose (15.7 versus 0% in controls,  $p=0.007$ ), and in females at the 7.0 mg chromium(VI)/kg/day (23.9 versus 2.2% in controls,  $p<0.001$ ). In both male and female rats, there was a significant dose trend for digestive tract neoplasms ( $p<0.001$ ). The carcinogenicity of chromium(VI) was evaluated in mice exposed to potassium chromate in drinking water at 9 mg chromium(VI)/kg/day for three generations (880 days) (Borneff et al. 1968). In treated mice, 2 of 66 females developed forestomach carcinoma and 9 of 66 females and 1 of 35 males developed forestomach papilloma. The vehicle controls also developed forestomach papilloma (2 of 79 females, 3 of 47 males) but no carcinoma. No evidence of carcinogenicity was observed in male or female rats fed diets containing chromium oxide at 2,040 mg chromium(III)/kg/day 5 days/week for 2 years. Moreover, no evidence of carcinogenicity was found in the offspring of these rats after 600 days of observation (Ivankovic and Preussmann 1975).

#### *Dermal Exposure*

*Hepatic Effects.* Information regarding liver effects in animals after dermal exposure to chromium or its compounds is limited. A single application of 0.5% potassium dichromate (0.175% chromium(VI)) to the shaved skin of rats resulted in increased levels of serotonin in the liver, decreased activities of acetylcholinesterase and cholinesterase in the plasma and erythrocytes, increased levels of acetylcholine in the blood, and increased glycoprotein hexose in the serum.

*Renal Effects.* Application of 50 mg chromium/kg/day (specific chemical or valence state not reported) for 30 days to clipped skin under occluded conditions to female guinea pigs produced increases in enzyme activities in renal tissue, specifically aspartate aminotransferase (8%), alanine aminotransferase (96%), and acid phosphatase (4%), compared to untreated controls (Mathur 2005).

Microscopic evaluation of the kidney showed lobularization of the glomerular tuft and congestion of capillaries. No additional information on renal effects of dermal exposure to chromium(VI) or chromium(III) compounds was identified.

*Dermal Effects.* Dermal application of chromium(VI) compounds to the clipped, nonabraded skin of rabbits at 42–55 mg/kg resulted in skin inflammation, edema, and necrosis. Skin corrosion and eschar formation occurred at lethal doses (Gad et al. 1986).

## Cobalt

### *Inhalation Exposure*

The following pages report considerations derived from the toxicological inhalation profile for cobalt (2014) written from the U.S. DEPARTMENT OF HEALTH AND HUMAN SERVICES. In the study male and female F344/N or F344/NTac rats were exposed to cobalt metal powders by inhalation for 2 weeks, 3 months, or 2 years.

*2-week study in rats.* Groups of five male and five female rats were exposed to cobalt metal particulate aerosol by inhalation at concentrations of 0, 2.5, 5, 10, 20, or 40 mg/m<sup>3</sup>, 6 hours plus 12 minutes per day, 5 days per week for 16 days. Additional groups of five female rats were exposed to the same concentrations for 16 days for tissue burden studies. All rats exposed to 40 mg/m<sup>3</sup> and all male and three female rats exposed to 20 mg/m<sup>3</sup> died before the end of the study. As Table 1 shows the mean body weights of males exposed to 10 mg/m<sup>3</sup> and of females exposed to 10 or 20 mg/m<sup>3</sup> were significantly decreased.

	Chamber Control	2.5 mg/m <sup>3</sup>	5 mg/m <sup>3</sup>	10 mg/m <sup>3</sup>	20 mg/m <sup>3</sup>	40 mg/m <sup>3</sup>
<b>Male</b>						
n	5	5	5	5	0	0
Necropsy body wt	144 ± 3	144 ± 2	140 ± 4	115 ± 6**		
L. Kidney						
Absolute	0.61 ± 0.02	0.61 ± 0.01	0.58 ± 0.01	0.52 ± 0.02**		
Relative	4.25 ± 0.06	4.26 ± 0.08	4.12 ± 0.09	4.57 ± 0.10*		
Liver						
Absolute	5.84 ± 0.16	5.10 ± 0.09**	5.08 ± 0.15**	4.29 ± 0.24**		
Relative	40.61 ± 0.46	35.40 ± 0.28**	36.35 ± 0.63**	37.43 ± 0.86**		
Lung						
Absolute	1.14 ± 0.10	1.16 ± 0.08	1.19 ± 0.04	1.28 ± 0.12		
Relative	7.91 ± 0.61	8.07 ± 0.55	8.49 ± 0.30	11.13 ± 0.50**		
L. Testis						
Absolute	0.886 ± 0.040	0.928 ± 0.017	0.852 ± 0.035	0.590 ± 0.088**		
Relative	6.165 ± 0.246	6.446 ± 0.155	6.103 ± 0.248	5.053 ± 0.502		
Thymus						
Absolute	0.374 ± 0.013	0.358 ± 0.025	0.358 ± 0.007	0.284 ± 0.008**		
Relative	2.605 ± 0.054	2.485 ± 0.161	2.560 ± 0.023	2.498 ± 0.112		

Table 1 (a): Selected Organ Weights and Organ-Weight-to-Body-Weight Ratios for Rats in the 2-Week Inhalation Study of Cobalt metal (Ntp,2014).

Females exposed to 20 mg/m<sup>3</sup> lost weight during the study. Exposure-related clinical findings included abnormal breathing, lethargy, and thinness in male rats exposed to 20 or 40 mg/m<sup>3</sup> and in females exposed to 40 mg/m<sup>3</sup>. Dark lungs were observed at necropsy in all rats exposed to 40 mg/m<sup>3</sup> and most rats exposed to 20 mg/m<sup>3</sup> that died early. The absolute lung weights of females exposed to

10 or 20 mg/m<sup>3</sup> and the relative lung weights of both sexes exposed to 10 mg/m<sup>3</sup> and females exposed to 20 mg/m<sup>3</sup> were significantly greater than those of the chamber controls. Absolute and relative liver weights of males exposed to 2.5 mg/m<sup>3</sup> or greater and absolute liver weights of females exposed to 5 mg/m<sup>3</sup> or greater were significantly less than those of the chamber controls. The relative liver weight of 20 mg/m<sup>3</sup> females was significantly greater than that of the chamber controls. Absolute kidney weights of males exposed to 10 mg/m<sup>3</sup> and females exposed to 20 mg/m<sup>3</sup> were significantly less than those of the chamber controls. The absolute testis weight of the 10 mg/m<sup>3</sup> group was significantly less than that of the chamber controls. Increased incidences of nonneoplastic lesions of the lung occurred in exposed male and female rats and included hemorrhage, acute inflammation, alveolar epithelium hyperplasia, histiocytic cellular infiltration of the alveolus, cytoplasmic vacuolization of bronchiolar epithelium, necrosis of the bronchiolar epithelium, and interstitial fibrosis of the alveolar epithelium. Increased incidences of nonneoplastic lesions of the nose occurred in exposed male and female rats and included olfactory epithelium necrosis, olfactory epithelium atrophy, respiratory epithelium necrosis, and respiratory epithelium squamous metaplasia. Tissue concentrations of cobalt increased with increasing exposure concentration in all tissues examined.

	Chamber Control	2.5 mg/m <sup>3</sup>	5 mg/m <sup>3</sup>	10 mg/m <sup>3</sup>	20 mg/m <sup>3</sup>	40 mg/m <sup>3</sup>
<b>Female</b>						
n	5	5	5	5	2	0
Necropsy body wt	112 ± 4	112 ± 2	107 ± 3	98 ± 4**	61 ± 5**	
L. Kidney						
Absolute	0.52 ± 0.02	0.50 ± 0.01	0.50 ± 0.02	0.46 ± 0.01*	0.35 ± 0.00**	
Relative	4.66 ± 0.11	4.46 ± 0.05	4.63 ± 0.08	4.74 ± 0.12	5.75 ± 0.42**	
Liver						
Absolute	4.07 ± 0.16	3.77 ± 0.05	3.61 ± 0.13**	3.44 ± 0.05**	2.57 ± 0.06**	
Relative	36.37 ± 0.49	33.59 ± 0.16	33.78 ± 1.08	35.17 ± 1.00	42.15 ± 2.12**	
Lung						
Absolute	0.86 ± 0.04	0.83 ± 0.01	0.91 ± 0.04	1.03 ± 0.06*	1.01 ± 0.04*	
Relative	7.71 ± 0.36	7.44 ± 0.07	8.49 ± 0.34	10.54 ± 0.69**	16.54 ± 0.56**	
Thymus						
Absolute	0.317 ± 0.016	0.324 ± 0.011	0.352 ± 0.022	0.289 ± 0.011	0.064 ± 0.016**	
Relative	2.842 ± 0.167	2.895 ± 0.126	3.289 ± 0.201	2.948 ± 0.092	1.024 ± 0.178**	

\* Significantly different (P<0.05) from the chamber control group by Williams' or Dunnett's test

\*\* P<0.01

Organ weights (absolute weights) and body weights are given in grams; organ-weight-to-body-weight ratios (relative weights) are given as mg organ weight/g body weight (mean ± standard error). No data are available for 20 mg/m<sup>3</sup> males or 40 mg/m<sup>3</sup> males or females due to 100% mortality.

Table 1 (b): Selected Organ Weights and Organ-Weight-to-Body-Weight Ratios for Rats in the 2-Week Inhalation Study of Cobalt metal (Ntp,2014).

*3-month study in rats.* Groups of 10 male and 10 female rats were exposed to particulate aerosols of cobalt metal by inhalation at concentrations of 0, 0.625, 1.25, 2.5, or 5 mg/m<sup>3</sup>, 6 hours plus 12 minutes per day, 5 days per week for 14 weeks. Additional groups of 10 male rats (clinical pathology study) and 32 to 36 female rats (special study) were exposed to the same concentrations for 14 weeks. All male and female rats survived to the end of the study. Final mean body weights of males and females exposed to 5 mg/m<sup>3</sup> were significantly less than those of the chamber controls, and the mean body weight gain of 5 mg/m<sup>3</sup> males was significantly less than that of the chamber controls. At necropsy, pale foci were noted in the lungs of most exposed male and female rats. In male rats, exposure concentration-related increases in the hemoglobin concentration, erythrocyte count, hematocrit value,

and manual packed cell volume occurred in the 2.5 and 5 mg/m<sup>3</sup> groups on days 3 and 23 and in all exposed groups by week 14; at week 14, female rats also had increases in these parameters. Exposure concentration-related decreases in cholesterol concentrations were observed at all three time points in male and female rats. While this change was not always observed in the lower exposure groups, decreases were consistently observed in the 2.5 and 5 mg/m<sup>3</sup> groups of both sexes on day 23 and at week 14. In addition, glucose concentration was decreased in males exposed to 1.25 mg/m<sup>3</sup> or greater at week 14. Lung weights of all exposed groups of males and females were significantly greater than those of the chamber controls. Sperm mobility was significantly decreased in male rats exposed to cobalt, suggesting a potential for cobalt metal to be a reproductive toxicant in male rats. In the lung, chronic active inflammation and alveolar proteinosis occurred in all exposed males and females, and bronchiole epithelium hyperplasia occurred in all males and females exposed to 1.25 mg/m<sup>3</sup> or greater. In the nose, incidences of olfactory epithelium degeneration and respiratory epithelium hyperplasia were significantly increased in males and females exposed to 2.5 or 5 mg/m<sup>3</sup>. The incidences of olfactory epithelium hyperplasia were significantly increased in 2.5 and 5 mg/m<sup>3</sup> males and in 5 mg/m<sup>3</sup> females. Significantly increased incidences of turbinate atrophy occurred in 2.5 mg/m<sup>3</sup> females and 5 mg/m<sup>3</sup> males and females. Tissue concentrations of cobalt increased with increasing exposure concentration in all tissues examined.

*S2-year study in rats.* Groups of 50 male and 50 female rats were exposed to cobalt metal particulate aerosol by inhalation at concentrations of 0, 1.25, 2.5, or 5 mg/m<sup>3</sup>, 6 hours plus 12 minutes per day, 5 days per week for up to 105 weeks. Additional groups of 35 lung burden study female rats were exposed to the same concentrations of cobalt metal for up to 105 weeks. Survival of female rats exposed to 2.5 mg/m<sup>3</sup> was significantly less than that of the chamber control group. As Figure 3 shows the mean body weights of 2.5 and 5 mg/m<sup>3</sup> males were at least 10% less than those of the chamber control group after weeks 99 and 12, respectively, and those of 2.5 and 5 mg/m<sup>3</sup> females (Figure 4) were at least 10% less after weeks 57 and 21, respectively.

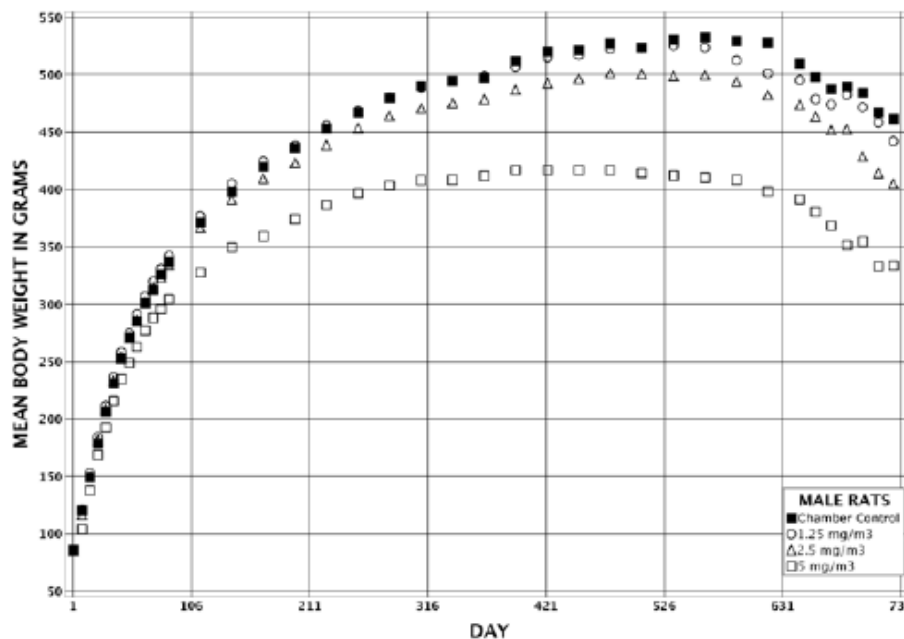


Figure 3: Growth Curves for Male Rats Exposed to Cobalt Metal by Inhalation for 2 Years (NTP, 2014).

Exposure-related clinical findings included abnormal breathing and thinness in male and female rats. In the lung, the incidences of alveolar/bronchiolar adenoma, alveolar/bronchiolar carcinoma, and

alveolar/bronchiolar adenoma or carcinoma (combined) occurred with positive trends in male and female rats and with the exception of the incidence of alveolar/bronchiolar adenoma in 1.25 mg/m<sup>3</sup> females, the incidences were significantly greater than those in the chamber controls. The incidences of multiple alveolar/bronchiolar adenoma and carcinoma generally increased with increasing exposure concentration, and the incidences of multiple carcinoma were significantly increased in all exposed groups of males and in 5 mg/m<sup>3</sup> females.

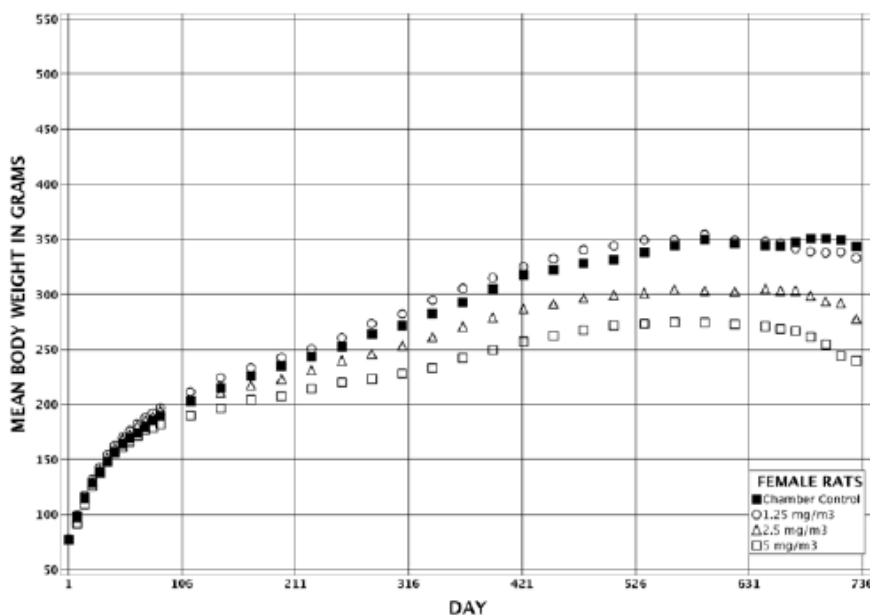


Figure 4: Growth Curves for Female Rats Exposed to Cobalt Metal by Inhalation for 2 Years (NTP, 2014).

The incidences of cystic keratinizing epithelioma were increased in exposed groups of female rats; cystic keratinizing epithelioma also occurred in two exposed males. One female rat exposed to 5 mg/m<sup>3</sup> had a squamous cell carcinoma. The incidences of alveolar epithelium hyperplasia, alveolar proteinosis, chronic active inflammation, and bronchiole epithelium hyperplasia in all exposed groups were significantly greater than those in the chamber control groups. A spectrum of nonneoplastic lesions occurred in the nose of exposed male and female rats including chronic active and suppurative inflammation, respiratory metaplasia, atrophy, hyperplasia, basal cell hyperplasia, and necrosis of the olfactory epithelium; hyperplasia, squamous metaplasia, and necrosis of the respiratory epithelium; and atrophy of the turbinate. In the adrenal medulla, incidences of benign pheochromocytoma, malignant pheochromocytoma, and benign or malignant pheochromocytoma (combined) occurred with positive trends in male and female rats, and with the exception of the incidence of malignant pheochromocytoma in 2.5 mg/m<sup>3</sup> females, the incidences in rats exposed to 2.5 or 5 mg/m<sup>3</sup> were significantly greater than those in the chamber controls. The incidences of bilateral benign and malignant pheochromocytoma were significantly increased in the 5 mg/m<sup>3</sup> groups. Incidences of hyperplasia were significantly increased in female rats exposed to 1.25 or 2.5 mg/m<sup>3</sup>. The incidences of carcinoma and adenoma or carcinoma (combined) of the pancreatic islets occurred with positive trends in male rats. The incidences of adenoma in 2.5 mg/m<sup>3</sup> males and of adenoma or carcinoma (combined) in males exposed to 2.5 or 5 mg/m<sup>3</sup> were significantly greater than those in the chamber controls. Incidences of neoplasms of the pancreatic islets in 5 mg/m<sup>3</sup> females were slightly increased. The incidences of mononuclear cell leukemia were significantly increased in all exposed groups of female rats. In the combined standard and extended (step-section) evaluations of the kidney, the incidence of renal tubule adenoma or carcinoma (combined) was increased in male rats exposed to 5

mg/m<sup>3</sup>. The incidence of infarct in the testes was significantly increased in male rats exposed to 5 mg/m<sup>3</sup>. Cobalt concentrations in the lung increased with increasing exposure concentration.

The following pages report considerations derived from the toxicological profile for cobalt (2004) written from the U.S. DEPARTMENT OF HEALTH AND HUMAN SERVICES.

### *Inhalation Exposure*

*Respiratory Effects.* Prolonged exposure (3–4 months) of rats and rabbits to mixed cobalt oxides (0.4–9 mg cobalt/m<sup>3</sup>) resulted in lesions in the alveolar region of the respiratory tract characterized histologically by nodular accumulation of Type II epithelial cells, accumulations of enlarged highly vacuolated macrophages, interstitial inflammation, and fibrosis (Johansson et al. 1984, 1987, 1991, 1992; Kyono et al. 1992; Palmes et al. 1959). Decreased lung compliance was found in pigs exposed to 0.1 mg cobalt/m<sup>3</sup> as cobalt dust for 3 months (Kerfoot 1975). Lifetime exposure of hamsters to 7.9 mg cobalt/m<sup>3</sup> as cobalt oxide resulted in emphysema (Wehner et al. 1977). In rats, chronic inflammation of the larynx was found at  $\geq 0.38$  mg cobalt/m<sup>3</sup>, and more severe effects on the nose, larynx, and lung were reported at higher exposures. In mice, acute inflammation of the nose was found at  $\geq 1.14$  mg cobalt/m<sup>3</sup>, and more severe effects on the nose, larynx, and lung were reported at higher exposures.

*Cardiovascular Effects.* Electrocardiogram abnormalities that may reflect ventricular impairment have been observed in miniature swine (n=5) exposed to 0.1 mg cobalt dust/m<sup>3</sup> for 6 hours/day, 5 days/week for 3 months (Kerfoot 1975).

*Hepatic, Renal Effects.* Necrosis and congestion of the liver were observed in both rats and mice that died following exposure to 19 mg cobalt/m<sup>3</sup> as cobalt sulfate over 16 days (Bucher et al. 1990; NTP 1991). No histological effects on the liver and on the kidneys were found in pigs exposed to up to 1.0 mg cobalt/m<sup>3</sup> as cobalt metal dust for 3 months (Kerfoot 1975).

*Neurological Effects.* Congestion in the vessels of the brain/meninges was reported in rats and mice exposed to 19 mg cobalt/m<sup>3</sup> or greater as cobalt sulfate over 16 days (Bucher et al. 1990; NTP 1991).

*Reproductive Effects.* In animals, long-term exposure to cobalt-containing aerosols has resulted in effects on reproductive end points. Testicular atrophy was reported in rats, but not in mice, exposed to 19 mg cobalt/m<sup>3</sup> as cobalt sulfate over 16 days (Bucher et al. 1990; NTP 1991). Following exposure of mice to cobalt (as cobalt sulfate) for 13 weeks, a decrease in sperm motility was found at 1.14 mg cobalt/m<sup>3</sup>, and testicular atrophy was found at 11.4 mg cobalt/m<sup>3</sup>. A significant increase in the length of the estrous cycle was reported in female mice exposed to 11.4 mg cobalt/m<sup>3</sup> for 13 weeks (Bucher et al. 1990; NTP 1991).

### *Oral Exposure*

*Cardiovascular Effects.* In an experiment designed to simulate conditions leading to beer-cobalt cardiomyopathy in humans, guinea pigs were given 20 mg cobalt/kg/day as cobalt sulfate by gavage either alone or in combination with ethanol (as part of a liquid diet) for 5 weeks (Mohiuddin et al. 1970). The experiment resulted in cardiomyopathy, which was characterized by abnormal electrocardiograms; increased heart weights; lesions involving the pericardium, myocardium, and endocardium; and disfigured mitochondria. Alcohol did not intensify the cardiac effects. Myocardia changes (proliferative interstitial tissue, swollen muscle fibers, and focal degeneration) were also found in rats following a single dose of 795 mg cobalt/kg administered as cobalt oxide (Speijers et al. 1982).

*Hematological Effects.* Significantly increased erythrocyte (polycythemia), hematocrit, and hemoglobin levels were found in animals treated orally with cobalt chloride as a single dose of 161 mg cobalt/kg (Domingo and Llobet 1984) or with longer-term exposure (3 weeks to 2 months) to  $\geq 0.5$  mg/kg/day (Brewer 1940; Davis 1937; Domingo et al. 1984; Holly 1955; Krasovskii and Fridlyand 1971; Murdock 1959; Stanley et al. 1947).

*Hepatic Effects.* Hyperemia of the liver and cytoplasmic changes in hepatocytes (clumpy cytoplasm located along the cell membrane) were found in rats administered a single dose of 68.2 mg cobalt/kg as cobalt fluoride or a single dose of 157.3 mg cobalt/kg as cobalt oxide (Speijers et al. 1982). Increased liver weight (17%) was found in rats exposed to 10 mg cobalt/kg/day (as cobalt chloride) for 5 months (Murdock 1959).

*Renal Effects.* Renal injury, evidenced by histologic alteration of the proximal tubules, was observed in rats after a single oral exposure to 42 mg cobalt/kg as cobalt fluoride (Speijers et al. 1982) and after exposure to 10–18 mg cobalt/kg/day as cobalt chloride for 4–5 months (Holly 1955; Murdock 1959). A slightly decreased urinary output was observed in rats exposed to 19.4 mg cobalt/kg as cobalt sulfate, but not in rats exposed to 4.25 mg cobalt/kg as cobalt chloride (Singh and Junnarker 1991).

*Endocrine Effects.* NTP (1998; Bucher et al. 1999) reported increased incidence of pheochromocytoma, a tumor of the adrenal medulla, in female rats exposed to 1.14 mg cobalt/m<sup>3</sup> for 2 years, but did not measure any other endocrine effects. Female mice exposed to 26 mg cobalt/kg-day in the drinking water for up to 45 days showed histopathological changes to the thyroid gland (Shrivastava et al. 1996).

*Body Weight Effects.* A significant decrease (33%) in body weight gain was observed following 8 weeks of exposure of rats to 4.2 mg cobalt/kg/day as cobalt sulfate (Clyne et al. 1988).

*Neurological Effects.* In Wistar rats, a single gavage dose of 4.25 mg cobalt/kg as cobalt chloride resulted in a moderate reduction in spontaneous activity, muscle tone, touch response, and respiration, while 19.4 mg cobalt/kg as cobalt sulfate caused a mild reduction the same parameters (Singh and Junnarkar 1991). In rats exposed to 4.96 mg cobalt/kg/day as cobalt chloride for 30 days in the drinking water, cobalt led to changes in sympathetically mediated contractile activity of isolated rat vas deferens (Mutafova-Yambolieva et al. 1994). Rats exposed to 6.44 mg cobalt/kg/day as cobalt nitrate in the drinking water showed an increased sensitivity and decreased maximal response to a cholinergic agonist (Vassilev et al. 1993).

Nickel

#### *Inhalation Exposure*

Oller et al. (2008) carried on a study on Wistar rats that were exposed by whole-body inhalation to 0, 0.1, 0.4, and 1.0 mg Ni/m<sup>3</sup> nickel metal powder for 6 h/day, 5 days/week for up to 24 months. A subsequent six-month period without exposures preceded the final euthanasia. The generation systems were optimized to produce an aerosol of 1.5–3.0  $\mu\text{m}$  Mass Median Aerodynamic Diameter (MMAD); this particle size range is considered optimal for delivery of nickel aerosols to all regions of the respiratory tract of the rat. Figure 5 shows the protocol used in this work for the inhalation carcinogenicity study with nickel metal powders. Significant nickel metal exposure-related effects on body weights were noted in the 0.1 (males only), 0.4 and 1.0 mg/m<sup>3</sup> groups (Figure 6 and Figure 7). Due to the high level of exposure the last day of exposure for the 1.0 mg/m<sup>3</sup> males and females was study day 375 (week 53, ~12 months), and study day 427 (week 61, ~14 months), respectively. Figure 8 (a), shows the blood levels of the rats, they were measured after 3 and 12 months of exposure. The



value at zero time of exposure is a calculated value based on the mean value for non-exposed animals and it is included here for the purpose of estimating the shape of the time-response curve for blood nickel levels in the various nickel exposure groups.

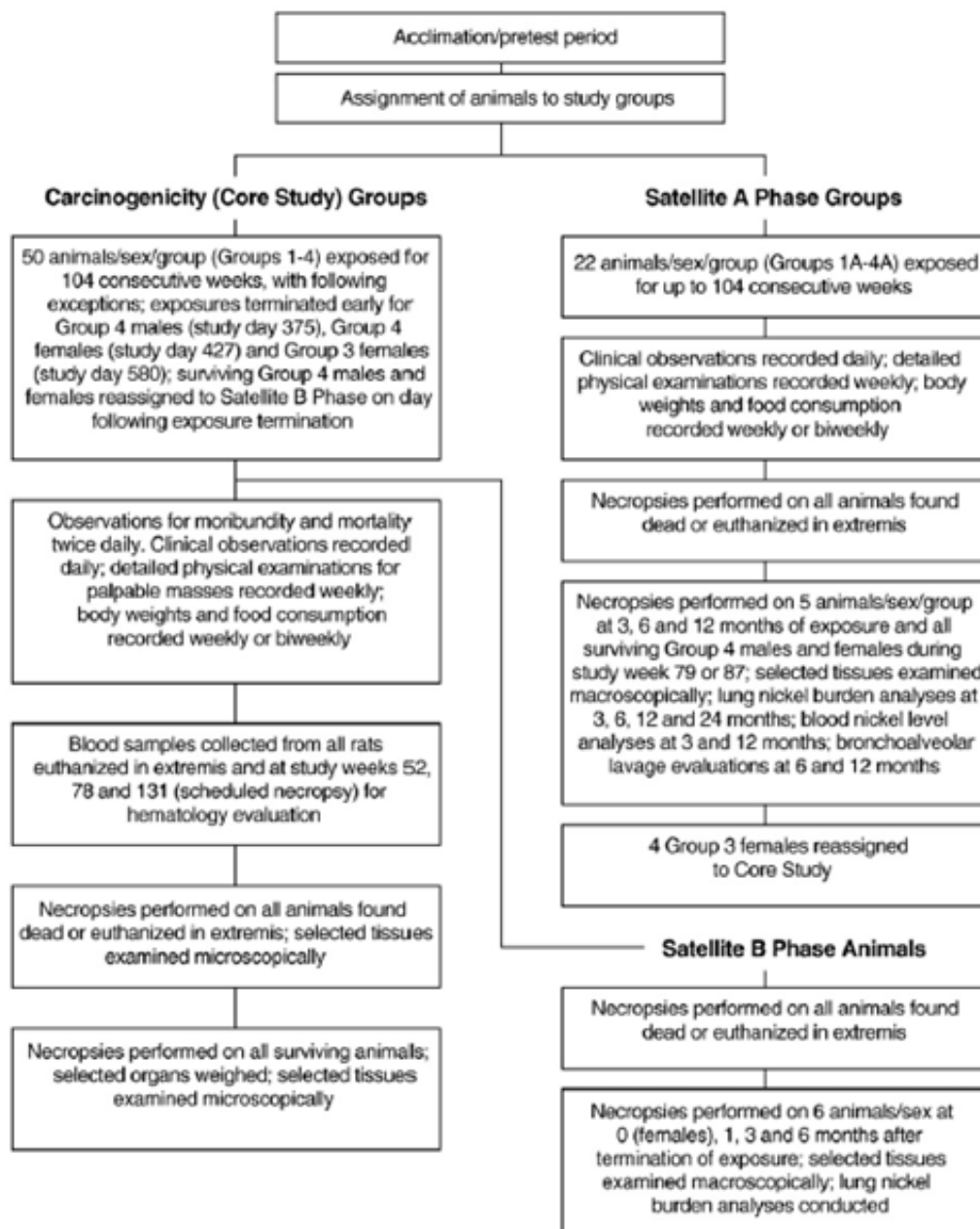


Figure 5: Protocol for the inhalation carcinogenicity study with nickel metal (Oller et al., 2008).

Figure 8 (b), shows the lung nickel burdens, they were measured after 3, 6, and 12 months of exposure in all exposure groups. After 24 months of exposure, lung nickel values were available for the 0, 0.1, and 0.4 (males only) mg Ni/m<sup>3</sup> groups. Both the blood and the lung nickel levels appear higher in females than in males in the present study. Alveolar histiocytosis was increased in incidence and severity in nickel metal-exposed rats compared to controls, but was not increased in severity with higher exposure concentration. Since alveolar macrophages play a primary role in clearance of inhaled particles from the alveolar region of the lung, an increased number of histiocytic alveolar macrophages is the expected adaptive response to repeated inhalation of particulates. Increases in erythropoiesis were observed in rats exposed to 0.1 and 0.4 mg/m<sup>3</sup> of nickel metal for 12 or 18 months in the present study. These increases were reflected in statistically significant elevation of red blood

cell levels and hemoglobin (up to 20% males, 30% females), as well as hematocrit values (up to 25% males, 40% females). These effects are considered primarily due to the hypoxia that ensues when the lung toxicity (resulting from inhalation of nickel metal powder) impairs proper gas exchange.

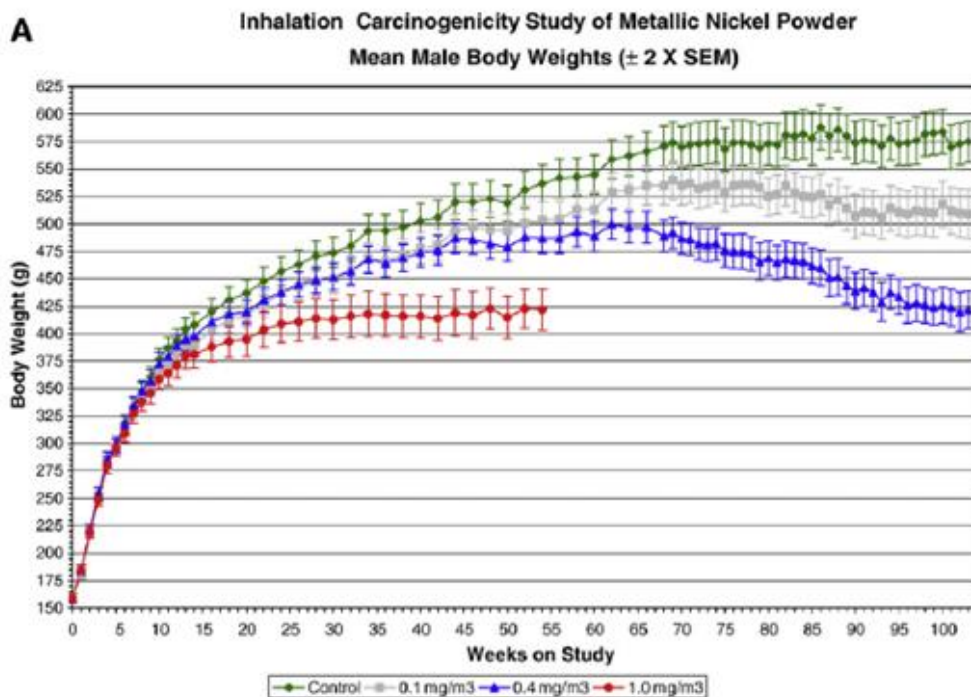


Figure 6: Rat body weights in grams. Panel A corresponds to male rats (Oller et al., 2008).

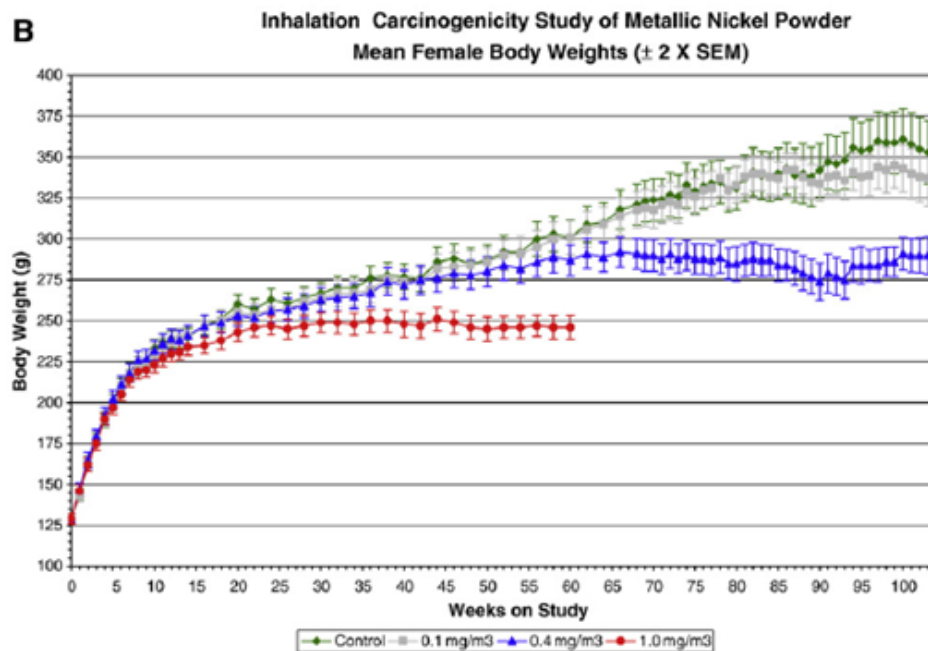


Figure 7: Rat body weights in grams. Panel B corresponds to female rats (Oller et al., 2008).

The inhalation treatment did not produce an exposure-related increase in tumors anywhere in the respiratory tract, including the nose. Significant dose-related increases in incidence of adrenal gland pheochromocytomas in males and combined cortical tumors in females were observed. Pheochromocytomas in males and combined cortical adenoma/carcinoma in females were statistically increased in the 0.4 mg/m<sup>3</sup> but not in the 0.1 mg/m<sup>3</sup> exposure groups compared to

controls. Multiple factors can contribute to the induction of pheochromocytomas, but the prolonged stimulation of catecholamine release by the endocrine cells may be a common step. An important factor in conclusively determining the lack of respiratory carcinogenic potential of nickel metal powder is to demonstrate that in this study: (1) there was an exposure group in which the Maximum Tolerable Dose (MTD) was achieved, and (2) mortality due to nickel exposure was low enough to preserve a sufficient number of animals for tumor analyses. The increased mortality seen in this study at the 1.0 mg/m<sup>3</sup> and 0.4 mg/m<sup>3</sup> (females only) exposure levels indicates that the MTD was reached and even exceeded. Despite the observed lethality, the number of males and females in the 0.4 mg/m<sup>3</sup> exposure group surviving at the end of the scheduled exposure period (24 months) and available for tumor examination was 36 and 26, respectively. These numbers meet the OECD criterion for sufficient power (50% survival of the OECD recommended 50 animals per group) to detect a positive effect if one exists. In summary, the authors of this work suggest that the results of this chronic inhalation carcinogenicity study in Wistar rats are definitive and do not show an association between nickel metal exposure and respiratory tumors.

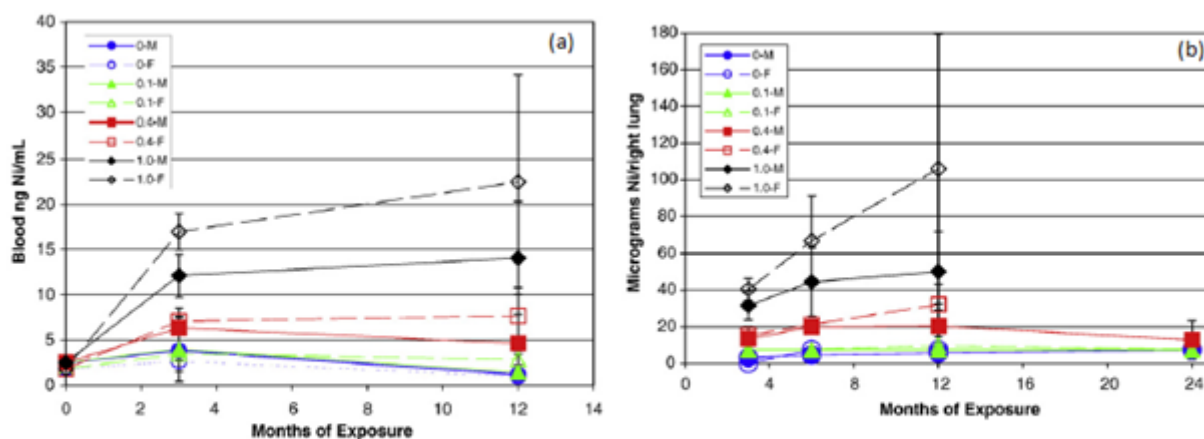


Figure 8: Blood nickel level (a) and lung nickel level (b) as a function of time of exposure to nickel metal powders (Oller et al., 2008).

The following pages report considerations derived from the toxicological profile for nickel (2005) written from the U.S. DEPARTMENT OF HEALTH AND HUMAN SERVICES.

### Inhalation Exposure

**Respiratory Effects.** In acutely-exposed rats, chronic lung inflammation was observed at the lowest nickel sulfate (0.7 mg Ni/m<sup>3</sup>) and nickel subsulfide (0.44 mg Ni/m<sup>3</sup>) concentrations tested in 12-day exposure studies (6 hours/day, 12 days in a 16-day period) (NTP 1996b, 1996c). Bronchiolar epithelium degeneration was also observed in rats exposed to 0.7 mg Ni/m<sup>3</sup> as nickel sulfate (NTP 1996c). Acute lung inflammation, consisting of neutrophilic infiltrates, was first observed in rats exposed to nickel oxide at 7.9 mg Ni/m<sup>3</sup> (NTP 1996a); chronic lung inflammation was not observed at doses as high as 23.6 mg Ni/m<sup>3</sup>. Mice appear to be less sensitive than rats to the acute toxicity of nickel with lowest observed adverse effect levels (LOAELs) for chronic inflammation of 0.7, 1.83, and >23.6 mg Ni/m<sup>3</sup> as nickel sulfate, nickel subsulfide, and nickel oxide, respectively (NTP 1996a, 1996b, 1996c). Alveolitis was reported in rats exposed to 0.11 mg Ni/m<sup>3</sup> as nickel sulfate and 1.96 mg Ni/m<sup>3</sup> as nickel oxide for 6 months (6 hours/day, 5 days/week) (Benson et al. 1995a) and interstitial pneumonia was observed at 0.5 mg Ni/m<sup>3</sup> as nickel oxide for 1 month (6 hours/day, 5 days/week) (Horie et al. 1985). Interstitial infiltrates were observed in rats exposed to  $\geq 0.11$  or 0.22 mg Ni/m<sup>3</sup> as nickel sulfate or nickel subsulfide (NTP 1996b, 1996c), granulomatous inflammation was observed in rats exposed to 3.9 mg Ni/m<sup>3</sup> as nickel oxide (NTP 1996a), alveolar wall thickening

was observed in rats exposed to 0.12 mg Ni/m<sup>3</sup> as nickel oxide (Bingham et al. 1972). The highest NOAEL values for respiratory effects in rats exposed to nickel sulfate, nickel subsulfide, or nickel oxide for intermediate durations were 0.06 mg Ni/m<sup>3</sup> (NTP 1996c), 0.11 mg Ni/m<sup>3</sup> (NTP 1996b), and 0.49 mg Ni/m<sup>3</sup> (Benson et al. 1995a). Chronic exposure to nickel (6 hours/day, 5 days/week for 2 years) resulted in chronic active lung inflammation (or pneumonia) in rats and mice at 0.06 mg Ni/m<sup>3</sup> as nickel sulfate, in rats at 0.11 mg Ni/m<sup>3</sup> and higher as nickel subsulfide (NTP 1996b; Ottolenghi et al. 1990), in mice at 0.44 mg Ni/m<sup>3</sup> and higher as nickel subsulfide (NTP 1996b), in rats at 0.2 mg Ni/m<sup>3</sup> and higher as nickel oxide (NTP 1996a; Tanaka et al. 1988), and in mice at 1 mg Ni/m<sup>3</sup> as nickel oxide (NTP 1996a). Additional lung effects that were found at the same dose levels as inflammation included alveolar epithelium hyperplasia (or bronchialization), fibrosis in rats and mice exposed to nickel subsulfide (NTP 1996b), and bronchialization and/or alveolar proteinosis in mice exposed to nickel oxide (NTP 1996a; Takenaka et al. 1985). Following acute- or intermediate-duration exposure, the toxicity of the different nickel compounds is related to its solubility, with soluble nickel sulfate being the most toxic and insoluble nickel oxide being the least toxic. The difference in the toxicity across compounds is probably due to the ability of water-soluble nickel compounds to cross the cell membrane and interact with cytoplasmic proteins. In contrast, the severity of inflammatory and proliferative lesions following chronic exposure was greater in rats exposed to nickel subsulfide or nickel oxide, as compared to nickel sulfate. Additionally, parenchymal damage secondary to inflammation was evident in the rats exposed to nickel subsulfide and nickel oxide, but not nickel sulfate. For all durations and nickel compounds tested, rats appear to be more sensitive to the lung effects than mice; significant increases in the incidence of chronic lung inflammation were observed at lower concentrations in the rats than mice. Intermediate-duration studies (Benson et al. 1995a; Horie et al. (1985) that monitored animals for months after exposure termination suggest that nickel-induced lung damage is not readily reversible after exposure termination. In the Benson et al. (1995a) studies, alveolitis was observed in rats exposed to 0.11 mg Ni/m<sup>3</sup> as nickel sulfate and 1.96 mg Ni/m<sup>3</sup> as nickel oxide at the end of the 6-month exposure period and 4 months after exposure termination.

*Cardiovascular Effects.* No cardiovascular effects were observed in rats or mice exposed to 0.44, 1.83, or 7.9 mg Ni/m<sup>3</sup> as nickel sulfate, nickel subsulfide, or nickel oxide, respectively, 6 hours/day, 5 days/week for 13 weeks (NTP 1996a, 1996b, 1996c). Similarly, chronic exposure (6 hours/day, 5 days/week) of rats to nickel sulfate, nickel subsulfide, or nickel oxide at concentrations up to 0.11, 0.73, or 2 mg Ni/m<sup>3</sup>, respectively, or exposure of mice to, 0.22, 0.88, or 3.9 mg Ni/m<sup>3</sup>, respectively, did not result in microscopic changes in the heart (NTP 1996a, 1996b, 1996c).

*Hematological Effects.* A number of hematological alterations were observed in studies by Weischer et al. (1980) and NTP (1996a, 1996b, 1996c). A decrease in hematocrit level was observed in male rats continuously exposed to 0.178 or 0.385 mg Ni/m<sup>3</sup> as nickel oxide for 28 days (Weischer et al. 1980); no significant alterations were observed at 0.785 mg Ni/m<sup>3</sup>. In non-pregnant females continuously exposed to nickel oxide for 21 days, increases in hematocrit and hemoglobin levels were observed at 0.8 mg Ni/m<sup>3</sup> and higher; an increase in mean cell volume and a decrease in erythrocyte levels were observed at 1.6 mg Ni/m<sup>3</sup> and higher (Weischer et al. 1980). As noted by NTP (1996b), increases in hematocrit, hemoglobin, and erythrocytes are consistent with erythropoietin production in response to tissue hypoxia, possibly as a result of the nickel-induced lung damage. Chronic exposure of rats to nickel oxide or nickel sulfate at concentrations up to 2 or 0.11 mg Ni/m<sup>3</sup>, respectively, and chronic exposure of mice to nickel oxide, nickel subsulfide, or nickel sulfate at concentrations up to 3.9, 0.88, or 0.22 mg Ni/m<sup>3</sup>, respectively, did not result in significant hematological effects (NTP 1996a, 1996b, 1996c).

*Musculoskeletal Effects.* No histological alterations were observed in bone of rats and mice exposed to nickel sulfate 6 hours/day for 12 days/16 days (highest No Observed Adverse Effect Level (NOAEL) is 12.2 mg Ni/m<sup>3</sup>), 5 days/week for 13 weeks (0.44 mg Ni/m<sup>3</sup>), or 5 days/week for 2 years (0.11 and 0.22 mg Ni/m<sup>3</sup> for rats and mice) (NTP 1996c). No alterations were observed in bone or muscle of rats and mice exposed to nickel oxide (6 hours/day, 5 days/week) at 23.6 mg Ni/m<sup>3</sup> for 16 days (12 days/16 days), 7.9 mg Ni/m<sup>3</sup> for 13 weeks, or 2 (rats) or 3.9 mg Ni/m<sup>3</sup> (mice) for 2 years (NTP 1996a).

*Hepatic Effects.* No histological alterations were observed in the livers of rats or mice exposed to nickel subsulfide, nickel sulfate, or nickel oxide at concentrations of 7.33, 12.2, or 23.6 mg Ni/m<sup>3</sup>, respectively, in rats and 1.4, 12.2, or 23.6 mg Ni/m<sup>3</sup>, respectively, in mice exposed 6 hours/day, 12 days in a 16-day period (NTP 1996a, 1996b, 1996c) or 1.83, 0.44, or 7.9 mg Ni/m<sup>3</sup> 6 hours/day, 5 days/week, for 13 weeks (NTP 1996a, 1996b, 1996c). Chronic exposure of mice to nickel oxide, nickel subsulfide, or nickel sulfate at concentrations up to 3.9, 0.88, or 0.22 mg Ni/m<sup>3</sup>, respectively, did not result in microscopic changes in the liver (NTP 1996a, 1996b, 1996c).

*Renal Effects.* No histological alterations were observed in the kidneys of rats or mice exposed to nickel sulfate, nickel subsulfide, or nickel oxide 6 hours/day, 5 days/week, at concentrations of ≤12.2, 7.33, or 23.6 mg Ni/m<sup>3</sup>, respectively, for 16 days (12 days in a 16-day period) (NTP 1996a, 1996b, 1996c), or ≤0.44, 1.83, or 7.9 mg Ni/m<sup>3</sup>, respectively, for 13 weeks (NTP 1996a, 1996b, 1996c), or 0.9 mg Ni/m<sup>3</sup> as nickel oxide for 12 months (Tanaka et al. 1988). Chronic exposure of rats to nickel oxide (NTP 1996a; Tanaka et al. 1988), nickel subsulfide (NTP 1996b), or nickel sulfate (NTP 1996c) at concentrations up to 2, 0.73, or 0.11 mg Ni/m<sup>3</sup>, respectively, did not result in histological alterations in the kidneys.

*Endocrine Effects.* Histological examinations did not reveal any changes in the adrenal glands, pancreas, parathyroid, pituitary, or thyroid glands in rats or mice exposed to nickel as nickel sulfate, nickel oxide, or nickel subsulfide for 12 6-hour exposures over 16 days or for 6 hours/day, 5 days/week for 13 weeks (NTP 1996a, 1996b, 1996c). The NOAEL values for endocrine effects were 12.2, 23.6, and 7.33 mg Ni/m<sup>3</sup> in rats and mice exposed to nickel sulfate, nickel oxide, and nickel subsulfide, respectively, for the shorter duration study and 0.44, 7.9, and 1.83 mg Ni/m<sup>3</sup>, respectively, for the 13-week study. In rats exposed intermittently to nickel subsulfide at 0.7 mg Ni/m<sup>3</sup> for 78 weeks, no histological changes were observed in the thyroid or adrenal glands (Ottolenghi et al. 1974). Adrenal medulla hyperplasia and increased incidences of benign pheochromocytoma were observed in female rats exposed to 2 mg Ni/m<sup>3</sup> as nickel oxide (NTP 1996a) and male and female rats exposed to 0.73 mg Ni/m<sup>3</sup> as nickel subsulfide for 2 years (NTP 1996b); an increased incidence of benign pheochromocytoma was also observed in male rats exposed to 0.11 mg Ni/m<sup>3</sup> as nickel subsulfide. These effects were not observed in rats exposed chronically to nickel sulfate at concentrations up to 0.11 mg Ni/m<sup>3</sup>, or in mice exposed to nickel oxide, nickel subsulfide, or nickel sulfate at concentrations of 3.9, 0.88, or 0.22 mg Ni/m<sup>3</sup>, respectively (NTP 1996a, 1996b, 1996c).

*Neurological Effects.* Microscopic examinations did not reveal any changes in the whole brains of rats or mice exposed to nickel as nickel sulfate, nickel oxide, or nickel subsulfide for 12 6-hour exposures over 16 days (NTP 1996a, 1996b, 1996c). The maximum concentrations that did not result in deaths or changes in brain histology were 3.1, 23.6, and 7.33 mg Ni/m<sup>3</sup> in rats for nickel sulfate, nickel oxide, and nickel subsulfide, respectively, and 0.7, 23.6, and 3.65 mg/m<sup>3</sup> in mice for nickel sulfate, nickel oxide, and nickel subsulfide, respectively. In intermediate-duration studies, no histological alterations were observed in the whole brains of rats and mice exposed to 0.44, 7.9, or 1.83 mg Ni/m<sup>3</sup> as nickel sulfate, nickel oxide, or nickel subsulfide, respectively, 6 hours/day, 5

days/week for 13 weeks (NTP 1996a, 1996b, 1996c). In rats exposed intermittently (6 hours/day, 5 days/week) to nickel subsulfide at 0.7 mg Ni/m<sup>3</sup> for 78 weeks, histological changes were not observed in the brain (Ottolenghi et al. 1974).

### *Oral Exposure*

*Respiratory Effects.* Significant increases in absolute and relative lung weights were observed in rats exposed to 28.8 mg Ni/kg/day as nickel sulfate in drinking water for 13 weeks (Obone et al. 1999). No histological alterations were observed in the lungs. In a multigeneration study (RTI 1988a, 1988b), increased lung weights were observed in rats provided with nickel chloride in the drinking water at 55 mg Ni/kg/day, and an increase in cellular infiltration of the lungs was observed at 20 mg Ni/kg/day.

*Cardiovascular Effects.* Rats exposed to 75 mg Ni/kg/day as nickel sulfate for 2 years had increased heart weight (Ambrose et al. 1976). Because the changes in heart weight were not accompanied by histological changes and decreases in body weight gain were also observed, the significance of these changes is not known.

*Gastrointestinal Effects.* During the first 3 days of a 2-year study, dogs vomited following treatment with nickel sulfate in the diet at 62.5 mg Ni/kg/day (Ambrose et al. 1976). The dose was lowered to 37.5 mg Ni/kg/day for 2 weeks, and then incrementally raised at 2-week intervals back to 62.5 mg Ni/kg/day, at which time, no further gastrointestinal distress was noted. These studies indicate that high doses of nickel can be irritating to the gastrointestinal tract, although acclimation to high levels of dietary nickel can occur.

*Musculoskeletal Effects.* Microscopic changes in skeletal muscle were not observed in rats or dogs fed nickel sulfate in the diet at doses up to 187.5 mg Ni/kg/day for rats (Ambrose et al. 1976; Springborn Laboratories 2002) and 62.5 mg Ni/kg/day for dogs (Ambrose et al. 1976).

*Hepatic Effects.* Decreased liver weight was observed in rats exposed to 0.97–75 mg Ni/kg/day as nickel chloride or nickel sulfate for 28 days to 2 years (Ambrose et al. 1976; American Biogenics Corporation 1988; Obone et al. 1999; Weischer et al. 1980) and mice exposed to 150 mg Ni/kg/day as nickel sulfate in drinking water for 180 days (Dieter et al. 1988).

*Renal Effects.* Renal tubular damage at the corticomedullary junction described as minor was observed in mice exposed to ≥108 mg Ni/kg/day as nickel sulfate in the drinking water for 180 days (Dieter et al. 1988). The renal effects included the loss of renal tubular epithelial cells and the presence of hyaline casts in the tubule (suggesting protein loss). Significant decreases in urine volume and urine glucose levels and increases in relative kidney weight at 14.4 or 28.8 mg Ni/kg/day and increases in blood urea nitrogen (BUN) at 28.8 mg Ni/kg/day were observed in rats exposed to nickel sulfate in drinking water for 13 weeks (Obone et al. 1999).

*Dermal Effects.* Histological changes in the skin have not been observed in rats and dogs exposed to nickel sulfate in the diet for 2 years at doses of 187.5 and 62.5 mg Ni/kg/day, respectively (Ambrose et al. 1976). These studies suggest that the skin is not affected by orally administered nickel in animals that have not been previously sensitized to nickel.

*Body Weight Effects.* Decreased body weight gain has been reported in mice treated with nickel sulfate in drinking water at a dose of 108 mg Ni/kg/day for 180 days (Dieter et al. 1988), and in dogs treated with nickel sulfate in the diet at a dose of 62.4 mg/kg/day for 2 years (Ambrose et al. 1976).

*Reproductive Effects.* Pandey et al. (1999) reported decreases in sperm count and motility in mice administered 2.2 mg Ni/kg as nickel sulfate, 5 days/week for 35 days; an increase in sperm

abnormalities was also observed at 1.1 mg Ni/kg. Although Pandey et al. (1999) did not report alterations in body weight gain, significant decreases in testes, epididymis, seminal vesicle, and prostate gland weights were observed.

*Cancer.* In lifetime drinking water studies in rats and mice, nickel acetate (0.6 mg Ni/kg/day for rats; 0.95 mg Ni/kg/day for mice) was found to be noncarcinogenic (Schroeder et al. 1964, 1974). The incidence of tumors was comparable to that observed in controls.

#### *Dermal Exposure*

*Hematological Effects.* Hematocrit and hemoglobin levels were not affected in guinea pigs treated with 100 mg Ni/kg/day as nickel sulfate placed on skin of the back for 15 or 30 days (Mathur and Gupta 1994).

*Endocrine Effects.* Blood glucose levels were significantly increased in guinea pigs treated with 100 mg Ni/kg/day as nickel sulfate placed on skin of the back for 15 or 30 days (Mathur and Gupta 1994).

*Dermal Effects.* Nickel sensitivity has been induced in guinea pigs following skin painting or intradermal injection with nickel sulfate (Turk and Parker 1977; Wahlberg 1976; Zissu et al. 1987). Effects on the skin were observed in rats treated dermally with  $\geq 40$  mg Ni/kg/day as nickel sulfate for 15 or 30 days (Mathur et al. 1977). The effects included distortion of the epidermis and dermis after 15 days and hyperkeratinization, vacuolization, hydropic degeneration of the basal layer, and atrophy of the epidermis at 30 days. Biochemical changes in the skin (enzymatic changes, increased lipid peroxidation, and an increase in the content of sulfhydryl groups and amino nitrogen) were observed in guinea pigs dermally exposed to nickel sulfate for up to 14 days (Mathur et al. 1988, 1992).

#### Stainless steel

##### *Inhalation Exposure*

In Hedberg et al. (2013) present an approach using metal release, explained by surface compositional data, for the prediction of inhalation toxicity of SS AISI 316L. AISI 316L was selected as a representative grade for SS alloys for further in vitro metal release and surface reactivity studies, and for a 28-day repeated dose inhalation study in rats. SS welding fume powder particles are significantly different from the inert gas-atomized SS powder. The most important difference from a toxicological perspective is that the gas-atomized SS particles have a thin (a few nanometre) surface oxide composed only of trivalent Cr and Fe, whereas welding fume particles reveal surface oxides that are at least >10 fold thicker compared with the particles investigated here and enriched in, for instance, chlorine, fluorine and potassium. It has, in addition, been shown in numerous publications that welding fume particles are composed of a large amount of soluble chromate or even only chromate (no trivalent Cr), which is dissolved as chromates into solution at concentrations about 30,000-fold higher in comparable solutions as in this study for inert gas-atomized particles. Their release is however strongly depending on welding conditions. The welding fume particles cause major health concerns due to their Cr(VI)-contents. No Cr(IV) is actually present in the AISI 316L SS powder selected for this study or on massive SS. Welding fumes can be considered as separate end use problems and are not directly related to health hazard assessments of metals or alloys as such. Therefore, welding fume particles are not in focus or relevant for comparison in this study. For the inhalation study and the in vitro release tests, fine SS 316L powder (geometrical diameter: 10% sized <1.1  $\mu\text{m}$ , 50% sized <1.8  $\mu\text{m}$  and 90% sized <3.6  $\mu\text{m}$ , based on supplier powder sizing data, here referred to as <4  $\mu\text{m}$ ) was used. The particles were produced by inert gas-atomization (the individual

particles were mainly spherical as a result of the gas-atomization production process. When the particles were immersed in solution, some agglomerates (50–300  $\mu\text{m}$ ) were formed, but most particles were sized less than 3  $\mu\text{m}$ .

*Metal release from the 316L powder - comparison with massive 316L and pure metal and  $\text{MnO}_2$  powders.* In summary, metal release was studied by immersing a powder (100 mg/L) for different periods into various synthetic biological fluids. The temperature was 37°C. The immersion studies were conducted under dark conditions in acid-cleaned polymethylpentene jars in incubators with controlled shaking (the acid solution is an artificial lysosomal fluid that has a high content of citric acid). Time-dependent studies were conducted using triplicate powder samples and one blank sample without any powder. After the exposures, the particles were separated from the solution by centrifugation. For comparative reasons, in addition, also manganese oxide ( $\text{MnO}_2$ ) particles were exposed to ALF, pH 4.5, for 168 h (1 week). The release of Fe, Cr and Ni from 316L powders has been thoroughly investigated as a function of particle size and in different synthetic media of relevance for inhalation and dermal contact. The total release of metals from 316L powders into the different test fluids is very low, although complexing solutions and proteins enhance the release of metals from the 316L powder (Figure 9).

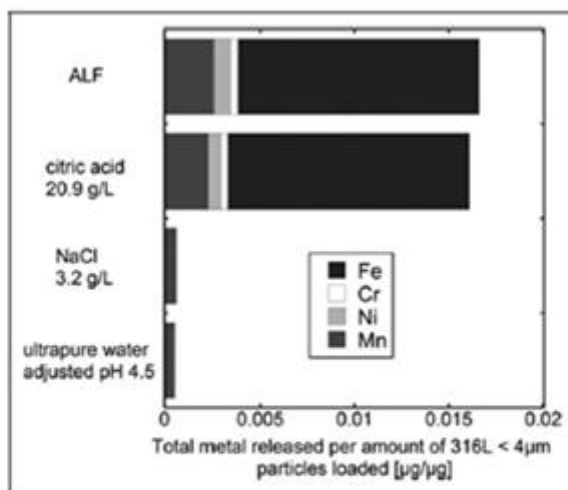


Figure 9: Metal (Fe, Cr, Ni and Mn) release (metal released per amount of particles loaded (microgram per microgram)) from the 316L powder (<4  $\mu\text{m}$ ) into different solutions, ALF, citric acid, sodium chloride and water (all initially at pH 4.5) after 24 h (Hedberg et al., 2013).

The release of Ni from SS powder into ALF was more than 1000-fold lower than the release of Ni from Ni metal powder (Figure 10). When normalized to the surface area, the release of Ni from the SS 316L powder compared with Ni powder was 1600-fold lower for the small powder particles (<4  $\mu\text{m}$ ) and 8400-fold lower for the <45  $\mu\text{m}$  particles. Similarly, significantly lower release of, for example, Fe from the fine 316L powder compared with Fe powder has previously been shown. Although the gas-atomization techniques used to produce the SS powders created a surface composition which was different from that of massive SS, the Ni release rate (normalized to the surface area) from SS powder was comparable with that of massive 316L (compare Figure 11). Ni release from the < 4- $\mu\text{m}$  powder was similar to that of abraded massive 316L in solutions with and without proteins (Figure 11, left). In ALF, it was comparable to that of as received 316L massive sheet and lower compared with abraded massive 316L. Recent studies have shown that the presence of proteins in solution can enhance the release of metals from massive 316L and Cr powders. Although complexing solutions and proteins do enhance the relative release of metals from 316L



(Figures 9 and 11), the release is still very low compared with pure Fe or pure Ni (compare Figure 10).

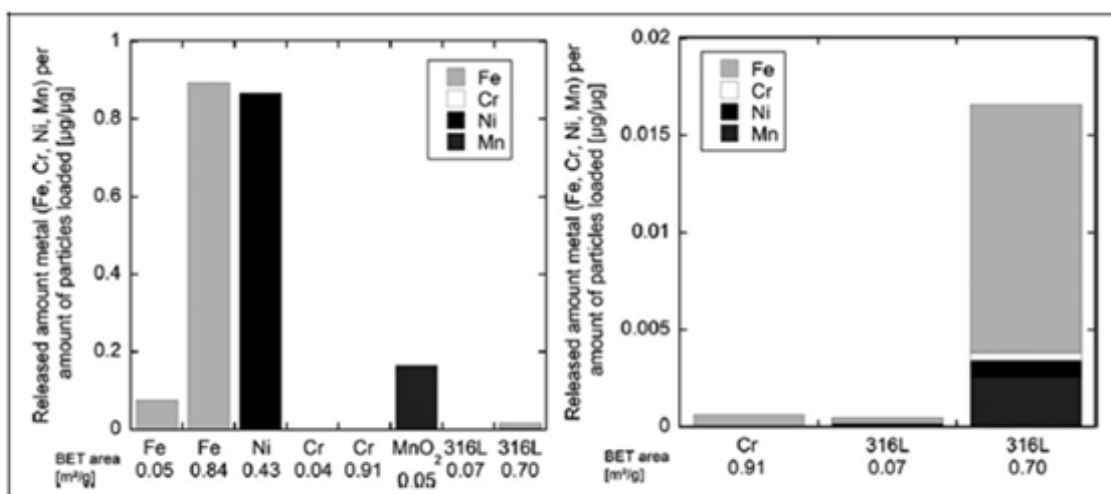


Figure 10: Released amount of metals (Fe, Cr, Ni and Mn) per amount of loaded powder (microgram per microgram) for differently sized metal powders of pure Fe, pure Ni, pure Cr, Mn dioxide and 316L powder, sized <4 mm (BET area 0.7 m<sup>2</sup>/g) and <45 mm (BET area 0.07 m<sup>2</sup>/g) into ALF (pH 4.5) after 168 h. The specific surface area (measured by the BET method<sup>8</sup>) is given for comparison. The graph to the right is of higher magnification. (Hedberg et al., 2013).

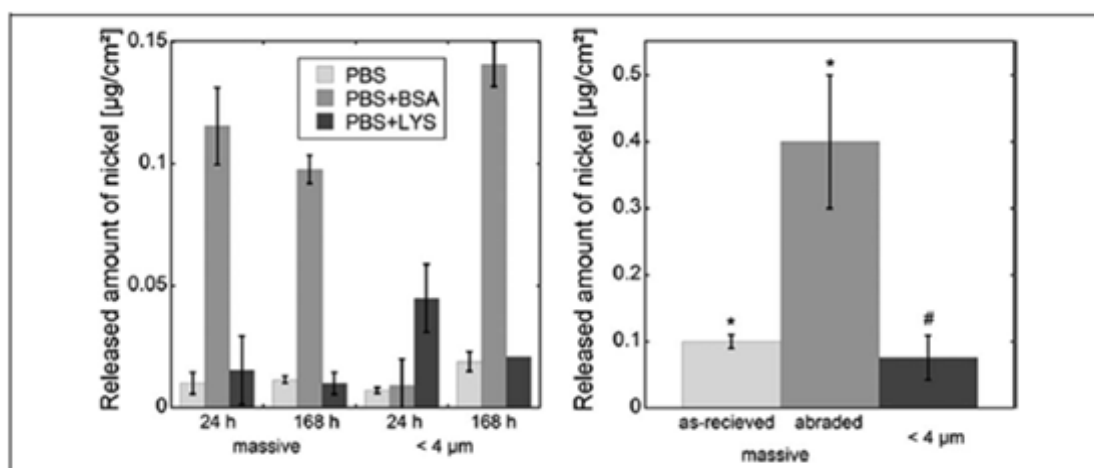


Figure 11: Released amount of nickel (microgram per centimetre square) from massive (abraded) 316L and the <4 mm stainless steel 316L powder after 24 and 168 h of exposure to PBS (pH 7.4) with and without 10 g/L bovine serum albumin (PBS + BSA) or 2.2 g/L lysozyme (from chicken egg white; PBS + LYS; left) and after 168 h of exposure in ALF (pH 4.5; right). (Hedberg et al., 2013).

*In vivo 28-day repeated dose toxicity test on rats.* A 28-day repeated dose nose-only inhalation study with rats using SS powder (grade 316L) was carried out. The animals were exposed to SS powder grade 316L (obtained from Osprey Metals Ltd) at target concentrations of 0.01, 0.10, 0.30 and 1.00 mg/L by inhalation (nose only). The particle size Mass Median Aerodynamic Diameter (MMAD) was  $\leq 3 \mu\text{m}$ . A control group (five female and five male rats) was treated in the same way as the study groups, but exposed to air only, at the same air-flow rates as in the 1.00 mg/L group. The exposures were carried out for 6 h/day, 5 days/week, followed by 2 days of rest, for a period of 4 weeks (28 days). All animals were killed at day 29. In this inhalation study with SS powder at concentrations of up to 1.0 mg/L (1 g/m<sup>3</sup>), no deaths or clinical signs of toxicity were observed during the exposure period, and the treatment did not affect food or water consumption. No statistically significant changes in body weights were seen (Table 2). No treatment-related changes were observed for the

haematological or blood chemical parameters investigated. Significantly elevated relative lung weights were observed for male and female rats treated with 0.3 and 1.0 mg/L SS powder when compared with the controls. This is the result of slight increases in absolute lung weights together with slight decreases in overall body weights (Table 2). These changes were not found to be related to lung inflammation. Grey discolouration of the lobes of the lungs was observed for all animals treated with 1.0, 0.3 or 0.1 mg/L. Two males and two females treated with 0.01 mg/L also showed grey discolouration of the lungs. No further macroscopic abnormalities were detected at the end of the study period. Accumulation of black pigment in the lung lobes was observed for all treated animals, being more severe at the highest exposure level. Alveolar macrophages, phagocytizing pigment, were found in high amounts in the lungs, but no signs of inflammatory responses, tissue degeneration or necrosis could be observed. Small amounts of black pigment were found in the nasal cavities at all exposure levels. No signs of inflammation, tissue degeneration or necrosis could be observed. Accumulations of black pigment were also seen in the trachea, larynx, pharynx and mediastinal lymph nodes of animals exposed to the highest concentration of SS powder. However, there was in no instance any associated inflammatory response. No treatment related changes in other organs were observed. Based on the lack of adverse effects of treatment in this study, the “no observed adverse effect concentration” was therefore considered to be 1.0 mg/L.

Treatment group	Control	Low	Intermediate (I)	Intermediate (II)	High
Target concentration (mg/L)	0	0.01	0.10	0.30	1.00
Mean achieved concentration (mg/L)	Not applicable	0.015 ± 0.007	0.141 ± 0.047	0.349 ± 0.070	1.040 ± 0.170
Overall body weight change – males (g)	111 ± 27	94 ± 29	106 ± 11	100 ± 22	89 ± 19
Overall body weight change – females (g)	49 ± 12	49 ± 10	41 ± 7	44 ± 6	46 ± 10
Dietary intake – males (g/rat/week)	154 ± 9	151 ± 7	157 ± 5	150 ± 7	147 ± 7
Dietary intake – females (g/rat/week)	117 ± 7	121 ± 6	110 ± 6	116 ± 8	111 ± 5
Absolute lung weight – males (g)	1.9972 ± 0.2361	1.8506 ± 0.2594	2.0639 ± 0.1383	2.2521 ± 0.2860	2.2856 ± 0.3285
Absolute lung weight – females (g)	1.5188 ± 0.1669	1.5254 ± 0.2483	1.5920 ± 0.1288	1.7523 ± 0.2214	1.8477 ± 0.2060
Body weight-relative lung weight – males (%)	0.6867 ± 0.0448	0.6538 ± 0.0222	0.6937 ± 0.0261	0.7916 ± 0.0330 <sup>a</sup>	0.8126 ± 0.498 <sup>b</sup>
Body weight-relative lung weight – females (%)	0.7915 ± 0.0474	0.7751 ± 0.0567	0.0877 ± 0.0309	1.9399 ± 0.1266 <sup>b</sup>	0.9909 ± 0.0770 <sup>a</sup>

<sup>a</sup>Statistically significant from control  $p < 0.01$ .

<sup>b</sup>Statistically significant from control  $p < 0.001$ .

Table 2: Summary table of in-life phase of the 28-day repeated dose exposures inhalation (nose only) toxicity study in rats (Hedberg et al., 2013).

*Considerations.* There were no indications that Fe would induce toxicity after inhalation, and as the release was much lower (70-fold) than from the fine Fe metal powder, Fe release is believed not to be of importance for the potential toxicity of SS. The release of Mn (microgram per microgram) in ALF was lower from the 316L powder than from the MnO<sub>2</sub> powder, but relatively higher if considering the total metal release and the nominal bulk composition of 316L. This is most likely specific for the powder of this investigation (inert gas atomization) and not relevant for SS produced

and cooled under normal conditions. ALF is considered as a worst case, as it causes the highest complexation-induced metal release and surface changes (Figures 2 to 4). The Cr release from 316L was higher when compared with pure Cr metal. This would be expected from a metallurgical point of view, because of the corrosion resistance and hence the inhibition of metal release decreases strongly with increasing Cr bulk content (above a certain threshold value of approximately 11 wt% Cr). It should be noted that the extent of Cr released from the 316L powder is still very low and only 5.6-fold higher compared with the Cr release from pure Fe metal powder, which contains approximately 0.1 wt% of Cr as an impurity. As Cr was the only alloying metal for which the release from SS 316L was similar to or higher than from the pure corresponding metal, and since it was enriched in the surface oxide over time (while Fe and Mn were depleted and Ni was completely absent), it can be assumed that the potential hazardous or non-hazardous effects of SS 316L are most likely driven by Cr. The results of our study show that the surface and metallurgical properties of an alloy play an extremely important role in its potential to elicit toxic effects. In the case of SS 316L, the potential toxicity or non-toxicity is likely to be driven by its Cr content and hence the surface composition, although the international rules for classification and labelling would require classification as hazardous due to the Ni in the bulk alloy composition. These findings support the hypothesis that in the case of alloys, the surface composition and the bioaccessible fraction of the released alloy constituents, rather than the nominal composition, is crucial for the eventual toxicity or non-toxicity of the alloy.

## Titanium

### *Inhalation Exposure - Oral Exposure*

Many of the commercially available, pigment-grade titanium dioxide products contain surface treatments/coatings with diverse compositions of alumina or alumina and amorphous silica adhered to the TiO<sub>2</sub> particle surface. However, with regard to the toxicity of TiO<sub>2</sub> and most other particle-types, it is noteworthy that virtually all of the inhalation/pulmonary hazard studies have been conducted with “standard reference” particle-types, containing few if any surface treatments. In Warheit et al. (2005) the objectives of their studies were (1) to assess in rats, the pulmonary toxicity of inhaled TiO<sub>2</sub> particle formulations with various surface treatments, ranging from 0–6% alumina (Al<sub>2</sub>O<sub>3</sub>) or alumina and 0–11% amorphous silica (SiO<sub>2</sub>). (2) To assess the acute pulmonary toxicity of several formulations of intratracheally instilled TiO<sub>2</sub> formulations and compare the effects with reference TiO<sub>2</sub>. (3) To bridge the results of the instillation study with data generated from inhalation study. The compositions of the nearly identical TiO<sub>2</sub> formulations for both inhalation and intratracheal instillation studies are presented in Table 3.

Six separate four-week inhalation studies were conducted with 6 different TiO<sub>2</sub> formulations. For each study, 25 male rats, approximately 50 days of age, were exposed to test atmospheres 6 h/day, 5 days/week over a 4–5 week period for a total of 20 exposures. Four groups of 25 age-matched male rats were similarly exposed to room air only and served as controls. Immediately following the last exposure, as well as 14 days, 3, 6, and 12 months postexposure, 5 rats from each of the control and test groups were sacrificed by chloroform anesthesia and exsanguinations and subjected to a histopathological evaluation. Body and lung weights were determined from all rats necropsied. Groups of male rats were exposed via intratracheal instillation to saline or the TiO<sub>2</sub> particle formulations listed in Table 3 at doses of 2 or 10 mg/kg. All particle-types were suspended in saline. The exposure period was followed by 24-h, 1-week, 1-month, and 3-month recovery periods. At the end of each recovery period, rats from each group were sacrificed for Bronchoalveolar Lavage (BAL) studies (4/group/time point) or for lower respiratory tract histopathology (4/group/time point).

*Inhalation Study.* During the 4-week exposure period, lower mean body weights of rats exposed to all of the TiO<sub>2</sub> formulations were measured when compared to controls. Mean body weights for groups exposed to TiO<sub>2</sub> formulations I and III were still depressed during the 12-month recovery period (Table 4), although these results were not statistically different from controls. Mean absolute lung weights of rats exposed to the different TiO<sub>2</sub> formulations were significantly elevated when compared to corresponding controls. The greater lung weights were evident at the end of the 4-week exposure period as well as throughout the 12-month recovery period.

	Inhalation studies	Instillation study
Base TiO <sub>2</sub>	99% TiO <sub>2</sub> -1% Al	99% TiO <sub>2</sub> - 1% Al
TiO <sub>2</sub> -I	99% TiO <sub>2</sub> -1% Al + organic	99% TiO <sub>2</sub> - 1% Al + organic
TiO <sub>2</sub> -II	96% TiO <sub>2</sub> -4% Al	96% TiO <sub>2</sub> - 4% Al
TiO <sub>2</sub> -III	85% TiO <sub>2</sub> -7% Al + 8% AMO	82% TiO <sub>2</sub> - 7% Al + 11% AMO
TiO <sub>2</sub> -IV	92% TiO <sub>2</sub> -2% Al + 6% AMO	92% TiO <sub>2</sub> - 2% Al + 6% AMO
TiO <sub>2</sub> -V	94% TiO <sub>2</sub> -3% Al + 3% AMO	94% TiO <sub>2</sub> - 3% Al + 3% AMO

*Note.* Al = alumina = Al<sub>2</sub>O<sub>3</sub>. AMO = amorphous silica - SiO<sub>2</sub>. Organic, refers to triethanolamine. Base TiO<sub>2</sub>, and TiO<sub>2</sub>-I, -II, -IV, and -V formulations are identical between the two studies. TiO<sub>2</sub>-III formulations differ slightly between the two studies.

Table 3: Composition of TiO<sub>2</sub> Particle Formulations with Surface Coatings (Warheit et al., 2005).

The pulmonary responses to the following TiO<sub>2</sub> formulations—Base, I, II, IV, and V generally were characterized by TiO<sub>2</sub> particle-containing macrophage accumulation reactions and light alveolar cell hyperplasia at the end of the 4-week exposure period. Small degrees of alveolar cell hyperplasia and macrophage accumulation were still evident at the 12-month postexposure time period. In addition, slight collagen deposition was observed only in rats exposed to TiO<sub>2</sub> formulation III, the formulation containing the largest composition of alumina and amorphous silica surface treatments, and having the largest surface area values.

*Intratracheal Instillation Exposures.* The results were quite similar for the two types of exposure and demonstrated that only the TiO<sub>2</sub> particle formulations, TiO<sub>2</sub>-V and TiO<sub>2</sub>-III which contained the largest concentrations of alumina and amorphous silica on their produced mildly adverse pulmonary effects compared to base TiO<sub>2</sub> control particle-types. This shows that the effects of the instilled material serve as a reference material and then are “bridged” to the inhalation toxicity data for that material, and to the new test materials being evaluated. It should be noted however, that these pulmonary bioassay studies are effective screening tools, but do not substitute for more substantial inhalation toxicity studies, such as 4-week inhalation, 90-day inhalation studies, or 2-year inhalation bioassay studies.

Time periods postexposure			
	0 days pe	3 months pe	12 months pe
Mean body weights of rats exposed to TiO <sub>2</sub> aerosol formulations (g)			
Control	369.0	574.4	767.6
Base TiO <sub>2</sub>	347.0	550.8	864.6
Control	412.6	636.4	897.8
TiO <sub>2</sub> -I	404.2	603.8	799.8
Control	412.6	636.4	897.8
TiO <sub>2</sub> -II	394.2	631.4	927.5
Control	392.6	603.2	795.0
TiO <sub>2</sub> -III	380.0	617.2	748.2
Control	392.6	603.2	795.0
TiO <sub>2</sub> -IV	372.8	633.8	801.4
Control	388.6	631.0	777.5
TiO <sub>2</sub> -V	365.6	615.6	778.6
Lung weights of rats exposed to TiO <sub>2</sub> aerosol formulations (g)			
Control	2.202	2.596	2.560
Base TiO <sub>2</sub>	2.986*	3.392*	3.146*
Control	2.332	2.292	2.747
TiO <sub>2</sub> -I	3.158*	3.110*	3.226
Control	2.332	2.292	2.747
TiO <sub>2</sub> -II	3.438*	3.958*	3.625*
Control	2.458	2.408	2.878
TiO <sub>2</sub> -III	4.288*	4.736*	4.650*
Control	2.458	2.408	2.878
TiO <sub>2</sub> -IV	3.304*	3.760*	3.538*
Control	2.028	2.416	2.703
TiO <sub>2</sub> -V	3.874*	4.846*	4.106*

\*Significantly different ( $p < 0.05$ ) from control group by Dunnett's test.

Table 4: Mean Body Weights and Lung Weights of Rats Exposed to TiO<sub>2</sub> Aerosol Formulations (g) (Warheit et al., 2005).

### Dermal Exposure

Tungsten alloys are composed of tungsten microparticles embedded in a solid matrix of transition metals such as nickel, cobalt, or iron. In Schuster et al. (2012) the carcinogenicity of three different pellet compositions; tungsten/nickel/cobalt, tungsten/nickel/iron, and pure tungsten is carried on. Cancer development was assessed in the context of metal mobilization, pellet corrosion, and gene expression.

WA pellets were manufactured by mixing powders of the metals in specified compositions (Table 5) followed by powder compaction/liquid phase sintering, after which pellets were machined to cylinders 2 mm high by 1-mm diameter. The resulting WA is a two-phase structure consisting of microparticles of W metal suspended in a matrix comprised of the specific transition metals. Pure W pellets (W) were machine cut from W wire.

Alloy	Ni:Fe:Co	Specified composition (wt%)	Matrix composition (wt%)
W/Ni/Co	6:0:3	91.1 W-6.0 Ni-2.9 Co	43 W-38 Ni-19 Co
W/Ni/Fe	7:3:0	97.1 W-1.7 Ni-1.2 Fe	22 W-51 Ni-27 Fe
Pure W	NA	99.9 W	NA

Pellet composition was not homogenous (see Fig. 3) but consisted of two distinct phases, tungsten microparticles embedded in a solid metal matrix. The matrix phase consisted of percentages of metal that were different than the specified composition of the alloy, as measured by this study.

Table 5: Metal composition pellets prior to implantation (Schuster et al., 2012).

Pre-sterilized pellets were aseptically inserted into the hind legs of male F344. All animals (except sham) received a total of 20 pellets, 10 in the gastrocnemius muscle of each hind leg. There were three treatment groups, as shown in Table 6, two of which (W/Ni/Fe and W), were administered at a high (10 pellets per leg) and a low dose (4 pellets per leg). W/Ni/Co, because of its known potent carcinogenicity, was only used as a low dose. Control animals (Ta) received 10 pellets of the non-toxic, non-carcinogenic metal tantalum in each leg, and 6 tantalum pellets were additionally used to balance the low-dose 4-pellet treatments. This ensured that each animal had an equal loading of 10 pellets in each leg (20 pellets in all) for all treatments. Consequently, high-dose groups contained 10 pellets of alloy in each leg e.g. no tantalum pellets added, while low-dose groups had 4 pellets plus 6 tantalum pellets in each leg. Briefly, the pellets were inserted into a sterile 16-gauge needle and anesthetized animals were surgically implanted by aseptically inserting the needle into the exposed gastrocnemius muscles and expelling the pellet from behind with a plunger. Pellets were implanted in a circular pattern and were approximately 1.5 mm apart. At necropsy, urine and serum samples were collected for analysis. Treatments and necropsy times (months) are listed in Table 6. The tumor appearance times at 12 months are shown in Table 7. Mean survival time for the W/Ni/Co group was  $36 \pm 5.5$  weeks. Tumors were initially detected as a palpable mass of ~3 mm between 17 and 36 weeks post-implantation that became externally visible between 1 and 21 weeks after initial detection. At 6 months post-implantation, malignant sarcomas were present in 10/15 (66%) of the animals, while the remaining 5 animals had atypical muscle fibers surrounding the pellet, suggesting early events in tumor formation. The sarcomas were grossly visible, but did not cause clinical signs of toxicity. Between 6 and 12 months post-implantation, 15/15 (100%) of the animals had developed aggressive tumors at the site of implantation and euthanasia was therefore required. In 5/15 animals (33%), tumors were found in both legs; thus not all pellets resulted in tumors. Half of the animals had metastases to multiple organs, including the lung, liver, prostate, and lymph nodes and histological assessment indicated that the metastases originated from the primary tumor in the leg. In the other groups, rats implanted with pellets of Ta, W or W/Ni/Fe had no significant changes in body weight, clinical chemistry, hematology, or urinalysis parameters. Histopathology revealed mild to moderate necrosis at 1 month post implantation (but no early tumors) for the W/Ni/Co treatment, which increased in severity and incidence at 3 months when compared to animals implanted with W/Ni/Fe or W alone. For W/Ni/Fe or W between 1 and 6 months post-implantation, there was also mild to moderate inflammation at the implant site but no pre-neoplastic changes were noted. This inflammation was resolved between 12 and 22 months post-implantation, and no other treatment-related effects were detected.

Treatments containing W had elevated levels of W in urine over time except for the W/Ni/Fe, low dose which had no (or very low) increases in metal concentrations. Levels of W in urine varied across time points but were particularly high for the W/Ni/Co, W/Ni/Fe (high), and the W (high) treatment groups. One noticeable trend was the decrease in W concentrations for W/Ni/Fe (high) from 1 to 3

months with the concentrations further decreased to very low levels by 6 months (Fig. 12c). For W/Ni/Co (Fig. 12a), Ni concentrations were highly elevated and continued increasing for W/Ni/Co over the first 6 months; and were at least threefold greater than that of the other Ni containing alloy W/Ni/Fe, which remained comparatively low at about 200 µg/L (Fig. 12c) through all time points. This was the case even with the high-dose W/Ni/Fe treated animals (20 pellets) that had five times more alloy pellets than the W/Ni/Co (4 pellets) treatment. The W/Ni/Fe low-dose Ni levels were at or less than 50 µg/L. For Co, the urinary concentrations were consistently 50% less than Ni at 1, 3, and 6 months. For W/Ni/Co, concentrations of W, Ni, and Co tracked each other over time with increases up to the 6-month time point.

Treatment group	Number of pellets	Dose	3 month N	6 month N	12 month N	24 month N
W/Ni/Fe	4 (16)	Low	15	15	15	15
W/Ni/Fe	20 (0)	High	15	15	15	15
W	4 (16)	Low	15	15	15	50
W	20 (0)	High	15	15	15	50
W/Ni/Co	4 (16)	Low	15	15	15	–
Ta	0 (20)	High	15	15	15	50
Control	0 (0)	Sham	–	–		50

(a) *N* = number of animals used for each treatment at each time point. Male F344 rats were implanted with a total of 20 pellets, 10 in the muscle of each hind leg. For each treatment except sham, tantalum (parenthesis) pellets were used to balance the total loading of pellets for each leg to 10 (20 pellets per treatment). Low dose = 4 pellets of indicated pellet type (W/Ni/Fe, W, W/Ni/Co) + 6 pellets of tantalum in each leg. High = 10 pellets of indicated pellet type (W/Ni/Fe, W, W/Ni/Co, or Ta) in each leg.

Table 6: Animal numbers, treatments, and dose groups (Schuster et al., 2012).

Animal Number	Time to tumor detection (weeks)	Time to euthanasia (weeks)	Metastases	Tumor location
569	17	30	Heart, lungs	Bilateral
581	17	43	None	Bilateral
607	23	25	Heart, prostrate, skin	Bilateral
596	25	34	Lungs, kidney, liver, lymph node	Bilateral
633	27	31	Lungs, skin	Bilateral
634	31	33	Lymph node	Bilateral
595	31	36	None	Bilateral
622	32	40	None	Right leg
570	33	34	Lungs	Bilateral
608	33	46	None	Bilateral
558	34	37	None	Left leg
584	34	37	None	Bilateral
582	34	38	None	Bilateral
557	34	42	Lungs	Bilateral
621	36	40	Lungs	Left leg

(b) Tumors appeared only in W/Ni/Co treatment; details of tumors at 12 months include time of appearance, metastasis, and whether tumors appeared in either or both legs. Tumors from shaded rows were used for microarray analysis.

Table 7: Animal numbers, time to tumor detection and tumor location (Schuster et al., 2012).

Tungsten treatments resulted in high concentrations throughout the 22-month period and there was a clear dose– response between the high and low-dose treatments. Both tantalum and sham controls

contained low levels of metals. Urinary iron (Fe) was not changed by the W/Ni/Fe or any of the other treatments (not shown). For W/Ni/Co at the 6-month period, normalization of each metal concentration to the total concentration of W, Ni and Co in urine resulted in relative concentrations of  $46.4 \pm 4.0$  wt.% of W,  $35.4 \pm 6.4$  wt.% Ni, and  $18.2 \pm 9.3$  wt.% of Co which is similar to the values found in the matrix phase of the W/Ni/Co alloy (43% W, 38% Ni, and 19% Co). W/Ni/Fe treatments had lower metal concentrations in urine than either of the other treatments and these metal concentrations stayed consistently low over a 22-month period. Twelve-month urine samples were not collected on the remaining W/Ni/Co animals (rhabdomyosarcoma), as the collection procedure was considered too stressful.

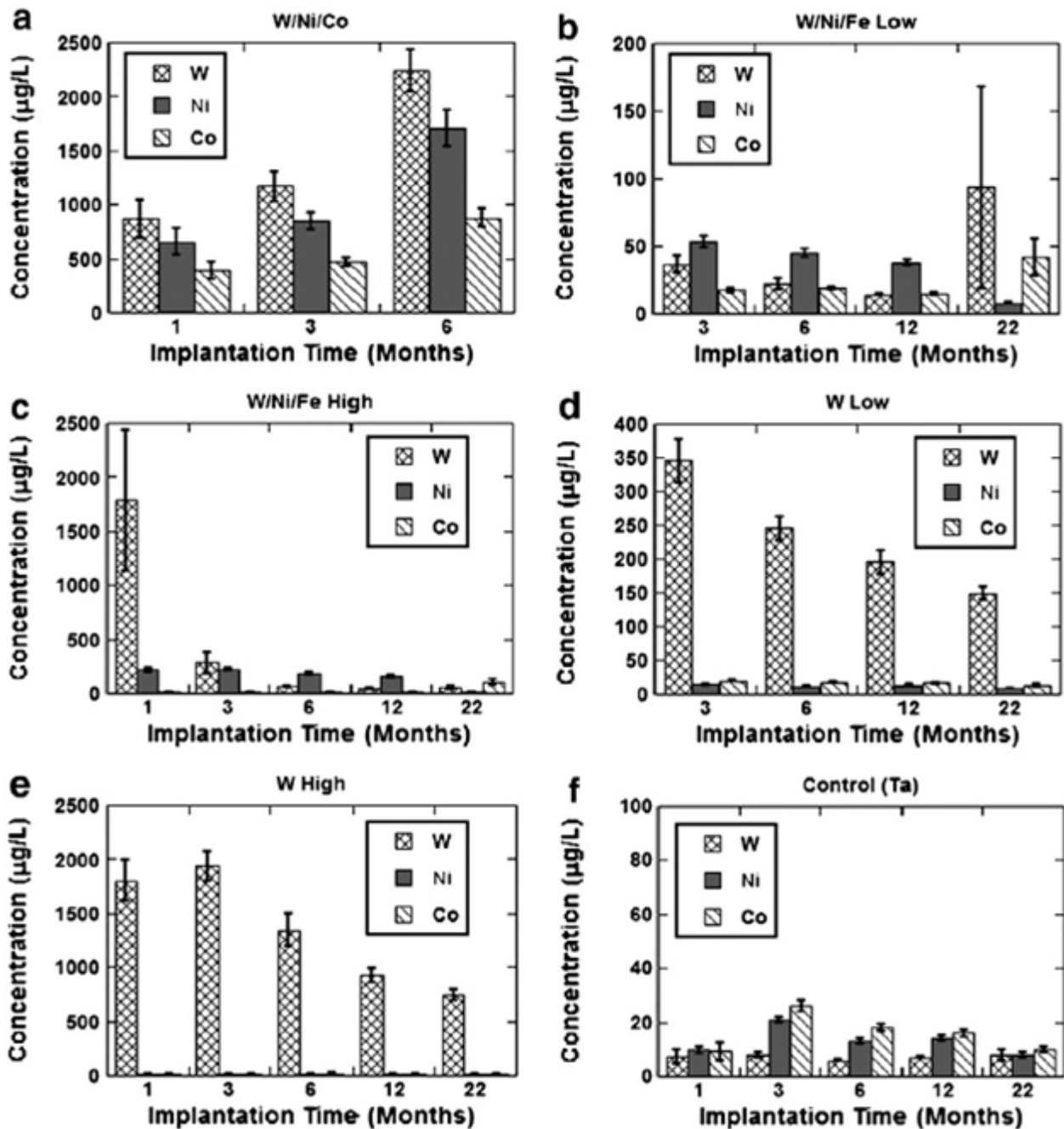


Figure 12: Metal concentrations in the urine of rats after implantation for all treatment groups including W/Ni/Co (a). W/Ni/Fe low (b). W/Ni/Fe high (c), W low (d), W high (e), Ta (f) (sham surgery). Analysis was by inductively coupled plasma-mass spectrometry (Schuster et al., 2012).



W alloys have an unusual two-phase structure, where pure W microparticles are embedded in a solid solution matrix of Ni, Co, Fe, and W that forms during the sintering process. Our work shows that the corrosion behavior of this matrix is a critical determinant in the carcinogenicity of these alloys. While the W/Ni/Co treatment resulted in 100% incidence of tumors, neoplasia were not found in the newly added treatments of W/Ni/Fe and W. Furthermore, there was a progressive and deep corrosion (~100 µm) of the W/Ni/Co matrix, with no appreciable loss of the embedded W microparticles; in contrast, W/Ni/Fe pellets showed little corrosion, and the loss of matrix never reached a depth greater than the diameter of a single W microparticle. Significantly for W/Ni/Co, the relative ratios of all three metals appearing in urine were similar to that of the disappearing matrix. Thus, the extensive corrosion of alloy matrix was the source of very high in vivo concentrations of the carcinogenic metals Ni and Co to which nearby cells were exposed. Even the high-dose W/Ni/Fe treatment (with 20 pellets) did not approach the urine concentrations of Ni seen in the W/Ni/Co low dose (4 pellets). Instead, urine concentrations in the W/Ni/Fe group remained relatively constant at ~200 µg/L, at least threefold less than the carcinogenic alloy.

### 2.1.2 Case studies of human exposure

Systematic studies of workers, suffering from diseases caused by contact with metal powders, requiring many years since the effects of these diseases are easily recognizable after decades of exposure. Since the additive manufacturing technologies relatively recent, it is very difficult to find studies about workers of these production places. The following sections present examples of studies on workers belonging to various production sectors, and where different routes of exposure are present.

#### Aluminium

The following pages report considerations derived from the toxicological profile for aluminum (2008) written from U.S. DEPARTMENT OF HEALTH AND HUMAN SERVICES, Public Health Service Agency for Toxic Substances and Disease Registry.

#### *Inhalation Exposure*

*Respiratory Effects.* Pulmonary fibrosis is the most commonly reported respiratory effect observed in workers exposed to fine aluminum dust (pyropowder), alumina (aluminum oxide), or bauxite. However, conflicting reports are available on the fibrogenic potential of aluminum. In some of the cases, the fibrosis was attributed to concomitant exposure to other chemicals. For example, pulmonary fibrosis has been observed in a number of bauxite workers or potroom workers (De Vuyst et al. 1986; Gaffuri et al. 1985; Gilks and Churg 1987; Jederlinic et al. 1990; Jephcott 1948; Musk et al. 1980; Riddell 1948; Shaver 1948; Shaver and Riddell 1947); in these workers, it is very likely that there was simultaneous exposure to silica and that the latter was the causative agent rather than the aluminum. However, other studies have not found any radiological evidence of pulmonary fibrosis in workers exposed to alumina (Meiklejohn and Posner 1957; Posner and Kennedy 1967) or fine aluminum powder (Crombie et al. 1944). There is also some evidence suggesting aluminum induced pneumoconiosis (Hull and Abraham 2002; Korogiannos et al. 1998; Kraus et al. 2000), pulmonary alveolar proteinosis (Miller et al. 1984b), interstitial pneumonia (Herbert et al. 1982), and granulomas (Cai et al. 2007; Chen et al. 1978).

*Cardiovascular Effects.* Dilation and hypertrophy of the right side of the heart were reported in male factory workers chronically exposed by inhalation to aluminum flake powder and who eventually died (McLaughlin et al. 1962; Mitchell et al. 1961).

*Hematological Effects.* No adverse hematological effects were noted in a group of seven workers following 6 months of exposure to aluminum fumes or dust (Mussi et al. 1984). Exposure levels from personal sampling ranged from 1 to 6.2 mg Al/m<sup>3</sup>, predominantly as aluminum oxide. Decreased red blood cell hemoglobin and increased erythrocyte sedimentation rates were reported in the case of a male aluminum industry worker chronically exposed by inhalation to aluminum flake powder (McLaughlin et al. 1962).

*Hepatic, Renal Effects.* Intermediate occupational inhalation exposure to aluminum fumes, dusts, or powders did not affect liver function, hepatic microanatomy, renal function in a group of seven workers as determined from biopsy samples (Mussi et al. 1984).

*Endocrine Effects.* Post-mortem enlargement of the thyroid was reported in the case of a male factory worker chronically exposed by inhalation to aluminum flake powder (McLaughlin et al. 1962).

*Ocular Effects.* No adverse effects were observed during an eye examination in a man chronically exposed by inhalation to metallic aluminum and aluminum oxide powders (De Vuyst et al. 1987).

*Neurological Effects.* A number of studies have investigated the neurotoxic potential in workers chronically exposed to aluminum. With the exception of isolated cases (for example, McLaughlin et al. 1962), none of these studies reported overt signs of neurotoxicity in workers exposed to aluminum dust (potroom and foundry workers) (Bast-Pettersen et al. 1994; Dick et al. 1997; Hosovski et al. 1990; Sim et al. 1997; White et al. 1992), in aluminum welders (Hänninen et al. 1994; Sjögren et al. 1996), or in miners exposed to McIntyre powder (finely ground aluminum and aluminum oxide) (Rifat et al. 1990). Subclinical effects have been reported in various types of aluminum workers. Significant alterations in performance tests assessing reaction time, eye-hand coordination, memory, and/or motor skills were found in aluminum foundry workers (Hosovski et al. 1990; Polizzi et al. 2001), aluminum welders (Akila et al. 1999; Bast-Pettersen et al. 2000; Buchta et al. 2005; Riihimäki et al. 2000; Sjögren et al. 1990), electrolyte workers (He et al. 2003), and miners exposed to McIntyre powder (Rifat et al. 1990). A higher incidence of subclinical tremors was found in a study of potroom workers (Bast-Pettersen et al. 1994).

*Cancer.* The International Agency for Research on Cancer (IARC) has stated (IARC 1984) that “the available epidemiological studies provide limited evidence that certain exposures in the aluminum production industry are carcinogenic to humans, giving rise to cancer of the lung and bladder. A possible causative agent is pitch fume.” It is important to emphasize that the potential risk of cancer in the aluminum production industry is probably due to the presence of known carcinogens (e.g., Polycyclic Aromatic Hydrocarbons) in the workplace and is not due to aluminum or its compounds.

### *Oral Exposure*

*Cardiovascular Effects.* Acute-duration oral exposure to aluminum phosphide has been shown to cause tachycardia, hypotension, cardiovascular electrocardiographic abnormalities, subendocardial infarction, and transient atrial fibrillation in persons who either ingested it accidentally or in suicide attempts (Chopra et al. 1986; Khosla et al. 1988). However, toxicity was probably due to the formation of highly toxic phosphine gas rather than to aluminum exposure.

*Neurological Effects.* Memory loss, fatigue, depression, behavioral changes, and learning impairment were reported in five children who, over a 5-day period, consumed drinking water containing unknown levels of aluminum sulfate, which was accidentally placed in a water-treatment facility in England (Ward 1989). The water also contained elevated levels of copper and lead, a highly neurotoxic element, which leached from the plumbing systems due to the greater acidity of the water.

Thus, the role of aluminum in the onset of the neurological symptoms is unclear. The possible association between aluminum and Alzheimer's disease was proposed over 40 years ago; however, the evidence that aluminum may or may not be a risk factor is inconsistent and inconclusive. A number of lines of evidence have been used to support the relationship between aluminum and Alzheimer's disease (Flaten 2001; Munoz 1998); these include elevated levels of aluminum in the brains of individuals with Alzheimer's disease, the well-established neurotoxicity of aluminum, and epidemiology studies finding a geographical association between aluminum levels in drinking water and Alzheimer's disease.

### *Dermal Exposure*

*Dermal Effects.* No studies were located regarding dermal effects in humans after dermal exposure to various forms of aluminum. Aluminum compounds are widely used in antiperspirants without harmful effects to the skin or other organs (Sorenson et al. 1974). Some people, however, are unusually sensitive to topically applied aluminum compounds. Skin irritation was reported in subjects following the application of aluminum chloride hexahydrate in ethanol used for the treatment of axillary or palmar hyperhidrosis (excessive sweating) (Ellis and Scurr 1979; Goh 1990) or the use of a crystal deodorant containing alum (Gallego et al. 1999).

### Chrome

The following pages report considerations derived from the toxicological profile for chrome (2002) written from U.S. DEPARTMENT OF HEALTH AND HUMAN SERVICES, Public Health Service Agency for Toxic Substances and Disease Registry.

### *Inhalation Exposure*

*Respiratory Effects.* In a chrome plating plant where poor exhaust resulted in excessively high concentrations of chromium trioxide fumes, workers experienced symptoms of sneezing, rhinorrhea, labored breathing, and a choking sensation when they were working over the chromate tanks. All five of the subjects had thick nasal and postnasal discharge and nasal septum ulceration or perforation after 2–3 months of exposure (Lieberman 1941). Chromium-induced asthma may occur in some sensitized individuals exposed to elevated concentrations of chromium in air, but the number of sensitized individuals is low and the number of potentially confounding variables in the chromium industry is high. Intermediate- to chronic-duration occupational exposure to chromium(VI) may cause an increased risk of death due to noncancer respiratory disease. In a retrospective mortality study of 1,288 male and 1,401 female workers employed for at least 6 months in a chrome plating and metal engineering plant in the United Kingdom between 1946 and 1975, a statistically significant excess of death from diseases of the respiratory system (noncancer) were obtained. Exposure was mainly to chromium trioxide. Alterations in lung function were reported in a study of 44 workers at 17 chromium electroplating facilities (Bovet et al. 1977). Statistically significant decreases in forced expiratory volume in 1 second and forced expiratory flow were observed. Lower lung function values were found among workers with high urinary chromium levels (exposure levels were not reported), and it was determined that cigarette smoking was not a confounding variable. In a survey of a facility engaged in chromate production in Italy, where exposure concentrations were  $\geq 0.01$  mg chromium(VI)/m<sup>3</sup>, high incidences of nasal septum perforation, septal atrophy and ulcerations, sinusitis, pharyngitis, and bronchitis were found among 65 men who worked in the production of dichromate and chromium trioxide for at least 1 year (Sassi 1956). Challenge tests with fumes from various stainless steel welding processes indicated that the asthma observed in two stainless steel

welders was probably caused by chromium or nickel, rather than by irritant gases (Keskinen et al. 1980).

*Cardiovascular Effects.* In a survey of a facility engaged in chromate production in Italy, where exposure concentrations were  $\geq 0.01$  mg chromium(VI)/m<sup>3</sup>, electrocardiograms were recorded for 22 of the 65 workers who worked in the production of dichromate and chromium trioxide for at least 1 year. No abnormalities were found (Sassi 1956).

*Gastrointestinal Effects.* In a NIOSH Health Hazard Evaluation of an electroplating facility in the United States, 5 of 11 workers reported symptoms of stomach pain, 2 of duodenal ulcer, 1 of gastritis, 1 of stomach cramps, and 1 of frequent indigestion. The workers were employed for an average of 7.5 years and were exposed to mean concentrations of 0.004 mg chromium(VI)/m<sup>3</sup> (Lucas and Kramkowski 1975). In a study of 97 workers from a chromate plant exposed to a mixture of insoluble chromite ore containing chromium(III) and soluble chromium(VI) as sodium chromate and dichromate, gastrointestinal radiography revealed that 10 of the workers had ulcer formation, and of these, 6 had hypertrophic gastritis. Nearly all of the workers breathed through the mouth while at work and swallowed the chromate dust, thereby directly exposing the gastrointestinal mucosa. Only two cases of gastrointestinal ulcer were found in 41 control individuals, who had the same racial, social, and economic characteristics as the chromium-exposed group (Mancuso 1951). In a survey of a facility engaged in chromate production in Italy where exposure concentrations were  $\geq 0.01$  mg chromium(VI)/m<sup>3</sup>, 15.4% of the 65 workers who worked in the production of dichromate and chromium trioxide for at least 1 year had duodenal ulcers and 9.2% had colitis. The ulcers were considered to be due to exposure to chromium (Sassi 1956).

*Hematological Effects.* Ninety-seven workers from a chromate plant were exposed to a mixture of insoluble chromite ore containing chromium(III) and soluble sodium chromate and dichromate. Hematological evaluations revealed leukocytosis in 14.4% or leukopenia in 19.6% of the workers. The leukocytosis appeared to be related primarily to monocytosis and eosinophilia, but controls had slight increases in monocytes and occasional increases in eosinophils without leukocytosis. Likewise, no effects on red blood cell counts, white blood cell counts, hemoglobin levels, or sedimentation rate were found in a case control study of 17 male manual metal arc stainless steel welders from six industries with mean occupational durations of 20 years (Littorin et al. 1984). The relationship between serum and urine chromium levels and blood hemoglobin was examined in workers exposed to chromium(III) at a tannery plant in Leon, Mexico (Kornhauser et al. 2002). Groups of workers were classified as unexposed (control; n=11), moderately exposed (n=14) or highly exposed (n=11) based on job type; exposure levels were not reported. Blood chromium levels of 0.13, 0.25, and 0.39  $\mu\text{g/L}$  and urine chromium levels of 1.35, 1.43, and 1.71  $\mu\text{g/L}$  were observed in the control, moderate, and high exposure groups, respectively; statistically significant differences were observed between the control group and both chromium groups for blood chromium and between the control and the high exposure groups for urine chromium. An inverse relationship was observed between urine chromium and blood hemoglobin ( $r=-0.530$ ), serum chromium and urine iron ( $r=-0.375$ ) and the chromium/iron ratio in urine and hemoglobin ( $r=-0.669$ ;  $<0.05$ ). Results indicate a potential effect of chromium(III) exposure on hemoglobin. No hematological disorders were found among 106 workers in a chromium(III) producing plant where workroom levels were  $\leq 1.99$  mg chromium(III)/m<sup>3</sup> as chromium(III) oxide and chromium(III) sulfate (Korallus et al. 1974a).

*Hepatic Effects.* Chromium(VI) has been reported to cause severe liver effects in four of five workers exposed to chromium trioxide in the chrome plating industry. Derangement of the cells in the liver, necrosis, lymphocytic and histiocytic infiltration, and increases in Kupffer cells were reported.

Abnormalities in tests for hepatic dysfunction included increases in sulfobromophthalein retention, gamma globulin, icterus, cephalin cholesterol flocculation, and thymol turbidity (Pascale et al. 1952). No indication was found that exposure to chromium(III) resulted in liver disorders in workers employed in two factories that produced chromium(III) oxide or chromium(III) sulfate (Korallus et al. 1974b).

*Renal Effects.* Workers exposed to chromium(VI) compounds in a chromate production plant were found to have higher levels of a brush border protein antigen and retinol binding protein in the urine compared with controls (Mutti et al. 1985a). These investigators believe that the presence of low molecular weight proteins like retinol binding protein or antigens in the urine are believed to be early indicators of kidney damage.

*Body Weight Effects.* In a report of a case of acute exposure to "massive amounts" of chromium trioxide fumes, the patient became anorexic and lost 20–25 pounds during a 3-month period following exposure (Meyers 1950).

*Neurological Effects.* In a chrome plating plant where poor exhaust resulted in excessively high concentrations of chromium trioxide fumes, workers experienced symptoms of dizziness, headache, and weakness when they were working over the chromate tanks (Lieberman 1941). Results of olfactory perceptions tests conducted in workers employed at chromium plating factories in An-San Korea (mean employment duration of 7.9 years) indicate that olfactory recognition thresholds were significantly higher in exposed workers compared to controls (Kitamura et al. 2003). No increases in vascular lesions in the central nervous system were evident in a cohort of 3,408 workers from four former facilities that produced chromium compounds from chromite ore in northern New Jersey (Rosenman and Stanbury 1996).

*Reproductive Effects.* Semen quality was evaluated in 61 workers in a chromium sulfate manufacturing plant in India (Kumar et al. 2005). Employment duration and chromium exposure levels were not reported. The study included a control group of 15 unexposed workers. Although no effect was observed on semen volume, liquefaction time, or pH or on sperm viability, count, motility, or concentration, a significant increase was observed in the number of morphologically abnormal sperm in exposed workers. In the exposed group, 53% of subjects had less than 30% normal sperm; in the control group, only 10% of subjects had <30% normal sperm. The effect of chromium(VI) on the course of pregnancy and childbirth was studied in women employees at a dichromate manufacturing facility in Russia. Complications during pregnancy and childbirth (not further described) were reported in 20 of 26 exposed women who had high levels of chromium in blood and urine, compared with 6 of 20 women in the control group. Toxicosis (not further described) was reported in 12 exposed women and 4 controls. Postnatal hemorrhage occurred in four exposed and two control women (Shmitova 1980).

*Cancer.* Sorahan et al. (1998) examined lung cancer risks in a cohort of nickel/chrome platters (n=1,762, hired during the period 1946–1975 with mortality follow-up through 1995). The same cohort was studied by Royle (1975a). Significant excess risks of lung cancer were observed among males and females working in the chrome bath area for <1 year (Standardized mortality ratio (SMR) =172; 95% CI 112–277; p<0.05) or >5 years (SMR=320; 95% CI 128–658; p<0.001), females working in the chrome bath area for <1 year (SMR=245; 95% CI 118–451; p<0.5), males starting chrome work in the period of 1951–1955 (SMR=210; 95% CI 132–317; p<0.01), and in male chrome workers 10–19 years after first chrome work (SMR=203; 95% CI 121–321; p<0.01). A significant

( $p < 0.01$ ) positive trend for lung cancer mortality and duration of exposure was found for the male chrome bath workers, but not for the female workers.

### *Oral Exposure*

*Cardiovascular Effects.* Case reports of humans who died after ingesting chromium(VI) compounds have described cardiovascular effects as part of the sequelae leading to death. In another case, cardiac output, heart rate, and blood pressure dropped progressively during treatment in the hospital of a 17-year-old male who had ingested 29 mg chromium(VI)/kg as potassium dichromate. He died of cardiac arrest. Autopsy revealed hemorrhages in the anterior papillary muscle of the left ventricle (Clochesy 1984; Iserson et al. 1983).

*Gastrointestinal Effects.* In a cross-sectional study conducted in 1965 of 155 villagers whose well water contained chromium(VI)/L as a result of pollution from an alloy plant in the People's Republic of China, associations were found between drinking the contaminated water and oral ulcer, diarrhea, abdominal pain, indigestion, and vomiting. The alloy plant began chromium smelting in 1961 and began regular production in 1965. Similar results were found in two similar studies in other villages, but further details were not provided (Zhang and Li 1987).

*Hematological Effects.* In a cross-sectional study conducted in 1965 of 155 villagers whose well water contained 20 mg chromium(VI)/L as a result of pollution from an alloy plant in the People's Republic of China, associations were found between drinking the contaminated water and leukocytosis and immature neutrophils. Similar results were found in two similar studies in other villages, but further details were not provided (Zhang and Li 1987).

*Hepatic Effects.* Liver damage, evidenced by the development of jaundice, increased bilirubin, and increased serum lactic dehydrogenase, was described in a case of a chrome plating worker who had accidentally swallowed an unreported volume of a plating fluid containing 300 g chromium trioxide/L (Fristedt et al. 1965).

*Renal Effects.* Acute renal failure, characterized by proteinuria, and hematuria, and followed by anuria, developed in a chrome plating worker who had accidentally swallowed an unreported volume of a plating fluid containing 300 g chromium trioxide/L. He was treated by hemodialysis (Fristedt et al. 1965).

*Body Weight Effects.* Although the role of chromium(III) in the regulation of lean body mass, percentage body fat, and weight reduction is highly controversial with negative and positive results being reported in the literature, studies assessing these effects were not designed to evaluate weight loss as a toxicological end point (Anderson 1998b). Thus, body weight effects associated with dietary supplementation with chromium(III) compounds is not considered adverse.

*Metabolic Effects.* Metabolic acidosis was observed in a 35-year-old female who died after ingesting approximately 257 mg chromium(VI)/kg (assuming a 70-kg body weight) as chromic acid in a suicide (Loubieres et al. 1999). No information on adverse metabolic effects of chromium(III) compounds in humans was identified.

*Cancer.* One study did find significantly higher stomach cancer death rates in areas where well water chromium levels had been elevated (Beaumont et al. 2008). An ecological study compared levels of chromium (and other chemicals) in drinking water in 453 Nebraska communities with death rates in these areas (Bednar and Kies 1991). Data on chromium in drinking water were obtained for the year period 1986–1987, and mortality data was obtained for the year 1986. Mean chromium concentration

in drinking water was 0.002 mg/L (range <0.001–0.01). Linear correlation (Pearson) between chromium levels and death from chronic lung disease was -0.101 ( $p=0.03$ ). A study of an area of Greece with elevated chromium(VI) levels in the public drinking water supply found significantly higher standardized mortality ratios (SMRs) for primary liver cancer (SMR=1104.2; 95% CI=403.2–2403.3), lung cancer (SMR 145.1; 95% CI=100.5–202.8), and cancer of the kidney and other genitourinary organs among women (SMR=367.8) (Linos et al. 2011). Chromium levels in the drinking water ranged from 8.3 to 51  $\mu\text{g/L}$ .

### *Dermal Exposure*

*Dermal Effects.* Skin burns, blisters, and skin ulcers, also known as chrome holes or chrome sores, are more likely associated with direct dermal contact with solutions of chromium compounds, but exposure of the skin to airborne fumes and mists of chromium compounds may contribute to these effects. Acute dermal exposure of humans to chromium(VI) compounds causes skin burns. Necrosis and sloughing of the skin occurred in individuals at the site of application of a salve containing potassium chromate. Twelve of 31 people died as a result of infection of these areas (Brieger 1920). Longer-term occupational exposure to chromium compounds in most chromium-related industries can cause deep penetrating holes or ulcers on the skin. In an extensive survey to determine the health status of chromate workers in seven U.S. chromate production plants, 50% of the chromate workers had skin ulcers or scars. In addition, inflammation of oral structures, keratosis of the lips, gingiva, and palate, gingivitis, and periodontitis due to exposure of these mucocutaneous tissues to airborne chromium were observed in higher incidence in the chromate workers than in controls. Chronic exposure of chrome chemical production workers produced dermal symptoms, including irritated and ulcerated skin, dermatitis, and burns (Gibb et al. 2000a). Medical records of 2,307 male workers employed at a chromate production plant in Baltimore, Maryland between 1950 and 1974 were evaluated to determine the percentage of workers reporting clinical symptoms, mean time of employment to first diagnosis of symptoms, and mean exposure to chromium(VI) at the time of first diagnosis (exposure for each worker was the annual mean in the area of employment during the year of first diagnosis). Ulcerated skin occurred in 31.6% of workers, at a mean exposure of 0.029 mg Cr(VI)/m<sup>3</sup> and a mean time to first diagnosis of 373 days. Ulcerated skin was significantly associated with chromium(VI) exposure ( $p=0.004$ ), with a relative risk of 1.11. Burns were observed in 31.4% of workers, with a mean exposure and time to onset of 0.027 mg/m<sup>3</sup> and 409 days, respectively. Dermatitis was observed in 18.5% of workers, with a mean exposure and time to onset of 0.029 mg/m<sup>3</sup> and 624 days, respectively. Irritated skin was observed in 15.1% of workers, with a mean exposure and time to onset of 0.025 mg/m<sup>3</sup> and 719 days, respectively. Irritation and ulceration of the buccal cavity, as well as chrome holes on the skin, were also observed in workers in a chrome plating plant where poor exhaust resulted in excessively high concentrations of chromium trioxide fumes (Lieberman 1941).

*Ocular Effects.* In an extensive study of chromate workers in seven U.S. chromate production plants, eyes were examined because accidental splashes of chromium compounds into the eye had been observed in these plants. Congestion of the conjunctiva was found in 38.7% of the 897 workers, discharge in 3.2%, corneal scarring in 2.3%, any abnormal finding in 40.8%, and burning in 17.0%, compared with respective frequencies of 25.8, 1.3, 2.6, 29.0, and 22.6% in 155 nonchromate workers. Only the incidences of congestion of the conjunctiva and any abnormal findings were significantly higher in the exposed workers than in the controls (PHS 1953).

### Cobalt

The following pages report considerations derived from the toxicological profile for cobalt (2004) written from U.S. DEPARTMENT OF HEALTH AND HUMAN SERVICES, Public Health Service Agency for Toxic Substances and Disease Registry.

### *Inhalation Exposure*

*Respiratory Effects.* The effects of chronic occupational exposure to cobalt and cobalt compounds on the respiratory system in humans are well-documented. These effects include respiratory irritation, diminished pulmonary function, wheezing, asthma, pneumonia, and fibrosis and occurred at exposure levels ranging from 0.007 to 0.893 mg cobalt/m<sup>3</sup> (exposure from 2 to 17 years) (Anttila et al. 1986; Davison et al. 1983; Demedts et al. 1984a, 1984b; Deng et al. 1991; Gennart and Lauwerys 1990; Gheysens et al. 1985; Hahtola et al. 2000; Hartung et al. 1982; Kusaka et al. 1986a, 1986b, 1996a, 1996b; Nemery et al. 1992; Raffn et al. 1988; Rastogi et al. 1991; Ruokonen et al. 1996; Shirakawa et al. 1988, 1989; Sprince et al. 1988; Sundaram et al. 2001; Swennen et al. 1993; Tabatowski et al. 1988; Van Cutsem et al. 1987; Zanelli et al. 1994). These effects have been observed in workers employed in cobalt refineries, as well as hard metal workers, diamond polishers, and ceramic dish painters (painting with cobalt blue dye). Swennen et al. (1993) performed a cross-sectional study on 82 workers in a cobalt refinery. Workers were examined for cobalt in blood and urine, a number of erythropoietic variables, thyroid metabolism, pulmonary function, skin lesions, and several serum enzymes. The concentrations of cobalt in blood and in urine after the shift were significantly correlated with those in air. Workers exposed to airborne cobalt metal, salts, or oxides (mean concentration 0.125 mg/m<sup>3</sup>, range 0.001–7.7 mg/m<sup>3</sup>) showed an increased ( $p < 0.05$ ) prevalence of dyspnea and wheezing and had significantly more skin lesions (eczema, erythema) than control workers. A dose-effect relation was found between the reduction of the Forced expiratory volume in the 1st second (FEV1) and the intensity of the current exposure to cobalt, as assessed by measurement of cobalt in blood, air, or urine. Nemery et al. (1992) conducted a cross-sectional study of cobalt exposure and respiratory effects in diamond polishers. Exposure occurred mainly from the generation of airborne cobalt resulting from the use of cobalt-containing polishing discs. The study groups were composed of 194 polishers working in 10 different workshops, and were divided into control, low-, and high-exposure groups. The low exposure group (n=102) was exposed to an average of 0.0053 mg cobalt/m<sup>3</sup>, based on personal sampling measurements, while the exposure level for the high dose group (n=92) was 0.0151 mg cobalt/m<sup>3</sup>; there was considerable overlap in the total range of concentrations for the low- and high-exposure groups. Workers in the high-exposure group were more likely than those in the other groups to complain about respiratory symptoms; the prevalence of eye, nose, and throat irritation and cough, as well as the fraction of these symptoms related to work, were significantly increased in the high-exposure group. Workers in the high-exposure group also had significantly reduced lung function compared to controls and low-exposure group workers, as assessed by Forced Vital Capacity (FVC), FEV1, Maximum Midexpiratory Flow (MMEF) (forced expiratory flow between 25 and 75% of the FVC) and mean Peak Expiratory Flow Rate (PEF). Results in the low-exposure group did not differ from controls.

*Cardiovascular Effects.* Occupational exposure of humans to cobalt-containing dust, either as cobalt metal or as hard metal, has been shown to result in cardiomyopathy, characterized by functional effects on the ventricles (Horowitz et al. 1988) and/or enlargement of the heart (Barborik and Dusek 1972; Jarvis et al. 1992), but the exposure levels associated with cardiac effects of inhaled cobalt in humans have not been determined. Horowitz et al. (1988) reported that in a cohort of 30 hard metal workers (exposure histories not specified), significant decreases in exercise right ventricular ejection fraction (EF) were seen in workers with abnormal chest x-rays relative to those with normal chest x-rays. It is possible that these effects were secondary to the respiratory effects of inhaled cobalt. It was



concluded that cobalt is a weak cardiomyopathic agent following occupational exposure (Horowitz et al. 1988).

*Hematological Effects.* Swennen et al. (1993) reported slightly, but statistically significantly, decreased levels of red cells and total hemoglobin (~4–5% decreases) in a group of 82 workers occupationally exposed to a mean concentration of 0.125 mg cobalt/m<sup>3</sup> as cobalt metal dust.

*Hepatic, Renal Effects.* Congestion of the liver and of the kidneys were observed upon autopsy of a metal worker (exposure history not reported) who had been occupationally exposed to an unknown level of cobalt for 4 years (Barborik and Dusek 1972). The cause of death was determined to be cardiomyopathy.

*Endocrine Effects.* A group of female workers occupationally exposed to a semisoluble cobalt glaze (cobalt-zinc silicate, estimated concentrations of 0.05 mg Co/m<sup>3</sup>) showed significantly elevated levels of serum thyroxine (T4) and free thyroxine, but no change in T3 levels (Prescott et al. 1992). In contrast to this, Swennen et al. (1993) reported no significant change in serum T4 levels, but a significant reduction in serum T3 in workers occupationally exposed to cobalt oxides, cobalt salts, and cobalt metal.

*Body Weight Effects.* Weight loss, measured individually from time of initial examination throughout followup, was observed in a group of five diamond polishers suffering from cobalt-induced interstitial lung disease (Demedts et al. 1984b), but the exposure level of cobalt was not reported.

*Neurological Effects.* Occupational exposure to cobalt in humans has been reported to cause several effects on the nervous system, including memory loss (Wechsler Memory Scale-Revised), nerve deafness, and a decreased visual acuity (Jordan et al. 1990; Meecham and Humphrey 1991). It should be noted, though, that both of these studies had small numbers of subjects (n=38 for Jordan et al. 1990, n=1 for Meecham and Humphrey 1991), and exposure characterization was not reported.

*Cancer.* The mortality of a cohort of 1,143 workers in a plant that refined and processed cobalt and sodium was analyzed (Mur et al. 1987); the French national population mortality data were used as a reference population. An increase in deaths due to lung cancer was found in workers exposed only to cobalt SMR of 4.66; four cases in the exposed group versus one case in the controls). A cohort of 5,777 males and 1,682 females who were exposed occupationally to cobalt (concentrations ranging from 1 to 515 µg/m<sup>3</sup>, means of exposure levels ranging from 39.37 to 169.0 µg/m<sup>3</sup>) and tungsten carbide (as hard metal dust) was examined by Moulin et al. (1998). A significantly increased mortality rate (SMR=1.30, 95% Confidence Interval (CI) =1.00–1.66) was seen for lung cancer in exposed workers, when compared to the national average. Within this study group, 61 cases and 180 controls were selected for a case-control study of cancer risk. When exposures during the last 10 years were ignored, presumably because cancer is a late-developing disease, a significant increase in lung cancer mortality (Odds Ratio (OR) =1.93, 95% CI=1.03–3.62) relative to controls was seen among workers simultaneously exposed to cobalt and tungsten carbide.

### *Oral Exposure*

*Cardiovascular Effects.* Beer-cobalt cardiomyopathy was observed in people who heavily consumed beer containing cobalt sulfate as a foam stabilizer (Alexander 1969, 1972; Bonenfant et al. 1969; Kesteloot et al. 1968; Morin et al. 1967, 1971; Sullivan et al. 1969). The beer drinkers ingested an average of 0.04 mg cobalt/kg/day (Morin et al. 1971, n=50) to 0.14 mg cobalt/kg/day for a period of years (Alexander 1969, 1972, n=28). The cardiomyopathy was characterized by sinus tachycardia, left ventricular failure, cardiogenic shock, diminished myocardial compliance, absence of a

myocardial response to exercise or catecholamine, enlarged heart, pericardial effusion, and extensive intracellular changes (changes in the myofibers, mitochondria, glycogen, and lipids).

*Gastrointestinal Effects.* In pregnant women given cobalt supplements (alone or combined with iron) to prevent the decrease in hematocrit and hemoglobin levels commonly found during pregnancy (n=78), a small percentage of those treated complained of gastric intolerance (Holly 1955). The women were treated with 0.5–0.6 mg cobalt/kg/day as cobalt chloride for 90 days. Nausea was reported in one anemic patient following treatment with 0.18 mg cobalt/kg/day as cobalt chloride (Duckham and Lee 1976b).

*Hematological Effects.* Cobalt has been shown to stimulate the production of red blood cells in humans. Davis and Fields (1958) exposed six apparently normal men, ages 20–47, to a daily dose of cobalt chloride, administered as a 2% solution diluted in either water or milk, for up to 22 days. Five of the six received 150 mg cobalt chloride per day for the entire exposure period, while the sixth was started on 120 mg/day and later increased to 150 mg/day. Blood was analyzed for red blood cell counts, hemoglobin percentage, leukocyte counts, reticulocyte percentages, and thrombocyte counts. Exposure to cobalt resulted in the development of polycythemia in all six subjects, with increases in red blood cell numbers ranging from 0.5 to 1.19 million (~16–20% increase above pretreatment levels). Polycythemic erythrocyte counts returned to normal 9–15 days after cessation of cobalt administration. Hemoglobin levels were also increased by cobalt treatment, though to a lesser extent than the erythrocyte values, with increases of 6–11% over pretreatment values. In five of the six subjects, reticulocyte levels were elevated, reaching at least twice the pre-experiment values. Thrombocyte and total leukocyte counts did not deviate significantly from pretreatment values.

*Hepatic Effects.* Liver injury was evident in patients with beer-cobalt cardiomyopathy, characterized by central hepatic necrosis accompanied by increased levels of serum bilirubin and serum enzymes (Serum Glutamic Oxaloacetic Transaminase (SGOT), Serum Glutamic Pyruvic Transaminase (SGPT), Lactate Dehydrogenase (LDH), creatine phosphokinase, ornithine carbamyl transferase, isocitric dehydrogenase, aldolase) (Alexander 1972; Morin et al. 1971). The hepatic injury may have resulted from ischemia, secondary to the cardiac effects of cobalt, and/or from excessive alcohol consumption.

*Endocrine Effects.* Roy et al. (1968) reported on 20 Québécois patients who died of beer drinkers' myocardiosis. Of these, 14 thyroids were available for examination. Three of those were normal, and the other 11 formed the basis of the study. "Abnormal" thyroids did not show gross changes, but upon histologic examination, they showed irregular follicle morphology and decreased follicular size.

#### *Dermal Exposure*

*Dermal Effects.* Dermatitis is a common result of dermal exposure to cobalt in humans that has been verified in a large number of studies (Alomar et al. 1985; Bedello et al. 1984; Dooms-Goossens et al. 1980; Fischer and Rystedt 1983; Goossens et al. 2001; Kanerva et al. 1988, 1998; Kiec-Swierczyńska and Kręcisz 2002; Marcussen 1963; Minamoto et al. 2002; Pryce and King 1990; Swennen et al. 1993; Romaguera et al. 1982; Valer et al. 1967). Using patch tests and intradermal injections, it has been demonstrated that the dermatitis is probably caused by an allergic reaction to cobalt. Contact allergy was reported in 22 of 223 (9.9%) nurses who were tested with a patch test of 1.0% cobalt chloride (Kiec-Swierczynska and Kręcisz 2000), as well as 16 of 79 (20.3%) of examined dentists (Kiec-Swierczynska and Kręcisz 2002).

Nickel

The following pages report considerations derived from the toxicological profile for nickel (2005) written from U.S. DEPARTMENT OF HEALTH AND HUMAN SERVICES, Public Health Service Agency for Toxic Substances and Disease Registry.

### *Inhalation Exposure*

*Respiratory Effects.* A significant excess of deaths from nonmalignant respiratory system disease was found among foundry workers that was associated with the duration of foundry employment, regardless of exposure to nickel (Cornell and Landis 1984). Other studies of refinery workers or workers exposed to nickel alloys have not found increases in deaths from respiratory disease (Arena et al. 1998; Cox et al. 1981; Cragle et al. 1984; Egedahl et al. 2001; Enterline and Marsh 1982; Redmond 1984; Roberts et al. 1989b; Shannon et al. 1984b, 1991). Two studies of welders also did not find significant increases in the risk of nonmalignant respiratory disease deaths (Moulin et al. 2000; Polednak 1981). A common limitation of the cohort mortality studies is that the number of observed deaths from all causes were lower (in many cases significantly lower) than the number expected deaths, suggesting a healthy worker effect. Additionally, the workers were exposed to other respiratory toxicants; this is particularly true for welders exposed to elevated levels of chromium. A single case of death from adult respiratory distress syndrome has been reported following a 90-minute exposure to a very high concentration (382 mg/m<sup>3</sup>) of metallic nickel of small particle size (<1.4 µm) (Rendell et al. 1994). Histological changes noted in the lungs of this case included alveolar wall damage, with fibrotic changes, and edema in the alveolar space. Another study found an increased risk of moderate pulmonary fibrosis, after controlling for age and smoking, among nickel refinery workers with cumulative exposure to soluble nickel or sulfidic nickel (Berge and Skyberg 2003).

*Cardiovascular Effects.* No increases in the number of deaths from cardiovascular diseases were reported in workers exposed to nickel (Cornell and Landis 1984; Cox et al. 1981; Cragle et al. 1984).

*Renal Effects.* Marked tubular necrosis was observed in the kidneys of a man who died of adult respiratory distress syndrome 13 days after a 90-minute exposure to a very high concentration (382 mg/m<sup>3</sup>) of metallic nickel of small particle size (<1.4 µm) (Rendall et al. 1994). Several days after the exposure, urinary concentrations of nickel were 700 µg/L, in comparison to levels of <0.1–13.3 µg/L in persons not occupationally exposed to nickel (Sunderman 1993). In nickel refinery workers, a significant association was found between increased levels of nickel in urine and increased urinary β<sub>2</sub>-microglobulin levels (Sunderman and Horak 1981).

*Reproductive Effects.* An increase in the rate of spontaneous abortions (15.9%) was reported among a group of 356 women who worked in a nickel hydrometallurgy refining plant in the Arctic region of Russia as compared to the rate (8.5%) in 342 local female construction workers (Chashschin et al. 1994). Exposure concentrations were 0.08–0.196 mg Ni/m<sup>3</sup>, primarily as nickel sulfate, and nickel concentrations in the urine were 3.2–22.6 µg/L. Nickel levels in the urine of persons not occupationally exposed are generally <0.1–13.3 µg/L (Sunderman 1993). The investigators noted that the nickel-exposed women manually lifted heavy nickel anodes and that they may have experienced heat stress. These confounders, plus the lack of information on the selection of control group subjects, possible acute exposure to high concentrations of chlorine, and the lack of adequate control of possible confounding variables such as smoking habits, use of alcohol, and intercurrent disease, preclude establishing a causative relationship between nickel exposure and reproductive toxicity from this study.

*Cancer.* A large number of epidemiology studies have assessed the carcinogenic potential of nickel; it has been estimated that over 100,000 nickel workers have been examined in epidemiology studies

(Seilkop and Oller 2003). These workers have been employed in nickel refinery facilities, nickel mining and smelting facilities, nickel alloy production facilities, stainless steel production facilities, nickel-cadmium battery production facilities, or as stainless steel welders. In the mid 1980s, a committee of epidemiologists was formed to investigate the human health risks associated with nickel exposure and to determine the specific forms of nickel that are associated with an increased risk of respiratory cancer (International Committee on Nickel Carcinogenesis in Man 1990). Based on information on the chemistry of the industrial process, total nickel exposure levels were divided into exposure to four nickel species: soluble nickel (including nickel sulfate and nickel chloride), sulfidic nickel (including nickel subsulfide), oxidic nickel, and metallic nickel. Statistically significant increases in the risk of nasal and/or lung cancer were found among nickel refinery workers (Andersen et al. 1996; Anttila et al. 1998; Chovil et al. 1981; Doll et al. 1977; Enterline and Marsh 1982; Grimmsrud et al. 2003; International Committee on Nickel Carcinogenesis in Man 1990; Karjalainen et al. 1992; Magnus et al. 1982; Muir et al. 1994; Pedersen et al. 1973; Peto et al. 1984; Roberts et al. 1989a). Sunderman and associates (Sunderman et al. 1989a) examined the histopathological diagnosis of 100 cases of sinonasal cancer and 259 cases of lung cancer among workers at three nickel refinery facilities. The primary sinonasal cancers were squamous cell carcinomas (48%), anaplastic and undifferentiated carcinomas (39%), and adenocarcinomas (6%). In an analysis of lung cancer, the cancers were primarily squamous cell carcinomas (67%), anaplastic, small cell, and oat cell carcinomas (15%), and adenocarcinomas (8%). The types of sinonasal and lung cancers were similar to those found in the general population, suggesting a lack of nickel-specific tumor types. Redmond (1984) and Arena et al. (1998) reported significant increases in lung cancer risks among high nickel alloy production workers as compared to the U.S. population. However, when the local population was used as the comparison group, the increase in lung cancer risk was no longer statistically significant (Arena et al. 1998). In general, workers employed in these industries were exposed to lower levels of sulfidic or oxidic nickel than the nickel refinery workers who were primarily exposed to metallic nickel (Cragle et al. 1984; Godbold and Tompkins 1979) or soluble nickel (Pang et al. 1996). Because nickel workers are exposed to several nickel species, it is difficult to assess the carcinogenic potential of a particular nickel species. The strongest evidence of carcinogenicity of a particular nickel species is for sulfidic nickel. The highest cancer risk levels were found in cohorts with the highest sulfidic nickel exposure levels, although high oxidic and soluble nickel levels were also found at these same facilities. The increased cancer risks in workers with high sulfidic nickel exposure and low oxidic and soluble nickel exposure suggests that sulfidic nickel is the causative agent. The evidence for oxidic nickel is weaker. No differences in cancer risks were seen among groups of workers with low sulfidic and soluble nickel exposures when the levels of oxidic nickel were varied. However, when high soluble nickel levels are present, oxidic nickel appears to be carcinogenic. The available weight of evidence does not suggest that exposure to soluble nickel, in the absence of carcinogenic compounds, will increase the risk of cancer. At low sulfidic and oxidic nickel levels, increasing soluble nickel levels do not increase the cancer risk. However, at high oxidic nickel levels, increasing the soluble nickel levels resulted in at least a 2-fold increase in the cancer risk. There is no evidence that metallic nickel is associated with increased lung or nasal cancer risks in nickel workers based on the results of the cross-classification analyses for two cohorts of nickel refinery workers and the lack of increased cancer risk in the workers exposed to metallic nickel alone at the barrier production facility (Cragle et al. 1984; Godbold and Tompkins 1979). The International Committee on Nickel Carcinogenesis in Man (1990) concluded that lung and nasal cancers were related primarily to exposure to less soluble nickel compounds at concentrations of  $\geq 10$  mg Ni/m<sup>3</sup> (primarily oxidic and sulfidic compounds). Exposure to soluble nickel compounds at concentrations of  $>1$  mg Ni/m<sup>3</sup> appeared to enhance the carcinogenicity of insoluble nickel compounds.

### *Oral Exposure*

*Hematological Effects.* A transient increase in blood reticulocytes was observed in workers who were hospitalized after drinking water during one work shift from a water fountain contaminated with nickel sulfate, nickel chloride, and boric acid (Sunderman et al. 1988). Thirty-five workers were exposed, 20 reported symptoms, and 10 were hospitalized. The workers who reported symptoms were exposed to an estimated dose of 7.1–35.7 mg Ni/kg. The contribution of boric acid to these effects is not known.

*Hepatic, Renal Effects.* A transient increase in serum bilirubin and urine albumin levels were observed in 3 of 10 workers (Sunderman et al. 1988).

*Dermal Effects.* Several studies indicate that a single oral dose of nickel given as nickel sulfate can result in a flare-up in the dermatitis in nickel-sensitive individuals (Burrows et al. 1981; Christensen and Moller 1975; Cronin et al. 1980; Gawkrödger et al. 1986; Hindsén et al. 2001; Jensen et al. 2003; Kaaber et al. 1978; Veien et al. 1987). Observed effects included erythema on the body, worsening of hand eczema, and a flare-up at the patch test site. Although some sensitive individuals may react to very low oral doses of nickel, the threshold for dermatitis in nickel-sensitized individuals appears to be around 0.01 mg Ni/kg; a dose of approximately 0.06 mg Ni/kg will result in a response in the most sensitized individuals. Nielsen et al. (1990) fed 12 women with hand eczema and known allergy to nickel a diet (oatmeal, soy beans, cocoa) with 5 times the normal level of nickel (about 0.007 mg/kg/day) for 4 days. An aggravation of hand eczema was found in 6/12 by day 4 after the start of the challenge, and although excess nickel was excreted by 2 days after the last treatment, further exacerbation of hand eczema was observed in 10/12 by day 11. This study also suggests that withdrawal of nickel rather than the peak nickel levels may contribute to the dermatitis observed in some sensitive individuals. Intermediate-duration studies suggest that longer-term oral exposure can be tolerated by some nickel-sensitive individuals and may even serve to desensitize some individuals. Jordan and King (1979) found flaring of dermatitis in only 1/10 nickel-sensitive women given nickel sulfate at 0.007 mg/kg/day for 2 weeks. Patch test responses to nickel were reduced in nickel-sensitive women given one weekly dose of 0.05 or 0.07 (but not 0.007) mg Ni/kg as nickel sulfate for 6 weeks (Sjovall et al. 1987). Santucci et al. (1994) gave increasing daily doses of nickel (0.01–0.03 mg/kg/day) as nickel sulfate to eight nickel-sensitive women for up to 178 days. A significant clinical improvement in hand eczema was observed in all subjects after 1 month of treatment, and continued treatment resulted in healing of all dermal lesions except for those on the hands. Measurement of urine and serum nickel suggested a decrease in the absorption of nickel and an increase in the excretion of nickel with longer exposure.

### *Dermal Exposure*

Hughson et al. (2009) summarize the development of a dermal exposure method and collection of workplace exposure samples from five different workplaces, including three nickel refineries producing a range of nickel metal products and nickel compounds; a stainless steel production plant, which used nickel briquettes and nickel cathode plates in the process; and a powder metallurgy facility using nickel powders to produce aluminium nickel cobalt magnets. Measurements of airborne nickel species were also collected to supplement the existing data set for this industry. The workplace surveys were carried out during 2004–2005 and all sites were within EU member states. The sampling method was designed to quantify the mass of nickel in the skin contaminant layer. Furthermore, laboratory procedures were developed to separate soluble and insoluble nickel species from the exposure samples and thereby allow separate quantification for both dermal and inhalation exposure

measurements. In the case of dermal exposures, this is because the risk of induction or elicitation of nickel sensitization is dependent on the skin absorption of the available free nickel ions. In the case of inhalation exposure, it is important to differentiate between soluble and insoluble nickel because soluble nickel compounds have been classified as respiratory sensitizers. Dermal exposure measurements were obtained using a removal method, i.e. samples were collected from the skin contaminant layer at predetermined anatomical locations. The dermal exposure samples were collected using commercial moist wipes using a template with an open aperture of 25 cm<sup>2</sup> pressed onto the skin. Each area of skin was wiped with three sequential wipes and a clean template was used on each occasion. For each subject, samples were collected on three separate occasions during the working day, i.e. before break times and at the end of the shift. For each of these three sampling periods, the palms and backs of both hands and both forearms were sampled. At the last sampling period, additional samples were collected from the neck, face (perioral region), and chest. All wipe samples were transferred to the laboratory in 250 ml wide-neck glass jars. The wipes contained in each sample jar were analysed to determine the soluble and insoluble nickel content. Inhalable dust sampling was carried out using personal sampling apparatus in accordance with Health and Safety Executive Methods for the Determination of Hazardous Substances (MDHS) 14/3 (HSE, 2000). This involved using an IOM inhalable dust sampler loaded with a pre-weighed cassette containing a 25 mm quartz fibre filter. The sampling apparatus was fitted to the worker near the start of the working shift and left running for the majority of the working day so that the inhalation exposures could be considered to be representative of average full-shift exposures. After sampling, the IOM cassettes were reweighed to determine the total inhalable dust concentration and the samples were then shipped to INCO Technical Services, Ltd, Mississauga, Ontario, Canada, for analysis of soluble/insoluble nickel species. The soluble and total nickel dermal exposure data for each process-task category were summarized in terms of the number of measurements (n), median, Geometric Mean (GM), Geometric Standard Deviation (GSD), and the range (maximum and minimum values). The inhalation exposure data for each category were also summarized in this manner for total inhalable dust and total inhalable nickel. Summary statistics were obtained using Microsoft Excel 2003 and box-whisker plots were produced using SigmaPlot version 11. A total of 67 sets of dermal exposure measurements were collected from 52 different workers (15 workers were sampled twice on different days). A total of 1547 dermal exposure samples (excluding blanks) were collected for nickel analysis. The data were tested for normality and found to have a log-normal distribution. Log transformation was performed to allow summary statistics to be presented. Although one of the study objectives was to collect a personal inhalable dust sample for each dermal exposure measurement, due to some workplace restrictions it was only possible to collect a total of 62 air samples from a possible total of 67. The results of the Pearson correlation tests showed a high level of correlation (for all tasks) between the hands and forearms and the neck, face, and chest, respectively. All upper body exposure measurements (neck, face, and chest) were highly correlated with each other. The highest correlations were for the hands and face ( $r = 0.754$ ), forearms and face ( $r = 0.732$ ), and face and neck ( $r = 0.644$ ). Except for the chest and forearm test, all P values were highly significant, with  $P < 0.001$ . When the dermal exposure data were compared with the inhalable dust concentrations, the correlations were not statistically significant. However, dermal exposure for all the anatomical areas was observed to be highly significantly associated with airborne nickel levels, with all P values  $< 0.001$ . Table 8 reports these numerical data. The summary of dermal exposure data for the seven process-task categories are presented in Table 9, for each anatomical area sampled and for both soluble and total nickel content. The highest overall dermal nickel exposures were recorded for workers involved with packing of nickel metal powder.

Anatomical area/correlation test		Forearms	Neck	Face	Chest	Inhalable dust	Inhalable Ni
Hands	Pearson correlation ( <i>r</i> )	0.766	0.567	0.754	0.548	-0.109	0.484
	Significance (two tailed) ( <i>P</i> )	<0.001	<0.001	<0.001	<0.001	0.401	<0.001
Forearms	Pearson correlation ( <i>r</i> )	—	0.694	0.732	0.536	-0.100	0.464
	Significance (two tailed) ( <i>P</i> )	—	<0.001	<0.001	0.001	0.438	<0.001
Neck	Pearson correlation ( <i>r</i> )	—	—	0.644	0.570	-0.058	0.548
	Significance (two tailed) ( <i>P</i> )	—	—	<0.001	<0.001	0.662	<0.001
Face	Pearson correlation ( <i>r</i> )	—	—	—	0.680	-0.039	0.530
	Significance (two tailed) ( <i>P</i> )	—	—	—	<0.001	0.767	<0.001
Chest	Pearson correlation ( <i>r</i> )	—	—	—	—	0.101	0.574
	Significance (two tailed) ( <i>P</i> )	—	—	—	—	0.439	<0.001
Inhalable dust	Pearson correlation ( <i>r</i> )	—	—	—	—	—	0.364
	Significance (two tailed) ( <i>P</i> )	—	—	—	—	—	0.004

Table 8: Dermal and inhalable nickel exposure relationships (all tasks) - log transformed (Hughson et al., 2009).

Task	Anatomical area	<i>n</i>	Soluble nickel ( $\mu\text{g cm}^{-2}$ )				Total nickel ( $\mu\text{g cm}^{-2}$ )			
			Median	GM	GSD	Range	Median	GM	GSD	Range
Front-end refinery	Hands and forearms	6	0.24	0.24	1.5	0.14–0.48	0.61	0.75	2.4	0.29–2.55
	Neck	6	0.21	0.14	4.4	<0.02–0.61	0.48	0.43	1.9	0.16–0.97
	Face	6	0.62	0.70	1.5	0.47–1.51	1.57	1.83	3.0	0.48–6.91
	Chest	6	0.24	0.15	4.1	<0.02–0.44	0.41	0.54	2.3	0.24–1.60
Electro-winning/ electrolysis	Hands and forearms	12	0.31	0.34	2.2	0.12–1.78	0.63	0.56	2.5	0.16–3.19
	Neck	12	0.17	0.16	4.7	<0.02–1.39	0.26	0.25	4.3	<0.02–2.21
	Face	12	0.49	0.24	5.6	<0.02–1.54	0.58	0.39	5.4	<0.02–4.32
	Chest	12	0.05	0.04	3.4	<0.02–0.21	0.06	0.06	2.9	<0.02–0.24
Packing nickel metal products	Hands and forearms	7	0.26	0.27	1.9	0.10–0.94	0.85	1.17	2.6	0.62–9.12
	Neck	7	0.33	0.24	2.3	0.09–0.83	1.65	1.18	4.0	0.10–5.39
	Face	7	0.70	0.55	1.9	0.24–1.18	2.47	2.99	3.2	0.55–16.20
	Chest	7	0.04	0.05	5.4	<0.02–0.40	0.63	0.28	8.3	<0.02–2.87
Packing nickel compounds	Hands and forearms	14	0.54	0.61	3.0	0.08–3.52	0.85	1.17	4.0	0.11–13.43
	Neck	14	0.49	0.27	3.9	<0.02–1.92	0.74	0.49	2.7	0.08–2.43
	Face	14	0.75	0.47	5.9	<0.02–2.55	1.08	0.73	4.9	<0.02–3.12
	Chest	14	0.24	0.14	7.0	<0.02–5.77	0.35	0.27	5.2	<0.02–6.23
Packing nickel powder	Hands and forearms	7	2.61	2.59	1.6	1.12–4.72	8.40	8.73	1.8	3.10–17.49
	Neck	6	2.18	2.03	1.9	0.69–4.27	6.16	6.20	1.5	3.67–10.23
	Face	6	4.17	3.29	2.0	1.28–7.29	17.41	15.16	2.3	3.87–44.51
	Chest	6	0.77	1.05	2.4	0.44–3.37	1.37	1.56	2.3	0.51–4.49
Powder metallurgy (magnet production)	Hands and forearms	8	0.12	0.08	3.4	<0.02–0.32	1.87	1.69	5.2	0.10–25.33
	Neck	8	0.17	0.08	6.5	<0.02–1.39	0.65	0.38	6.8	<0.02–4.34
	Face	8	0.17	0.18	8.1	<0.02–2.15	1.82	1.54	7.4	0.13–33.23
	Chest	8	0.10	0.08	4.6	<0.02–0.67	0.28	0.40	7.1	<0.02–4.56
Stainless steel production	Hands and forearms	13	0.01	0.02	1.8	<0.02–0.05	0.08	0.11	2.7	<0.02–0.84
	Neck	13	0.04	0.03	3.8	<0.02–0.37	0.14	0.13	3.2	<0.02–0.66
	Face	13	0.03	0.03	3.3	<0.02–0.20	0.22	0.14	3.5	<0.02–0.84
	Chest	13	0.01	0.02	3.0	<0.02–0.18	0.12	0.10	3.8	<0.02–1.33

Notes: There was an incomplete set of measurements for one worker involved in nickel powder packing. This resulted in seven sets of hand/arm data and six measurements for face, neck, and chest, respectively. It is emphasized that the exposures for the hands and forearms are an average of measurements obtained from the palms and backs of both hands and both forearms. Also, the individual measurements of the hands and forearm exposures (not detailed here) are averages of the levels recorded at three periods over the working shift.

Table 9: Summary of dermal nickel exposure by category and anatomical area sampled (Hughson et al., 2009).

The dermal nickel exposures for the hands/forearms of these workers were GM = 2.59  $\mu\text{g cm}^{-2}$  (soluble nickel) and GM = 8.73  $\mu\text{g cm}^{-2}$  (total nickel) with GSDs of 1.6 and 1.8, respectively. This group of workers, together with those at the magnet production plant that handled nickel powders, had exposures to the face and neck regions, which were greater than those observed for most of the other process-task categories. The inhalation exposure measurements are detailed in Table 10 using the same exposure categories as the dermal exposure data. The results of the analysis of nickel species in the air samples are summarized in Table 11, where the quantity of soluble, sulfidic, metallic, and oxidic nickel is expressed as a percentage of the total nickel content in the airborne dust samples. As with the dermal exposures, the stainless steel workers had very low inhalable total nickel exposures with GM 5 0.03  $\text{mg m}^{-3}$  (GSD 5 2.3), although the total inhalable dust levels were the highest overall at GM 5 3.9  $\text{mg m}^{-3}$  (GSD 5 2.1). This confirms that while the process was generally dusty, the nickel content of the airborne dust was low. Considering the nickel content of the inhalable dust, the exposures in the electro-winning, electrolysis processes and tasks involving packing of nickel compounds (nickel chloride, nickel sulphate hexahydrate, and nickel hydroxycarbonate) had the highest proportions of soluble nickel, with few other nickel species being present.

Industry/task	n	Inhalable dust ( $\text{mg m}^{-3}$ )				Total nickel ( $\text{mg m}^{-3}$ )			
		Median	GM	GSD	Range	Median	GM	GSD	Range
Front-end refinery	6	1.2	1.4	1.9	0.8–3.5	0.16	0.13	2.3	0.05–0.40
Electro-winning/electrolysis	12	0.8	0.9	1.5	0.4–1.7	0.04	0.04	3.0	0.01–0.18
Packing nickel metal products	7	0.8	0.8	1.2	0.6–1.2	0.10	0.08	3.3	0.01–0.34
Packing nickel compounds	12	0.4	0.5	2.8	0.1–5.9	0.02	0.02	2.6	0.01–0.10
Packing nickel powders	7	1.6	1.7	2.3	0.5–5.0	0.81	0.77	3.0	0.13–2.81
Powder metallurgy (magnet production)	8	1.0	1.0	1.8	0.4–2.6	0.03	0.05	3.9	0.01–0.36
Stainless steel production	10	4.7	3.9	2.1	1.2–11.6	0.04	0.03	2.3	0.01–0.12

Table 10: Summary of inhalable dust and nickel exposures for primary nickel production and primary user sites (Hughson et al., 2009).

Process/task	n	Airborne nickel species (percentage of total nickel content)			
		GM (and GSD) values			
		Soluble	Sulfidic	Metallic	Oxidic
Front-end refinery processes	6	25 (1.6)	44 (1.5)	3 (6.8)	13 (3.1)
Electro-winning/electrolysis	12	82 (1.5)	1 (8.7)	<1 (6.3)	1 (9.5)
Packing nickel metal products	7	21 (1.5)	1 (7.0)	30 (1.2)	41 (1.4)
Packing nickel compounds	12	76 (1.3)	2 (12)	<1 (1.0)	3 (12)
Packing nickel powders	7	2 (2.3)	1 (2.1)	33 (1.5)	60 (1.3)
Powder metallurgy (magnet production)	8	1 (10)	3 (6.3)	42 (2.1)	35 (1.4)
Stainless steel production	10	1 (10)	1 (8.8)	<1 (7.2)	89 (1.1)

Table 11: Airborne nickel species by process area (Hughson et al., 2009).

## Titanium

The published epidemiological literature consists of mortality studies of two independent multi-plant cohorts of cobalt–tungsten carbide hard-metal manufacturing workers, one in France (Moulin et al. 1998) and one in Sweden (Hogstedt and Alexandersson 1990), and cohort studies of two individual factories included in the French multi-plant cohort (Lasfargues et al. 1994, Wild et al. 2000). The French multi-plant cohort included all 10 cobalt–tungsten carbide manufacturing plants in France; in addition, a nested case-control study of lung cancer was conducted within this cohort. The nested case-control study is most informative for evaluating cancer risk, because it used a semi-quantitative exposure scale to evaluate exposure-response relationships and considered potential confounding by



exposure to tobacco smoking and other known or suspected occupational carcinogens. The cohort study of the largest French factory shares these advantages; however, because the workers were included in the multi-plant study, it does not provide independent evidence for carcinogenicity. In these two studies, four metrics of exposure were evaluated: (1) exposure level, which was the highest exposure score experienced during an individual's work history (on a scale of 0 to 9), (2) duration of exposure at a level of 2 or higher, (3) unweighted cumulative dose, which assigned the same level to occasional and full-time exposure, thus favoring peak exposure, and (4) frequency-weighted cumulative dose, which weighted exposure level by the frequency of exposure, thus reducing the effect of occasional exposure. The Swedish study, although limited in size, provides supporting information for an independent population. Excess lung-cancer mortality (of approximately 30%) was found in both multi-plant cohort studies (Hogstedt and Alexandersson 1990, Moulin et al. 1998); risk estimates were significantly higher among individuals with higher measures of exposure or longer time since first exposure (latency). In the nested case-control study (Moulin et al. 1998), lung cancer risk was significantly higher (OR = 1.93, 95% CI = 1.03 to 3.62, 35 exposed cases) among workers exposed to cobalt-tungsten carbide (exposure level  $\geq 2$ ) than among workers with little or no exposure (exposure level  $< 2$ ). In exposure-response analyses using workers in the lowest exposure category as the comparison group, lung-cancer risk was significantly higher (by up to fourfold) for workers in the highest categories of both measures of cumulative dose, and an elevated risk of borderline statistical significance was found for workers in the highest exposure-level category. Positive exposure-response relationships were observed for all four measures of exposure: duration (Ptrend = 0.03), unweighted cumulative dose (Ptrend = 0.01), frequency-weighted cumulative dose (Ptrend = 0.08), and exposure level (Ptrend = 0.08). Adjustment for tobacco smoking or exposure to known or suspected carcinogens did not change the results. The Swedish study had limited ability to evaluate exposure-response relationships because of small numbers of exposed workers with lung cancer. Nevertheless, the risk of lung cancer mortality was significantly increased for workers with exposure duration of over 10 years and latency of over 20 years (SMR = 2.78, 95% CI = 1.11 to 5.72, 7 exposed cases). Analyses restricted to workers with at least 10 years' exposure or at least 20 years' latency found somewhat higher SMRs for "high-exposed" than "low-exposed" workers (Hogstedt and Alexandersson 1990). Excess risks of lung-cancer mortality were also found in studies of the two individual French factories. Wild et al. (2000) reported significantly elevated SMRs (by approximately twofold) for lung cancer among all male workers and among male workers ever employed in presintering workshops or with exposure levels of at least 2. The highest SMRs were observed for male workers in the highest exposure categories of all four exposure metrics (level, duration, and both measures of cumulative dose), although the trends were not statistically significant, and the risk estimates were imprecise. In the study by Lasfargues et al. (1994), the entire cohort had a significantly increased risk of lung cancer, and the risk was highest among workers in the highest exposure-level category. Although small, this study provides supporting evidence that the findings for the French industry-wide cohort were not due solely to the results for the large factory studied by Wild et al. Both the French multi-plant cohort study (Moulin et al. 1988) and the larger study of an individual French factory (Wild et al. 2000) found higher risks of lung cancer for exposure to cobalt-tungsten carbide before sintering than after sintering. The authors stated that exposure was highest during presintering processes; however, there is no evidence of toxicological differences between presintered and sintered materials, and both materials release similar amounts of cobalt ions. It is unlikely that the excess risks of lung cancer found in the French studies were due to confounding by tobacco smoking or co-exposure to other known carcinogens. In the multi-plant study, the smoking-adjusted odds ratio for cobalt-tungsten carbide exposure (OR = 2.6, 95% CI = 1.16 to 5.82) was similar to the unadjusted risk (OR = 2.29, 95% CI = 1.08 to 4.88). Neither study found increased risks

of smoking-related diseases, such as chronic bronchitis and emphysema, and adjustment for smoking or exposure to other occupational carcinogens did not change the findings in the exposure-response analyses (Moulin et al. 1988, Wild et al. 2000). Neither the Swedish multi-plant study (Hogstedt and Alexandersson 1990) nor the small French cohort study (Lasfargues et al. 1994) adjusted for smoking; however, surveys of smoking habits among a subset of workers found smoking rates similar to those in the general population. Overall, the studies are limited by the lack of quantitative exposure assessment and potential confounding; however, exposure misclassification would most likely reduce the likelihood of detecting a true effect.

The following sections present a short list of some of the most common diseases among people that are in close contact with hard metal powders. These disease are divided on acute, subacute and chronic diseases.

**Acute diseases.** In acute phases, the most common diseases caused by cobalt exposure are characterized by productive cough and chest tightness, often the presence of expiratory wheezes. Symptoms resolve during periods of absence from work. The exposure of tungsten carbide powder alone does not produce any sensitization (Chiappino et al. 2011).

**Subacute diseases.** To this group belong the fibrosing alveolitis that appears in susceptible individuals after about a year of exposure to dust of hard metals. It common symptoms are dyspnea, weight loss, chest tightness and coughing often productive. Often patients have positive feedback from the patch test of cobalt. Cytology exam of BAL may show an increase in total cellularity, with numerous lymphocytes and rare reversal of the ratio of CD4<sup>+</sup>/CD8<sup>+</sup> (used as a progressive biomarker for monitoring of people with HIV), many macrophages, multinucleated giant cells and bizarre cells. The histological aspect of lung biopsy specimens may show thickened walls of the alveoli and infiltrated by lymphocytes, plasma cells, macrophages. In case of lack of exposure, patients can have a natural improvement of their clinical picture. In some workers these diseases can naturally evolve to fibrosis (Chiappino et al. 2011, Kusaka et al. 1989).

**Chronic diseases.** These diseases are related to a cumulative exposure of several years, in susceptible individuals. Some of these are the hard-metal disease and lung cancer. The hard-metal disease is also known by other names such as "Hard Metal Interstitial Lung Disease" (HMILD), "hartmetall lungenfibrose", "hard metal pneumoconiosis", "tungsten carbide pneumoconiosis", "Giant Cell Interstitial Pneumonitis"(GIP). This disease was first identified in 1940 by doctors Jobs and Ballhausen in a worker from a manufacturer of hard metals in Krefeld (Germany). The presence of the disease ranges from less than 1% and 10% in long time exposed workers, and a fundamental role is taken from the individual susceptibility rather than a cumulative exposure to the substance (Nemery et al. 2001, Chinarro et al. 2008, Choi et al. 2005). The symptomatology is characterized by a persistent dyspnea, which may occur gradually or brusquely, and by non-productive cough (dry coigh). The High Resolution Computed Tomography (HRCT) can show diffuse opacities, irregular linear opacities, and, depending on the specific context, may also be present honeycombing, nodules, consolidation, emphysema, mediastinal lymphadenopathy and pleural effusion (Montero et al. 2010). The analysis of the BAL may show the presence of numerous mononuclear cells and multinucleated giant cells, some of which "bizarre" and "cannibalized" (Kusaka et al. 1989, Chinarro et al. 2008, Paris et al. 2011). With the electron microscope it is possible to see the tungsten carbide in macrophages and alveolar walls of lung biopsy specimens (Chiappino et al. 2011). Cobalt is detectable in the tissues only in 10% of cases (Chinarro et al. 2008). In the lung tissues of these patients are often detected traces of other substances such as titanium, miobio, iron, nickel and silica. Many authors believe that they play a fundamental role, not yet fully understood, in triggering and

perpetuating the disease. The two main components of carbides (WC and Co) act synergistically through a peculiar physical-chemical reaction. Studies in biological fluids, in vitro systems, experimental animals, and humans have demonstrated that cobalt is rapidly solubilized from cobalt–tungsten carbide. Cobalt dissolution rates were similar for presintered and sintered cobalt–tungsten carbide incubated in various artificial biological fluids (Stopford et al. 2003). Tungsten is not rapidly solubilized from cobalt–tungsten carbide, but can be phagocytized by macrophages (Lombaert et al. 2004). Cobalt was also released from hard-metal dust incubated with plasma and lung tissue (Edel et al. 1990). In experimental animals administered cobalt–tungsten carbide by intratracheal administration, cobalt was solubilized rapidly, cleared from the lung, distributed in the body, and excreted in the urine (Lison 1996). Rats exposed intratracheally to cobalt–tungsten carbide had more cobalt in the urine than did rats administered cobalt alone, suggesting that tungsten carbide increases the bioavailability of cobalt (Lasfargues et al. 1992). Several biomonitoring studies detected elevated levels of cobalt in the urine, lungs, and other tissues of workers exposed to cobalt–tungsten carbide hard metals (Rizzato et al. 1986, Nicolaou et al. 1987, Gallorini et al. 1994, Sabbioni et al. 1994b, Scansetti et al. 1994, 1998, Linnainmaa and Kiilunen 1997, Goldoni et al. 2004). Cobalt is naturally able to ionize and to reduce the oxygen, generating reactive species, while the tungsten carbide is biologically inert, but it is an excellent conductor of electrons. The close contact of these two components, that are deposited in the lung tissue microenvironment, causes that the cobalt rapidly transfers on the surface of the tungsten its electrons that react with the near oxygen. This phenomenon generates large amounts of reactive oxygen species (ROS) capable of oxidative and proinflammatory effects leading recruitment of immune cells in site. The detection of multinucleated giant cells and "bizarre cells" and "cannibalized cells" appears to be due to the peculiar activation suffered by macrophages. They are probably stimulated by toxic, inflammatory and immunological mechanisms or by gene induction (that is promoted by hard metals) (Chinarro et al. 2008). It is suspected that the people most susceptible to this disease are those that have a low antioxidant defense (Choi et al. 2005). The exclusive exposure to cobalt does not seem to be able to cause such pulmonary toxicity (U.S. Department of Health and Human Services Public Health Service 2009). It was found a link between lung cancer and exposure to hard metals. The International Agency for Research on Cancer (IARC) metallic considers cobalt combined with tungsten carbide belongs to the group 2A, "probably carcinogenic to humans". Cobalt alone belongs to Group 2B, "possibly carcinogenic to humans" (U.S. Department of Health and Human Services Public Health Service National Toxicology Program Morrisville 2011). The Twelfth Report on Carcinogens (National Toxicology Program) has classified the carbide powders of tungsten and cobalt and hard metal powders as "reasonably anticipated to be human carcinogens". The carcinogenic mechanisms appear to be due to the combination of the direct effects of the Co ionized and to the response of the oxidative stress due to the generation of ROS (U.S. Department of Health and Human Services Public Health Service 2009, Simonsen et al. 2012). The cobalt ions can compete with zinc of the zinc-finger proteins (enzymes that control the transcription of genes involved in DNA repair and cell cycle regulation. They are also responsible for the activation of hypoxia regulatory genes, implicated in cell survival in the absence of oxygen) (Chinarro et al. 2008, Simonsen et al. 2012, Liebow et al. 1969). The ROS that are formed in the microenvironment in which are deposited hard metals, in addition to producing oxidative and pro-inflammatory effects, can directly damage DNA and alter gene expression (U.S. Department of Health and Human Services Public Health Service 2009, Simonsen et al. 2012). The combination of the high cytotoxic, pro-inflammatory, toxic, genotoxic effects are the events that induces the neoplastic effect [U.S. Department of Health and Human Services Public Health Service 2009]. In some studies it is seen that cobalt ions disrupt cell-signaling pathways (Murata et al. 1999), inhibit DNA repair (Hartwig 2000, Hartwig et al. 2002), regulate genes involved in the response to hypoxia

(Beyersmann 2002), replace or mimic essential divalent metal ions, thus altering cellular reactions (Nackerdien et al. 1991, Beyersmann and Hartwig 1992, Kawanishi et al. 1994, Lloyd et al. 1998), and interfere with mechanisms involved in cell-cycle control and modulation of apoptosis (DeBoeck et al. 2003b,c). Numerous in vitro studies (reviewed in NTP 2009) and in vivo studies (Huaux et al. 1995, Lasfargues et al. 1995) have shown greater cytotoxic effects (measured primarily by lactate dehydrogenase release) for cobalt–tungsten carbide than for either cobalt powder or tungsten carbide alone.

## 2.2 explosions, fires, protection, safety rules

Although there is no single, universally accepted definition of “combustible dust,” nor a standard method for sampling dust to determine its combustibility, OSHA has defined “combustible dust” in at least one rulemaking document to include “all combustible particulate solids of any size, shape, or chemical composition that could present a fire or deflagration hazard when suspended in air or other oxidizing medium.” Any combustible material can burn rapidly when in a finely divided form. If such a dust is suspended in air in the right concentration, under certain conditions, it can become explosible. Even materials that do not burn in larger pieces (such as aluminum or iron), given the proper conditions, can be explosible in dust form. The force from such an explosion can cause employee deaths, injuries, and destruction of entire buildings. For example, 3 workers were killed in a 2010 titanium dust explosion in West Virginia, and 14 workers were killed in a 2008 sugar dust explosion in Georgia. The U.S. Chemical Safety and Hazard Investigation Board (CSB) identified 281 combustible dust incidents between 1980 and 2005 that led to the deaths of 119 workers, injured 718, and extensively damaged numerous industrial facilities. A wide variety of materials that can be explosible in dust form exist in many industries. Examples of these materials include: food (e.g., candy, sugar, spice, starch, flour, feed), grain, tobacco, plastics, wood, paper, pulp, rubber, pesticides, pharmaceuticals, dyes, coal, metals (e.g., aluminum, chromium, iron, magnesium, and zinc). The following section summarizes the findings of one in-depth U.S. Chemical Safety Board (CSB) investigation of dust explosion incidents. On October 29, 2003, aluminum dust exploded (Figure 13) at the Hayes Lemmerz International facility in Huntington, Indiana, killed one worker and injured several others. This explosion, which involved equipment used to remelt scrap aluminum, occurred in a part of the building where Hayes made cast aluminum and aluminum alloy automobile wheels. Scrap aluminum from the wheel manufacturing lines was chopped into small chips, pneumatically conveyed to the scrap processing area, dried, and fed into a melt furnace. Transporting and drying the aluminum chips generated explosive aluminum dust, which was then pulled into a dust collector. The CSB determined that the explosion likely originated in the dust collector, which had not been adequately vented or cleaned, and was located too close to the aluminum scrap processing area. The initial explosion spread through ducting, causing a large fireball to emerge from the furnace. The dust collector system was not designed or maintained to prevent dust explosions, or to prevent a dust collector explosion from spreading through ducting. When the scrap and dust collector systems were added to the facility, Hayes did not follow management of change procedures that might have identified the dust explosion hazard. Hayes had also not cleaned dust from overhead beams and other structures. Some of this accumulated dust exploded (a secondary explosion), damaging the building roof. As known a material in the powder form can burn more easily than the same material in the bulk form. This is due to many factors but chiefly because the material surface area has been greatly increased, the powder configuration is more conducive to ignition and the air around supplies enough oxygen to readily support combustion, see Figure 14 (a). In this case, combustible dust is the fuel. Oxygen is usually available in the ambient air. In addition to, or in place of the oxygen, another chemical oxidizer may simulate oxygen in the combustion reaction. The following information

discusses the additional elements needed for a flash fire or explosion to occur. If the powders are composed by really fine particles and they are suspended in a cloud with air around all of the many particles, the dust cloud will burn so violently, a flash fire will occur, see Figure 14 (b).



Figure 13: Intense fire following an aluminium dust explosion at Hayes Lemmerz International (Huntington, Indiana, October 29, 2003).

If this flash fire occurs in an open field it is often called fireball or deflagration. If that same energy release in a confined space, such as a machine or a building, which acts like a vessel to contain the deflagration. The pressure wave from the rapid burning of the dust cloud tries to expand quickly. The vessel contains the pressure and allows it to build until it bursts out of its confinement in a rapid fashion. This is a dust explosion, see Figure 14 (c).

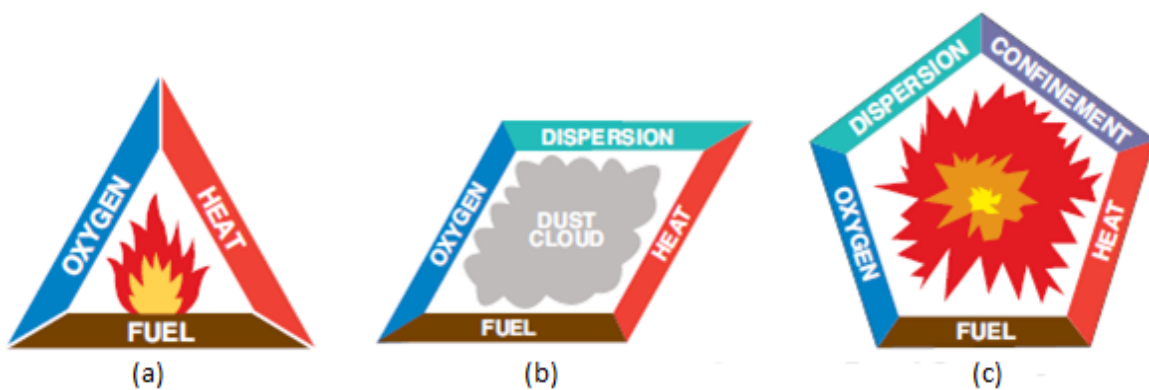


Figure 14: Fire triangle (a), elements of a flash fire (b) and explosion pentagon (c).

The blast wave can also disperse accumulated combustible dust in work or storage areas, fueling one or more subsequent explosions. These secondary explosions are often more destructive than the initial incident due to the large quantities of dust dispersed. Secondary explosions can continue to ignite in sequence, cascading throughout a facility.

To better understand a dust explosion event Figure 15 and Figure 16 (pictures prepared by Joseph P. Howicz CSP, CFPS Accident Prevention Corporation) shows a possibly timeline (timing of actual events may vary) of the series of events that take place in this case.

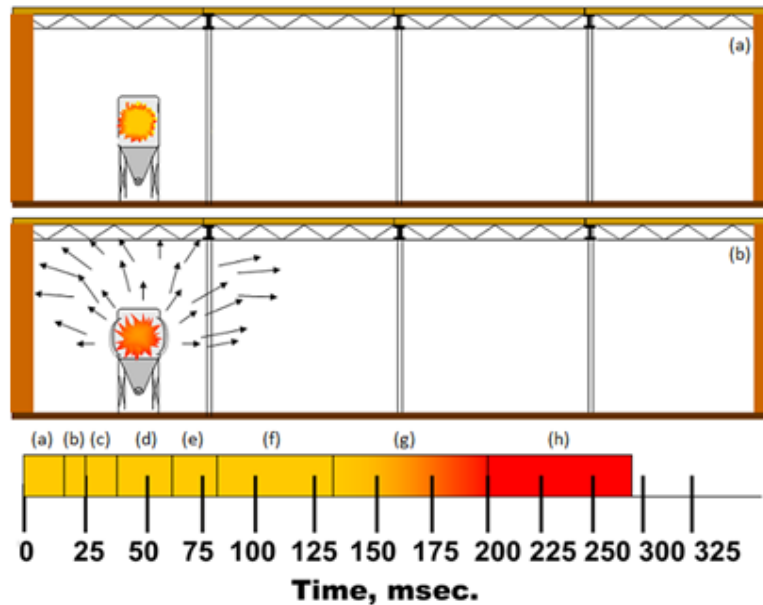


Figure 15: A dust explosion event with an orientative timeline (timing of actual events may vary). Primary deflagration inside process equipment (a); shock wave caused by primary deflagration (b).

As summarized on the investigation report on combustible dust hazard (2006) of the U.S. Chemical safety and hazard investigation board, scientific and engineering experts, industry, labor, and regulatory bodies recognize that the NFPA voluntary consensus standards provide effective technical guidance to prevent industrial dust explosions. The NFPA standards that address combustible dust explosion hazards provide the basis for the technical requirements of the two fire codes widely used in state fire systems across the United States: the NFPA’s Uniform Fire Code (UFC) and the ICC’s International Fire Code (IFC). The NFPA’s two principal voluntary consensus standards to prevent and control dust explosion risks are NFPA 654 (Standard for the Prevention of Fire and Dust Explosions from the Manufacturing, Processing, and Handling of Combustible Particulate Solids–2006) and NFPA 484 (Standard for Combustible Metals–2006). These standards, typically updated every five years, have long been recognized as the benchmarks for good engineering practice for handling most combustible dusts in general industry. NFPA 654, Standard for the Prevention of Dust Explosions, was issued in 1942, and the NFPA combustible dust standards have been regularly expanded and revised since. In addition to being incorporated into the NFPA Fire Code, the standards are used directly by many industry professionals (designers, engineers, health and safety experts, etc.) as guidance to prevent dust explosions.

NFPA 654. This standard applies to the manufacturing, processing, blending, conveying, repackaging, and handling of combustible particulate solids and their dusts. It covers all combustible dusts, except those specifically addressed in other NFPA standards, and it is one of the most cited documents for control measures for combustible dust hazards. NFPA 654 details the hazards of combustible dusts, specifies building construction requirements and the type of equipment to use in dust-handling operations. It addresses selection and design of protective systems by referencing other NFPA standards (Section 7.1.3). The standard also recommends that facilities implement management systems to prevent dust explosions, addressing: 1) Hazard evaluation; 2) Change management; 3) Maintenance and inspection; 4) Housekeeping; 5) Procedures and training. NFPA 654 requires, for example, that “spaces inaccessible to housekeeping shall be sealed to prevent dust accumulation” and that “interior surfaces where dust accumulations can occur shall be sealed and constructed so as to facilitate cleaning and to minimize combustible dust accumulations.”

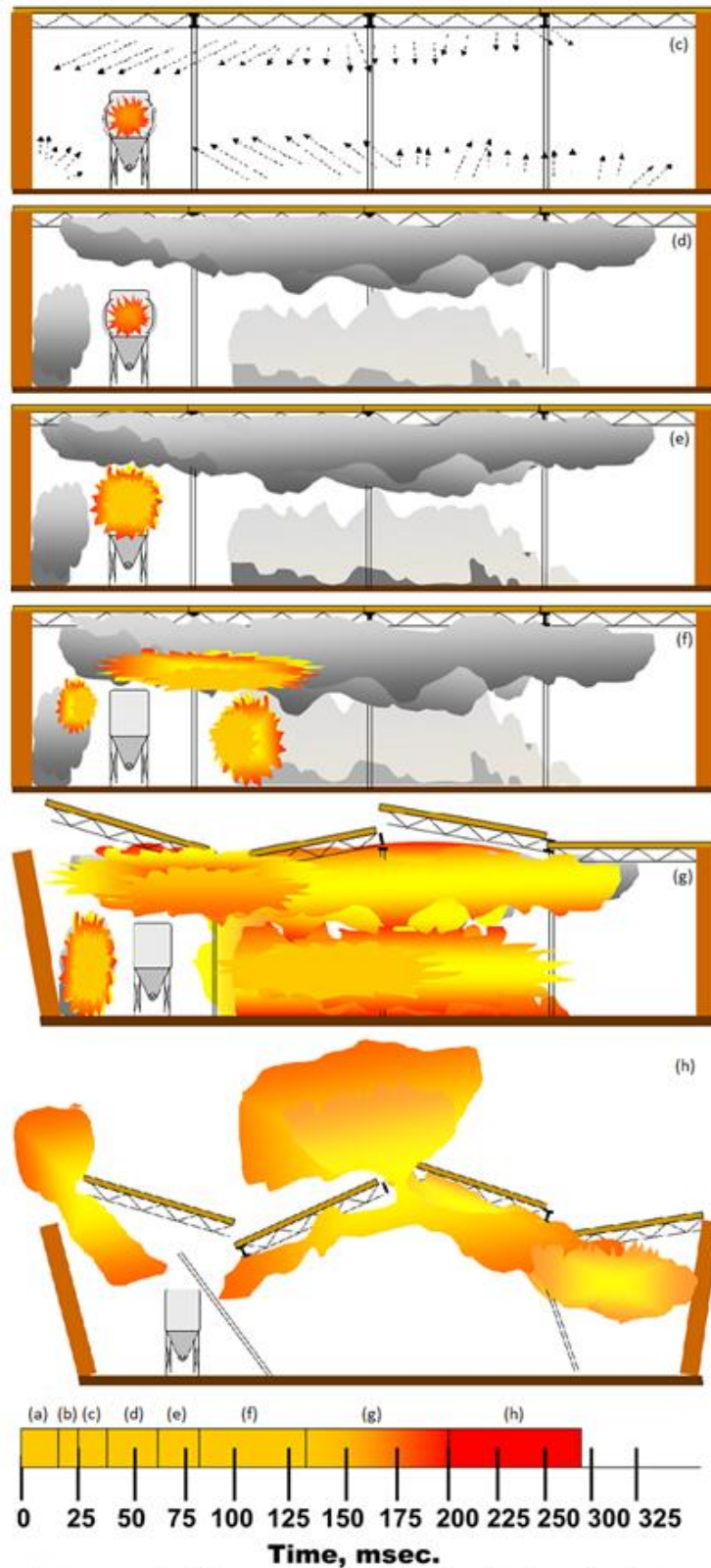


Figure 16: A dust explosion event with an orientative timeline (timing of actual events may vary. Shock waves reflected by surfaces within the building cause accumulated dust to go into suspension (c); dust clouds thrown in the air by the shock waves (d); primary deflagration breaks out of the equipment enclosure - creating a source of ignition (e); secondary deflagration ignited (f); secondary Deflagration is propagated through the dust clouds (g); secondary deflagration bursts from the building (h).

NFPA 484. This standard applies to fine particles of metals, including aluminum, magnesium, and others, and is distinct from NFPA 654 because the nature of metallic dusts makes them exceptionally

vulnerable to ignition. Once ignited, metal dusts release large amounts of energy; therefore, some of the protective systems required by NFPA 654 would be inappropriate for metal dust hazards. NFPA 484 provides detailed information about equipment design and explosion protection systems, and required management systems to address combustible dust hazards, and discusses appropriate testing to determine if a dust explosion hazard exists. The CSB found that the consequences of the Hayes Lemmerz incident could have had less severe if NFPA 484 been applied, especially in terms of location, design, maintenance, and explosion protection for dust collectors, all factors in the Hayes incident.

Several other NFPA standards address facilities that produce or handle specific combustible dusts or other factors related to dust explosions (Table 12a). These standards are typically cross-referenced when relevant issues overlap, and are incorporated into the NFPA’s UFC.

An important standard is NFPA 77, Recommended Practice on Static Electricity. NFPA 2113 is another important standard and its title is Standard on Selection, Care, Use and Maintenance of Flame-Resistant Garments for Protection of Industrial Personnel Against Short-Duration Thermal Exposures.

Standard	Title	Coverage or Purpose
NFPA 68	<i>Guidelines for Deflagration Venting – 2002</i>	Provides technical guidance on designing, sizing, installing, and maintaining deflagration vents.
NFPA 69	<i>Standard on Explosion Prevention Systems – 2002</i>	Addresses the design of explosion prevention, protection, and mitigation systems.
NFPA 70	<i>The National Electric Code® – 2005</i>	Addresses electrical equipment and wiring requirements for special situations, including those in which an explosive atmosphere may exist. Defines combustible dust classified locations.
NFPA 499	<i>Recommended Practice for the Classification of Combustible Dusts and Hazardous (Classified) Locations for Electrical Installations in Chemical Process Areas – 2004</i>	Provides guidance for classifying dust processing locations for electrical equipment installation.

Table 12a: Other NFPA Standards related to combustible dust explosion hazards.

As exposed from Gary Q. Johnson (principal consultant of the company Workplace Exposure Solutions) in the article “How to safely clean up combustible dusts”, there are various methods to safely clean up combustible dust accumulations in a plant, as long as they are applied appropriately. These methods include compressed- air blowdown, sweeping, water washdown, and vacuum cleaning. Some information here is from NFPA 654, which covers all of the methods except water washdown; however the vacuum cleaning is the safest cleanup method for combustible dust.

*Compressed-air blowdown.* Using compressed air to blow dust off equipment and surfaces can create dust clouds with a concentration exceeding the dust’s (minimum explosible concentration) MEC. Key NFPA 654 safety strategies for compressed-air blowdown are to limit ignition sources in the area and minimize dust cloud size by limiting how extensively the method is used. This standard limits the use



of compressed-air blowdown to areas that can't be reached with vacuum cleaning. For instance, the standard allows using compressed air only for blowing dust off the inaccessible sections of a machine into an adjoining aisle. Then sweeping or vacuum cleaning, not compressed air, can be used to consolidate the dust into piles and clean the aisle. Section 8.2.2.2 in NFPA 654 permits compressed-air blowdown for dust cleanup only when the cleanup worker follows these steps, in this order, for de-energizing and cooling down any ignition sources in the area: 1) Vacuum all accessible dust. 2) De-energize any nearby electrical equipment that isn't rated for combustible dust. 3) Allow any hot equipment or other surfaces to cool below the dust's Minimum Ignition Temperature (MIT). 4) Use 15-psig compressed air or steam to move dust out of inaccessible areas. 5) Vacuum all accessible dust.

*Sweeping.* Vigorously sweeping dust from floors and other surfaces with a broom can also generate dust clouds. The same key NFPA 654 safety strategies apply: limit area ignition sources and minimize dust cloud size by limiting sweeping's use. If the dust is easily ignited by static electricity, the cleanup worker should use a broom with soft, natural bristles to avoid generating static during sweeping and use a conductive, nonsparking dust pan, such as one made of aluminum or conductive plastic, to collect the dust. Sweeping a floor creates a dust cloud that's close to the ground, so the cloud generally won't be denser than the dust's MEC unless the sweeping is extremely vigorous. But sweeping dust from overhead piping, conduit, steel structures, and other surfaces can create a dust cloud denser than your dust's MEC. Before sweeping, the cleanup worker must meet the same Section 8.2.2.2 requirements as for compressed-air blowdown, in the same order, to de-energize and cool down any ignition sources in the area.

*Water washdown.* It is used by some bulk solids plants to clean up combustible dust. Such plants already use water to wash floors, so the floors are equipped with drains to direct the waste water to an appropriate treatment system, and the plant's electrical equipment is watertight. For nonmetal combustible dusts, the safety strategy for water washdown is to wet the dust, thus increasing its conductivity and reducing the potential for static electricity to ignite the dust. However, water washdown must be done correctly to avoid creating a combustible dust cloud. When washing down a dusty area, the cleanup worker should wet the accumulated dust by first applying a water mist to it, then increase the flow to a high-velocity water stream to remove the wet dust from the area. If the worker uses a high-pressure stream of water at the start, not much dust will be wetted, because the air induced alongside the high velocity water stream will fan the dust cloud away from the area where the water is applied. One caution: If the dust doesn't dissolve in water, it's best to push the wet dust to an area where it can easily be cleaned up rather than have it run into a floor drain; the drain piping can plug if there isn't enough water to convey the dust to the waste water treatment system. Using a water mist is also a good way to reduce the airborne dust around a dust pile fire; the mist will wet the dust without creating a dust cloud that can move into the fire area and cause a dust explosion. However, water washdown has some disadvantages: 1) The mess from water washdown can trickle over a large area, requiring widespread cleanup. 2) The residue must be collected somewhere that can be cleaned. 3) The electrical system must be watertight to prevent shorting out the equipment. Water washdown isn't covered in NFPA 654, and because metal combustible dusts can cause water to break down and release hydrogen gas, NFPA specifically recommends against using this method in plants handling combustible metals.

*Vacuum cleaning.* Vacuum cleaning is NFPA 654's preferred dust cleanup method because it provides some dust containment as the dust-laden air enters the vacuum cleaner's pickup point (the vacuum tool attached to the hose), just like dust-laden air entering a capture hood in a dust collection system. Cleanup workers can vacuum dust with a portable vacuum cleaner or a central vacuum

cleaning system. Determining which is right for the particular plant requires looking at the pros and cons for each, as listed in Table 12b.

	Portable	Central system		Portable	Central system
<b>Pros</b>	<ul style="list-style-type: none"> <li>Has lower capital cost</li> <li>Is easy to operate</li> <li>Has clear ownership by one worker</li> <li>Allows relocation to other cleanup sites</li> <li>Malfunction affects only one unit</li> </ul>	<ul style="list-style-type: none"> <li>Has readily available hose inlets to provide cleanup at logical sites</li> <li>Allows multiple users</li> <li>Provides faster response to dust spills because only hose and tool must be transported</li> <li>Provides low-dusting, ergonomic, permanent central waste disposal outside of operating areas</li> </ul>	<b>Cons</b>	<ul style="list-style-type: none"> <li>Is heavy and cumbersome to transport to cleanup site</li> <li>Allows only one user per unit</li> <li>Requires "fleet" management when multiple units are used</li> <li>Is dusty and poses ergonomic problems during waste emptying</li> <li>Requires significant maintenance when multiple units are used</li> </ul>	<ul style="list-style-type: none"> <li>Has higher capital cost</li> <li>Ownership may be unclear because system has multiple users</li> <li>Malfunction affects cleanup capability of entire system</li> <li>Occupies dedicated floor space</li> </ul>

Table 12b: Comparing portable vacuum cleaner with central vacuum cleaning system.

*Portable vacuum cleaner.* A portable vacuum cleaner includes a tank on wheels, a vacuum producer (mounted on the tank), filters (inside the tank), one vacuum hose connected to the tank, and several vacuum tools for the hose. The vacuum producer can be an electric blower with an explosion-rated motor or a nonelectric compressed-air venturi eductor, as shown in Figure 17. A disposable plastic bag is often used inside the tank to collect dust. In operation, the cleanup worker moves the portable vacuum cleaner, along with the vacuum hose and required tools, to the location to be cleaned. The worker repeats this process for each area to be cleaned. When the tank is filled with dust, the worker removes the tank's top lid and removes the plastic bag filled with dust or lifts and empties the tank into a waste disposal container.



Figure 17: Vacuum producers for portable vacuum cleaner.

NFPA 654 outlines two safety strategies for portable vacuum cleaning: limiting ignition sources and keeping the contained dust volume small.

Limiting ignition sources. This strategy requires choosing an appropriate vacuum producer — an electric blower with an explosion-rated motor or a nonelectric venturi educator — and using conductive components to dissipate static electricity. The electric blower motor and controls must be rated for Electrical Hazard Class II material Groups E (metal dusts), F (carbonaceous dusts), or G (general combustible dusts). The portable vacuum cleaner must be carefully grounded by running a bonding cable between the tank and its connected components to a nearby ground. The unit must also have a conductive vacuum hose (a hose with a resistance of <1 million ohms meets NFPA’s minimum resistance requirement for dissipating static electricity). If the unit uses a venture educator, the compressed-air hose leading to the venture educator should also be conductive.

Keeping dust volume small. The portable vacuum cleaner’s tank is typically no larger than a 55-gallon drum, which will limit the contained dust’s volume.

A variation of the conventional portable vacuum cleaner, known as a submerged- or liquid-recovery unit, is suitable for certain highly combustible dusts. This unit, as shown in Figure 18, safely removes metal combustible dusts or other easily ignitable dusts such as gunpowder, toner, rocket propellant, and sodium azide (used as automobile airbag propellant) by submerging the collected dust in an appropriate liquid in the vacuum tank. The solids can then be drained as a sludge from the tank for disposal.



Figure 18: Submerged- (or liquid-) recovery portable vacuum cleaner.

*Central vacuum cleaning system.* A central vacuum cleaning system includes a dust collector (typically a pulse-jet baghouse) containing multiple filters; a high-vacuum exhaustor; a metal tubing network with multiple spring-closed hose inlets; and vacuum hoses and tools. The hose inlets are installed at points around the plant where powder is often spilled, such as near equipment access doors

or material transfer points. In operation, the cleanup worker inserts a vacuum hose fitted with the required tool into a hose inlet in the area to be cleaned. Multiple workers can use the system to clean several areas at once. Because the collected dust is discharged from the system's dust collector hopper, workers don't have to manually dispose of the dust. The central system's exhauster must be a blower to achieve the high vacuum this system requires. Compared with a dust collection system, which typically requires vacuum of 0.44 to 0.88 inches mercury (6 to 12 inches water column), the central system needs much more - about 6 to 12 inches mercury (82 to 164 inches water column). The greater vacuum is required to provide enough suction to overcome the flow resistance of the vacuum hoses, tools, and tubing between each hose inlet and the dust collector; overcoming the hoses' and tools' flow resistance alone consumes about 25 to 50 percent of the system's total suction, depending on the system's layout. The blower can be a multistage, positive displacement, or regenerative type. Which is best for your application depends on the number of workers using the system at one time and the cost of operating the blower. One way to limit the blower's size and power consumption, and thus keep operating costs low, is to try to keep the system's tubing network no longer than necessary to handle the distance the dust will be conveyed and to size the blower no larger than necessary to handle the maximum number of workers who will use the system at one time. The safety strategy for the central vacuum cleaning system is the same as for a dust collection system: The system components must meet combustible dust standards. This means that the system's tubing, vacuum hoses, and tools must be conductive and grounded. The dust collector must be equipped with an explosion protection system or devices, such as those shown in Figure 19, and the tubing network must have an isolation device to prevent a flame front from traveling outward to workers using the system.

The combustibility characterization of a particular dust is complex. ASTM International provides many standards to understand if a particular dust might explode (ASTM-E1226-12A, Standard Test Method for Explosibility of Dust Cloud; ASTM - E789 Standard Test Method for Dust Explosions) and in which conditions this might happen (ASTM-E1515, Standard Test Method for Minimum Explosible Concentration of Combustible Dusts; ASTM-E2019, Standard Test Method for Minimum Ignition Energy of a Dust Cloud in Air; ASTM-E1491, Standard Test Method for Minimum Autoignition Temperature of Dust Clouds; ASTM-E2021, Standard Test Method for Hot-Surface Ignition Temperature of Dust Layers; ASTM-D257 Standard Test Methods for DC Resistance or Conductance of Insulating Materials (Charging)). Another important standard is the EN 14034-4, Determination of the Limiting Oxygen Concentration of Dust Clouds.

## Aluminium

As exposed from Gesamtverband der Aluminiumindustrie (GDA) in the article "Safety instructions for handling and processing aluminium powder" (2007), aluminium powder can be safely transported, stored and processed if a few basic safety instructions are followed. Aluminium powder is combustible and classified as being flammable. Mixtures of aluminium powder and air are ignitable over a wide range of concentrations and can cause violent dust explosions. Highly flammable hydrogen can form on contact with water or other chemicals and present an additional risk of explosion, and possibly be responsible for causing a secondary dust explosion. The strong electrostatic charge on aluminium powder can lead to electrical discharges, which can possibly ignite a cloud of aluminium dust. When aluminium powder burns, aluminium oxide is produced. A strongly adherent, compact oxide film protects the aluminium surface. Some hazardous reactions are listed below. Aluminium reacts strongly with acids and alkalis (and also with water after prolonged contact) with the formation of highly flammable hydrogen. There is a danger of a fire or an explosion. Aluminium reacts strongly with oxidants (e.g. nitrates, sulphates, halogens, peroxides). There is a

danger of a fire or an explosion Aluminium can react strongly on contact with halogens and simple halogenated hydrocarbons with the formation of, for example, hydrogen chloride or hydrochloric acid vapour.

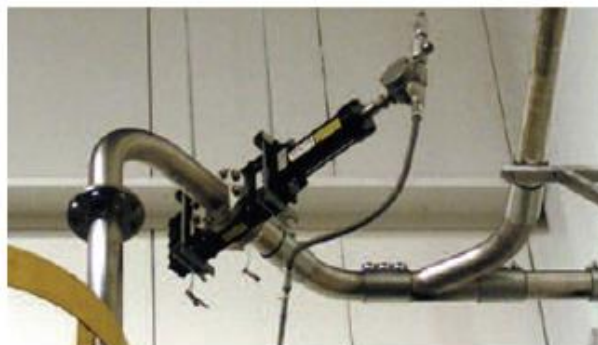
**a. Chemical suppression device on system's dust collector**



**b. Flame-arresting vent on system's dust collector**



**c. High-speed isolation valve on system's tubing leading to dust collector**



Courtesy of Vac-U-Max, Belleville, N.J.

Figure 19: Explosion protection devices for central vacuum cleaning systems.

The use of loading aids is imperative when unloading or placing in storage. Storage should preferably be in rooms with a fire-resistant or non-combustible construction. One should ensure that there is good natural or forced ventilation of the storeroom and areas used for processing. Only those containers used by the metal pigment manufacturer for transport purposes should be used for storage. These original containers should be kept tightly sealed at all times. Aluminium powder should not be stored in areas where there are flammable liquids or other combustible materials. The reason for this is that different firefighting techniques are used in the event of a fire. Aluminium powder should not be stored together with incompatible substances, such as oxidants. Avoid accumulations of dust on floors, walls and other places in storage areas. In this respect, attention should be given to avoiding grooves and potential sites for deposits. Aluminium powder should be stored in a cool place, i.e. in the open it should be protected against direct sunlight. In addition, containers should be stored far enough away from steam pipes or radiators to prevent heating. Aluminium powder should be stored dry and any contact with water avoided. One should ensure that the containers are always protected against rain, snow and humidity. Leaks in steam pipelines, water pipes, radiators or roofs should be repaired immediately in order to avoid products coming into contact with water. There should not be any automatic fire-extinguishing systems (e.g. using sprinklers or carbon dioxide) in areas where aluminium powder is stored.

Personal protective equipment. Whenever dealing with aluminium powder in the open one should always wear at least the following personal protective equipment and no-one without protection should be allowed into the area. Respiratory protection: dust mask filter class FFP 1 (DIN EN 149) for normal dust formation; depending on the legal requirements, choose a higher class of protection for high dust concentrations (P2). Hand protection: leather gloves with long cuffs (DIN EN 388/407). Head / face protection: helmet with mesh for protection against heat or flames (DIN EN 166, wire mesh or plastic visor). Work wear: fire-retardant special fabric, rendered conductive (EN 531/1149-1/2), trousers without turn-ups, closed pockets. Foot protection: conductive safety shoes (DIN EN 345 S1-3).

Possible sources of ignition for aluminium powder. Naked flames e.g. flames from matches or cigarette lighters, furnaces, blowtorches, welding or cutting flames, combustion engines. Hot surfaces e.g. walls of boilers, hot pipe work, soldering irons, parts of machines (bearings) that overheat, hot gases. Electric sparks and sources of sparks e.g. loose contacts, overloaded power cables, faulty control systems, arcs and sparks on switches, light bulbs, flashlights, electrical as well as battery-operated equipment. Electrostatic discharges e.g. non-earthed parts of plant or containers, unsuitable tools and fixtures, unsuitable clothing. Friction or mechanical sparks e.g. grinding, hammering of machine parts, tools, containers. Lightning strikes e.g. voltage surges in cables or plant caused by a lightning strike.

Protection against electrostatic discharges is essential, particularly in view of the low minimum ignition energy of fine powders (< 1 mJ). Only use conductive tools and containers (do not use plastic tools or plastic containers, or plastic sacks for transfer processes) as aluminium powder builds up an electrical charge when in contact with a non-conductive surface. When cleaning, for example, must be brushes with natural bristles (coconut, horsehair, etc.). Earthing is absolutely essential. When handling and processing aluminium powders it is essential that there is electrical contact between the plant components and that they are earthed to discharge static electricity. Portable items (e.g. for filling containers or transferring the contents from one container to another) also have to be connected in an electrically conductive manner and earthed. Thus even when transferring the contents by hand connect earthing, clips to the containers and ensure that the tools used are adequately earthed via the person using them or earth them separately.

Permissible exposure limit (PEL). In accordance to the OSHA permissible exposure limits for chemical contaminants, the current OSHA standard for aluminium total dust (Alumina; Aluminum soluble salts; Aluminum metal and oxide) is 10 milligram per cubic meter of air ( $\text{mg}/\text{m}^3$ ) (with a respirable fraction of  $5 \text{ mg}/\text{m}^3$ ). The Threshold Limit Value is of  $15 \text{ mg}/\text{m}^3$ .

Chrome, Cobalt, Nickel, Titanium

The following pages report considerations derived from the occupational health guideline for Chromium Metal and insoluble Chromium Salts (19978), Chromic Acid and Chromates (1978), Cobalt Metal Fume and Dust (1978), Nickel Metal and Soluble Nickel Compounds (1978), and Titanium Dioxide (1978) written by the U.S. department of labor, Occupational Safety and Health Administration (OSHA).

*Permissible exposure limit (PEL).* The current OSHA standard for chromium metal or insoluble chromium salts is 1 milligram of chromium metal or insoluble chromium salts per cubic meter of air ( $\text{mg}/\text{m}^3$ ) averaged over an eight-hour work shift. The current OSHA standard for chromic acid or chromates is a ceiling of 0.1 milligram of chromic acid or chromates per cubic meter of air ( $\text{mg}/\text{m}^3$ ). Certain forms of chromium (VI) have been found to cause increased respiratory cancer among workers. Certain other forms of chromium (VI) are currently believed to be non-carcinogenic: The non-carcinogenic forms are the monochromates and bichromates (dichromates) of hydrogen, lithium, sodium, potassium, rubidium, cesium, and ammonium, and chromium (VI) oxide (chromium acid anhydride). NIOSH has not conducted an in-depth study of the toxicity of chromium metal or compounds containing chromium in an oxidation state other than 6. NIOSH recommends that the permissible exposure limit for carcinogenic chromium (VI) compounds be reduced to  $0.001 \text{ Cr (VI) mg}/\text{m}^3$  and that these compounds be regulated as occupational carcinogens. NIOSH also recommends that the permissible exposure limit for non-carcinogenic chromium (VI) be reduced to  $0.025 \text{ Cr (VI) mg}/\text{m}^3$  averaged over a work shift of up to 10 hours per day, 40 hours per week, with a ceiling level of  $0.05 \text{ Cr (VI) mg}/\text{m}^3$  averaged over a 15-minute period. It is further recommended that chromium (VI) in the workplace be considered carcinogenic, unless it has been demonstrated that only the noncarcinogenic chromium (VI) compounds mentioned above are present. The current OSHA standard for cobalt metal fume and dust is 0.1 milligram of cobalt metal fume and dust per cubic meter of air ( $\text{mg}/\text{m}^3$ ) averaged over an eight-hour work shift. The American Conference of Governmental Industrial Hygienists has recommended for cobalt metal fume and dust a Threshold Limit Value of  $0.05 \text{ mg}/\text{m}^3$ . The current OSHA standard for nickel metal and soluble nickel compounds is 1 milligram of nickel metal and soluble nickel compounds per cubic meter of air ( $\text{mg}/\text{m}^3$ ) averaged over an eight-hour work shift. NIOSH has recommended that the permissible exposure limit for nickel be reduced to  $0.015 \text{ mg}/\text{m}^3$  averaged over a work shift of up to 10 hours per day, 40 hours per week, and that nickel be regulated as an occupational carcinogen. The NIOSH Criteria Document for Inorganic Nickel and the Special Occupational Hazard Review for Nickel Carbonyl should be consulted for more detailed information. The current OSHA standard for titanium dioxide is 15 milligrams of titanium dioxide (total dust) per cubic meter of air ( $\text{mg}/\text{m}^3$ ) averaged over an eight-hour work shift. The American Conference of Governmental Industrial Hygienists has recommended for titanium dioxide a Threshold Limit Value of  $10 \text{ mg}/\text{m}^3$ .

*Reactivity and Flammability.* Chromium metal in contact with strong oxidizers may cause fires and explosions. Chromic acid or chromates contact with any combustible, organic, or other readily oxidizable materials such as paper, Wood, sulfur, aluminum, plastics, etc. may cause fires and explosions. Chromic acid or chromates will attack most forms of metals, cloth, leather, plastics, rubber, and coatings and may cause spontaneous ignition. Contact of Cobalt dust with strong

oxidizers may cause fire and explosions. Contact of nickel with strong acids may form flammable and explosive hydrogen gas. Nickel contact with sulfur may cause evolution of heat. Contact of nickel nitrate with wood and other combustibles may cause fire. Hazardous decomposition products: Toxic gases and vapors (such as nickel carbonyl and oxides of nitrogen) may be released in a fire involving nickel or in the decomposition of nickel compounds. Titanium Dioxide incompatibilities: none. Chromium Metal and insoluble Chromium Salts minimum ignition temperature (metal): 400 °C (layer); 580 °C (cloud). Chromium Metal and insoluble Chromium Salts minimum explosive dust concentration (metal): 230 grams/m. Chromium Metal and insoluble Chromium Salts extinguishant: Dry sand, dry dolomite, dry graphite. Chromic acid is not combustible in itself, but is a powerful, oxidizing material. It will ignite on contact with acetic acid and alcohol. Cobalt autoignition temperature: specially prepared (the form prepared by reducing the oxides in hydrogen) very fine cobalt dust will catch fire at room temperature. Cobalt extinguishant: Dry sand, dry dolomite, dry graphite powder. Nickel extinguishant: Dry sand, dry dolomite, dry graphite powder. Titanium Dioxide flammability: not combustible.

*Personal protective equipment.* Employees should be provided with and required to use impervious clothing, gloves, face shields (eight-inch minimum), and other appropriate protective clothing necessary to prevent repeated or prolonged skin contact with solids or liquids containing insoluble chromium salts, solids or liquids containing chromic acid or chromates, cobalt dust, powdered metallic nickel or solids or liquids containing soluble nickel compounds. If employees' clothing may have become contaminated with solids or liquids containing chromic acid or chromates, cobalt dust, powdered metallic nickel or solid soluble nickel compounds, employees should change into uncontaminated clothing before leaving the work premises. Clothing contaminated with these substances should be placed in closed containers for storage until it can be discarded or until provision is made for the removal of these materials from the clothing. If the clothing is to be laundered or otherwise cleaned to remove these materials, the person performing the operation should be informed of these substances' hazardous properties. Non-impervious clothing which becomes contaminated with these materials should be removed promptly and not reworn until these materials are removed from the clothing. Employees should be provided with and required to use dust- and splash proof safety goggles where solids or liquids containing insoluble chromium salts, solids or liquids containing chromic acid or chromates may contact the eyes. Where there is any possibility that employees' eyes may be exposed to solids or liquids containing chromic acid or chromates, an eye-wash fountain should be provided within the immediate work area for emergency use. Where there is any possibility of exposure of an employee's body to solids or liquids containing chromic acid or chromates, facilities for quick drenching of the body should be provided within the immediate work area for emergency use. Further information on respiratory protections for all these metal substances are reported on the Appendix A.

*Sanitation.* Skin that becomes contaminated with these materials should be immediately washed or showered with soap or mild detergent and water to remove any such substance. Workers subject to skin contact with solids or liquids containing chromic acid or chromates should wash with soap or mild detergent and water any areas of the body which may have contacted such a substance at the end of each workday. Eating and smoking should not be permitted in areas where these substances are handled, processed, or stored. Employees who handle solids or liquids containing these materials should wash their hands thoroughly with soap or mild detergent and water before eating, smoking, or using toilet facilities. Areas in which exposure to a carcinogenic form of chromium (VI) or nickel metal and soluble nickel compounds may occur should be identified by signs or other appropriate means, and access to these areas should be limited to authorized personnel only.



*Spill leak, and disposal* procedures. Persons not wearing protective equipment and clothing should be restricted from areas of spills until cleanup has been completed. If these materials are spilled, the following steps should be taken: 1) Ventilate area of spill (In case of chromium metal or insoluble chromium salts remove all ignition sources where metallic chromium has been spilled before point 1)). 2) Collect spilled material in the most convenient and safe manner and deposit in sealed containers for reclamation or for disposal in a secured sanitary landfill. Liquid containing these materials should be absorbed in vermiculite, dry sand, earth, or a similar material. Waste disposal method: these materials may be disposed of in sealed containers in a secured sanitary landfill.

Much of what exposed in this section assumes a great importance also for additive manufacturing processes. Although these technologies are relatively new, it is also necessary to apply the standards and the rules exposed above in these processes. Below it is presented a case of accident in an industry that produce metal components through additive manufacturing processes, in order to confirm the dangers that can arise in these new technologies. As written on the web page of Beveridge & Diamond PC, by the lawyer Heidi P. Knight, in the spring of 2014, a Woburn, Massachusetts-based 3-D printing company, Powderpart Inc., was cited by OSHA for multiple alleged violations involving combustible dust hazards, including violations of the GDC for failure to furnish employment and a place of employment “which are free from recognized hazards that are causing or are likely to cause death or serious physical harm to his employees.” The inspection followed a November 5, 2013 explosion and fire that inflicted third-degree burns on a company employee. OSHA’s then acting regional administrator for New England stated, “Establishments that use metal powders in this new technology need to scrutinize their processes and take steps to prevent and protect their employees from fire and explosion hazards that arise with these materials.” The company faces a total \$64,400 in penalties. OSHA said it found that the company failed to prevent and protect its workforce from the fire and explosion hazards of reactive, combustible metal powders, such as titanium and aluminum alloys, which are used in the company's 3D printing process. "The fire and explosion hazards when working with titanium and aluminum are established, particularly when the materials are in powder form," said Jeffrey Erskine, OSHA's area director for Middlesex and Essex counties. "Just as it's easier to start a campfire with kindling than with logs, it's easier for a metal fire to start when you're working with metal powder that is as fine as confectioner's sugar." In addition to the fire and explosion dangers, other serious hazards included: 1) The use of unapproved electrical equipment; 2) Electrical equipment and wiring that were unsuitable for a hazardous location; 3) Failure to train employees on chemical hazards and safeguards; 4) Failure to supply employees with all necessary protective clothing, equipment and training; 5) No written respiratory protection program; 6) Failure to post danger tags in potentially explosive areas. "Establishments that use metal powders in this new technology need to scrutinize their processes and take steps to prevent and protect their employees from fire and explosion hazards that arise with these materials," said Robert Hooper, OSHA's acting regional administrator for New England. "The market for 3-D printed parts made from titanium and aluminum alloys includes the automotive, aerospace, defense, medical, dental and jewelry industries. Basic safety measures must be incorporated into this 21st century technology, so that it can grow without harming the employees who are building this new industry.” One willful violation, with a \$14,000 penalty, was cited for Powderpart's failure to have any Class D metal fire extinguishers. OSHA said it found that Powderpart was aware that titanium and aluminum fires cannot be extinguished with a regular fire extinguisher or with water, and knew that its manufacturing process presented potential fire hazards; however, there were no Class D metal fire extinguishers on-site during the explosion and fire. Nine serious violations, with \$50,400 in penalties, were cited for the remaining hazards. Powderpart has 15 business days from receipt of its citations to comply or contest the findings. Under the Occupational Safety and Health Act of 1970, employers are responsible for

providing safe and healthful workplaces for their employees. More information on the alleged violations, is available at the OSHA website.

## Chapter 3: Process phenomena models

### 3.1 Cost estimation and energy demand models

In according with Ruffo et al., (2006) there are some principal quantitative approaches to cost estimation for building the mathematical model: 1) Analogy-based techniques. These are based on the concept of deriving an estimation from actual information regarding similar real products. 2) Parametric models. Here, the cost is expressed as an analytical function of a set of variables, usually called Cost-Estimation Relationships (CERs). 3) Engineering approaches. Here, the estimated cost is calculated in a very analytical way as the sum of its elementary components, constituted by the value of the resources used in each step of the production process. This approach can only be used when the characteristics of the processes are well defined. 4) There is also a different approach developed by Cavalieri et al., (2004). They studied the possibility of replacing a classic costing model with one based on an artificial neural network. The results obtained in a case study confirm the validity of this innovative method, giving results similar and sometimes better than classical approaches, but with the limitation of a reduced possibility of interpreting and modifying data. Moreover, besides the mathematical model approaches, there are different methodologies to split costs to different sections of the model. In Brinke (2002), the author explain as the most common steps in cost modelling involve the determination of: 1) The scope, i.e. costs are subdivided into different types, which have to be modelled; 2) The allocation base for (overhead) costs; 3) The cost functions, i.e. the relationships between product parameters and costs.

In Hopkinson and Dickens (2003) the authors provide a direct comparison between Rapid Manufacturing (RM) approaches with Injection Moulding (IM) for the manufacture of selected geometries in various quantities. The cost analysis was performed in a manner that assumed that production criteria may be applied to Rapid Prototyping (RP) machines; e.g. machine depreciation was set as 8 years, straight line for RP machines, as this was used for injection moulding equipment. Also, using the RP machine for production means that the preprocessing time, such as part orientation and placement, is reduced as standard builds would be used. It was assumed that an RP machine would achieve 90 per cent uptime (as would an injection moulding machine) if used for production. The costs for injection moulding were obtained by quotes for tooling plus unit costs for each moulding produced. During initial calculations for costs, factors such as machine power consumption and space rental had been considered. However, these contributed such a small total to the final costs (less than 1 per cent) that they have not been included. No inclusion of overhead costs, such as for part design and testing, etc., have been included as these were not included in the quotes for costs by injection moulding. A significant assumption is that the material properties, surface finish and accuracy of parts produced by RP are not an issue. The costs for producing parts by RP processes were broken down into: 1) Machine costs; 2) Labour costs; 3) Material costs.

Costs for producing parts by RM were calculated by assuming that a machine produces one part consistently for 1 year, although one of the benefits of RM is the ability to simultaneously produce numerous parts, say a complete assembly, on a single machine.

Calculating machine costs. Table 13 (left) shows the build parameters and machine costs that were considered. These were required to formulate the total machine cost per part produced by each of the RP processes. Costs for ancillary equipment vary according to location; e.g. air-conditioning systems depend on the climate in which the machine is located. Ancillary costs for RP machines play only a

very small percentage of the total price for the machinery; for this reason, basic machine costs from manufacturers have been used. In each case, the highest rate of maintenance cost currently available from the equipment supplier was used.

Calculating labour costs. Table 13 (right) shows the build parameters and labour costs that were required to formulate the labour costs per part for each RP process used. An hourly rate of 5.30 euros was used for injection moulding, remembering that for production purposes, highly skilled staff would not be needed.

	Source of cost			Source of cost	
	Variable	Obtained by		Variable	Obtained by
Number per platform	$N$	Maximum possible in one build	Number per platform	$N$	Maximum possible in one build
Platform build time	$T$	Hours	Platform build time	$T$	Hours
Production rate per hour	$R$	$N/T$	Production rate per hour	$R$	$N/T$
Hours per year in operation	$HY$	$365 \times 24 \times 90\% = 7884$	Hours per year in operation	$HY$	$365 \times 24 \times 90\% = 7884$
Production volume total per year	$V$	$R \times 7884$	Production volume total per year	$V$	$R \times HY$
<i>Machine costs</i>			<i>Labour costs</i>		
Machine and ancillary equipment	$E$	Machine purchase cost	Machine operator cost per hour	Op	Minimum wage 5.30 euros
Equipment depreciation per year	$D$	$E/8$	Set-up time to control machine	Set	Timed
Machine maintenance per year	$M$	Most comprehensive package	Post-processing time per build	Post	Timed
Total machine cost per year	$MC$	$D + M$	Labour cost per build	$L$	$Op \times (Set + Post)$
Machine cost per part	$MCP$	$MC/V$	Labour cost per part	$LCP$	$L/N$

Table 13: Calculation of machine costs (left) and calculation of labour costs (right) (Hopkinson and Dickens, 2003).

Calculating material costs. The method for calculating material costs for each process is shown in Table 14.

	Source of cost	
	Variable	Obtained by
Number per platform	$N$	Maximum possible in one build
<i>Material costs for SL</i>		
Material per part including support (kg)	$SLMass$	Weighing finished parts
Material cost per kg	$SLcost$	Quote = 275.20 euros
Material cost per SL part	$SLMCP$	$SLMass \times SLcost$
<i>Material costs for FDM</i>		
Material per part (kg)	$FDMPM$	Weighing finished parts
Support material per part (kg)	$FDMSM$	Weighing finished supports
Build material cost per kg	$FDMPC$	Quote = 400.00 euros
Support material cost per kg	$FDMSC$	Quote = 216.00 euros
Material cost per FDM part		$(FDMPM \times FDMPC) + (FDMSM \times FDMSC)$
<i>Material costs for LS</i>		
Material cost per kg	$LSC$	Quote = 54.00 euros
Mass of each part	$LSM$	Weighing finished parts
Volume of each part	$VP$	Found with Magics software
Total build volume	$TBV$	$34 \times 34 \times 60 \text{ cm}^3$
Mass of sintered material per build	$LSMS$	$N \times LSM$
Mass of unsintered material per build	$LSMU$	$(TBV - N \times VP) \times 0.475^*$
Cost of material used in one build	$LSMC$	$(LSMU + LSMS) \times LSC$
Material cost per LS part	$LSMCP$	$LSMC/N$

\* Published density of unsintered LS powder is 0.45–0.5 g/cm<sup>3</sup> [11].

Table 14: Calculation of material costs for each process (Hopkinson and Dickens, 2003).

The different nature of the three RP processes employed necessitated the use of slightly different means for calculating material costs. For Stereolithography (SL), it was sufficient to weigh completed parts with supports in order to calculate material costs; this assumes that no material is wasted by replacing vats, etc. In the case of Fused Deposition Modelling (FDM), it was sufficient to weigh parts and support separately and then to multiply these by the associated material costs to find the material cost. In this case, the weight of purged material that is used in the build process was not considered. A more complex system to calculate costs with Laser Sintering (LS) was required. It was assumed that no material was to be recycled to ensure consistent part quality (although in practice material is recycled and some organizations practising RM could recycle material without compromising part functionality, depending on their product's function). The mass of material used was calculated in terms of sintered material (by weighing parts) and unsintered material (by calculating the volume of unused material and multiplying this by its unsintered density). In this work, the part selected is shown in Figure 20 (a).

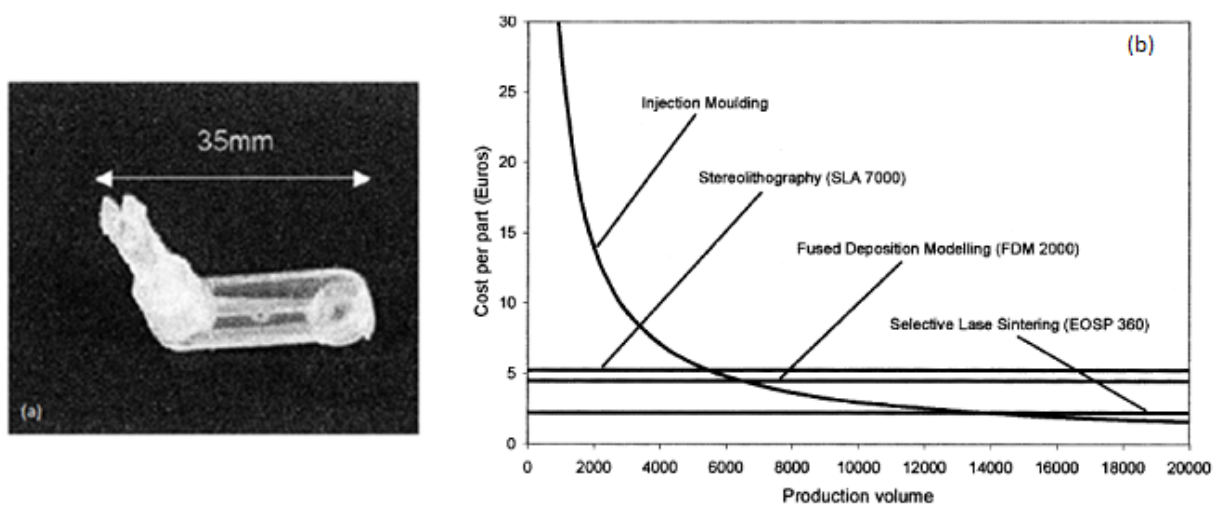


Figure 20: Small lever part selected for cost analysis (a) and cost comparison for the lever by different processes (b) (Hopkinson and Dickens, 2003).

Laser sintering. Table 15 shows the building parameters and cost associated with LS when building the lever part in nylon on an EOSP360 machine. The costs for LS appear to be significantly cheaper than those for SL and FDM. In the case of LS, material provided the highest cost as it was assumed that none of the unsintered material could be recycled. Close inspection of Table 15 shows that sintered material only comprised one-tenth of the material used for the lever; with more efficient packing of parts, the cost should be able to be reduced significantly. The machine costs for LS are lower than for the other processes, mainly because the machine is capable of building a higher number of parts by stacking vertically and because the build rate is higher. Figure 20 (b) shows a cost comparison for the lever according to production volume when produced by each method. As expected, injection moulding is the most expensive process for small volumes due to the cost of tooling. SL and FDM both appear to be more suitable methods of manufacture than injection moulding for volumes up to around 6,000. LS, which incurs a unit cost of around half of that for SL and FDM, appears to be a more viable option than injection moulding for production volumes up to around 14,000. The reducing slope of the injection moulding cost line indicates that a cost reduction of 25 per cent for LS would suggest an economical production volume up to around 20,000 parts. As mentioned above, more efficient packing of parts in the build volume may achieve this kind of reduction in cost.

	SL	FDM	LS
Number per platform	190	75	1056
Platform build time (h)	26.80	67.27	59.78
Production rate per hour ( $h^{-1}$ )	7.09	1.11	17.66
Hours per year in operation (h)	7884	7884	7884
Production volume total per year	55 894	8790	139 269
<i>Machine costs</i>			
Machine and ancillary equipment (euro)	1 040 000	101 280	340 000
Equipment depreciation cost per year (euro)	130 000	12 660	42 500
Machine maintenance cost per year (euro)	89 000	10 560	30 450
Total machine cost per year (euro)	219 000	23 220	72 950
Machine cost per part (euro)	3.92	2.64	0.52
<i>Labour costs</i>			
Machine operator cost per hour (euro)	5.30	5.30	5.30
Set-up time to control machine (min)	33	10	120
Post-processing time per build (min)	49	60	360
Labour cost per build (euro)	7.24	6.18	42.37
Labour cost per part (euro)	0.04	0.08	0.04
<hr/>			
SL			
<i>Material costs</i>			
Material per part including support (kg)	0.0047		
Material cost per kg (euro)	275.20		
Material cost per part (euro)	1.29		
<hr/>			
FDM			
<i>Material costs</i>			
Material per part (kg)		0.0035	
Support material per part (kg)		0.0016	
Build material cost per kg (euro)		400.00	
Support material cost per kg (euro)		216.00	
Material cost per part (euro)		1.75	
<hr/>			
LS			
<i>Material costs</i>			
Material cost per kg (euro)			54
Mass of each part (kg)			0.0036
Volume of each part ( $cm^3$ )			4.3
Mass of sintered material per build (kg)			3.8016
Mass of unsintered material per build (kg)			32
Cost of material used in one build (euro)			1725.72
Material cost per part (euro)			1.63
<hr/>			
Total cost per part (euro)	5.25	4.47	2.20

Table 15: Detailed cost breakdown for SL, FDM and LS (Hopkinson and Dickens, 2003).

In Ruffo et al., (2006) the authors make first of all a revision of the paper Hopkinson and Dickens (2003). They explain that IM curve decreases because the initial cost of the mould is amortized across the production volume (see Figure 20). The RM line is constant, supposing that all indirect costs are charged on every single part, dividing the total indirect cost for the number of parts produced (i.e. machine depreciation in 8 years). This model is a good approximation, but only valid where the RM method is making copies of the same part with a relatively high production volumes. The flexibility of additive techniques allows the production of more than one part at a time. In addition, the parts in production can be different from one another. For this reason it is possible to define RM as a parallel process, where different parts can be built contemporaneously. Also, if the production regards only copies of the same part, the graph of Figure 20 is incorrect for lower production volumes. In fact, just as the IM process has to amortize the initial cost of the tool, the RM process needs to amortize the

investment of buying the machine. Therefore, the RM production curve must have a deflection for low-volume production, taking into consideration the fixed time and cost described above. It is the object of this study to do a production analysis of copies of the same part, which leads to a model, valid for both low- and high-volume production, expanding on the existing model of Hopkinson and Dickens (2003).

The model presented in this paper is placed between the parametric model and the engineering approach, as the relationships found are approximations based on statistics, although most of the data are defined. Moreover it has been formulated in order to attribute the full cost of an RM organization. This includes all costs of plant and production, costs of administration, and costs of the necessary overheads. The methodology used in this paper is general and open to any additive manufacturing technique, although the particular case studied here regards an LS machine, the 3D-Systems Vanguard.

*Scope: activities involved with RM*

The different costs can be split into two categories: direct and indirect costs. In the model presented, only the activity ‘material’ was considered to be a direct cost. Labour and machine maintenance, which could be seen as direct costs, were allocated indirectly as they are annual payees with regular contracts. Moreover, it was supposed that the technician is working full-time only on RM, setting up machines and cleaning parts; this is a conservative model because the entire salary is allocated to RM production instead of supposing the operator is working on different tasks. An important assumption was made about the productivity of the LS machine, which was estimated to work 100 hours/week for 50 weeks/year (utilization of 57 percent). The indirect activities can be summarized into four categories. Table 16 shows the categories with the associated cost/build hour. Table 17 includes a detailed breakdown of the indirect costs used in the model.

Main activities	Cost/h (€)
Production labour/machine hour	7.99
Machine costs	14.78
Production overhead	5.90
Administrative overhead	0.41

Table 16: Main indirect, cost activities and hourly rate (Ruffo et al., 2006).

<i>Production overhead</i>	€	<i>Production labour</i>	€
Yearly rent rate (per m <sup>2</sup> )	130.5	Technician annual salary + employer contributions	32 770 (+ 22%)
Building area (m <sup>2</sup> )	246.5		
Energy consumption/h	1.5	<i>Machine costs</i>	€
		Machine & breakout station purchase	362 500 + 24 360
<i>Administration overhead</i>	€	Purchase cost/year*	45 313 + 3045
Hardware purchase	2175	Maintenance/year	21 750
Software purchase	2175	Software purchase	7250
Hardware cost/year*	435	Hardware purchase	4350
Software cost/year*	435	Software cost/year*	1450
Consumables per year	1450	Cost of software upgrades/year	1450
		Hardware cost/year	870

\* Depreciation time for computer hardware and software is 5 years, for the RM machine purchase is 8 years

Table 17: Indirect cost details (Ruffo et al., 2006).

The only direct cost used in this model was the material purchase; Duraform PA is the material selected for the case study and sold at around €58 per kg (UK 2005). The machine purchase absorption and other indirect costs were allocated to each individual product by the time in which the machine

takes to produce them. Machine set-up and cleaning, warming up, and cooling down phases imply times in which the machine is not building layers. However, they must be considered for cost allocation, as each new build needs these fixed times (equivalent to a fixed cost).

#### *Cost estimation relationships (CERs)*

The cost of a build ( $Cost_B$ ) is the sum of the indirect cost associated with the time of building ( $t_B$ ) and the direct cost associated with the material used during manufacture ( $m_B$ )

$$Cost_B = Cost(t_B) + Cost(m_B)$$

Where

$$Cost(m_B) = \frac{direct\_Cost}{mass\_unit} * m_B ; Cost(t_B) = \frac{\sum direct\_Cost}{working\_time} * t_B$$

The time and material used during the build ( $t_B$  and  $m_B$  respectively) are the main variables of the costing model. Time refers to how long the machine works for the build; part mass (or volume) is an index of the raw material used.

The material that has not been sintered is, in theory, recyclable. However, recycled powder has suffered from a thermal treatment and its mechanical properties are modified from the virgin state. Therefore, recycle is possible but with limitations. In this case the threshold value was set to 67 per cent of the total. Moreover, after a few recycles it is advisable to discard the old powder, operating with virgin powder once more. The quantity of material sintered can be calculated if the density of the material (In this case  $\rho=0.6 \text{ g/cm}^3$ ) and the volume of the build ( $V_B$ ) are known. In formulae

$$m_B = \rho * V_B$$

Where

$$V_B = V_P * n_P$$

$V_B$  is the volume of the entire build, sum of the parts volume included in the production;  $V_P$  is the volume of a single part; and  $n_P$  is the total number of parts. The number of parts that fit in a bed is described by the Packing Ratio ( $PR \in [0,1]$ ), which is defined as follows

$$PR = \frac{V_B}{V_{beds}} = \frac{V_P * n_P}{V_{beds}}$$

where  $V_{beds}$  is the total beds volume, which is the sum of the machine bed volumes required for the planned production. The value of PR can vary: between zero, in the case of an empty bed (no production), and one, if the volume of the components equalizes the volume of the beds. The higher the packing ratio, the lower the waste in material and the production time per component, with a consequent cost saving. The material used is the sum of the material sintered by the laser and the material lost during parts-cleaning or similar. The equation of  $m_B$  was extended as

$$m_B = \rho * (V_B + W_B)$$

where  $W_B$  is the volume of the material wasted. In this model the material wasted was calculated by setting a waste factor indicating the percentage of recycled powder

$$W_B = (V_{beds} - V_B) * \alpha$$

where  $\alpha \in [0,1]$  is the waste factor, depending on the manufacturer. In Grimm (2004), the author affirms that the ratio of unsintered powder to part volume is always high (typically 10:1) and this leads to used powder that will never be claimed, with a stockpile of expensive unusable material as a consequence. Therefore, the powder recycle is set at 50 per cent as default, which seems to be the maximum value admissible, realistically.

*Equations for time*

There are three different times to calculate: (1) Time to laser scan the section and its border in order to sinter the powder ( $t_{xy}$ ); (2) Time to add layers of powder (recoating time,  $t_z$ ); (3) Time to heat the bed before scanning and to cool down slowly after scanning, adding layers of powder or just waiting time to reach the correct temperature ( $t_{HC}$ ). The sum of the above-mentioned times is the total time necessary to complete a build ( $t_B$ ). In formulae

$$t_B = t_{xy} + t_z + t_{HC}$$

An empirical time estimator was developed by the current authors and it was used in this model to estimate all the times presented. In particular, the estimator was based on simulation results obtained with Build Setup ver3.4, which is the software driving the LS machine. This estimator did not consider directly the laser power and similar deep-technical variables, but these parameters were included in some macro parameters which assure an overestimation of the total production time. Estimation results were confirmed and validated by real builds. The layer thickness was fixed to 0.1mm. A detailed description of the time estimator can be found in Ruffo, Tuck and Hague (2006).

The resulting curve relating the cost/part with the production volume is shown in Figure 21. A full machine bed envelope comprised 896 components, with each lever having a volume of 7106 mm<sup>3</sup>. The packing ratio intuitively varies with the number of components “nested” in the build envelope, so each increment on the x axis corresponds to a different packing ratio. The optimum packing ratio was 0.12 for any full bed (896 components and multiples thereof).

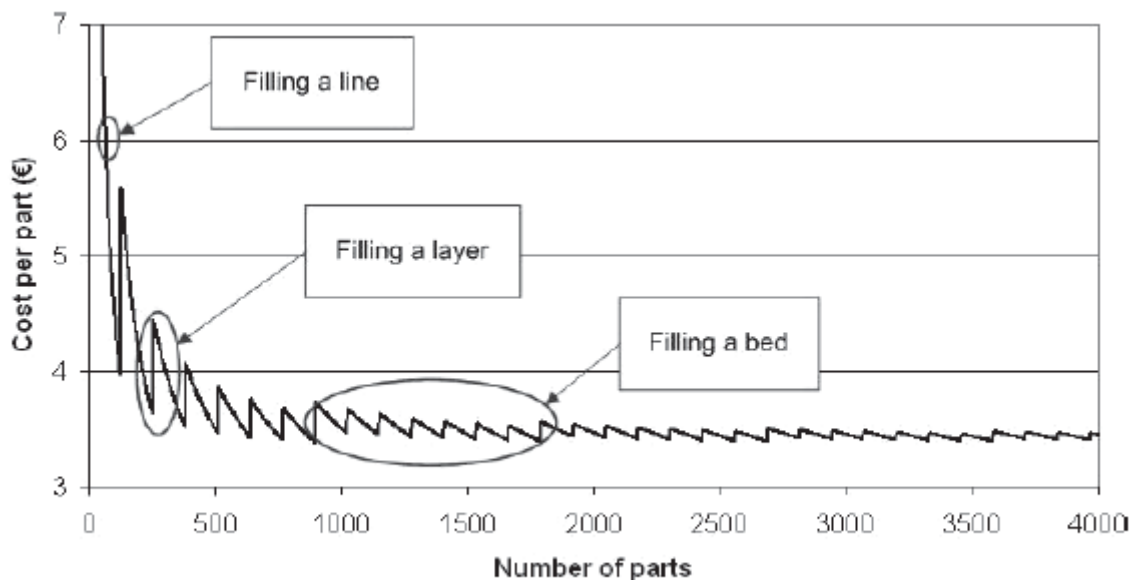


Figure 21: Production curve for the lever (Ruffo et al., 2006).

The curve has a deflection for low production volumes (less than 1,500 parts in the case presented) and a change in the curve tendency whenever one of three following cases arise. 1) It is necessary to use a new row in the x direction for the addition of a part (i.e. every 16 parts for the lever). 2) It is



necessary to add a new vertical layer for the addition of a part (i.e. every 128 parts for the lever). 3) It is necessary to start a new bed for the addition of a part (i.e. every 896 parts for the lever). Each of the three situations listed causes an increase of the manufacture time and the relative addition of indirect costs to the parts in production. For high production volumes the curve tends to stabilize. This happens because the indirect costs are split on a higher number of parts. Both the initial transition and the final stabilized value of the curve depend upon: 1) the part size – big parts quickly fill layers and machine beds, splitting the additional cost between fewer parts; small parts allow a more fractionated assignment of indirect costs; 2) The PR – it influences both build time and material waste, being a fundamental parameter for cost estimations.

*Effect of different orientations on the part cost*

The new model was also used to compare the manufacture of the same part built in different orientations. For example, Figure 22 presents a manufacture simulation of a simple geometrical box built horizontally and vertically. The investigation shows that setting parts flat is not always the economical best solution. In fact, for convenience, it is possible to switch between different configurations, depending on the number of parts produced and the relative packing ratio.

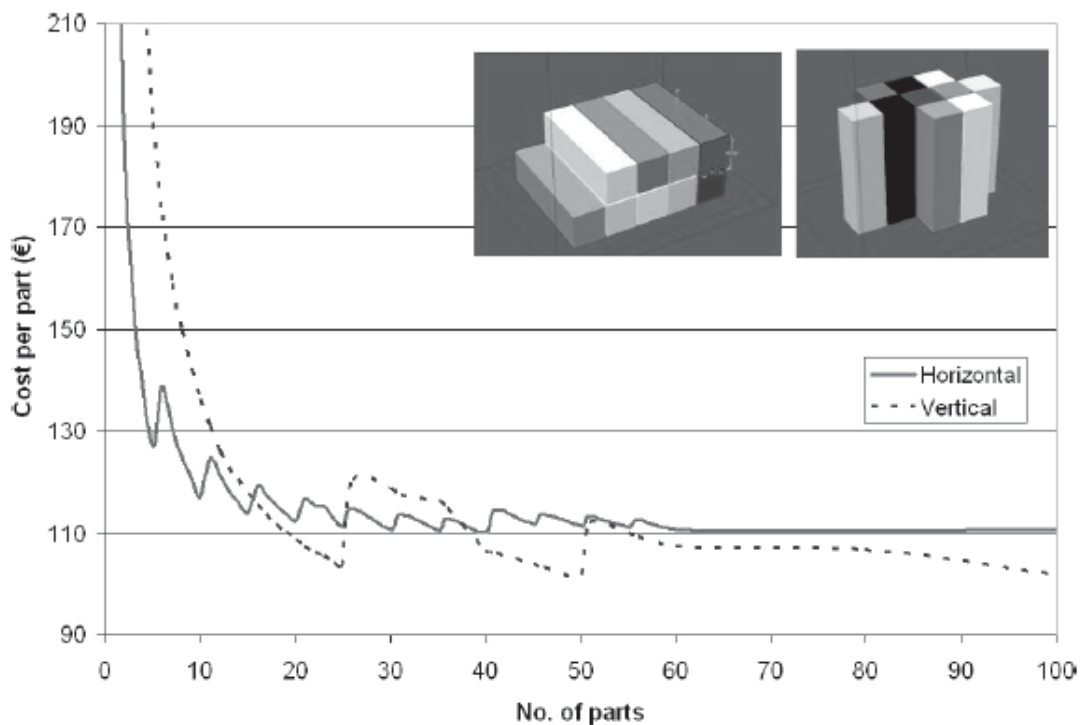


Figure 22: Effect of different orientations on the cost (Ruffo et al., 2006).

However, the limitation previously exposed about mixed parts production has not yet been solved in Ruffo et al., (2006). Therefore, the development of a method for cost calculation of mixed parts in the same build envelope is the aim carried on Ruffo et al. (2007). From now onwards, the term ‘original model’ will be used to identify the cost model of Ruffo et al. (2006), which is used as the basis of this work. This means that the case studies in this work are developed by using the cost model mentioned, and therefore all the assumptions made in the original model are also used for this study. In particular, it should be recalled that the LS machine used was a 3D Systems Vanguard Model and the material was Duraform.

The aim of this study was equitably to split the total cost of manufacture,  $Cost_B$ , into the different costs for the different parts,  $Cost_{P_i}$ , in the scenario of mixed components manufacture. When the

planned production consists of copies of a single part, the cost per part,  $Cost_P$ , is intuitively equal to the entire cost of the build,  $Cost_B$ , divided by the number of parts placed in it,  $n$ . Three different mathematical methods for RM cost assignment are presented in the following pages.

*First assignment method – based on parts volume*

A possible estimation is based on the components volume. Once the cost of the entire build is found, the cost of a single part can be calculated as a fraction of the total cost using the ratio between the volume of the part,  $V_P$ , and the total volume of production,  $V_B$

$$Cost_{P_i} = \left( \frac{V_{P_i}}{V_B} \right) * Cost_B$$

where  $V_B$  is the volume of the entire build,  $Cost_{P_i}$  is the cost of part  $i$ ,  $V_{P_i}$  is the volume of part  $i$ , and  $i$  is an index going from one to the number of different parts present in the build.

*Second method – based on the cost of building a single part*

The part volume, considered singularly, is not enough for time and cost estimation purposes. Therefore, a different solution is proposed in order to split the full build cost into the different parts placed on the machine bed. A coefficient  $\gamma \in [0,1]$  is introduced as a weight; its purpose is to identify the build cost of the part when manufactured alone in the machine bed. This method ensures that both volume and bounding box volume are used for the estimation, following the directives of the original cost model. When calculating the single part cost, the constants referring to machine set-up, warming up, and cooling down are excluded. This is because the single part cost should be a ‘naked’ production cost, depending only on the part size and geometry. Therefore, the coefficient  $\gamma$  includes the variables identifying part size and build time and it works as a weight for the assignment of the full build cost

$$Cost_{P_i} = \frac{\gamma_i * Cost_B}{n_i}$$

Where  $\gamma_i = \frac{Cost^*_{P_i} * n_i}{\sum_j (Cost^*_{P_j} * n_j)}$

and  $i$  is the index of the part under cost calculation,  $j$  is the index that refers to all the parts manufactured on the same bed,  $\gamma_i$  is the above-mentioned factor for part  $i$ ,  $n_{(\_)}$  is the number of parts identified with the subscript  $(\_)$ , and  $Cost^*_{P_{(\_)}}$  is the cost obtained with the original model for the building of the single part  $(\_)$ , but where the constant  $t_{HC}$  is missing from the equations and the time function is reduced to

$$t_B = t_{xy} + t_z$$

This second method is logically correct but introduces a significant error. In the presence of a small part (i.e. small in the  $x$  and  $y$  directions), the machine bed is partially empty and thus the packing ratio used for calculation is poor – in reality manufacturers set every build with the highest packing ratio possible. This makes the  $\gamma$ -based method very inaccurate because this weight is based on manufacturing conditions very far from the ones used in practice. Figure 23 shows the provenance of the factor  $\gamma_i$  on the production curve of an automotive component (which is used in the next section of this paper for a case study).

*Third method – based on the cost of a part built in high-volume production*

In order to overcome the problem described above, an effective solution appears to be the replacement of the cost of the single part,  $Cost^*_{P_i}$ , with a cost calculated in hypothetical high-volume production using RM. The explanation of the solution proposed is based on the fact that the RM curve tends to stabilize for a high number of parts and the packing ratio is then optimized. Conceptually, it is possible to extrapolate the cost for the production of an infinite number of parts. In practice, a high part number is used instead, with the condition that this production volume makes the production curve flat, as shown in Figure 23. It is then reasonable to use the following equations

$$Cost_{P_i} = \frac{\gamma_i^\infty * Cost_B}{n_i}$$

Where  $\gamma_i^\infty = \frac{Cost^\infty_{P_i} * n_i}{\sum_j (Cost^\infty_{P_j} * n_j)}$

$\gamma_i^\infty$  is the weight for the assignment of the full build cost, and  $Cost^\infty_{P_i}$  is the cost described above for a hypothetical infinite number of manufactured parts  $i$ . The use of “infinite parts production” is not credible for engineering problems, and thus its value is set by the cost for high production, where the curve is flat or, at least, has very low oscillations (with a consequent low error).

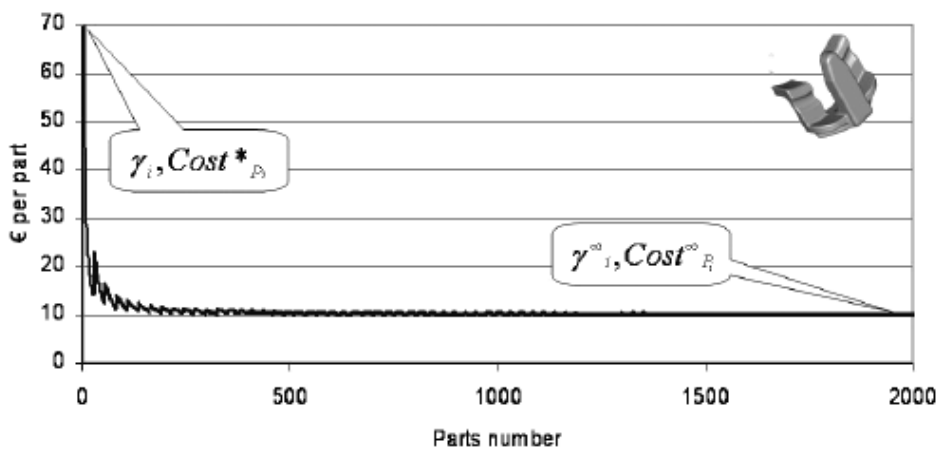


Figure 23: Graphical aid to understand the source of weights  $\gamma_i$  and  $\gamma_i^\infty$  (Ruffo et al., 2007).

In order to determine the efficiency of the three models proposed, a brief case study is analysed. Figure 24 shows two automotive components, one of small and one of large physical dimensions (not to scale in the figure).

Their RM production costs were calculated (a) as if produced separately, and (b) as if produced simultaneously in the same machine, and then compared. The maximum number of consoles that can fit the Vanguard machine chamber was two, and 200 small spring clips were added around the consoles in order to fill the build capacity. Costs for RM production were estimated, using the original model, as follows: (a) €526,752 to build separately 20,000 clips (€199,218) and 200 consoles (€327,533); (b) €382,967 to build together the same number of parts in parallel production. The cost saving is evident for components mixing, as expected. Table 18 shows the resulting costs per part using the three different assignment techniques. In Table 18, the values indicating a cost reduction are shown in bold italic, while the values indicating a cost increase are underlined. Intuitively, only the third model is a fair assignment method. In fact, the first two methods tend radically to reduce the cost of larger components at the expense of smaller parts. In contrast, the last model equitably splits the cost saving, typical of mixed production, between each component.



Spring Clip	Centre Console
	
Volume: 19634 mm <sup>3</sup> Bounding box dimensions: X=51.6 mm Y=54.1 mm Z=39.2 mm	Volume: 387821 mm <sup>3</sup> Bounding box dimensions: X=200.7 mm Y=256.9 mm Z=383.5 mm

Figure 24: Automotive components (Ruffo et al., 2007).

Method	Equation number	Cost per part (€)	
		Console	Spring clip
a) Multiples of the same parts (only consoles first and only spring clips then)	(3)	1637.6	10.0
b) Mixed production			
1st – volume based	(4)	<b>315.8</b>	16.0
2nd – single part cost based	(5)	<b>162.3</b>	<u>17.5</u>
3rd – high volume production based	(8)	<b>1188.7</b>	<u>7.3</u>

Table 18: Comparison between different cost assignments for mixed production (Ruffo et al., 2007).

The use of the third cost assignment method can be used graphically to show the advantage of mixed parallel production. A clear example follows for the production of the spring clip described previously. In the first scenario there is a need to build 200 spring clips and a machine is reserved for this work. Figure 25 shows the same cost curve shown in Figure 23 but focuses on low-volume production, for the building of up to 200 clips. In the second scenario there is a machine already set up for the manufacture of two consoles – some spring clips can be added to the same build. Figure 25 shows a comparison between the two production curves plotted under the assumptions of scenarios 1 and 2, being respectively curves for copies of the same part and mixed production of consoles and clips. The dashed curve has been modelled using the third cost assignment for the simultaneous production of two different components on the same machine. For scenario 2, owing to the absorption of indirect costs on the two different components, the spring clip curve deflection for low volumes is not as steep as in scenario 1. This indicates the advantage of mixing components in the machine bed envelope in order to increase the build density and optimize the build space. Moreover, Figure 25 confirms that a smart mixing of parts allows the manufacture of one-off components (or very low volumes) without incurring in a high cost, which is typical of the absorption of indirect costs.

In Lindemann et al. (2012), the authors in the first section of their work make a review of some approaches used to calculate the production costs of AM. Some of the most influencing authors were Augsburg, Hopkins/Dickens (HD), Ruffo/Tuck/Hague (RTH) and Gibson/Rosen/Stucker (GRS). A comparison of the models shows that all authors have chosen a similar approach for the calculation of costs in their models. Each of them has set a specific emphasis on a certain topic. The model of Augsburg for example describes manual process steps (e.g. removal of support structure, machine preparation), which helps to assign the labor costs directly to the product.

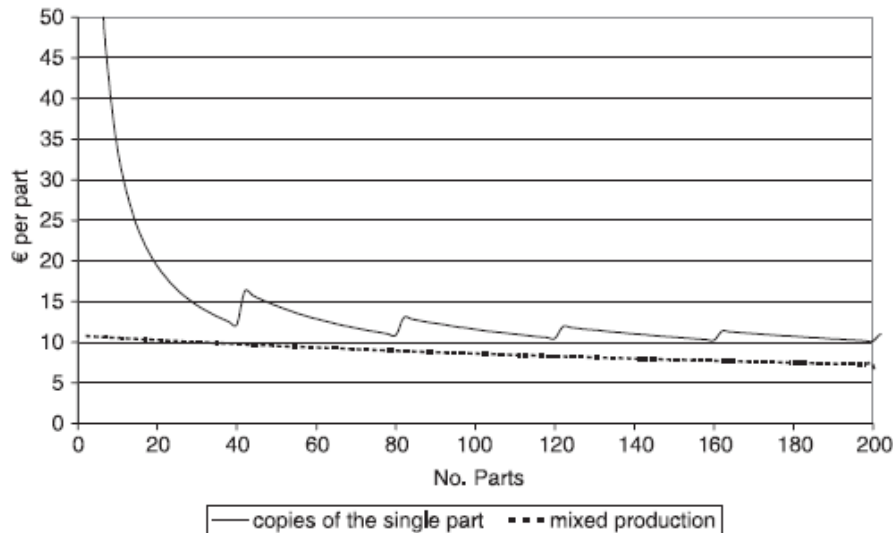


Figure 25: Comparison between production curves for the spring clip. Scenario 1 (only copies of the clip) versus scenario 2 (mixed production of clips with two

The model of RTH is the only model showing the composition of the indirect costs and the composition of the cost rate for the build time. The costs of additive manufacturing are separated in four main categories in the model of GRS. They relate to the cost of the machine, production costs, material costs and labor costs. The sum of these cost categories represents the total costs. The production costs are mainly depending on the time of printing. In this model the print time is calculated more accurately than in any other cost model. As well as the print time, Gibson, Rosen and Stucker designed the calculation of material cost applicable for several additive manufacturing processes. This calculation is based on the mathematical approach that the machine has to measure vectors to build up the product. This means that all kind of processes can be modeled that build products in single layers e. g. by the use of nozzle, laser or welding torch (Gibson et al., 2010). In summary, one could say that each of the existing costing models has advantages and disadvantages, but no model meets all criteria satisfactory. Thus, there is a need to combine the strengths of the existing models without including their weaknesses and to develop a new costing model that is suitable for the calculation of today's AM. A model considering the whole production process completely and correctly will be the basis for research how to include for instance development and lifecycle costs.

Lindemann et al. (2012) in their work, prior to the development of a cost model, investigated and modeled all cost relevant processes of the metal AM production process with Event Driven Process Chains (EPC). Business process models, especially EPC's, have been proven in the past that they are capable to represent knowledge. They are the basis for an aggregation of different types of information. This should help to understand the processes in detail. As a calculation method a "Time driven Activity Based Costing" (TD-ABC) approach has been taken. For the estimation of cost relevant processes, the process steps of the initial model have been simplified into four main

processes: (1) Preparation of the building job; (2) Production of the building job; (3) Manual removing of sample parts and support; (4) Post processing to enhance material properties. The main processes have been selected in order to be able to represent different cost centers. This facilitates the calculation and makes it easier to adopt the model to different production environments.

The costing center “preparation” includes all steps from the initial CAD data, placement of the parts in the building chamber and creating the support structures. The costs in this step are highly dependent on the complexity of the different parts and the complexity of the building job itself. Therefore, a complexity factor has been introduced in the calculation of this cost center, which is capable of estimating the duration of this task. This is especially important, as this process requires an experienced engineer, whose labor costs represent the main costing factor in this step. Furthermore, this factor allows distinguishing between the variation of an existing building job as well as the creation of a new one.

The costing center “machine” can be seen in detail in Figure 26 and is mainly based on the work of RTH and Dietrich et al., (2010).

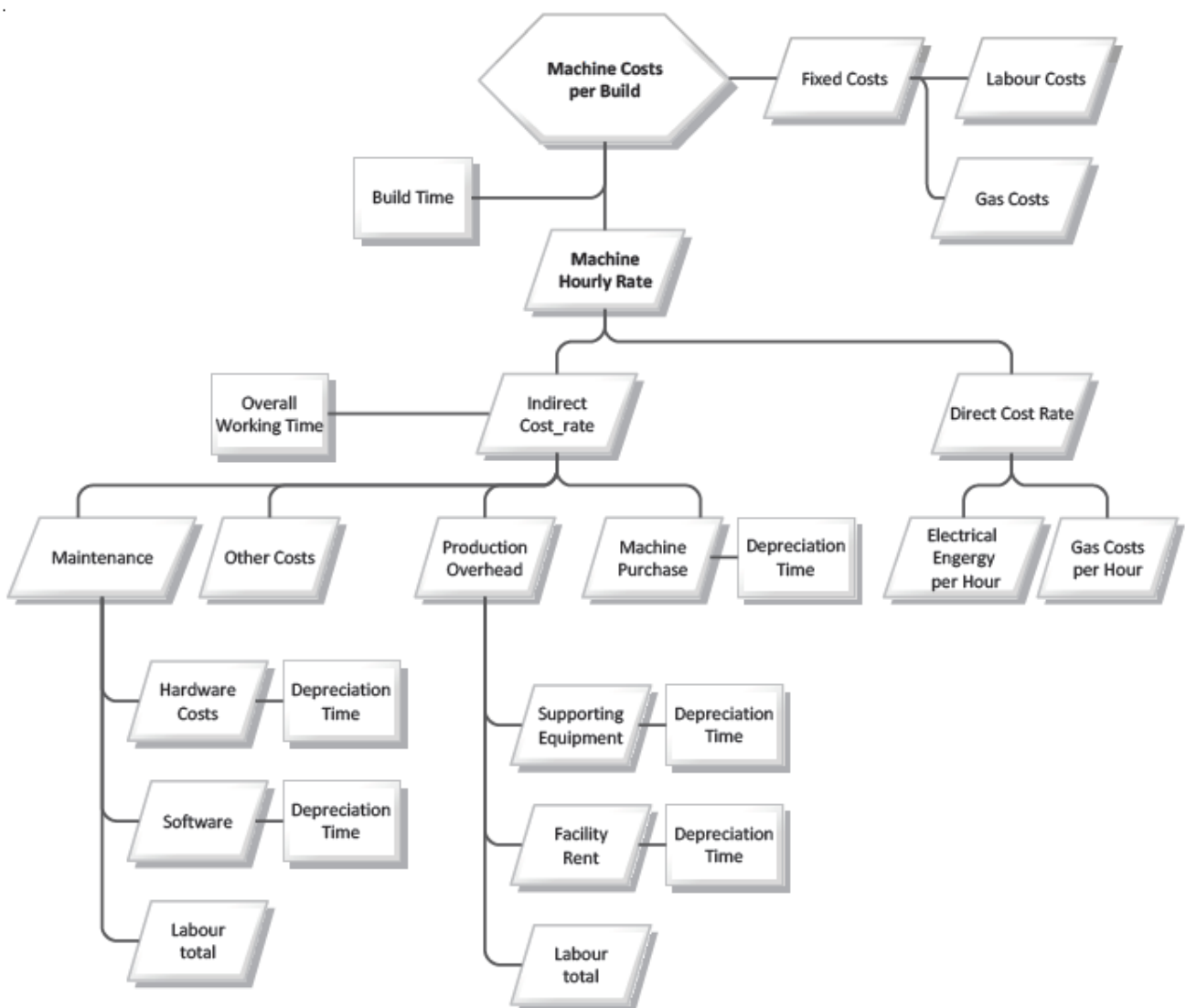


Figure 26: Machine Costs per build (Lindemann et al., 2012).

This production model is completely time driven and gets an additional fixed cost rate for the initial gas flooding of the machine as well as a fixed labor cost rate, as the processes are considered constant

for each building process. The hourly machine rate consists of an indirect and a direct cost rate and is multiplied with the build time afterwards. Many factors are already available as the energy consumption of different machines.

$$\text{CostsBuild} = \text{CostsFixed} + \text{MachineHourlyRate} * \text{Buildtime}$$

The estimation of the build time is certainly one of the most important factors in costing models as it influences the costs of the build significantly. A lot of authors have put some effort in the calculation of the building time. Therefore, different approaches can be taken. As stated above the model of GRS is the most detailed concerning the estimation of the build time. Hence, the equations from GRS have been adopted for that model. Further research attempts to find a way to simplify the estimation of the building time depending on factors such as standard elements, material selection, part density and part alignment. As material usage is not directly related to the build time these costs will be allocated in an additional step.

After the building process, the costing model allows different treatments to enhance the mechanical properties of the build. This process step can be considered additionally because it depends strongly on the product requirements if a pretreatment is necessary. As heat relief treatments or Hot Isostatic Pressing (HIP) have proven to improve material properties significantly this was found useful by the authors to estimate total part cost for AM. An hourly machine rate, which consists of direct and indirect costs, is multiplied by the processing time.

The last costing factor sums up all necessary manual processing steps. These include steps like support removal, polishing and quality control. An average value for the processing time has been taken which is multiplied with the labor costs per hour. These can be estimated lower than in the preparation phase because only a minimally skilled worker is needed to perform the tasks. The whole processing time will be multiplied with a complexity factor capturing the different efforts that it takes to remove support structures.

As the material costs have not been part of the machine costs per build, they need to be added to the costs of the other cost centers. The formula to calculate the material costs is the same as used by GRS as it is suitable for the FDM, SLM and LS processes.

$$\text{MaterialCost} = \text{Supportstructure} * \text{Wastefactor} * \text{Number of Parts} * \text{Partsvolume} * \text{MaterialPrice} * \text{MassDensity}$$

This paper discusses metal AM-production-costs on the basis of a sample part shown in Figure 27 (a). As a first evaluation of the costing model the cost of this sample metal part has been calculated.

Some major parameters for the Model were: 1) AM-machine utilization: 4500 h/year; 2) Depreciation time: 5 years; 3) Investment costs: 500,000€; 4) Costs for maintenance 21,666 €/ Year; 5) Build rate: 6.3 cm<sup>3</sup>/h; 6) Build Material: Stainless Steel 316L; 7) Material Price 89 €/kg; 8) Part Volume: 1cm<sup>3</sup>; 9) Layer thickness 0.3 μm. In Figure 27 (b) one can see the relationship between costs per unit and the number of manufactured parts. The star indicates the production quantity, which is used for the following part of the paper. It can be seen that the initial costs for a single piece rapidly drop as more parts are being placed in the building chamber. The developed costing model does not show the typical chainsaw effect, which can be seen in RTH for example. A slight effect can be noticed after a new production process has been initiated and the building chamber is not fully utilized. Over the time, this effect minimizes as the costs are split on more parts. Figure 28 shows variation of some of the above stated cost drivers. For each column one cost driver has been varied in order to see the effects on the composition of the total costs (Only Material cost quotes are showed in €).

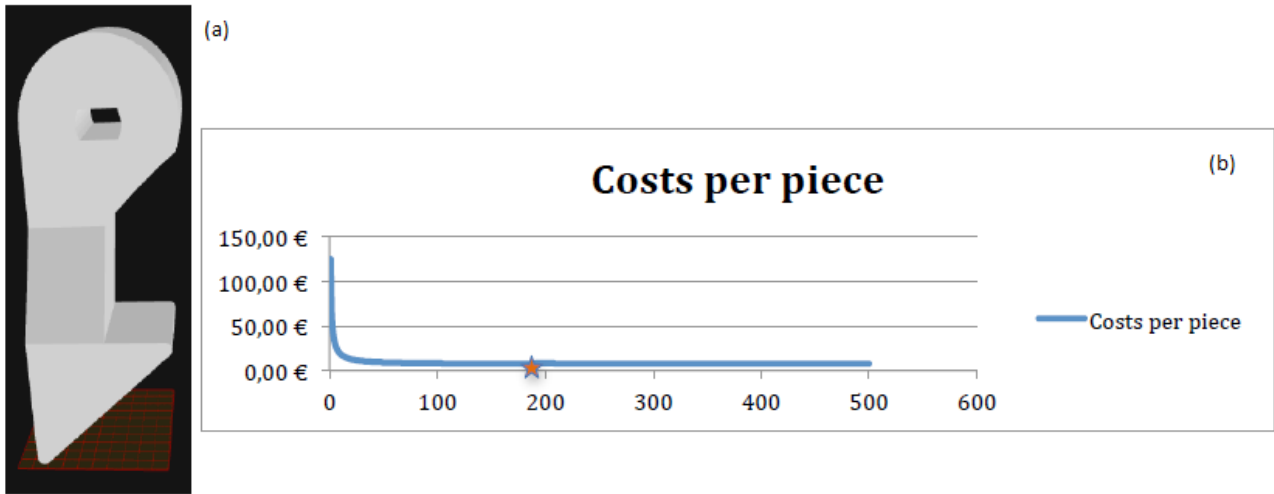


Figure 27: Sample Part (a) and the Costing Curve depending on the numbers of the build (b) (Lindemann et al. 2012).

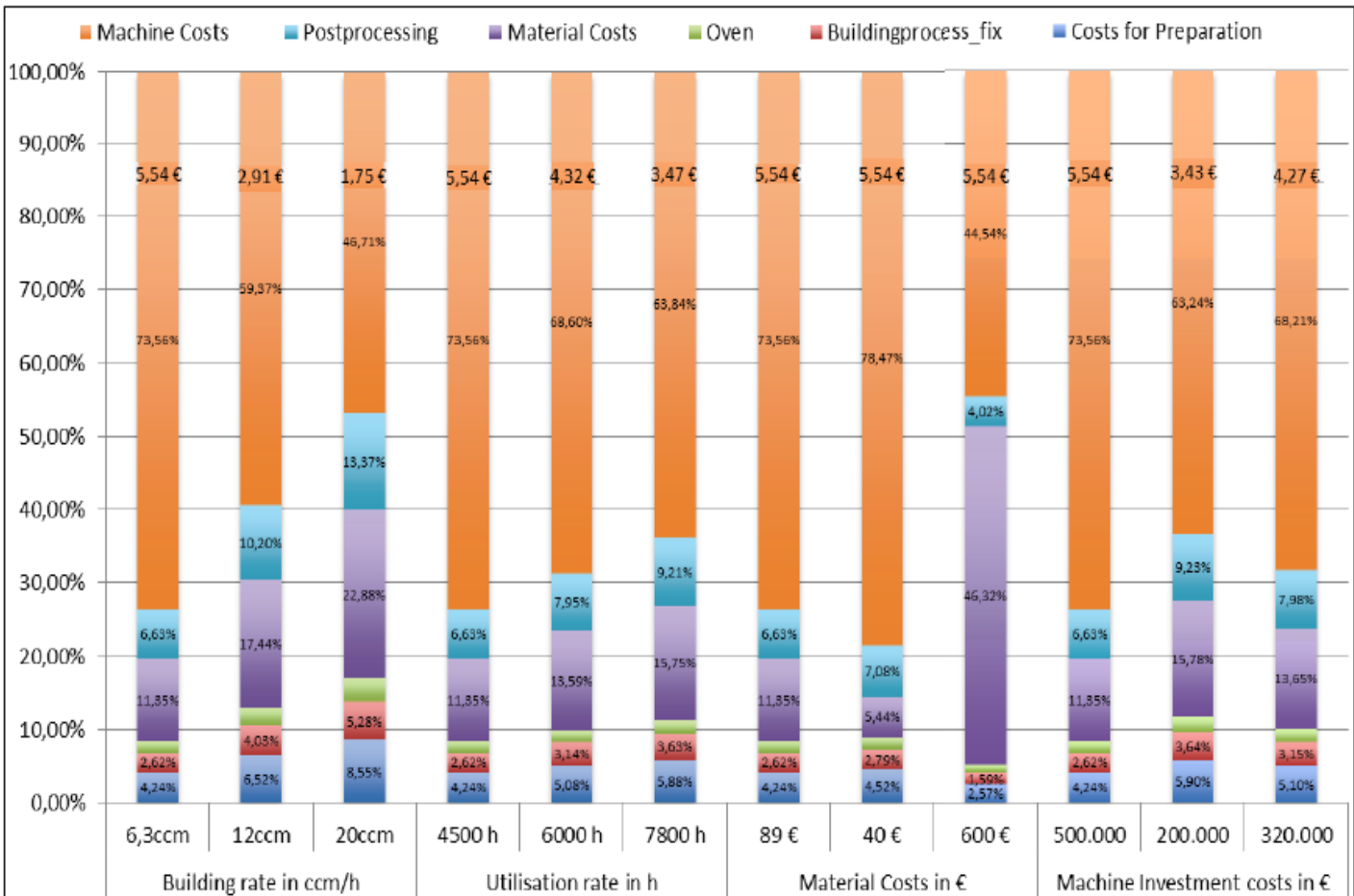


Figure 28: Variation on different Influence Factors in % (Only Material Cost quotes are showed in €) (Lindemann et al., 2012).

The largest contributor for building costs are the machine costs. The variation of influence factors have shown that a reduced machine rate cost can be achieved but will stay one of the dominant factors in the production process. One reason is that the labor costs for the AM building process itself can be reduced to the loading and unloading of the machine, as the production process is a blind process. As the material costs are not considered as a part of the building process, these cannot contribute to a decrease in machine rate costs. As the process is a fully automated and “lights-out” process it is logical that the machine rate costs have the greatest contribution to the total costs of a build. The



changing allocation of the overhead costs to the production enhances this effects. The material costs as the second largest cost driver has a certain influence on the building costs as well. For the sample part this is smaller than for a single piece high volume build. In general, the volume of additively manufactured parts will decrease constantly as the designer is able to construct independently of manufacturing restrictions. Lattice structures have the potential to reduce material volume and therefore the cost of the build. Materials like titanium are still very expensive and can raise costs up to nearly 50% even for low volume parts. These two cost drivers are followed by the post and preprocessing of the parts. While the production process itself is nearly labor-free, the post processing is not yet automated. In fact, the only two processes in which labor costs are significant, are the data preparation as well as the post processing, because it is necessary to remove the support structures etc. The direct labor costs for the production process are locked in the cost driver “Building process fix” which amount to a very small portion of the total part cost. The third largest cost driver is represented by the costs for the data preparation. This influence may be greater than the expected, since only a simple building job has been investigated. For the preparation process a skilled and experienced engineer is necessary. Thus, the main cost driver of the data preparation process is represented by labor costs. Knowledge is necessary to place the parts in the building chamber. Further research will bring more knowledge about the placing of parts and new software will automate this process so that a computer-based placement of parts in the building chamber will reduce the cost driver and make the technology more viable. As the main factor for the preparation is labor costs to place the parts in the building chamber, it only has to be performed once for larger series of parts. This will decrease the costs for the data preparation. Thus, the developed cost model allows a differentiation between mass produced parts (only place parts once) and customized combination of parts in the building chamber. An automated placing of parts in the building chamber on the other hand would make this differentiation obsolete.

The available additive manufacturing (AM) platforms differ in terms of their operating principle, but also with respect to energy input usage. The study of Baumers et al. (2011) presents an overview of electricity consumption across several major AM technology variants, reporting specific energy consumption during the production of dedicated test parts (ranging from 61 to 4849 MJ per kg deposited). Applying a consistent methodology, energy consumption during single part builds is compared to the energy requirements of full build experiments with multiple parts (up to 240 units). It is shown empirically that the effect of capacity utilization on energy efficiency varies strongly across different platforms. Table 19 summarizes the technology that have been assessed experimentally for this research and it also shows the manufacturer reference, operating principle and nominal build volume size of the machines assessed in the performed experiments. Is also provided an indication of the layer thickness and the build material selected for the performed power monitoring experiments.

The energy consumption characteristics of various additive systems have been the subject of a number of publications. Table 20 provides an overview of the cited energy consumption results. Moreover the table states if the data are derived from build experiments or estimated using secondary data. Regarding the work based on experimental results, it also reports whether the data were obtained from build configurations holding only a single test part or from builds with multiple parts. The specific energy consumption results reported in the literature for the same additive technology variant can differ significantly, as noted by Telenko and Seepersad (2010), who suggest that differences in Z-height and density of the build experiments are responsible. This supports the assumption that the degree of capacity utilization is very likely to have a bearing on energy requirements. To produce

consistent results, such data should ideally be collected from experiments with a controlled degree of capacity utilization.

System	Manufacturer reference	Operating principle	Nominal build vol. size (X * Y * Z)	Layer thickness	Build material
SLM250	MTT Group, UK (2009)	Selective laser melting (SLM)	250 × 250 × 300 mm	50 µm	Stainless steel 316L
M3 Linear	Concept Laser GmbH (2011)	Selective laser melting (SLM)	250 × 250 × 250 mm (used configuration)	30 µm	Stainless steel 316L
EOSINT M 270	EOS GmbH (2011)	Direct metal laser sintering (DMLS)	250 × 250 × 215 mm	20 µm	Stainless steel 17-4 PH
A1	Arcam AB (2010)	Electron beam melting (EBM)	200 × 200 × 180 mm	70 µm	Ti-6Al-4V
EOSINT P 390	EOS GmbH (2011)	Laser sintering (LS)	340 × 340 × 620 mm	100 µm	PA 12
FDM 400 mc	Stratasys Inc. (2011)	Fused deposition modeling (FDM)	406 × 355 × 406 mm	178 µm (nozzle Ø)	Polycarbonate

Table 19: Machine characteristics and build material in the performed experiments (Baumers et al., 2011).

The approach taken in the current paper rests on the assumption that for the efficient operation of additive manufacturing processes, it is necessary to produce parts in fully utilized build volumes, thereby operating the machinery at maximum capacity. This premise is confronted with the empirical data collected.

Study	Technology variant	Energy consumption result	Methodology
Luo et al. (1999)	Stereolithography	74.52 – 148.97 MJ / kg	Energy consumption not empirically measured
	LS	107.39 – 144.32 MJ / kg	
	FDM	83.09 – 1247.04 MJ / kg	
Mognol et al. (2006)	3D Printing	7.56 – 13.68 MJ per part	Single part build experiments, in various orientations
	FDM	1.80 – 4.50 MJ per part	
	DMLS	115.20 – 201.60 MJ per part	
Sreenivasan and Bourell (2009)	LS	52.20 MJ / kg	Empirical energy results not reported
Kellens et al. (2010a & 2010b)	LS	129.73 MJ / kg*	Full build experiments
	SLM	96.82 MJ / kg*	
Baumers et al. (2010)	SLM	111.60 – 139.50 MJ / kg†	Single part and full build experiments, compared
	EBM	61.20 – 176.67 MJ / kg†	

\* - Calculated from data provided by Kellens et al. (2010a; 2010b)

† - Calculated from data provided by Baumers et al. (2010)

Table 20: Specific energy consumption results for additive processes in the literature (Baumers et al., 2011).

The underlying experimental strategy is to record the energy consumption during two specifically designed build experiments for each additive technology variant: 1) In a first build experiment, the additive system is operated at full capacity. This is achieved by placing as many test parts as possible on the available substrate area. Hence, in this case the available build capacity is exhausted in the X/Y plane. For technology variants allowing an unconstrained three-dimensional placement of parts in the build volume (for example LS), full capacity operation necessitates a three dimensional workspace configuration that uses up all available space in the X/Y/Z dimensions. 2) The second experiment surveys the production of a single test part located in the center of the build volume floor plane. This experiment provides information on the energy consumption characteristics if the available capacity is only minimally used, thereby allowing an analysis of the impact of capacity utilization on process energy efficiency.

Due to additive manufacturing platforms normally being single-machine electricity driven systems, the measurement of electric energy inputs to build experiments is not complex. For the current research, process energy consumption was recorded using a digital power meter (Yokogawa CW240) attached to each systems AC power supply. Energy consumption was monitored throughout the entire build process, including any necessary process steps preceding and following the actual build activity. This includes, for example, process elements such as bed heating or vacuum drawing. The implementation of power monitoring experiments with consistent packing efficiency is based on the use of a standardized test part, shown in Figure 29. A reason for the “spider” shape is that it has a relatively large footprint in the X/Y dimensions, thereby limiting the achievable overall packing density and improving the economy and manageability of the experiments. Due to the two-dimensional method of build volume packing found on some additive platforms, this is particularly effective for approaches that require every part to be attached to the build substrate. A further consideration in the design of the test part is that it should not require auxiliary structures for the support of overhanging areas or the dissipation of heat.

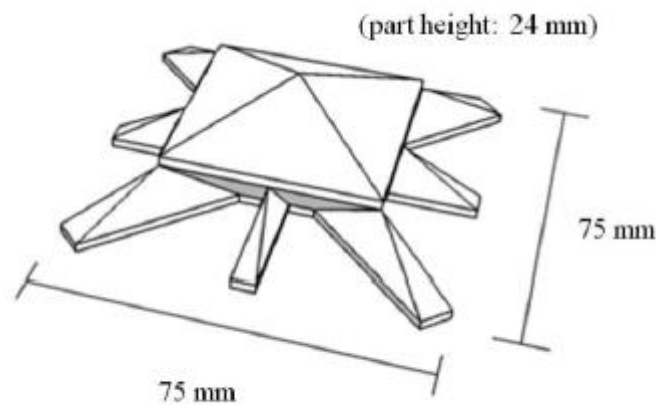


Figure 29: A standardized test part (Baumers et al., 2011).

Figure 30 reports the specific energy consumption per kg of material deposited during the build experiments for both the single part (dark column) and full build (light column) experiments. For all surveyed systems, as expected, full capacity utilization results in a lower specific energy consumption. However, the size of this saving varies heavily from platform to platform. It appears that for the energy efficient operation of some additive systems, capacity utilization is critical. The two polymer-processing systems form the extremes in this comparison. While the specific energy consumption observed on the FDM 400 mc appears relatively insensitive to the switch to full capacity utilization (-3.17 %), the change to full utilization produces a huge specific energy saving on the

EOSINT P 390 (-97.79 %). Contributing factors to the disproportionately large variation are likely to be the extensive energy investments in machine warm-up and cool-down.

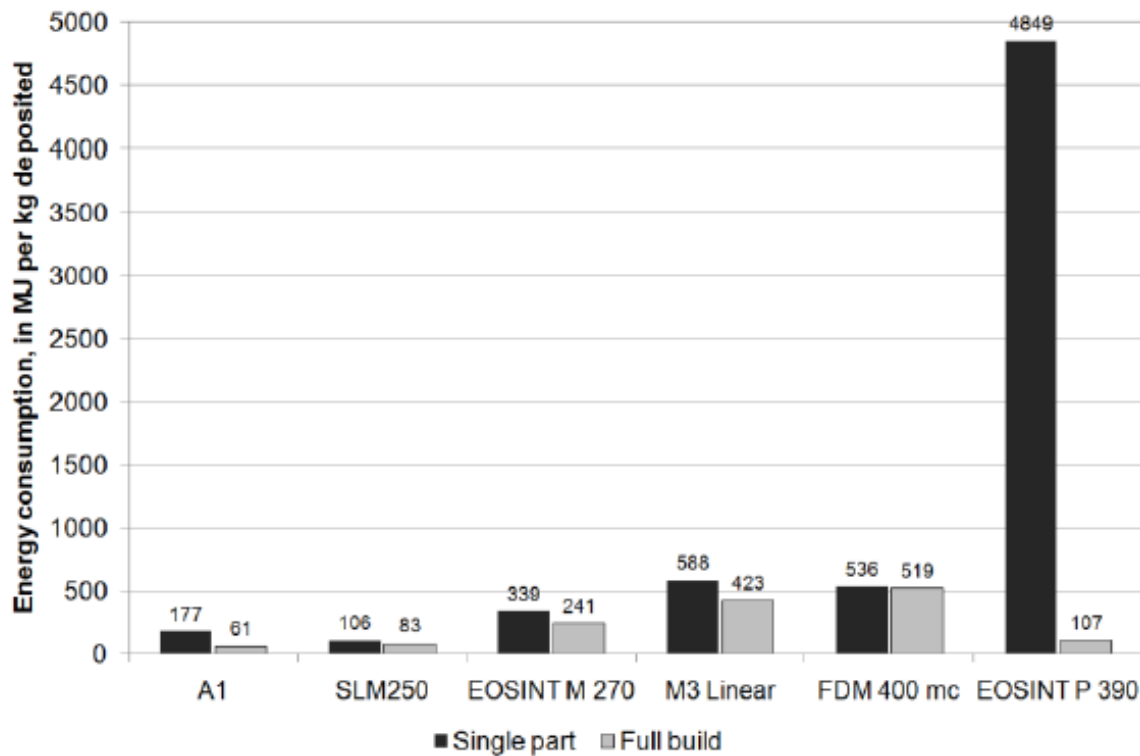


Figure 30: Single part and full build energy consumption per kg deposited (Baumers et al., 2011).

As Table 21 shows, these energy investments are large during both build experiments on the EOSINT P 390. The much greater number of parts generated in a full build configuration (240) enables the listed energy consumption to be allocated to a far greater part mass, thereby producing a favorable process energy consumption result (107 MJ per kg). Contrary to this, the FDM 400 mc is assumed to operate continuously. Therefore, extra energy consumption increments for build volume warm-up and cool-down are unnecessary.

Build phase	Single part build		Full build experiment	
	Energy consumption	Duration	Energy consumption	Duration
Warm-up	31.55 MJ	125 min	37.96 MJ	160 min
Cool-down	66.94 MJ	600 min	97.33 MJ	914 min

Table 21: EOSINT P 390 warm-up and cool-down energy consumption and time (Baumers et al., 2011).

The substrate carrying the produced parts is removed from the machine at operating temperature and replaced by an empty substrate for the next build. This, of course, ignores periods in which the machine may in practice sit idle due to other reasons. The metallic platforms exhibit a smaller variation in specific energy consumption. Operating at full capacity, the Arcam A1 exhibits a far greater energy saving (-65.54 %), than the MTT SLM250 (-21.70 %). Again, the reason for this is likely to be the significant energy expenditure for build volume pre-heating and cool-down procedures. While consuming markedly more energy per kg of material deposited than the other metallic systems, the EOSINT M 270 and Concept Laser M3 Linear, show a similar variation in specific energy consumption (-28.91 % and -28.06 %). A possible reason for the comparatively high

specific energy consumption levels observed during both experiments is the small layer thickness setting used on these platforms (20  $\mu\text{m}$  and 30  $\mu\text{m}$ ).

Considering the LS and EBM processes, which include extensive energy expenditure for atmosphere generation, warm-up and cool-down, full capacity utilization will result in far greater energy efficiency compared to a single part mode of production. This may pose problems in the estimation of process energy consumption for additively produced parts if the composition of the production build is unknown. Contrasting this, the results indicate that the FDM process (where system warm-up and cool-down do not enter the energy consumption metric at all) does not benefit significantly from full capacity utilization. It appears that FDM can be applied in a serial fashion generating output part-by-part without incurring a significant energy efficiency loss. Operating LS or EBM equipment in this way would result in a severe penalty to the environmental performance of the process.

In Baumers et al. (2012), the authors discuss the implementation of a tool for the estimation of process energy flows and costs occurring in the AM technology variant direct metal laser sintering. The authors apply the model to the EOSINT M270 platform (EOS GmbH 2010).

In the first part of their work, the authors make a review about build time estimation models, because as they explain these tools forms the starting point for AM production cost estimation models. In comparison with published works on metallic AM the papers related to build time estimation are scarce. Di Angelo and Di Stefano (2011) argue that the existing approaches can be divided into “detailed-analysis” methods based on knowledge of the inner workings of AM systems and “parametric” methods informed by data on a set of process characteristics such as layer thickness, hatch distance, and laser scan velocity. Munguia (2009) suggests also an artificial neural network time estimation approach for metallic AM. In the paper Baumers et al. (2012), the authors also make a review on AM Energy Consumption. Mognol and colleagues (2006) report the energy usage of a now obsolete version of the DMLS system investigated in this research, analyzing the energy inputs to single-part build experiments. Reporting a mean real power consumption of 4.00 kilowatts (kW), Mognol and colleagues conclude that part orientation affects total energy consumption due to the large effect of a part’s Z-height on overall energy consumption. For the production of a test part with a volume of 8.00 cubic centimeters ( $\text{cm}^3$ ), the authors cite a minimum total energy consumption of 115.2 megajoules (MJ). Kellens and colleagues (2010) investigate the energy consumption of the Concept Laser M3 linear selective laser melting system, which is technologically closely related to the investigated DMLS system. For the production of a batch of parts with a mass of 409 grams (g), a total energy consumption of 39.60 MJ is reported, which allows the calculation of a specific energy consumption of 96.82 MJ/kg of material deposited. This corresponds to the specific energy consumption rates reported by Baumers and colleagues (2010) for the two metallic AM technology variants EBM and SLM. Specific energy consumption of the EBM platform is measured at 61.20 MJ while the SLM system consumes 111.60 MJ/kg of material deposited. Corresponding to these results, Strutt (1980) notes that laser-based manufacturing processes may be much less energy efficient than comparable systems utilizing an electron beam, due to lower energy transfer efficiency. While energy consumption estimators analogous to AM cost estimators are not documented, one result from the AM cost estimation literature is transferrable to energy inputs: overall energy consumption is affected by capacity utilization (Baumers et al., 2010). It is also likely that the mix of parts in an individual build influences the energy efficiency of the process.

To provide the empirical data, a series of build experiments was performed on the EOSINT M270 DMLS system with factory settings. This set of default operating parameters includes the following: 1) Layer thickness of 0.02 mm, set in conjunction with the used stainless steel raw material (grade

17–4 PH) in powder form; 2) Scan path overlap of 0.5 mm; 3) Hatch scan strip width of 10 mm; 4) Contour scanning: scan speed of 700 mm/s, 60W nominal beam power, 40W for downward-facing surfaces; 5) Outer skin scanning: scan speed of 1,000 mm/s, 195 W nominal beam power; 6) Postcontour scanning: scan speed of 1,000 mm/s, 195 W nominal beam power. For the energy component in life cycle inventory analyses, the variable of interest is mean real power consumption per measurement interval. The energy inputs during these build experiments were recorded using a Yokogawa CW240 digital power meter attached to the main power connection, in the same configuration used by Baumers and colleagues (2010). This setup takes into account the energy used to provide the nitrogen (N<sub>2</sub>) required to shield the process from oxygen as the N<sub>2</sub> generator is attached to the system’s power supply. To simplify this analysis, the impact of the used compressed air (supplied by the local facility) is ignored. In total, four build experiments were undertaken.

In the work of Baumers et al. (2012), the first experiment was performed to collect energy consumption and build time data. To achieve this, a specifically designed test part (shown in Figure 31 (a)) was built directly on the build platform. To ensure sufficient data resolution, mean real power consumption was logged in 100 millisecond (ms) intervals. Three further experiments were conducted to validate the combined energy consumption and time estimator. This included a multipart build at full machine capacity, as well as two single-part builds to test model accuracy in single-part configurations. As cumulative energy consumption values were in the foreground in these experiments and the power meter logs the largest number of power-related variables in this setting, the data were recorded with a time resolution of 1 s. To populate the workspace, emulating a realistic application of AM, a basket of five test parts was defined (shown in Figure 31 (b)).

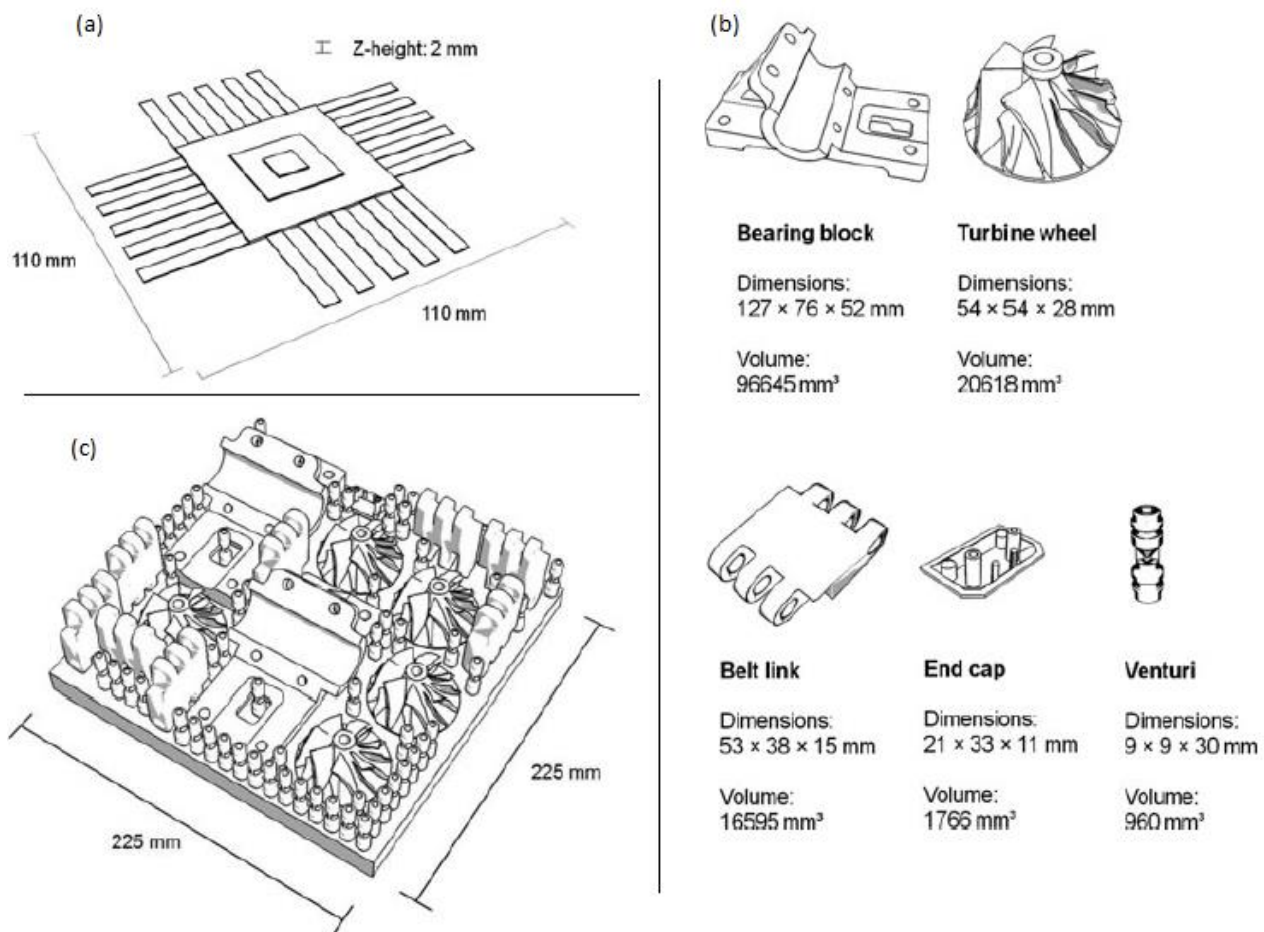


Figure 31: Power monitoring test part (a), basket of sample parts (b) and full build configuration (c) (Baumers et al., 2012).

The composition of this basket was chosen to be representative of the products commercially manufactured using DMLS and to reflect variation in product size, geometry, and application. The energy consumed by the separation of the parts from the removable build plate in an ancillary wire erosion process was also monitored. The wire erosion process operates by passing an electrically charged brass wire along the surface of the build substrate from one side of the build plate to the other. The energy usage of the wire erosion process depends heavily on the cutting time, which in turn depends on the length of the interface connecting the parts to the substrate. Experiments show that the amount of energy used in the wire erosion process tends to be independent of part geometry and build volume utilization. The mean real power consumption of the wire erosion process is measured at 3.96 kW. On the CUT20, the separation of a full build of parts from the metal substrate is observed to take approximately 600 minutes (36,000 s). Thus, for each build, the energy investment for the wire erosion process is assumed to be constant at 142.46 MJ. The estimator applies this amount of energy consumption to the energy consumption estimate of every build, irrespective of build configuration. Moreover, the wire erosion process for full builds and single-part builds is thus treated identically, which may be a further simplification. However, the authors did not include this element of energy consumption for the validation of the estimator.

Cost estimation is based on a combination of data published by Ruffo et al. (2006) and expenditure data provided by the EOSINT M270 machine operator, Bentley Motors, in Crewe (UK). Table 22 presents the data informing the cost model specified for the EOSINTM270, including the cost arising from the ancillary wire erosion process.

<i>Cost elements</i>			<i>Cost elements (cont.)</i>		
<i>Production overhead</i>			<i>Equipment</i>		
Rent, building area cost	4.53	£/h	AM equipment and wire eroder	8.00	years
			Hardware and software	5.00	years
<i>Administration overhead</i>			<i>Machine costs</i>		
Hardware purchase	1,670.27	£	Machine purchase	364,406.80	£
Software purchase	1,670.27	£	Machine purchase cost per year	45,550.85	£
Hardware cost/year	334.05	£	Maintenance cost per year	22,033.90	£
Software cost/year	334.05	£	Machine consumables per year	2,542.37	£
Consumables per year	1,113.52	£	Wire erosion machine purchase	55,000.00	£
Total administration overhead	0.31	£/h	Total wire erosion costs per year	8,165.00	£
<i>Production labor</i>			Total machine costs per year	78,292.12	£
Technician annual salary	25,165.45	£	Total machine costs	15.66	£/h
Employer contributions	22.00	%			
Total production labor	6.14	£/h			
<i>Utilization</i>			<b>Total indirect costs per machine hour</b>	<b>26.64</b>	<b>£</b>
Utilization rate	57.04	%	<b>Direct cost for 17-4 PH powder/kg</b>	<b>78.81</b>	<b>£</b>
Annual machine operating hours	5,000.00	h	<b>Direct electricity costs per MJ</b>	<b>0.018</b>	<b>£</b>

Notes: £ = 2010 pounds sterling; h = hours; kg = kilograms; MJ = megajoules.

Table 22: Direct and indirect cost elements (adapted from Ruffo et al., 2006), (Baumers et al., 2012).

### *Demand Profile Definition*

An intertemporal production scheduling decision will usually mean that total demand for parts exceeds machine capacity available at a given point in time. This is modeled by allowing the total demand for parts to exceed available machine capacity, which may be interpreted as demand extending into the future. The construction of an energy and cost estimator allowing for such excess demand in the multiproduct case can be facilitated by the definition of some order of precedence for k different parts. This can be interpreted as a measure of comparative urgency of the production of

individual components. In a situation of demand exceeding the available capacity, this precedence order is likely to govern the composition of a build. Thus the demand profile faced by the AM user in this specification contains two elements: first, the demand level for each of the  $k$  parts, and second, an indication of the order of precedence. The instantaneous demand level measured in integer units for each of the  $k$  parts can be expressed as a  $k$  element vector  $dd$ , where  $dd_i \in \mathbb{N}$ ,  $dd = [dd_1 \ dd_2 \ \dots \ dd_{k-1} \ dd_k]$ . The assignment of an order of precedence to each of the  $k$  parts results in a vector  $p$  with  $k$  elements, where  $\{p_i \in \mathbb{N} | 0 < p_i \leq k\}$  and  $p_i \neq p_j$ :  $p = [p_1 \ p_2 \ \dots \ p_{k-1} \ p_k]$ .

### *Build Time Estimation*

Once the build configuration is determined by executing the build volume packing algorithm, the next step is to estimate build time, which forms a prerequisite for cost estimation. The estimate for total build time,  $T_{Build}$ , is obtained by combining data from a hierarchy of elements of time consumption: 1) Fixed time consumption per build operation,  $T_{Job}$ , including, for example, machine atmosphere generation and machine warm-up; 2) Total layer dependent time consumption, obtained by multiplying the fixed time consumption per layer,  $T_{Layer}$ , by the total number of build layers  $l$ ; 3) The total build time needed for the deposition of part geometry approximated by the voxels. The triple  $\Sigma$  operator in the following equation is used to express the summation of the time needed to process each voxel,  $T_{Voxel_{xyz}}$ , in a three-dimensional array representing the discretized build configuration:

$$T_{Build} = T_{Job} + (T_{Layer} * l) + \sum_{z=1}^z \sum_{y=1}^y \sum_{x=1}^x T_{Voxel_{xyz}}$$

No allowance is made for build preparation and machine cleaning. It is felt that the time spent on these activities is difficult to measure and very much at the discretion of the machine operator. It could be argued that these activities take place during the 42.96% of nonoperational hours (as shown in Table 22). In the commercial setting surveyed, the EOSINT M270 is kept in a standby state when idle, except during holidays or maintenance, when it is switched off completely. In this standby state, the  $N_2$  supply is shut down, with only the laser chiller, the control computer, and some secondary functions active. However, this configuration does not reflect energy-conscious technology usage. For energy consumption minimization, the system should be deactivated completely or as far as possible during inactive periods, perhaps through the addition of an energy-saving mode.

### *Energy Consumption Estimation*

Total energy investment,  $E_{Build}$ , can be modeled similarly to the equation for Build Time Estimation. However, a purely time-dependent element of power consumption must be expected in the continuous operation of the AM machine. This is denoted by the energy consumption rate  $E_{Time}$  (measured in MJ/s), which is multiplied by  $T_{Build}$  to estimate total time-dependent energy consumption. Modeling  $E_{Time}$  as a constant reflects its interpretation as a mean baseline level of energy consumption throughout the build, originating from continuously operating machine components such as cooling fans, pumps, and the control system.  $E_{Job}$  contains all energy consumption attributable to the build job, including energy consumed by the wire erosion process to remove the parts from the build plate. Analogous to build time estimation,  $E_{Layer}$  denotes fixed elements of energy consumption per build and layer, for a total number of layers,  $l$ . Further, the geometry-dependent energy consumption is obtained by adding all energy consumption associated with voxel deposition,  $E_{Voxel_{xyz}}$ , throughout the discretized workspace. Please note that  $E_{Voxel_{xyz}}$  does not contain time-dependent power consumption. The empirical data on  $E_{Voxel_{xyz}}$  were obtained by monitoring machine energy



consumption during scanning and then subtracting the energy associated with the energy consumption rate  $E_{Time}$ . Thus  $E_{Build}$  can be modeled as follows:

$$E_{Build} = E_{Job} + (E_{Time} * T_{Build}) + (E_{Layer} * l) + \sum_{z=1}^z \sum_{y=1}^y \sum_{x=1}^x E_{Voxel_{xyz}}$$

This energy consumption model should not be interpreted as showing how total AM energy consumption can be attributed to individual subunits of the platform. The specification was chosen to implement a voxel-based energy consumption estimator. Moreover, both the time and energy estimation implementations possess additional information on the real Z-height of the parts contained in the build. This approach is chosen to avoid large estimation errors arising from the inclusion of empty layers.

### *Cost Estimation*

For the current research, an activity-based cost (ABC) estimator of the type devised by Ruffo and colleagues (2006) is employed. The cost estimate for the build,  $C_{Build}$ , is constructed by combining data on the total indirect costs and direct costs incurred, thereby providing a measure of “relatively well-structured” costs (Son 1991) ignoring costs arising from risk of failure, setup, waiting, idleness, and inventory. Indirect costs, expressed as a cost rate,  $C_{Indirect}$ , measured per machine hour, contain costs arising from administrative and production overheads, production labor, as well as machine costs (including depreciation). As listed in Table 22, the current research estimates the total indirect cost rate of operating the EOSINT M270 at £26.64 per hour. It is noteworthy that the system incorporates an  $N_2$  generator, hence no protective gas from external sources is needed. Unlike in the work by Ruffo and colleagues (2006), two direct costs enter the total cost estimates: raw material costs and energy costs. Total raw material costs are calculated by multiplying the total weight  $w$  of all parts included in the build (including support structures) with the price per kilogram of the stainless steel 17-4 PH powder,  $Price_{Raw\_material}$  (£78.81/kg). The expenditure for energy enters the model by multiplication of the energy consumption estimate,  $E_{Build}$ , with the mean price of electricity for the manufacturing sector in the UK,  $Price_{Energy}$ , currently around £0.018/MJ. Thus the total cost estimate for the build,  $C_{Build}$ , can be expressed as

$$C_{Build} = (C_{Indirect} * T_{Build}) + (w * Price_{Raw\_material}) + (E_{Build} * Price_{Energy})$$

### *Model Specification*

The final specifications of the time and energy estimators are obtained from a least squares regression of the time and energy consumption data recorded during the deposition of each layer of the power monitoring test part, using the area scanned per layer as the independent variable. The obtained intercept parameters  $\alpha_{Time}$  (10.82 s) and  $\alpha_{Energy}$  (0.008 MJ) are multiplied by the number of layers in the build  $l$  in order to obtain layer-dependent time and energy consumption. The slope parameters expressing the time and energy attributable to the scanning of  $1 \text{ mm}^2$  during the build,  $\beta_{Time}$  (0.0125 s) and  $\beta_{Energy}$  (0.000013 MJ), are then used in conjunction with the layer thickness  $l_t$  (0.02 mm) and a measure of occupancy of each voxel to calculate total time and energy consumption per voxel,  $T_{Voxel_{xyz}}$  and  $E_{Voxel_{xyz}}$  respectively. The rate of occupancy ( $RO_i$ ) in each voxel depends on the ratio of the volume of part  $i$  occupying this voxel ( $VP_i$ ) and the volume of the voxel approximation for part  $i$  ( $VA_i$ ):

$$RO_i = \frac{VP_i}{VA_i}$$

Thus, for each (5 mm)<sup>3</sup> voxel in the position xyz holding 250 (= 5 mm/l<sub>t</sub>) layers and containing part i, the build time and energy consumption can be approximated:

$$T_{Voxel_{xyz}} = \beta_{Time} * 5^2 * \frac{5}{l_t} * RO_i$$

$$E_{Voxel_{xyz}} = \beta_{Energy} * 5^2 * \frac{5}{l_t} * RO_i$$

This is combined with an estimated fixed time and energy consumption for machine startup, T<sub>Job</sub> (63 s) and E<sub>Job</sub> (142.58 MJ, including wire erosion). The startup process is very rapid on this system, as no system warm-up is required and the build chamber is continuously flooded with N<sub>2</sub> during build activity. It should be noted that E<sub>Build</sub> also contains the time-dependent power consumption, obtained by multiplying the baseline energy consumption rate  $\dot{E}_{Time}$  (0.0015 MJ/s) by T<sub>Build</sub>. The estimates of T<sub>Build</sub> and E<sub>Build</sub> are obtained as follows:

$$T_{Build} = T_{Job} + (\alpha_{Time} * l) + \sum_{z=1}^z \sum_{y=1}^y \sum_{x=1}^x T_{Voxel_{xyz}}$$

$$E_{Build} = E_{Job} + (\dot{E}_{Time} * T_{Build}) + (\alpha_{Energy} * l) + \sum_{z=1}^z \sum_{y=1}^y \sum_{x=1}^x E_{Voxel_{xyz}}$$

### Validation of the Model

The time and energy consumption model specified in the last two equations can be validated by comparing the calculated estimates to the real time and energy consumption during three build experiments. Validation is performed for the full build at maximum machine capacity (shown in Figure 31 (c)) and two builds of single components from the basket of sample parts, the bearing block and the turbine wheel. The results of the validation experiments and the corresponding estimates of T<sub>Build</sub> and E<sub>Build</sub> are presented in Table 23. Note that the validation does not include the energy consumed by the ancillary wire erosion process, as the emphasis of this study is the core AM process. Compared to other build time estimators (Campbell et al. 2008; Munguia 2009; Ruffo et al. 2006b; Wilson 2006), the mean absolute errors show that the developed time estimation functionality performs robustly.

Experiment	Time consumed	Model time estimate, T <sub>Build</sub>	Error	Energy usage	Model energy estimate, E <sub>Build</sub>	Error
Full build experiment	388,031 s	354,806 s	-8.56%	917.10 MJ	879.93 MJ	-4.05%
Single bearing block	93,302 s	92,338 s	-1.03%	215.48 MJ	223.13 MJ	3.55%
Single turbine wheel	31,224 s	28,504 s	-8.71%	72.73 MJ	66.80 MJ	-8.15%

Notes: s = seconds; MJ = megajoules.

Table 23: Confronting the estimates with experimental results (Baumers et al., (2012).

According to the experimental data (including the wire erosion process), the full build experiment consumed a total of 1059.56 MJ of energy. Using the specified cost model, C<sub>Build</sub> is estimated at £3,218.87. Individual part shares of cost and energy usage are identified through their share of total

product mass, which includes any support structures connecting the parts to the substrate (4.167 kg). Figure 32 thus shows the process energy consumption and production cost attributable to each part.

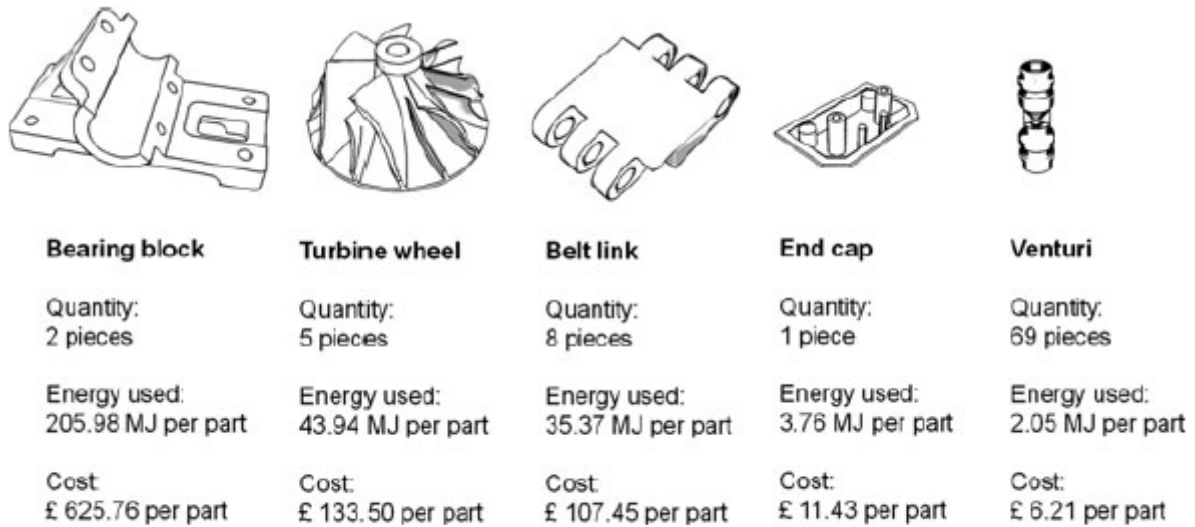


Figure 32: Process energy consumption and cost by part (Baumers et al., 2012).

The average cost functions for AM products proposed by Ruffo and colleagues (2006) are downward sloping and stabilize asymptotically for large production quantities, suggesting that part quantity is a determinant of the process efficiency of AM. The current article argues that such considerations do not correspond to AM technology usage in practice, which is marked by AM users trying to operate their machinery as efficiently as possible by packing as many parts as possible into each build. Moreover, AM is used in a parallel mode of production that mixes multiple parts in varying quantities in each build. So if production quantity is not a useful determinant of AM production efficiency, what is? The current article instead argues that the demand profile faced by the AM user has a significant impact. The combined energy consumption and cost estimator can be used to test the effect of different demand profiles. Table 24 lists eight such specifications, which are then used for cost and energy consumption estimation. The different demand profiles enter the estimator through the instantaneous demand vector  $dd$ . Note that demand for a particular part is allowed to exceed the available build volume capacity, and hence also exceeds the real number of parts that can be produced in one build (reported in brackets). The concepts of full capacity utilization and technical efficiency are related, so this research takes the standpoint that technically efficient operation of the DMLS machinery does not imply the full exhaustion of the build volume capacity, which is an idealized situation that does not normally occur in practice. Rather, the position is taken that the non-exhaustion of the demand faced by the AM user signals technically efficient machine operation. Following this, the demand profiles A, B, C, E, F, and G satisfy the criterion. Moreover, Table 24 lists the fraction of the build volume floor voxels that are occupied. It is noteworthy that for the builds deemed to be technically efficient, this fraction ranges from 50.07% (profile E) to 97.53% (profile G). A possible criticism of this methodology is that by letting the packing algorithm select parts, the composition of the demand profile changes, eventually leading to a mismatch with what is demanded by the user. However, the presented model, based on the instantaneous demand profile  $dd$ , aims to reflect the situation at a particular point in time. Adding a temporal dimension would improve realism, but would also greatly increase model complexity. By cumulating the total part volume resulting from each of the eight demand profiles, summary metrics (per cubic centimeter) of comparative process efficiency are derived, as shown in Figure 33. Demand profiles A through D reflect situations of uniform demand, in which the number demanded of each type is equal (see Table 24). Demand profiles E

through G demonstrate how changes to the mix of parts in the build volume affect production cost, even if the criterion of technical efficiency is satisfied. The main insight won from the demand profiles A, B, and C is that production quantity is only an indirect determinant of manufacturing costs and energy consumption. Ruffo et al. (2007) argue that increases in production quantity diminish the average cost by enlarging the allocation base for the total cost of the build.

Demand profile	Quantity of parts demanded					Build volume floor area occupation (voxels)	Description
	Bearing block	Turbine wheel	Belt link	End cap	Venturi		
A	∞ (2)	∞ (5)	∞ (8)	∞ (1)	∞ (69)	92.59%	Uniform demand, excess
B	5 (2)	5 (5)	5 (5)	5 (4)	5 (5)	79.80%	Uniform demand, high
C	3 (2)	3 (3)	3 (3)	3 (3)	3 (3)	62.27%	Uniform demand, intermediate
D	1 (1)	1 (1)	1 (1)	1 (1)	1 (1)	26.32%	Uniform demand, low
E	∞ (3)	—	—	—	—	50.07%	Excess demand, largest part
F	—	∞ (10)	∞ (13)	—	—	82.37%	Excess demand, medium parts
G	—	—	—	∞ (45)	∞ (100)	97.53%	Excess demand, small parts
H	1 (1)	—	—	—	—	16.69%	Single-part build, bearing block

Notes: Values in parentheses show the actual number of parts inserted by the build volume packing algorithm. ∞ = infinity.

Table 24: Different demand profiles and realized part quantities (Baumers et al., 2012).

In contrast, this work argues that not unused capacity, but the ability of the AM user to fill the available build volumes drives manufacturing costs. The results for the other three demand profiles leading to technically efficient builds—E, F, and G—show that changes in the part mix create an unpredictable effect on the efficiency of the investigated AM process. It appears that some part mixes will idiosyncratically lead to more efficient builds than others. In terms of energy consumption, specification A is the most efficient, despite profile G exhibiting a higher build volume voxel utilization metric (97.53%, Table 24). Though not by a wide margin, profile A is also the most cost-effective configuration (570.69 pence/cm<sup>3</sup> versus 571.15 pence/cm<sup>3</sup> in profile F). This indicates that builds with a wide variety of parts are likely to lead to improved process economics through the AM user’s increased ability to compose builds freely.

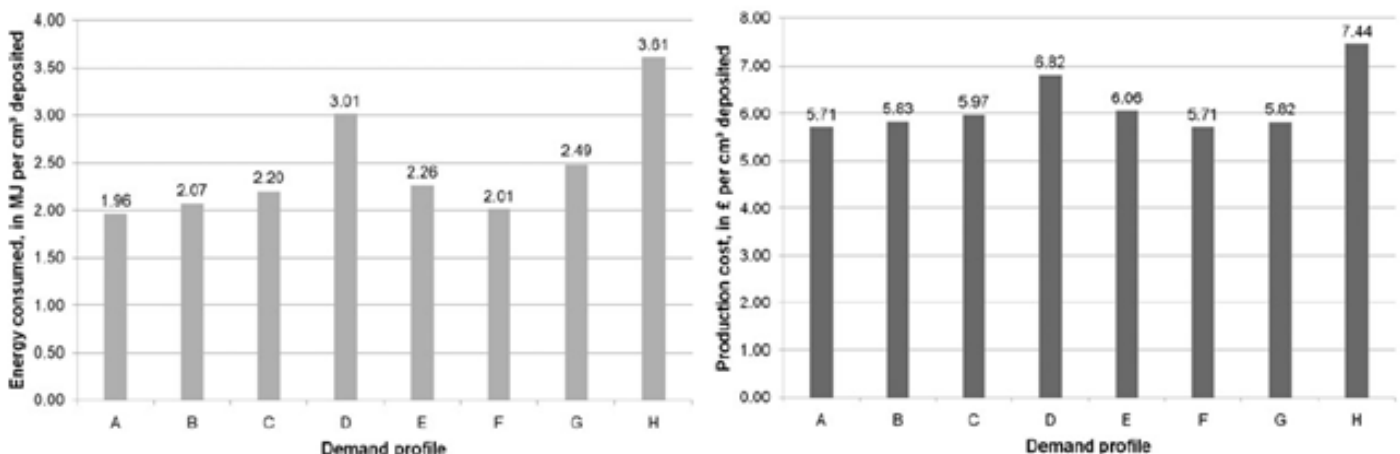


Figure 33: Effect of demand scenario on estimated energy consumption and cost (Baumers et al. 2012).

In Baumers et al. (2016), the authors study the effect of a variation in product shape complexity on process energy consumption, using experimental data collected during the manufacture of a titanium test part on a variant of AM technology, electron beam melting (EBM). This is done by applying a computationally quantifiable convexity-based characteristic associated with shape complexity to the test part and correlating this quantity with per-layer process energy consumption on the EBM system.

The methodology used in this paper is based on the assumption that using such a primarily process-flavored approach to the measurement of complexity does not provide a suitable pathway for the investigation of marginal effects of changes of shape complexity. The reason for this is that if manufacturing process characteristics are present in the formulation of the complexity metric it is difficult to identify any changes of process characteristics, such as energy consumption, in response to changes in shape complexity. Therefore, this paper views shape complexity as a characteristic derived from the geometry manufactured, implicitly accommodating aspects of the processes, rather than deriving from the processes used to generate them.

### *Methods and Implementation*

To facilitate this investigation, it was decided to base power monitoring experiments on the same test part geometry showed in Figure 29. The layer-by-layer operating principle of EBM allows the design of a power monitoring geometry tailored for the analysis of the impact of geometric variables on energy consumption by varying the part's cross-section along the vertical ("Z") direction. The resulting test part exhibits a suitable variation in two parameters, shape complexity and cross-sectional area, as will be explored in the following sections. The part's lower half is designed to assess the effect of shape complexity on energy inputs. This is done by changing a complex, star-shaped cross-section with a square cutout in the center into a square cross-section (at 12 millimeters [mm] Z-height). In the upper half of the geometry, the effect of cross-sectional area, reflective of overall part size, is explored. This is achieved by simply reducing cross-section area  $A$  down to a value of zero, forming a single vertex in a pyramid-like upper tip. A further point of consideration in the design of the "spider" shape was that some areas of the geometry feature negative wall angles. To avoid the use of support structures in the build experiments on the EBM system, the part was designed to not exceed negative wall angles of  $45^\circ$ .

*Implementing a Complexity Measurement Algorithm.* An algorithmic approach suitable for this article was developed by Psarra and Grajewski (2001), associating the measurement of two-dimensional (2D) shape complexity with various convexity-based classes of regularity. This technique was designed with the original intent of computationally assessing floor plans in architecture. In an adapted form, and combined with an implementation inspired by radar systems, this article develops the technique to be able to quantify shape features associated with complexity in the test part shown in Figure 29 (and indeed any other part). This approach is particularly useful because it is able to capture aspects associated with both the topological and geometrical aspects of shape complexity. Transferring the technique to the analysis of three-dimensional (3D) solid object geometry, the special layer-by-layer operating principle of AM allows the underlying 2D method to be maintained. This is possible because current additive equipment, such as the analyzed EBM platform, operates in a strictly sequential manner completing each horizontal layer before depositing the next layer onto the existing geometry. Thus, AM permits a separate analysis of every 2D cross-section. By subjecting the cross-section of a test part to a controlled variation along the test part's Z-axis, this research extends the original algorithmic approach by Psarra and Grajewski (2001). Effectively, a continuous 3D solid is split into a sequence of 2D layers, so that the level of shape complexity can be varied within one build. The effect of the variation of shape complexity on process energy consumption of

AM can then be studied. The first step toward the computational approach is, of course, a discretization process. The complexity measurement algorithm is based on a manually discretized version of the test part, which is hard coded in a 3D array. Corresponding to the discretization resolution in  $(1\text{ mm})^3$  volumetric pixels (“voxels”), the variation of shape complexity is measured in 1-mm intervals of Z-height. This resolution was chosen to balance the computational power needed for this approach (written in C++) with sufficient accuracy. Once the specifically designed power monitoring geometry is discretized, the next step is to develop an algorithm that is designed to assess each discrete voxel element of the part’s surface for complexity in a succession of horizontal cross-sections (analogous to build layers). Expressed intuitively, the proportion of other surface elements that are directly visible from specific loci in a layer can thus be identified. The outcome of this calculation is a Mean Connectivity Value (MCV) characterizing the shape complexity of each horizontal slice of the test part. Mimicking the layer-by-layer principle of AM, the resulting algorithm assesses each layer separately, resulting in a series of MCV values for each horizontal layer of the discretized test geometry. The actual algorithm underlying the measurement of such “visibility” is inspired by radar systems used to measure the distance of surrounding objects relative to a location. Radar systems operate by emitting signals in predetermined directions, often using antennae rotating around a Z-axis. A Cartesian coordinate system is used in the implementation, which may deviate from the original inspiration of radar. The principle of the measurement algorithm is very similar, however. Starting with the first element of the perimeter of the initial layer under consideration, a “radar signal” is emitted. Once the signal has been sent, it travels through the discretized voxel space in the predetermined direction. Where it strikes another element of the surface, the location is recorded. If it does not strike the perimeter at any location, for example, if it is emitted toward the outside of the shape, no impact location is registered. This radar-inspired implementation works as follows: As illustrated in Figure 3a, the algorithm reads discretized information on part geometry in a particular direction, recording the content of the voxel cells approximating the part in a onedimensional (1D) array (Figure 34b).

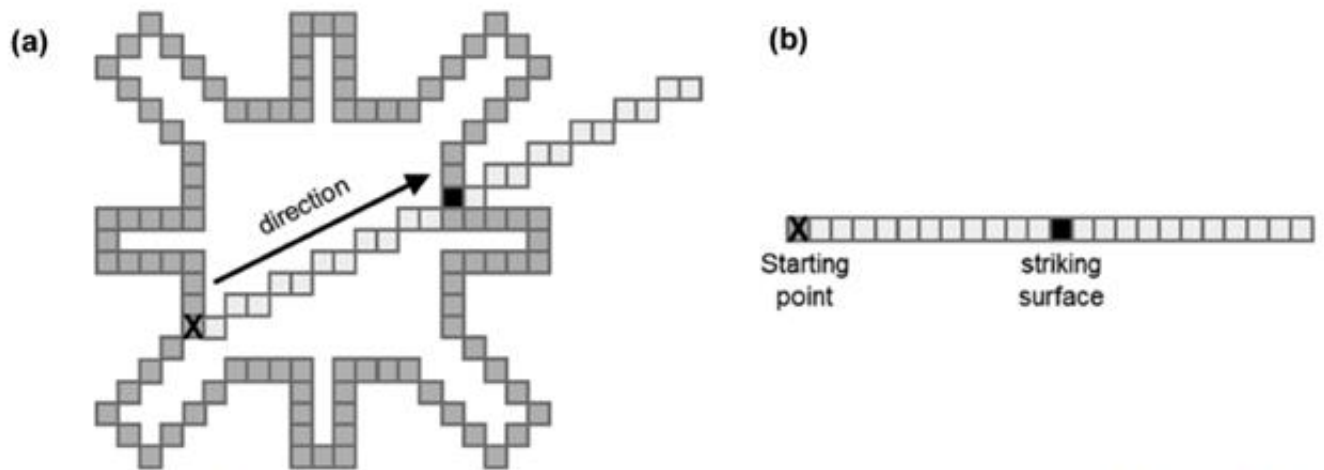


Figure 34: Implementation of occlusion measurement: (a) top view on a discretized layer (voxel resolution and scale not accurate) and (b) illustration of a one-dimensional array for the determination of visible voxels (Baumers et al., 2015).

In this sequence, beginning from the starting point, each entry is interrogated for a surface hit. The location of the first cell struck in this sequence is then recorded in a further array. The direction, or gradient, of the “radar beam” is then changed by one increment in counterclockwise direction and new information is read into the 1D array (Figure 34b). This is repeated in a loop, until the full 360° circle is complete around the starting point and all visible cells have been recorded. In the following step, the algorithm compares the location of the recorded visible elements to what should be visible

without occlusion. If every existing surface element is visible, the shape is deemed fully convex, as proposed by Psarra and Grajewski (2001). For intermediate results, a value of connectivity  $CV \in [0, 1]$  will be the result. This procedure is repeated for all “n” elements of the perimeter in layer “i”, enabling the calculation of the mean connectivity value  $MCV_i$  for each layer, where:

$$MCV_i = \frac{\sum_{m=1}^n CV_m}{n}$$

MCV is calculated for all layers in the discretized approximation of the test part. Effectively,  $MCV_i$  reflects shape complexity present in the “i”th horizontal cross-section of the part and thus forms a measure of 2D shape complexity. The measurement algorithm is available in the form of pseudocode in the Supporting Information available on the Journal’s website.

*Power Monitoring Experiments.* To assess the effect of a variation in part geometry on the energy consumed to deposit a layer, a build experiment has been performed on the Arcam A1 EBM system. Acknowledging that AM systems of this type only operate efficiently if the available build capacity is utilized (Baumers et al. 2011), a batch of five power monitoring test parts was produced in a full build experiment. As required by the methodology, all test parts were built in the same orientation directly onto the removable build plate, without any connecting or support structures. The electricity consumption during the build experiments was recorded using a Yokogawa CW240 digital multipurpose power meter (Yokogawa ElectricCorp. 2004), the main variable of interest being mean real power consumption across the three phases and the neutral line. To assemble the required data set, it is necessary to synchronize the collected energy consumption data with the log files created by the A1’s operating system, providing information on machine state and build progress.

### Results

Figure 35 shows the variation of three parameters along the test part’s Z-axis: the total area of the part’s cross-section; the cross-sectional perimeter length; and the parameter of shape complexity.

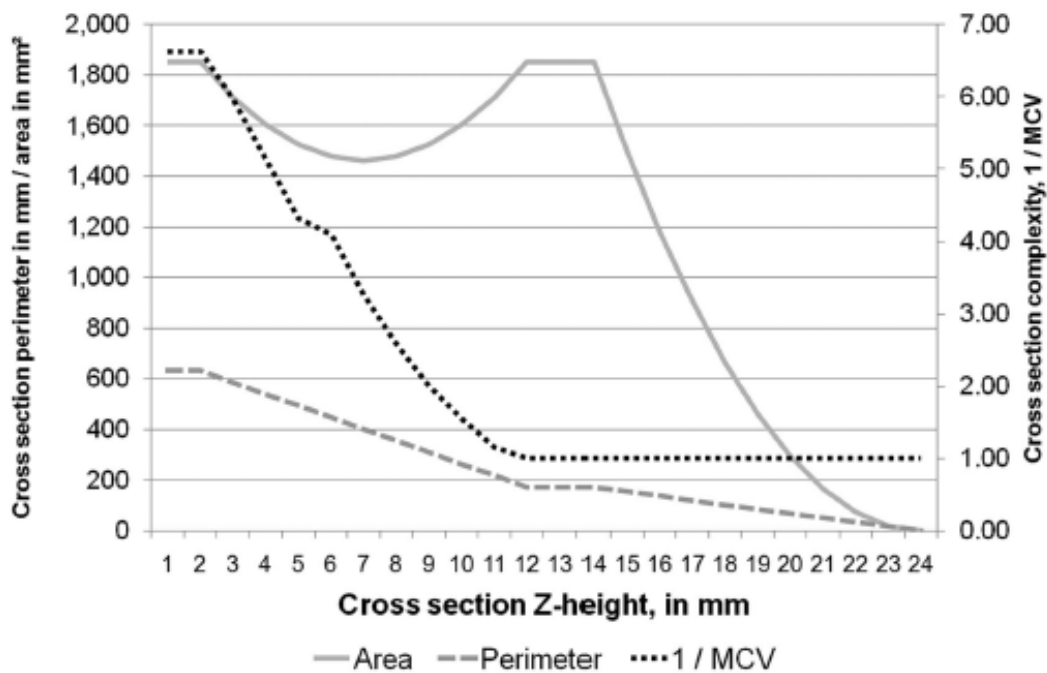


Figure 35: Variation of parameters of geometry (Baumers et al., 2016).

For exposition, MCV is shown in inverted form, such that a high value of MCV-1 indicates high cross-sectional shape complexity. As Figure 35 demonstrates, the area of the cross-sections dips between 2 and 12 mm of Z-height, from an initial value of 1,850 square millimeters (mm<sup>2</sup>) to around 1,450 mm<sup>2</sup>. This fluctuation occurs alongside the controlled variation of MCV. The fact that both parameters are varied in parallel complicates the analysis of the pure effect of a variation of MCV. The irregularity in the MCV-1 curve at a Z-height of 6 mm results from the use of a discretized voxel representation of part geometry. It is thus an artefact of the discretization technique and should be ignored. It has been argued that for any measure of complexity to be useful, at least one of the surveyed features must exhibit high complexity (Gell-Mann 1995). Figure 35 demonstrates that the design of a test part jointly varying parameters of complexity and cross-sectional area is successful by this standard. The effect of these variations of area and complexity along the Z-axis can now be explored in terms of the per-layer process energy consumption data.

*Power Monitoring Results.* Build operations on an EBM platform consist of four phases: system startup; preheating; build phase; and machine cooldown. The energy consumption results are reported in Table 25, listing process time, mean real power consumption, and cumulative energy consumption during the various phases of the build.

Category	Characteristic	Value
Process time	Warm-up time: machine startup	10 min
	Warm-up time: preheating	14 min
	Build time	260 min
	Cool-down time	17 min
	<b>Total build time</b>	<b>301 min</b>
Power consumption	Mean real power consumed: machine startup	1.09 kW
	Mean real power consumed: preheating	3.90 kW
	Mean real power consumed: build	2.22 kW
	Mean real power consumed: cool-down	0.60 kW
	<b>Mean real power consumed, overall</b>	<b>2.17 kW</b>
Absolute energy consumption	Energy consumption: machine startup	0.62 MJ
	Energy consumption: preheating	3.27 MJ
	Energy consumption: build time	34.66 MJ
	Energy consumption: cool-down	0.61 MJ
	<b>Total energy consumption</b>	<b>39.16 MJ</b>
Specific energy consumption	<b>Energy consumed per part (5 in total)</b>	<b>7.83 MJ</b>
	<b>Energy consumed per cm<sup>3</sup> deposited</b>	<b>0.27 MJ</b>
	<b>Specific energy consumption per kg deposited<sup>a</sup></b>	<b>59.96 MJ</b>

<sup>a</sup>Assuming 100% part density, at 4.43 g/cm<sup>3</sup>.

EBM = electron beam melting; cm<sup>3</sup> = cubic centimeters; kg = kilogram; min = minutes; kW = kilowatts; MJ = megajoules; g/cm<sup>3</sup> = grams per cubic centimeter.

**Table 25: EBM power monitoring results (Baumers et al. 2016).**

This results in a specific energy consumption of 59.96 megajoules (MJ) per kilogram (kg) deposited. It should be noted that the power consumed by the platform’s internal chiller is included in the measurement. By combining the energy consumption data with the information retrieved from the machine’s log file, it is possible to divide the energy invested during the core build time into three machine activities: 1) layer preparation; 2) layer preheating; and 3) melting. Figure 35 shows that the energy expended during layer preparation fluctuates around a constant mean throughout the build (approximately 10 kilojoules per layer). In contrast, the energy expended during the preheating state exhibits a linear, slightly negative, trend— most likely owing to a gradual warming up of the machine



frame during the build process, decreasing the requirement for energy expenditure for layer preheating over time. More interestingly, the energy expended for the selective melting of the cross-sections fluctuates strongly. The initial spike in energy consumption (during the first layer) is explained by repeat melting to ensure full attachment of parts to the build platform.

*Correlation between Complexity and Energy.* Visual inspection of Figure 36 suggests that the observed pattern of energy expenditure for melting (dashed line) can be explained by cross-sectional area. The Pearson product-moment correlation coefficient  $\rho_{X,Y}$ , where:

$$\rho_{X,Y} = \frac{cov(X,Y)}{\sigma_X\sigma_Y}$$

and  $\sigma_X\sigma_Y$  is the product of the standard deviations of variables X and Y, can be used to express the degree of linear dependence between two variables. A sample correlation coefficient  $\rho_{Area,Layer\ Energy} = 0.9699$  between selective melting energy and cross-sectional area (in 1-mm intervals of Z-height) suggests that total melting energy consumption is indeed determined by cross-sectional area and thus by overall part mass. Further applying correlation coefficients, the effects of various aspects of geometry on the energy expended for layer melting can be studied. Focusing on the portion of the build containing variation of shape complexity (1 to 12mm Z-height, as shown in figure 29), correlation coefficients between layer energy and cross-sectional perimeter length, complexity, and melting area can be compared:

$$\rho_{Perimeter,Layer\ Energy} = 0.6568$$

$$\rho_{Area,Layer\ Energy} = 0.8265$$

$$\rho_{MCV,Layer\ Energy} = -0.3544$$

The coefficients demonstrate that melting energy consumption correlates strongly with cross-section area (0.8263) and, to a lesser extent, with perimeter length (0.6568).

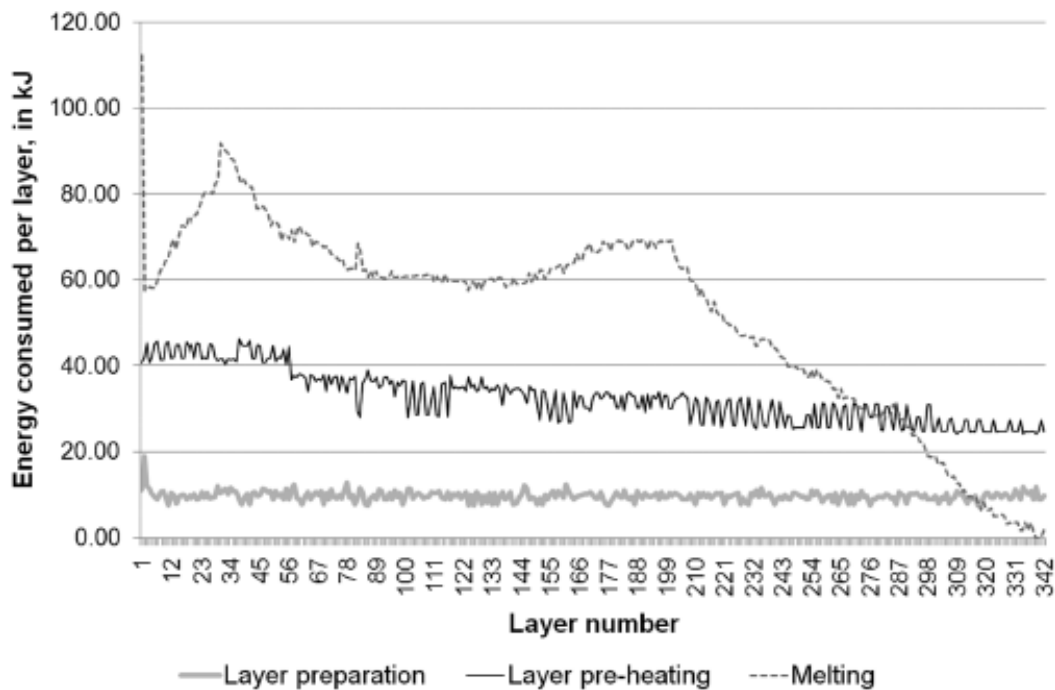


Figure 36: EBM energy invested per layer, by activity (Baumers et al., 2016).

The correlation coefficient between layer energy consumption and the used measure of shape complexity ( $-0.3544$ ) is small. This can be viewed as evidence of a weak or potentially absent association between EBM energy consumption and cross-sectional shape complexity. It should be noted that the negative correlation coefficient originates from the formulation of  $MCV_i$  (a high value indicates a small degree of shape complexity and vice versa). This article acknowledges that the test part geometry was selected to avoid the requirement to deposit support structures. This is, of course, a simplification that routinely does not hold in reality and must flow into the consideration of the calculated correlation coefficients.

The experimental results presented in this article suggest that EBM does not exhibit a strong direct linkage between energy consumption and shape complexity, at least on a per layer basis. Rather, it appears that process energy consumption is driven by cross-sectional area and hence by overall part mass. It should be remarked at this point that the used test geometry, featuring a controlled variation along the Z-axis, may resemble a relatively noncomplex component, especially when compared to some applications of EBM incorporating internal or external lattice structures. Further, the test specimen does not necessitate expendable support structures, which are routinely required in the EBM process. Moreover, this analysis forms an investigation of energy consumption at the process level. It thus does not investigate the environmental impact occurring during other stages in the product life cycle. By concentrating on the core process level, this research ignores aspects of postprocessing. Such postprocessing for EBM products can be performed by light finish machining or shot blasting. The additional energy consumption required to postprocess products may be related to the shape complexity exhibited by designs, dependent on the used technique. Unlike machining processes, the results presented in this article show that a minimization of deposited volume can be expected to lead to a minimization of process energy consumption in EBM. An important linking argument is the assumption that process energy consumption and production cost correlate positively, which has been observed for the AM process variant, direct metal laser sintering (Baumers et al. 2013), which is closely related to EBM. This implies that cost minimization by the technology operator should coincide with the minimization of process energy consumption. The described relationship produces a situation of correctly aligned incentives: The private incentive of cost minimization will motivate the deposition of the smallest possible amount of material, which, in turn, will result in the smallest amount of process energy consumption. Such an alignment of the private cost minimization incentive with configurations minimizing energy consumption, and hence a significant external environmental footprint, has been classed as an important prerequisite for the reduction of energy inputs. By minimizing energy consumption during the manufacturing stage of applications in which component mass plays a role for product performance, end-use efficiency may also be improved. This results in lower operating and lower environmental impacts associated with, for example, reduced fractional fuel consumption. Further savings may be enabled through secondary mass reductions that become possible through the lightweighting of structural or other components.

In Baumers et al. (2015), the authors establish a detailed technical understanding of the determinants of manufacturing cost by comparing two different technology variants, Electron Beam Melting (EBM) (Arcam AB, 2013) and Direct Metal Laser Sintering (DMLS) (EOS GmbH, 2013). Table 26 summarises the two platforms analysed for this paper. This paper employs a computational build volume packing algorithm developed for previous research (Baumers et al., 2012). This ensures that the build operations providing the data are performed with a sufficient and consistent degree of efficiency.

	Electron Beam Melting (EBM)	Direct Metal Laser Sintering (DMLS)
System model	S12	EOSINT M 270
Beam type	Electron beam	Yb-fibre laser
Beam power	3500 W	200 W
Build material used for this research	Titanium, Ti-6Al-4 V	Stainless Steel, 17-4 PH
Material density	4.43 g/cm <sup>3</sup>	7.78 g/cm <sup>3</sup>
Nominal build volume size, X × Y × Z	250 mm × 250 mm × 200 mm	250 mm × 250 mm × 215 mm
Usable build area, X × Y	200 mm × 200 mm	225 mm × 225 mm
Layer thickness	70 μm	20 μm
Process atmosphere	Vacuum (with the addition of Helium)	Nitrogen
Part retrieval	Automatic separation from steel substrate through thermal expansion	Wire erosion
Manufacturer reference	Arcam AB Arcam AB (2013)	EOS GmbH EOS GmbH (2013)

Table 26: Specifications of the analysed systems (Baumers et al., 2015).

Figure 37 shows the packing configurations generated for both systems using the build volume packing algorithm (layout (b) and test parts from Baumers et al., 2012). The very similar build volume occupation measures (93.00% for EBM and 92.59% for DMLS) indicate that the build volume packing algorithm has exhausted the available capacity almost equally well on both systems.

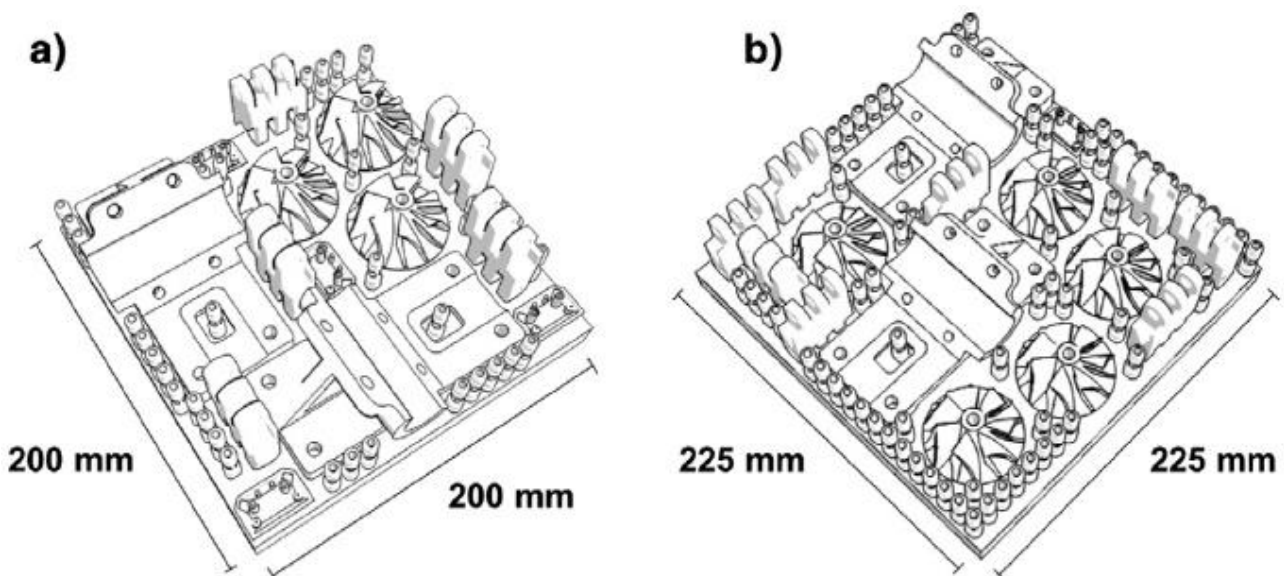


Figure 37: Full capacity utilisation for EBM (a) and DMLS (b) (Baumers et al., 2015).

The cost model used in this paper draws on two direct costs of manufacturing, raw material cost and energy consumption, which are combined with the total indirect (time-dependent) costs incurred during the build. The total cost  $C_{\text{Build}}$  of the build can be expressed as in Baumers et al. (2012). Table 27 summarises the published data used in this interprocess comparison.

As can be seen, a number of costs are shared between both systems, such as overheads, labour, depreciation periods and utilisation rates. These are viewed as highly similar across both platforms, which is a simplifying assumption. The results of the build experiment on the EBM system are compared with data generated during previous research on the DMLS platform (Baumers et al., 2012). Details of the build time and energy consumption elements are shown in Table 28, together with estimates of the full costs of the two builds, calculated according to the above cost model. Note that despite the EBM system's substantial warm up and cool down procedure, which the DMLS platform does not require, the total build time  $T_{\text{Build}}$  measured on the EBM system was much shorter (25.65 h

vs. 107.79 h). Corresponding to this, the total energy consumed,  $E_{\text{Build}}$ , during the full build experiment was also significantly lower (200.80 MJ vs. 917.10 MJ). EBM's advantage in process speed leads to a shorter build time, 20.97 h vs. 107.77 h, and results in a higher build rate, 15.63 cm<sup>3</sup>/h vs. 4.83 cm<sup>3</sup>/h. This can be identified as the central reason for the lower total cost and energy consumption estimates. Two further technical remarks should be made at this point. Unlike the DMLS system, EBM does not require an ancillary wire erosion process to remove the parts from the substrate after the build is complete.

	EBM		DMLS	
<i>Production overhead*</i>				
Rent, building area cost	4.53		£/h	
<i>Administration overhead*</i>				
Hardware purchase	1,670.27		£	
Software purchase	1,670.27		£	
Hardware cost/year	334.05		£	
Software cost/year	334.05		£	
Consumables per year	1,113.52		£	
Total administration overhead	0.31		£/h	
<i>Production labour*</i>				
Technician annual salary	25,165.45		£	
Employer contributions	22.00		%	
Total production labour	6.14		£/h	
<i>Utilization*</i>				
Utilization rate	57.04		%	
Annual machine operating hours	5,000.00		h	
<i>Equipment depreciation*</i>				
AM equipment and wire eroder	8		Years	
Hardware and software	5		Years	
<i>Machine costs</i>				
Machine purchase	348,772.73	£	364,406.80	£
Machine purchase cost per year	43,596.59	£	45,550.85	£
Maintenance per year	27,758.69	£	22,033.90	£
Consumables per year	5,783.06	£	2,542.37	£
Wire erosion machine purchase			55,000.00	£
Total wire erosion costs per year			8,165.00	£
Total machine costs per year	77,138.34	£	78,292.12	£
Total machine costs	15.43	£/h	15.66	£/h
<i>Total indirect costs per machine hour (<math>\dot{C}_{\text{indirect}}</math>)</i>	<b>26.41</b>	<b>£/h</b>	<b>26.64</b>	<b>£/h</b>
Direct cost for build material powder ( $Price_{\text{Raw material}}$ )	<b>156.97</b>	<b>£/kg</b>	<b>78.81</b>	<b>£/kg</b>
Direct electricity costs ( $Price_{\text{Energy}}$ )	<b>0.018</b>	<b>£/MJ</b>	<b>0.018</b>	<b>£/MJ</b>

\*Adapted from Ruffo et al. (Ruffo and Hague, 2007), converted into 2010 pounds sterling (£).

Table 27: Data used in the cost model (Baumers et al., 2015).

In EBM, the titanium parts separate from the steel build plate during cool down due to differences in thermal expansion behaviour. Moreover, the low density of the Ti-6Al-4 V material used ( $\rho=4.43 \text{ g/cm}^3$ ) has also led to comparatively moderate raw material costs, despite the high specific cost of the material (156.97 £/kg, see Table 27). Table 28 illustrates the dominance of machine costs for both systems, which are build-time dependent. As a summary metric for the comparison of manufacturing cost, the total cost per cm<sup>3</sup> of material deposited is useful. This specific cost metric can be calculated by attributing total cost,  $C_{\text{Build}}$ , to the total volume of manufactured parts, net of anchor structures. The build experiment performed on the EBM system resulted in a total specific cost of 2.39 £/cm<sup>3</sup> which is far lower than the result for DMLS of 6.18 £/cm<sup>3</sup>.

Category	Break down	unit	EBM	DMLS Arcam (2013)
Build time	Warm up (h)	h	1.69	0.02
	Build time (h)	h	20.97	107.77
	Cool down (h)	h	2.99	N/A
	Total build time, $T_{\text{Build}}$ (h)	h	25.65	107.79
Energy	Energy consumed, $E_{\text{Build}}$ (MJ)	MJ	200.80	917.10
Indirect costs	Production overhead	£	116.19	488.27
	Administration overhead	£	7.95	33.41
	Production labour*	£	157.49	661.81
	Machine costs	£	395.78	1511.75
Direct costs	Wire eroder costs	£	N/A	176.02
	Raw material costs	£	278.78	328.40
	Electricity costs	£	3.61	16.51
Total cost of build, $C_{\text{Build}}$		£	959.81	3218.87

\*Assuming 100% operator attendance during the build process (Ruffo and Hague, 2007).

Table 28: Build time, energy consumption and cost results (Baumers et al., 2015).

In this context, a crude, yet interesting, measure illustrating the two technologies' efficacy in turning raw material and energy into products is the ratio  $r$  of all direct costs over total cost,  $C_{\text{Build}}$ , which can be obtained at follows:

$$r = \frac{(w * Price_{\text{Raw material}}) + (E_{\text{Build}} * Price_{\text{Energy}})}{C_{\text{Build}}}$$

For the experimental results reached on the EBM platform, the result is  $r=0.42$ , suggesting that for every pound spent for this processes, raw materials and energy worth £0.42 are converted into products (and anchor structures). This ratio appears less favourable for DMLS, at  $r=0.12$ , suggesting that DMLS is less effective in the conversion of raw materials and energy into products. The presented results show that system productivity has a very significant effect on the cost performance of the assessed AM processes. Noting that two different build materials are used, the mass-based material deposition rate observed on the S12 EBM system (69.24 g/h) is 84% greater than that observed on the M270DMLS system (37.58 g/h). This demonstrates that system productivity is a central driver of manufacturing cost on these variants of AM technology.

#### *Contextualisation of the experimental results*

After assessing the build speed and cost performance of two major AM platforms, it is now interesting to put these results into the context of the wider literature. Two themes of particular interest have been identified for this research.

*System productivity as a driver of cost in AM.* The inter-platform comparison between EBM and DMLS has provided evidence that system productivity is a main driver of manufacturing cost. Deposition rates of 37.58 g/h (DMLS) and 69.24 g/h (EBM) were measured, resulting in mean cost estimates of 6.18 £/cm<sup>3</sup> (DMLS) and 2.39 £/cm<sup>3</sup> (EBM). For conventional manufacturing processes such as machining or injection moulding, Gutowski et al. (2009) report typical process rates of well over 100 kg/h. Acknowledging the substantial difference between AM and conventional processes, current AM systems are almost in all cases unable to support high-volume production. Further refinement to this point can be added by arguing that even if the average unit cost of the output could be depressed by reducing the system purchase price, rather than increasing system productivity, the overheads resulting from running a large number of unproductive systems may result in prohibitive total expenditure. In the development of next-generation production-ready AM systems, the focus should lie on reducing the various operating costs rather than on the purchase cost of the AM equipment itself.

*Demand-pull versus technology-push innovation.* According to Hull (2012), the first variant of additive technology, stereolithography, was developed in response to the clearly identified market need to speed up the creation of design prototypes. Such explicit needs form a central characteristic of the demand-pull mode of innovation (Martin, 1994). With a narrow aim on automating the prototyping process, the technology, known then as Rapid Prototyping, quickly gained market share in these applications. The following major step in the evolution of the AM industry was the introduction of the notion that these new technologies could be used as manufacturing processes for end-use products (Rudgley, 2001; Hopkinson and Dickens, 2001). Proposing additive techniques for the manufacture of final products had two consequences: Initially, this greatly expanded the potential market in which AM could be adopted, promoting a specific process for prototyping applications to (in principle) almost limitless applications as a general purpose manufacturing technology. The second, perhaps more subtle, consequence was that a prototyping technology was now proposed for manufacturing settings for which it was not designed. Differences in the mentality associated with the requirements of prototype creation, rather than finished products, have been emphasized (Bourell et al., 2009). Within AM processes, the 'prototyping mind set' has manifested itself in the observed generic barriers to AM adoption, including lacking cost effectiveness compared to conventional processes. Where an innovation has been induced by technological capability rather than expressed market need, the concept of technology-push applies (Martin, 1994). This suggests that as Rapid Prototyping evolved into AM, the accompanying mode of innovation rolled over from the demand-pull of the prototyping industry to the conceptual opposite of technology-push in the manufacturing industry. This paper argues that unit cost levels low enough to compete with incumbent high volume conventional manufacturing processes did not feature in the market-pull of prototyping applications. However, following the emergence of the concept of AM, the switch to true manufacturing applications has placed a significant focus on this aspect. The identification of this pattern leads to the question of whether ongoing AM technology development efforts and accompanying complementary innovation in supporting input markets are appropriate for AM's innovation context. This is of relevance as it has been suggested that such a transition is likely to have significant consequences for various aspects of strategy in an emerging industry (Brem and Voigt, 2009). Table 6 maps out possible consequences for the AM industry. Due to the large number of potential applications for AM in the general manufacturing sector, this paper takes the position that there is

also high market uncertainty once the economic barriers described in this paper have been overcome. According to the framework presented in Table 6, the appropriate response includes investing heavily in background and exploratory research, engaging the future technology users in the innovation process, and to explore novel business models.

	Rapid prototyping (demand-pull)	AM (technology-push)
Uncertainty of technology	Low	High
Required R&D funding	Low	High
Duration of R&D programmes	Short	Long
Market related uncertainty	Low	High
Time-to-market	Known	Uncertain/unknown
User integration into R&D	Easy	Difficult
Mode of market research	Verification	New discovery
Need for user business models to adapt	Minimal	Extensive

Table 29: Consequences of the transition to AM (Baumers et al., 2015).

In Rickenbacher et al. (2013), the authors present a new cost-model for the SLM process, taking into account all the process characteristics, as the other models are not appropriate for the application of AM with SLM and as they do not take into account adequately any pre- and post-processing operations.

#### Model formulation

Each process will be separately analysed and modelled in detail allowing an evaluation of the influences of the different geometries  $G_i$  in various quantities  $N_i$  on the cost of the parts. Initially it is assumed that an error-free CAD model exists for each geometry  $G_i$  and their quantities  $N_i$ . Therefore, each part  $P_i$  exhibits an assigned geometry  $G_i$ .  $T_{prep}$  represents the operator's required time to orient the geometry in the build space and to apply process-related support structures. Numerous geometry specific boundaries have to be taken into account to achieve optimal quality. Therefore, this operation is still done manually or at most half-automated, despite numerous analyses regarding optimal geometry orientation and corresponding software algorithms exists.  $T_{prep}$  depends highly on the complexity of the specific geometry  $G_i$ . Said process step has to be done once for each geometry  $G_i$ , therefore the time required can be evenly allocated on all parts with the same geometry  $G_i$ :

$$C_{Prep}(P_i) = (C_{Oper} + C_{PC}) * \frac{T_{Prep}(G_i)}{N_i}$$

where:

$C_{Prep}$  – cost for preparing geometry data (orientation, support structures, etc.) (€).

$P_i$  – part with  $i$ th geometry (-).

$C_{Oper}$  – operator's hourly rate (€/h).

$C_{PC}$  – hourly rate of the workstation including costs of required software and tools (€/h).

$T_{Prep}$  – time required for preparing CAD data (h).

$G_i$  –  $i$ th geometry (-).

$N_i$  – quantity of parts with  $i$ th geometry (–).

The time required to arrange all parts into a build job on the machine depends on part quantity. Therefore, the costs for this operation as well as for the build job parameterization can be evenly distributed on all parts:

$$C_{Buildjob}(P_i) = T_{Buildjob} * \frac{(C_{Oper} + C_{PC})}{\sum_i N_i}$$

where:

$C_{Buildjob}$  – cost for build job assembly (€).

$P_i$  – part with  $i$ th geometry (–).

$T_{Buildjob}$  – time required for build job assembly (h).

During data import and machine setup, the SLM machine is blocked during the time  $T_{Setup}$ . Additional time  $T_{Mat.change}$  is needed, if the material inside the machine has to be changed, whereby the effort per build job is considered by the factor  $F_{Mat.change}$ . Depending on the material used, a handling under protective gas can be mandatory resulting in supplementary effort, e.g. while processing Titanium-based alloys. This additional work is taken into account by factor  $F_{Inertgas}$ . Assuming 25 per cent additional effort when handling under protective gas, the factor  $F_{Inertgas}$  equals 1.25, if no additional effort is required  $F_{Inertgas}$  equals 1. In general, the machine setup time is independent of the part quantity and therefore can be evenly distributed on all parts, leading to a further cost reduction resulting from simultaneous manufacturing of multiple parts:

$$C_{Setup}(P_i) = F_{Inertgas} * \frac{(C_{Oper} + C_{Machine})}{\sum_i N_i} * (T_{Setup} + (F_{Mat.change} * T_{Mat.change}))$$

where:

$C_{Setup}$  – machine set up costs (€).

$F_{Inertgas}$  – factor to model extra effort required for handling in protective gas environment (–).

$T_{Setup}$  – time required for machine set up (h).

$F_{Mat.change}$  – factor to model the frequency of material changes (–).

$T_{Mat.change}$  – time required to change material (h).

$C_{Machine}$  – machine's cost per hour (€/h).

$T_{Mat.change}$  represents a constant amount of time, which is in average required for a material change. It is assumed that  $T_{Mat.change}$  is independent of the affected materials. Factor  $F_{Mat.change}$  allows to determine how this effort is assigned on a build job basis. Its value can either be 1 or 0, if there is a material change or not, respectively. In these cases, the costs will be directly assigned to the specific build job. Alternatively, if the costs shall be equally divided on multiple build jobs, the corresponding frequency can be used as value. For example, if a material change occurs in average each fifth build job, factor  $F_{Mat.change}$  equals 0.2. A build time estimator is included in many of today's AM machines or software solutions, respectively. Hence, this topic will be only slightly touched herein. However, some aspects are essential for a precise cost allocation when building up different parts simultaneously. To estimate the build time, a linear regression model was derived from 24 different



build jobs, including multiple geometries in different quantities. All parts were built up with the same process parameter set allowing to analyse separately the specific influences of composition and geometric properties on total build time. Table 30 summarizes the data of the 24 jobs

Nr.	$T_{Build}$ (h)	$N_L$ (-)	$N_i$ (-)	$V_{tot}$ (mm <sup>3</sup> )	$S_{Supptot}$ (mm <sup>2</sup> )	$S_{tot}$ (mm <sup>2</sup> )
1	5.783	850	5	11,405	4,257	8,880
2	24.783	3,123	3	17,625	50,007	20,931
3	5.767	1,282	2	2,610	1,451	2,640
4	25.517	3,774	18	35,832	0	36,559
5	12.067	1,485	13	15,906	40,671	39,713
6	12.183	1,485	10	17,653	41,356	40,365
7	12.200	1,485	10	17,963	41,163	41,251
8	11.750	1,485	10	16,496	39,188	39,019
9	12.483	1,287	15	17,746	39,878	46,372
10	6.550	690	22	13,864	3,141	41,814
11	18.117	1,368	26	34,763	26,304	39,712
12	9.700	1,136	4	21,006	7,680	19,561
13	8.717	1,294	14	10,489	0	20,427
14	12.800	1,313	6	28,843	13,606	23,186
15	13.350	2,863	1	3,353	7,517	4,611
16	24.600	2,318	9	68,790	33,447	38,848
17	20.017	4,102	4	31,208	0	14,408
18	18.083	4,102	4	31,208	0	14,408
19	27.900	5,061	1	13,305	36,580	18,639
20	17.483	2,434	1	13,165	35,811	18,300
21	2.167	635	4	964	0	2,348
22	8.983	707	6	28,197	12,919	17,841
23	34.117	4,150	2	51,988	66,364	29,516
24	31.000	4,148	2	65,116	33,002	38,774

Table 30: Data table of the 24 build jobs serving as basis for the linear regression model (Rickenbacher et al., 2013).

. The following equation results from the linear regression to estimate the total build time of a build job:

$$\sum_i T_{Build}(P_i) = a_0 + a_1 * N_L + a_2 * V_{tot} + a_3 * S_{Supptot} + a_4 * \sum_i N_i + a_5 * S_{tot}$$

where:

$T_{Build}$  – building time (h).

$P_i$  – part with  $i$ th geometry (-).

$a_0, \dots, a_5$  – regression coefficients.

$N_L$  – number of layers (-).

$V_{tot}$  – total volume of the build job (mm<sup>3</sup>).

$S_{Supptot}$  – total surface area of the support structures (mm<sup>2</sup>).

$S_{tot}$  – total surface area of the build job ( $mm^2$ ).

For a precise cost allocation it is crucial to divide accordingly the time fractions on all parts. Thus, different rules and algorithms have to be applied to each fraction contributing to the total build time. As shown in Figure 38, during manufacturing the amount of processed parts varies from layer to layer, since the parts heights are different. In the dark grey slice three parts are affected, two in the grey slice and finally in the light grey slice only the king is built up. Therefore, time fraction resulting from the total amount of layers has to be allocated to each part on a layer-wise basis. Otherwise smaller parts will be wrongly priced up because of the simultaneous build up. To avoid this, the following algorithm was developed: 1) Ordering of the parts by increasing height; 2) Calculation of the time fraction resulting from the amount of layers up to the smallest part height and divide it equally on all parts. Another approach would be to divide it proportional to the corresponding cross-section. This would require a layer-wise analysis of each part resulting in a more complex algorithm inappropriate for industrial use. Therefore, the first approach was chosen; 3) Choose of the next taller part; 4) Calculation of the time fraction from the previous to the height of the actual part; 5) Division of the calculated time equally on all parts with a part height equal or greater than actual part's height; 6) Repetition of steps 3)-5) until all parts are processed.

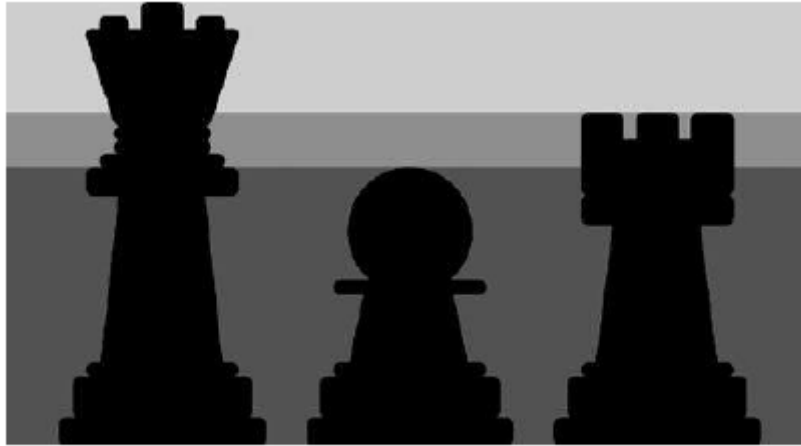


Figure 38: Simultaneous build-up of multiple parts with different heights requires a layerwise time allocation (Rickenbacher et al., 2013).

This algorithm allows calculating the layer-dependent fraction  $T_L(P_i)$  of total build time per part. The geometry dependent factors can be easily allocated based on part's geometry properties. Remaining regression coefficients  $a_0$  and  $a_4$  can be split equally on each part, resulting in the following equation to calculate the total build time of each part:

$$T_{Build}(P_i) = \frac{a_0}{\sum_i N_i} + T_L(P_i) + a_2 * V(P_i) + a_3 * S_{Supp}(P_i) + a_4 + a_5 * S(P_i)$$

where:

$T_L$  – layer-dependent fraction (h).

$V$  – volume of the part ( $mm^3$ ).

$S_{Supp}$  – surface area of the support structures ( $mm^2$ ).

$S$  – surface area of the part ( $mm^2$ ).

Based on the part's total build time, the SLM manufacturing costs of each part can be calculated as follows:

$$C_{Build}(P_i) = T_{Build}(P_i) * (C_{Machine} + C_{Inertgas}) + V(P_i) * C_{Material}$$

where:

$C_{Build}$  – cost for building up the part (€).

$C_{Inertgas}$  – cost per hour for inert gas consumption (€/h).

$C_{Material}$  – material costs (€/kg).

Since the material degradation in the SLM process is of less importance compared to SLS, it is assumed herein, that the compensation for any material degradation or losses is already included in the material costs  $C_{Material}$ . Alternatively, an additional factor can be introduced in the precedent equation to compensate material degradation and losses. The required time to extract the substrate plate and the parts, to recycle and sieve the powder as well as for the machine clean-up is assumed to be independent of the part quantity and geometry. Therefore, this time  $T_{Removal}$  can be evenly allocated on all parts. Throughout the needed time  $T_{Removal}$  the machine is blocked for other tasks. Again, a potential handling under protective gas atmosphere is taken into account with the corresponding factor  $F_{Inertgas}$ :

$$C_{Removal}(P_i) = F_{Inertgas} * T_{Removal} * \frac{(C_{Oper} + C_{Machine})}{\sum_i N_i}$$

where:

$C_{Removal}$  – costs for removing the part from the SLM machine (€).

$T_{Removal}$  – time required for removing parts from the SLM machine (h).

Removing built parts from the substrate plate can be done by means of wire electrical discharge machining (EDM), sawing or the like. In the present work, EDM is assumed to be used. Thereby, the required effort is always proportional to the area of each part, over which it is connected with the substrate plate. The connection area can be approximately derived from the geometry  $G_i$  related bounding box, whereby no distinction between the connection via support structures or bulk material is made. Therefore, the costs  $C_{EDM}$  correspond to a fixed price per plate, resulting in the following cost allocation:

$$C_{Substrate}(P_i) = \frac{C_{EDM}}{\sum_i A_{Con}(G_i)} * A_{Con}(G_i)$$

where:

$C_{Substrate}$  – costs to separate parts from substrate plate (€).

$C_{EDM}$  – costs for EDM process to separate parts from substrate plate (€).

$A_{Con}$  – connection area between parts and substrate plate (mm<sup>2</sup>).

$G_i$  –  $i$ th geometry (–).

Part post-processing includes removal and mending of support structures as well as possible surface post treatment, e.g. by sand or steel grit blasting. The operator's time required for post-processing

$T_{Postp}$  strongly depends on specific geometry  $G_i$ .  $C_{Tools}$  represents the hourly rate of all tools and machines needed for post-processing:

$$C_{Postp}(P_i) = T_{Postp}(G_i) * (C_{Oper} + C_{Tools})$$

where:

$C_{Postp}$  – costs for post-processing (€).

$T_{Postp}$  – time required for post-processing (h).

$C_{Tools}$  – cost per hour for a workplace including all required tools for post-processing (€/h).

Total cost  $C_{Total}$  per part results from summing up costs of each process step:

$$C_{tot}(P_i) = C_{Prep}(P_i) + C_{Buildjob}(P_i) + C_{Setup}(P_i) + C_{Build}(P_i) + C_{Removal}(P_i) + C_{Substrate}(P_i) + C_{Postp}(P_i)$$

where:

$C_{tot}$  – total manufacturing costs (€).

$C_{Build}$  – cost for building up the part (€).

### Results

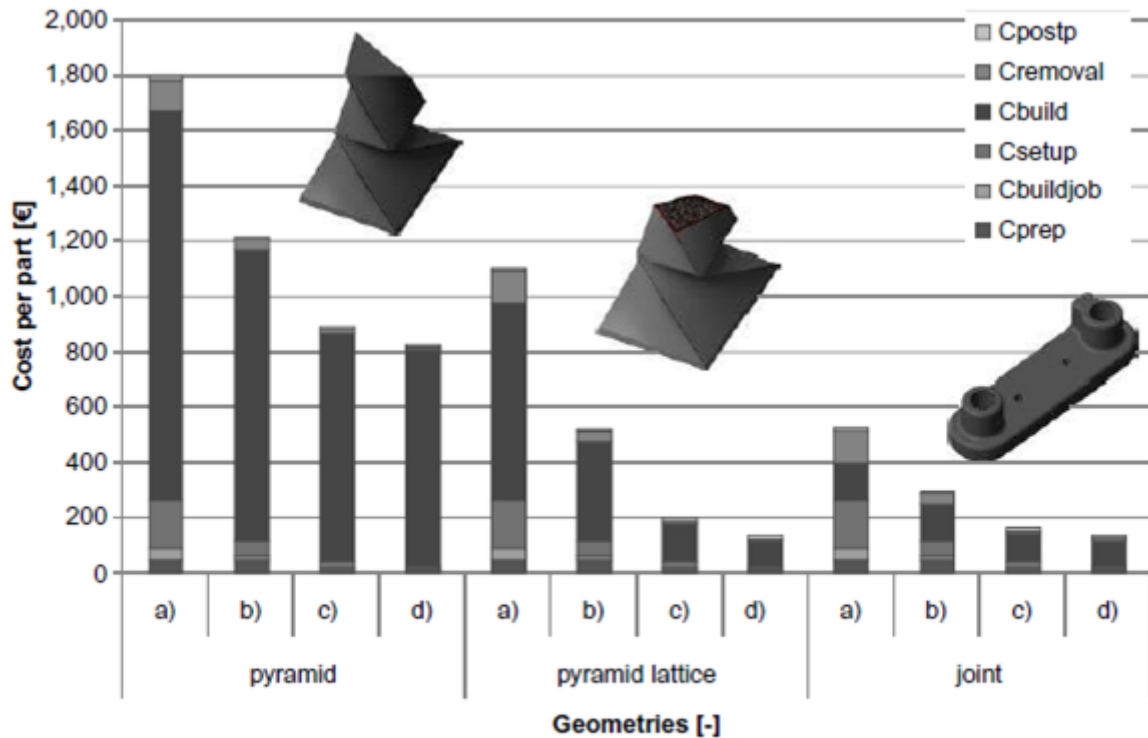
The costs of each process step as well as the achievable cost reduction by building up multiple parts simultaneously will be analysed on the basis of a case study, where an example build job will be manufactured. The build job is summarized in Table 31 and the parts are shown in Figure 39. It is assumed in the following that a quotation shall be calculated and therefore data mainly consist of estimated values.

Geometry ( $G_i$ )	Volume ( $\text{mm}^3$ )	Surface ( $\text{mm}^2$ )	Bounding-box ( $W \times L \times H$ ) (mm)
$i = 1$	14,650	4,912	$42 \times 48 \times 51$
$i = 2$	4,900	18,767	$42 \times 48 \times 51$
$i = 3$	2,020	1,783	$12 \times 42 \times 10$

Table 31: Build job composition used for the case study (Rickenbacher et al., 2013).

The presented equations and algorithms were used to estimate cost per part of the geometries shown in Figure 39. If each geometry is built up in a separate build job, the resulting cost split can be found in Figure 39 case (a). The results of the cost model are shown in Figure 39 cases (b)-(d) if one, three or five pieces of each geometry are built up simultaneously together in one build job, respectively. The parameter values used for this case study can be found in Table 32. As can be seen from Figure 39, in average a cost reduction of 41 per cent can be achieved, when building one part of each geometry together in a single build job. When building up three or five parts of each geometry a further reduction of 38 and 12 per cent results, respectively, indicating that the better the build space is used, the higher the potential savings. Furthermore, by reducing the volume of bulk material by substituting bulk material with lattice structures inside the pyramid, another cost reduction of approximately 40 per cent is achievable. Besides, post-processing, all cost fractions contribute to the cost reduction as can be seen from Figure 39. With decreasing part volumes as well as simultaneous

manufacturing, thereby reducing SLM build up time per part, the fraction on cost per part of pre- and post-processing steps increases. By analysing the manufacturing time more closely, it can be seen from Figure 40, that auxiliary process time, including the coating time needed for the creation of the powder layers, contributes on average 23 per cent and scanning time approximately with 77 per cent to the total time needed.



Notes: Case (a) separate manufacturing of each geometry; cases (b)-(d) part-costs for each geometry, when manufactured together in the same build process for one, two or five parts of each geometry, respectively

Figure 39: Cost splitting for each geometry according to the cost model (Rickenbacher et al., 2013).

The coating time depends only on the total height of the build job and not on the amount of parts. Therefore, when building parts simultaneously the coating time can be divided on more parts, thereby reducing time required per part. Since this alone would not result in a build time reduction of 41 per cent, as shown in the example above, it is evident that further synergies regarding scanning and auxiliary processes can be used. For example, this could be time required for parameter loading, parameter adjusting as well as time required to move the laser beam from one part to another. Although additive manufacturing (AM) and Subtractive Methods (SMs) offer several unique advantages, there are technological limitations such as tolerance and surface finish requirements; tooling and fixturing, etc. that cannot be met by a single type of manufacturing. In Manogharan et al. (2015), the authors present economic models for a new hybrid method where AM and SM are integrated. The authors outline the operations of a hybrid direct manufacturing system that uses an additive manufacturing process (e.g. EBM) followed by the use of CNC-RP to form a hybrid direct manufacturing process. However, it should be noted that the developed AIMS system can be implemented using any AM process. In the AIMS hybrid system, the part is processed in two separate machines: 1) the near-net shape fabrication through additive manufacturing (e.g. EBM or direct metal laser sintering (DMLS)), and then 2) a CNC-RP ‘finish’ machining where in a layered manner in a 4-axis CNC machining centre, the part is produced within specified tolerances. The processing

environment in powder bed fusion processes such as EBM or DMLS is not ideal to incorporate machine tools within the build volume.

Parameter	Description	Value	Unit
$T_{Prep}$	Time required for preparing CAD data	0.25	(h)
$C_{Oper}$	Operator's hourly rate	90	(€/h)
$C_{PC}$	Hourly rate of the workstation including costs of required software and tools	90	(€/h)
$T_{Buildjob}$	Time required for build job assembly	0.25	(h)
$T_{Setup}$	Time required for machine set up	0.75	(h)
$F_{Inertgas}$	Factor to model extra effort required for handling in protective gas environment	1	(-)
$F_{Mat.change}$	Factor to model the frequency of material changes	0	(-)
$T_{Mat.change}$	Time required to change material	0.75	(h)
$C_{Machine}$	Machine's cost per hour	90	(€/h)
$a_0$	Regression coefficient	-1.29	(h)
$a_1$	Regression coefficient	$4.53 \cdot 10^{-3}$	(h)
$a_2$	Regression coefficient	$1.80 \cdot 10^{-4}$	(h/mm <sup>3</sup> )
$a_3$	Regression coefficient	$1.59 \cdot 10^{-4}$	(h/mm <sup>2</sup> )
$a_4$	Regression coefficient	0.348	(h)
$a_5$	Regression coefficient	$-1.33 \cdot 10^{-4}$	(h/mm <sup>2</sup> )
$C_{Inertgas}$	Cost per hour for inert gas consumption	20	(€/h)
$C_{Material}$	Material costs	150	(€/kg)
$T_{Removal}$	Time required for removing parts from the SLM machine	0.5	(h)
$C_{EDM}$	Costs for EDM process to separate parts from substrate plate	150	(€)
$T_{Postp}$	Time required for post-processing	0.1	(h)
$C_{Tools}$	Cost per hour for a workplace including all required tools for post-processing	40	(€/h)

Table 32: Parameter values used in the case study (Rickenbacher et al. 2013).

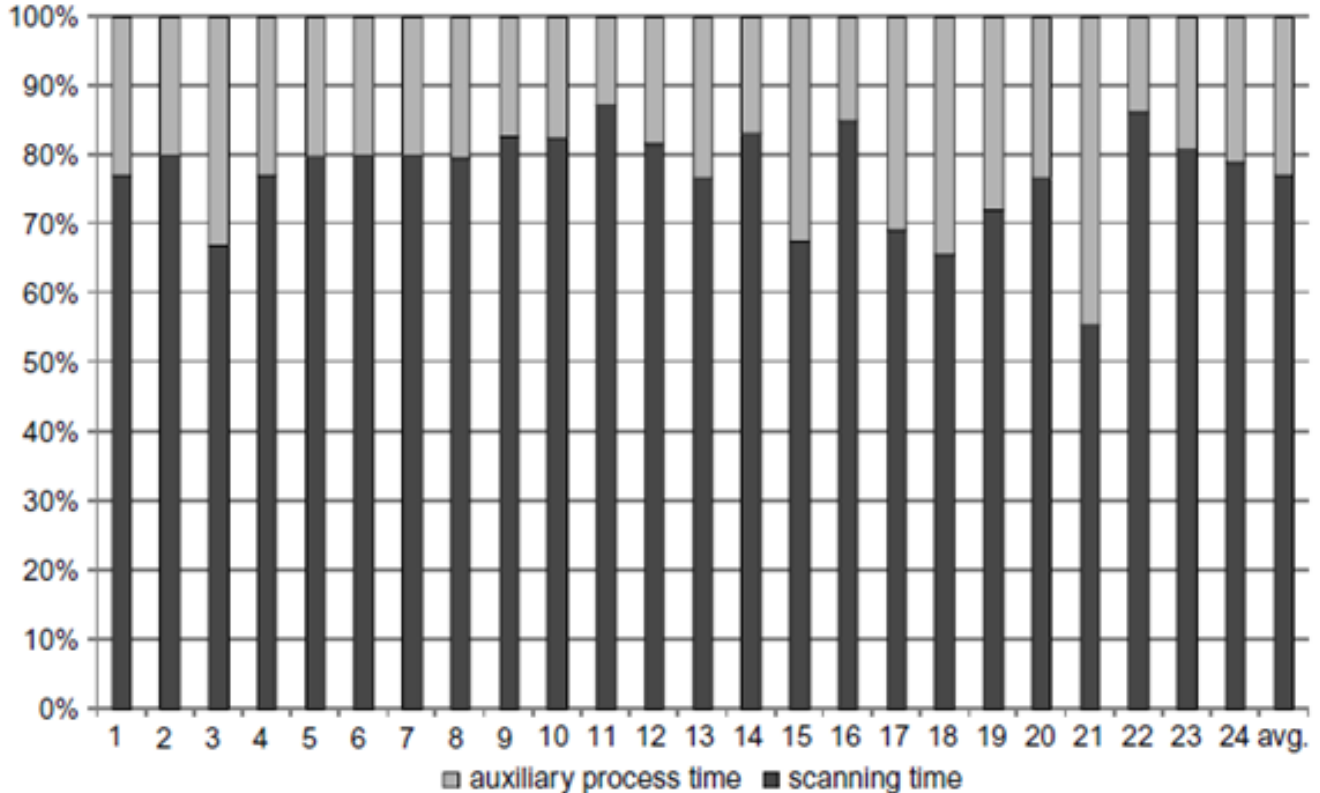


Figure 40: Manufacturing time of 24 different build jobs, divided in scanning and auxiliary process time (Rickenbacher et al.; 2013).

This approach expedites the hybrid production of multiple batches (depending on batch build time and only finish machining time) by increasing the availability and efficiency of both the machines. In other words, additive manufacturing of batch ‘x’ and subtractive only finish machining of near-net shape units in batch ‘x – 1’ in CNC-RP can be simultaneously conducted. Since, relatively lower percentage of production time per unit part is spent on CNC-RP processing when compared to AM processing, the CNC machine can then be used to process multiple (or other) unit parts when the AM machine processes the next batch.

### Economic model

In this cost model, the energy costs of AM and CNC-RP are included in their respective manufacturing cost. The time for preparation of process parameters in terms of NC codes (CNC-RP) and additive manufacturing process files are approximately the same (and small typically < 60 minutes), and the engineering cost is not included in the model. For highly complex geometries, it is recommended to include this cost. The cost model is material and activity-based, and the notation for all the major cost factors is detailed in Table 33.

General factors			CNC-RP specific factors		
$C_{unit}$	\$	Cost per unit	$S_v$	mm <sup>3</sup>	Volume of bar stock
$P_v$	mm <sup>3</sup>	Part volume	$t_{hog}$	hr	Time for hogging operation
$SP_v$	mm <sup>3</sup>	Support volume-sacrificial supports	$t_{rough}$	hr	Time for roughing operation
$C_{process}$	\$/hr	Operating cost for each process	$t_{finish}$	hr	Time for finishing operation
$C_{mat}$	\$	Cost of the material in each process	$t_{tool\_life}$	hr	Cutting tool life duration
$t_{build}$	hr	Time to fabricate the part in the additive process	$t_{tool\_change}$	hr	Time for changing tool and tool set-up time
$t_{setup\_process}$	hr	Setup time in each process	$\Delta V$	mm <sup>3</sup>	Total volume removed at each stage in CNC-RP
$t_{post\_process}$	hr	Post-processing time in each process	<b>MRR</b>	mm <sup>3</sup> /hr	Material removal rate at each stage in CNC-RP
<b>EBM specific factors</b>			$C_{tooling}$	\$/tool	Cost of cutting tools
$n_{EBM}$	–	Number of layers in EBM fabrication	$Nf$	–	Number of tool changes in each stage
$P$	kg/mm <sup>3</sup>	Density of metal powder used	$C_{tooling}$	\$/tool	Cost of cutting tools
$t_{EBM}$	hr	Total build time in EBM			
$t_{plate}$	hr	Time to pre-heat the start plate to required temperature before fabrication			
$t_{cool}$	hr	Time to cool the build volume, retrieve part and recycle unused powder			

Table 33: Nomenclature used for cost models for additive, subtractive and hybrid processes (Manogharan et al., 2015).

**Additive manufacturing cost model.** For many additive manufacturing processes, unit cost can be simplified as a function of set-up time, part height (i.e. number of layers), summation of cross-sectional area of each layer and post-processing time. For a part with n layers, where  $t_{build\_i}$  is the build time for layers  $i = 1, 2, \dots, n$ , the total manufacturing time and unit cost are formulated as:

$$C_{unit} = C_{material} + (C_{add} * t_{add})$$

$$t_{add} = t_{setup\_add} + \sum_{i=1}^n (t_{build\_i}) + t_{post\_process}$$

The generic model presented in these two equations can be adapted to any layer-by-layer manufacturing methods depending on individual cost components in each layer (e.g. different part

and support generation parameters) and the corresponding setup and post-processing time such as annealing. In the following sections, this model is extended to two specific systems: CNC-RP and the AIMS hybrid process.

*CNC-RP cost model.* In the case of CNC-RP, the manufacturing cost is a function of: cost of the stock, total machining time and the tooling cost. The machining time is determined based on the total volume of metal to be removed from the stock ( $\Delta V$ ) for a given Mean Reciprocal Rank (MRR), i.e.  $\Delta V/MRR$ . Furthermore, the tool geometry, feed rates and depth of cut will vary in hogging, roughing and finishing stages, leading to decreasing MRR. The setup time ( $t_{setup\_CNC-RP}$ ) is assumed to be uniform irrespective of the part volume (because the stock is fixtured across two chucks). Furthermore, the material cost ( $S_v$  – stock volume) is based on part orientation (a cylinder with a minimum diameter equal to the diagonal of the part). The post-processing step in CNC-RP is the removal of sacrificial supports which takes negligible time and is not considered in the cost model derived from the following equations as shown below:

$$C_{unit} = (S_v * C_{mat_{CNC-RP}}) + (C_{CNC-RP} * t_{CNC-RP}) + (C_{tooling} * n_{stage})$$

$$t_{CNC-RP} = t_{setu_{CNC-RP}} + t_{hog} + t_{rough} + t_{finish}$$

$$n_t = \frac{\Delta V}{MRR} * \left( \frac{1}{t_{tool\_life}} \right)$$

$$t_{stage} = \frac{(\Delta V)}{MRR} + (n_t * t_{tool\_change})$$

At every ‘stage’ of CNC-RP (roughing, semi-roughing and finishing), there are two time components namely; machining time and tool change operations. Subsequently, the unit cost of the CNC-RP made part is derived from the manufacturing time ( $t_{CNC-RP}$ ), material cost and tooling cost.

*AIMS cost model.* The developed hybrid process has two steps: AM and ‘finishing’ stage of CNC-RP. First, the cost model for AM is developed by integrating EBM-specific process steps for the total build time in the following equation:

$$\sum_{i=1}^n (t_{build\_i}) = t_{plate} + t_{raking} + t_{preheating} + t_{melt\_i} + t_{support\_i} + t_{postheating}$$

In this process cost model, the total build time is further expanded to differentiate individual operations in each layer ‘i’ namely; pre-heating of the plate, raking of the metal powder, pre-heating the powder bed, melting the contour (or edges) and part volume, support structures and finally, post-heating scan. Constant plate pre-heating, raking, pre-heating and post-heating duration are assumed. For each layer ‘i’, the melting and support generation time are formulated based on EBM process parameters as shown below:

$$t_{melt\_i} = \sum_{i=1}^n \left( \frac{Contour\ scan\ length}{Contour\ speed} \right) + \sum_{i=1}^n \left( \frac{Melt\ scan\ length}{Melt\ speed} \right)$$

$$t_{support\_i} = \sum_{i=1}^n \left( \frac{Support\ scan\ length}{Support\ speed} \right)$$



In the case of EBM, the post-processing involves cooling down of the build chamber, part retrieval and recovery/recycling of unused powder. Hence, the overall cost-time of the EBM component in this hybrid process is defined as:

$$t_{EBM} = t_{setup\_EBM} + \sum_{i=1}^n (t_{build\_i}) + t_{cool}$$

$$C'_{EBM} = (\eta * (P_v + SP_v) * \rho * C_{kg}) + (C_{EBM} * t_{EBM})$$

Unlike the complete CNC-RP, the subtractive stage of the hybrid system consists of only the finishing stage. Since the sacrificial fixtures used in the subtractive stage are considered as ‘EBM-made part volume’, there is no additional material cost associated with the subtractive stage. The ‘near net’ part from EBM is the stock volume and hence the cost-time CNC-RP component in this hybrid process is defined as:

$$C_{Hybrid} = (C_{CNC-RP} * (t_{setup\_CNC-RP} + t_{finish})) + (C_{tooling} * n_{finish}) + C'_{EBM}$$

In the Chapter 4 will be presented the cost model used in Priarone et al. (2017). This model is applied to the case study build in the AM laboratory of Norwegian University of Science and Technology.

### 3.2 Footprints emission models

As presented in Fishedick et al. (2014), Figure 41 (a) which shows a breakdown of total global anthropogenic Greenhouse Gas (GHG) emissions in 2010 based on Bajželj et al. (2013), illustrates the logic that has been used to distinguish the industry sector from other sectors.

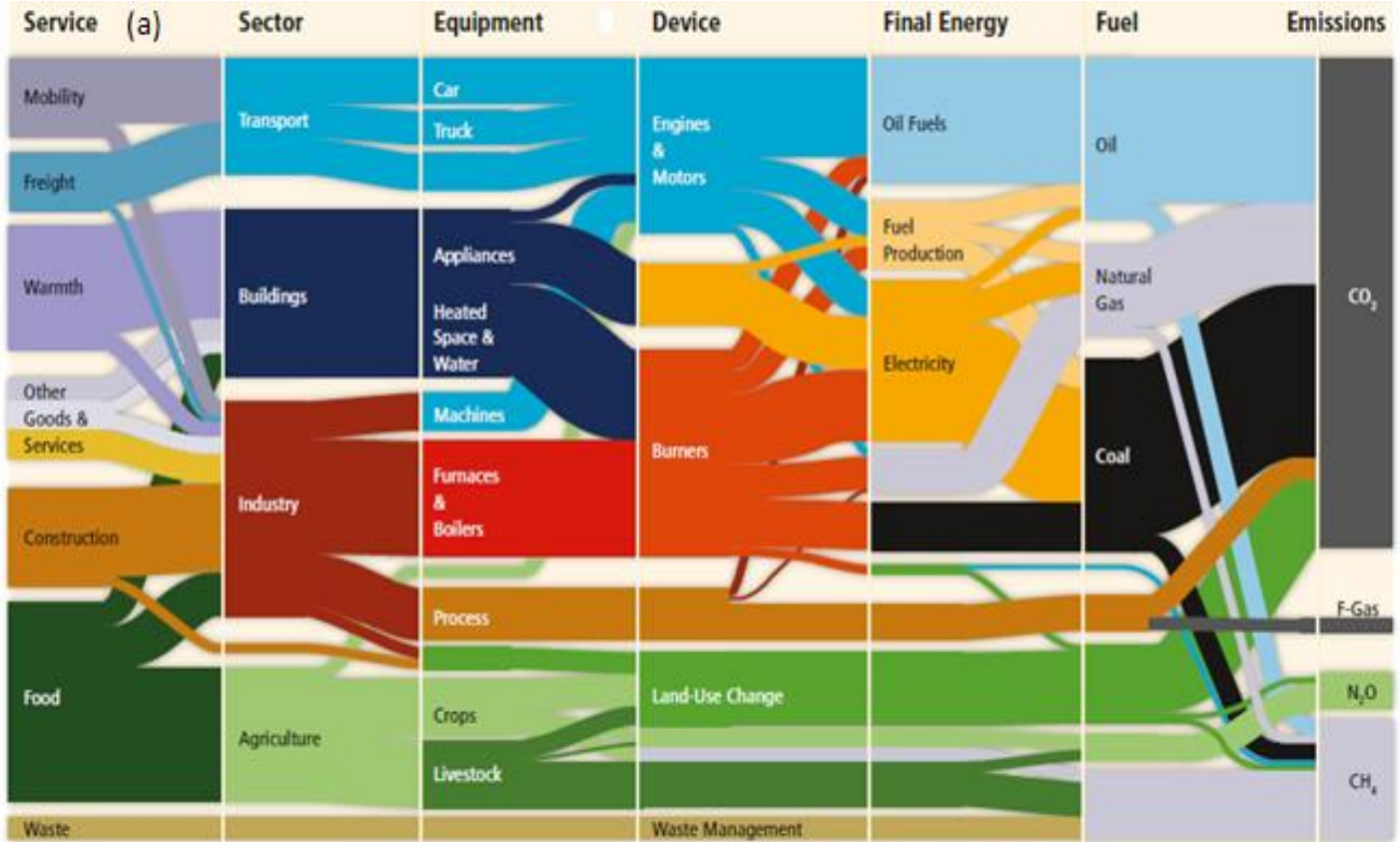


Figure 41: A Sankey diagram showing the system boundaries of the industry sector and demonstrating how global anthropogenic emissions in 2010 arose from the chain of technologies and systems required to deliver final services triggered by human demand (Fishedick et al., 2014).

The figure shows how human demand for energy services, on the left, is provided by economic sectors, through the use of equipment in which devices create heat or work from final energy. In turn, the final energy has been created by processing a primary energy source. Combustion of carbon-based fuels leads to the release of GHG emissions as shown on the right. As assessed by IEA (2016), climate scientists have observed that carbon dioxide (CO<sub>2</sub>) concentrations in the atmosphere have been increasing significantly over the past century, compared to the pre-industrial era level of about 280 parts per million (ppm). In 2015, the average concentration of CO<sub>2</sub> (399 ppm) was about 40% higher than in the mid-1800s, with an average growth of 2 ppm/year in the last ten years. Two sectors produced nearly two-thirds of global CO<sub>2</sub> emissions from fuel combustion in 2014: electricity and heat generation, by far the largest, which accounted for 42%, while transport accounted for 23%. Globally, per-capita emissions increased by 16% between 1990 and 2014, however, contrasting trends were observed amongst the top five emitting countries, generally reducing gaps (Figure 41 (b)).

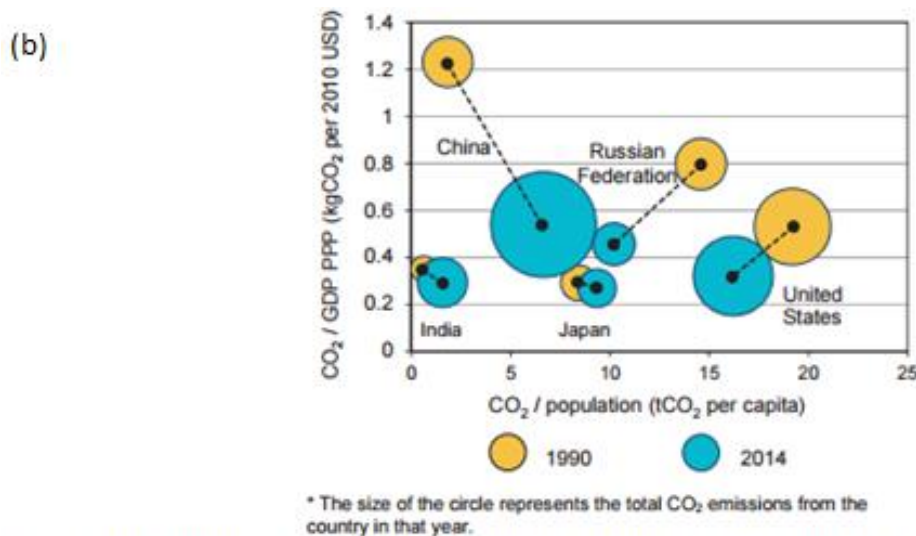


Figure 41: Trends in CO<sub>2</sub> emission intensities for the top five emitting countries (by IEA, 2016).

China more than tripled its per-capita emissions, while India more than doubled theirs (as did some other rapidly expanding economies), reflecting strong per-capita Gross Domestic Product (GDP) growth. Manufacturing accounts for about 98% of the total direct CO<sub>2</sub> emissions from the industrial sector, and is responsible for about 35% of the global electricity use and over a quarter of the primary resource extraction (Fischedick et al., 2014; UNEP, 2011).

The manufacturing of a product is connected directly to the amount of carbon emitted in producing electrical energy for that manufacturing process. In Jeswiet et al. (2008) a new, simple Carbon Emission Signature, CES<sup>TM</sup>, is proposed. The objective of the work in this paper is to develop a method that connects the electrical energy used in manufacturing directly to the carbon emissions (CE) that are created in using the electrical energy. There are two types of energy available: 1) Clean energy, no carbon emissions; 2) Carbon-based energy, with carbon emissions. The environmental goal is to reduce or eliminate carbon emissions. Energy use is benign when no carbon is emitted at the fuel source. In general, energy distribution occurs through electrical power grids. The energy available on an electrical power grid depends upon the primary energy source(s) used; see Figure 42. For instance, if either hydro, solar or wind energy is used to generate electrical energy on a power grid, the energy available on that grid is clean energy. A manufacturing process is carbon free if it uses electrical energy from an electrical power grid that does not use any fossil fuels. This means that between steps A and B in Figure 42 is no combustion. The steps that occur when proceeding from primary energy supplies to energy used in manufacturing, with potential carbon emissions, are shown

in Figure 42. An electrical power grid is supplied by primary energy sources. A list of primary energy sources is given in Figure 42, where fossil fuels are shown at the top, and primary energy sources that do not produce carbon emissions are shown as “green energy”.

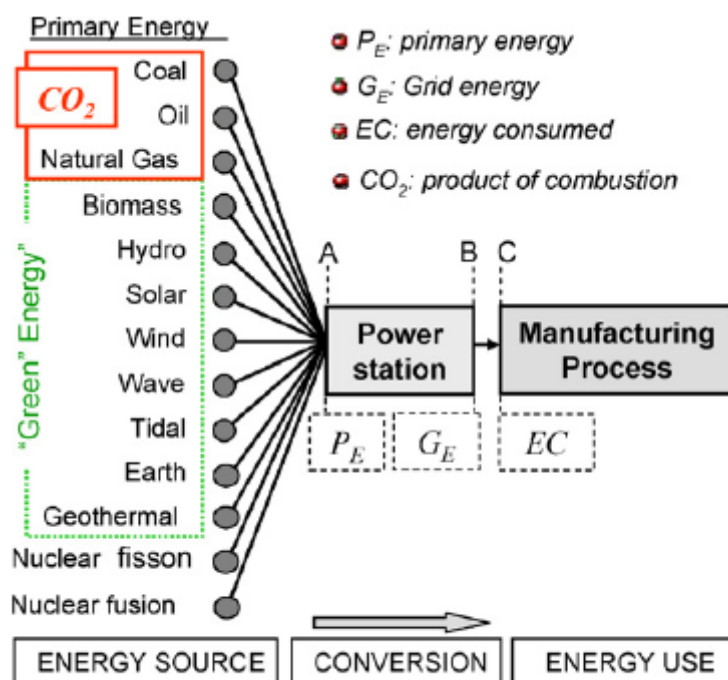


Figure 42: Primary energy supplies available (Jeswiet et al., 2008).

Carbon emissions occur at the point where the primary energy is converted to electricity; this is indicated by the box labeled power station. A primary energy source will have energy content, P<sub>E</sub>. The primary energy is converted to electric energy, G<sub>E</sub>, which is placed on a power supply grid. Electricity is the energy transport medium used. For carbon free primary energy carriers, the energy conversion is direct, without any carbon emissions; hydropower is an example. Whether carbon is a byproduct depends upon the energy carrier. Fossil fuels inherently have carbon emissions. At present, the majority of energy supplied via electrical power grids comes from fossil fuels, hence the concern with carbon emissions. Power grids use a variety of energy sources, including fossil fuels where carbon emission is an inevitable fate of combustion. These are converted into electric energy at the point shown in Figure 42. The four carbon content fossil fuels are: coal, oil, gas and biomass. Combustion reactions and the magnitude of enthalpy changes that occur are shown in Table 34.

Type of fuel	1 GJ of heat produced releases	$\Delta H$ (kJ)	CO <sub>2</sub> (kg)
Coal	$C + O_2 \Rightarrow CO_2$	-394	112
Heavy oil	$C_{20}H_{42} + 30O_2 \Rightarrow 20CO_2 + 21H_2O$	-13300	66
Natural gas	$CH_4 + 2O_2 \Rightarrow CO_2 + 2H_2O$	-890	49
Biomass	$CH_2O + O_2 \Rightarrow CO_2 + H_2O$	-440	100

$\Delta H$  = Enthalpy: heat content; thermodynamic potentia.

Table 34: Energy production fuels, the heat and CO<sub>2</sub> released (Jeswiet et al., 2008).

An electrical power supply grid is the sum of the fractions of primary fuel sources used to create electrical energy for that grid. Examples of two electrical power grids are used for purposes of this paper as shown in Table 35. Fossil fuels often form a fraction of the grid fuel supplies. The fraction of fossil fuel used will determine the amount of carbon created, thereby giving an electrical power grid a Carbon Emission Signature or CES<sup>TM</sup>. The following is a way of accounting for carbon

emissions in systems that use electric power grids. It uses a Carbon Emission Signature, CES<sup>TM</sup>, which has units of kg CO<sub>2</sub>/GJ. CES is a function of a power grid.

Fuel supply	Ontario (%)	NSW (%)
Coal (C)	19	83.9
Natural gas (NG)	7	8.5
Petroleum (P)		0.3
Biomass (B)		
Hydropower (H)	23	7.3
Solar (S)		
Wind (W)		
Geothermal (G)		
Earth (E)		
Wave (Wa)		
Tidal (T)		
Nuclear (N)	51	
Total	100	100
Total renewable	23.0	

Table 35: Power supply grids for two legal jurisdictions, Ontario, Canada, and New South Wales, Austria (Jeswiet et al., 2008).

The Carbon Emitted, CE, due to consumption, can be found by multiplying energy consumed, EC, by the Carbon Emission Signature, CES:

$$CE = EC(GJ) * CES(kgCO_2/GJ)$$

A grid provides electrical energy ( $G_E$ : grid energy) and is made up of the sum of fractions of the primary sources multiplied by the conversion efficiency,  $\eta$ , for each energy source. Each electrical power grid has a Carbon Emission Signature, CES. The CES can be found from:

$$CES = \eta * [112x\%C + 49x\%NG + 66x\%P]$$

The coefficients, 112, 66, and 49 are an inevitable fate of combustion and are the kilograms of carbon emitted per gigajoule of heat released in each case. These can be found in Table 34. These always occur. A conversion efficiency of  $\eta = 0.34$  is common and is used in this paper. Therefore for any system that uses electrical energy from a power grid, the carbon emissions can be calculated by multiplying energy consumed by the Carbon Emission Signature, CES. Table 36 shows examples of CES values for Table 34.

Place of production	CES <sup>TM</sup> (kg/GJ)	C (%)	NG (%)	P (%)
ONT	74	0.19	0.07	0
NSW	295	0.84	0.085	0.003

Table 36: CES values for Ontario, NSW electrical grids (Jeswiet et al., 2008).

### *Manufacturing a single part*

If a part is manufactured using a local power grid, the carbon emitted in manufacturing the single part,  $CE_{part}$ , can be found by applying equation:

$$CE_{part} = EC_{part}(GJ) * CES(kgCO_2/GJ)$$

$EC_{part}$  is the energy consumed in making a part (GJ). This is for one part. However, the energy consumed in making a part,  $EC_{part}$ , can be broken down into components, including energy for ancillary operations ( $EC_{ancillary}$ ).

$$EC_{part} = EC_T + EC_{ancillary}$$

ECT is the energy consumed for a type of production process.  $EC_{ancillary}$  is the energy for operations needed to run the process, such as pumps, cooling media, etc. It should be noted that  $EC_{ancillary}$  can be large in a manufacturing process where supporting equipment such as hydraulic pumps run continuously while the primary process is idle. If all the parts, called NP, to be manufactured are included, the foregoing simply becomes:

$$EC_{parts} = EC_{part} * NP$$

The need for environmental impact analyses becomes more and more urgent if the increasing success of additive manufacturing (AM) approaches is taken into account.

### Manufacturing examples

*Energy consumption in turning.* The following is an example for turning a high strength titanium alloy bar and an aluminum bar. A single cut is made at  $N = 800$  rpm. The workpiece dimensions are: 152.4 mm long with a 12.7 mm diameter. Final dimension is 12.2 mm. The tool travels at 3.39 mm/s. A specific energy can be found on the literature, at  $5 \text{ J/mm}^3$  for titanium and at  $1 \text{ J/mm}^3$  for aluminum. The energy consumed in turning titanium is 7722 J, and for aluminum it is 1699 J.

*Energy consumption for open die forging.* A round aluminum billet, 25.4 mm diameter by 25.4 mm high is compressed. The strain is  $\epsilon = 0.181$ . The model used is  $s = 172e^{0.25}$  MPa. The energy,  $EC_{part}$ , is 592 J.

*Carbon emitted.* The carbon emitted is found for the two foregoing production, for two grids, each having its own CES. The results are presented in tabular form in Table 37. The values shown are very small. However, each is for one part and if larger production quantities are taken into account, along with the difference in CES of 4, then the economic consequences become important.

CES <sup>TM</sup>	ONT	NSW	EC (kJ)	Process
	74	295		
g CO <sub>2</sub>	0.000572	0.002279	8	(1)
g CO <sub>2</sub>	0.000126	0.000501	2	(2)
g CO <sub>2</sub>	0.000044	0.000176	0.6	(3)

Process (1), turning titanium bar; Process (2), turning aluminum bar; Process (3), compressing aluminum billet.

Table 37: CE (g CO<sub>2</sub>), turning and open die forging (Jeswiet et al., 2008).

The electrical energy is the source of alimentation for additive manufacturing processes, not only for the printing phase but also to supply the others necessary tools like cooling and atmosphere generator system, etc., and all the ancillary activities like machining operations. The energy input is higher in metal AD technologies because they use tools that produce laser or electronic beams, necessary to bring at the right temperature the metal powders. Moreover the atomization process for the creation of metal powders is known for being a high CO<sub>2</sub> quantity producer. Because of the strong diffusion of these technologies it is important to study models able to evaluate their emissions.

The growing interest in quantifying the CO<sub>2</sub> footprint of processes has led to the development of a methodology for the systematic analysis and improvement of the manufacturing Unit Process Life Cycle Inventory (UPLCI). It is also interesting to make comparisons between AD and Conventional Manufacturing (CM) processes not only about the energy necessary to build the same product but also to the CO<sub>2</sub> emissions.

In Ingarao et al. (2017) is presented a model used to assess the life-cycle impact of metal-based components produced via 1) conventional subtractive manufacturing (CM hereafter), and 2) additive manufacturing plus finish machining (AM + FM hereafter). According to Ashby (2013), the environmental impacts of material production, part manufacturing, transportation, use, and disposal should be included when considering a cradle-to-grave system boundary. Figure 43 schematizes the main flows that characterize the life cycle of a component manufactured by means of CM and AM + FM. The functional unit is a single produced part. The different contributions to the primary energy demand and CO<sub>2</sub> emissions are presented and discussed in the following subsections.

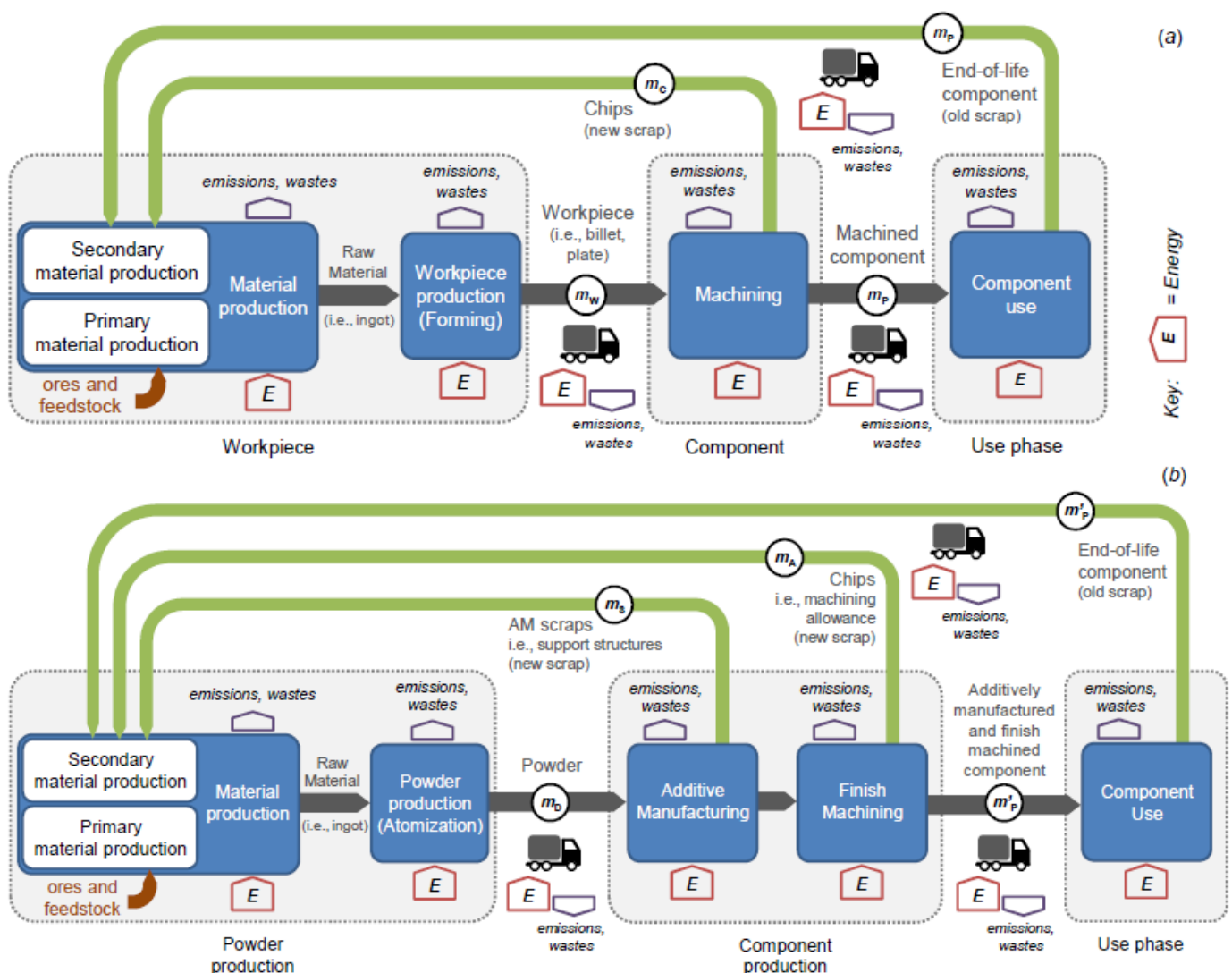


Figure 43: The main flows in conventional machining (a) and additive manufacturing plus machining (b) approaches, showing the recycling paths (Ingarao et al., 2017).

### Material production

The material of the workpiece for CM has to be made by way of primary or secondary production, and then formed to get the desired geometry (i.e., a billet, a slab, a block, etc.). An atomization

process, which is needed to obtain the metal powder, follows the material production phase for AM. The workpiece mass ( $m_w$ , in kg) for CM consists of the mass of the component ( $m_p$ ) plus the mass of the machined chips ( $m_c$ ). The required powder mass ( $m_D$ , in kg) for AM is made up of the masses of the component ( $m_p$ ), of the built-up supports ( $m_s$ ), and of the machining allowance ( $m_A$ ) for the post-process finishing operations. In addition, the process scraps should include, among others, the amount of metal powder that cannot be recovered and/or reused (e.g., as a consequence of thermal degradation phenomena). As far as EBM processes are concerned, some authors have proved that the chemical contents of the powder material are maintained even after numerous reuses, with no measurable undesired effects on the process. Petrovic and Ninerola (2015), for instance, studied the level of atomized Ti-6Al-4V powder recyclability, in compliance with aeronautical standards, while Nandwana et al. (2016) studied the recyclability of both Inconel 718 and Ti-6Al-4V powders. Moreover, it is worth remarking that material losses during the parameter setting and optimization phases for AM processes (i.e., at the beginning of a new batch production) have been neglected in the present model. The primary energy demand for material production ( $E_{MAT}$ , in MJ per produced part) is computed by applying the following two equations in the CM approach and the AM + Finish Machining (FM) approach, respectively.

The amount of material required for all the subsequent processing operations ( $m_w$  or  $m_D$ ) is multiplied by the corresponding embodied energy  $E_E$  (in MJ/kg). In addition, as shown in Figure 43, the energy necessary for forming ( $E_F$ , in MJ/kg) the workpiece (in the case of machining) as well as the energy for the atomization ( $E_A$ , in MJ/kg) of the metal powder (in the case of additive manufacturing) are both accounted for.

$$E_{MAT}^{CM} = \overbrace{(m_p + m_c)}^{m_w} \cdot (E_E + E_F) \quad \left( \frac{MJ}{part} \right)$$

$$E_{MAT}^{AM+FM} = \overbrace{(m'_p + m_A + m_s)}^{m_D} \cdot (E_E + E_A)$$

$$= \overbrace{(k \cdot m_p + m_A + m_s)}^{m_w} \cdot (E_E + E_A) \quad \left( \frac{MJ}{part} \right)$$

Furthermore, the particular features of the layer-by-layer production, coupled with the design for AM methodologies and the topological/topographical optimization, could lead to a reduction in the masses of the components, while ensuring the same in-work performance of conventionally machined products (as highlighted by Huang et al., 2016). As a result, the mass of the component produced via AM + FM ( $m'_p$ ) could be lower than that of CM ( $m_p$ ). The  $k$  factor, which is smaller than or equal to 1, is introduced into the second equation, in order to account for the weight reduction potential of the components produced via AM. If  $k = 1$ , no weight reductions are considered. If  $k = 0.9$ , a weight reduction of 10% is expected when the AM + FM approach is used.  $CO_2$  emissions could be assessed in a similar way by replacing the energy factors  $E_E$ ,  $E_F$ , and  $E_A$  in the two equations with the carbon footprints arising from material production ( $CO_{2E}$ ), forming ( $CO_{2F}$ ), and atomization ( $CO_{2A}$ ). The embodied energy ( $E_E$ ) and the carbon emissions ( $CO_{2E}$ ) for material production have been computed by applying the substitution method presented in the following two equations, respectively, as a function of the fraction of recycled material at its end of life ( $r$ ). The full benefit of recycling the material is allocated to the end of life, and no benefit is considered for incoming recycled materials, which are effectively neglected (Hammond and Jones, 2010). The new scraps (such as the chips obtained from the machining process) as well as the old scraps (derived from the part disposed of at the end of its first life) are both considered in this research (as presented in Priarone et al., 2016a).

$$E_E = E_V - r \cdot (E_V - E_R) \quad \left( \frac{\text{MJ}}{\text{kg}} \right)$$

$$\text{CO}_{2E} = \text{CO}_{2V} - r \cdot (\text{CO}_{2V} - \text{CO}_{2R}) \quad \left( \frac{\text{kg}}{\text{kg}} \right)$$

### Manufacturing

The primary energy demand for part manufacturing ( $E_{\text{MFG}}$ ) is assessed (in MJ/part) by means of the two following equations for the CM approach and the AM + FM approach, respectively. In both cases, the material involved in the manufacturing process (the removed material  $m_C$  and  $m_A$ , or the deposited material  $m_D$ ) is multiplied by the specific primary energy demand of each approach ( $U_E$ , in MJ per kg of processed material), which could include the contributions of the consumables, such as the lubricants and the cutting tools used for machining (Priarone et al., 2016b), or the supply gases necessary for additive manufacturing (Baumers et al., 2016). This black-box modelling method empirically correlates the main process parameters to the energy demand. The modelling detail is lower than that of bottom-up methods, which split the total energy consumption into the contributions from the machine states and/or components (Guo et al., 2015). However, the accuracy of the model is assumed to be satisfactory for the purposes of the present paper. A finish machining (FM) approach is envisaged for AM for the removal of the machining allowance  $m_A$ .  $\text{CO}_2$  emissions arising from the manufacturing stage could be assessed by substituting the  $U_E$  value with the specific carbon footprint per each kg of processed material ( $U_{\text{CO}_2}$ , in kg/kg).

$$E_{\text{MFG}}^{\text{CM}} = m_C \cdot U_E^{\text{CM}} \quad \left( \frac{\text{MJ}}{\text{part}} \right)$$

$$\begin{aligned} E_{\text{MFG}}^{\text{AM+FM}} &= \overbrace{(k \cdot m_P + m_A + m_S) \cdot U_E^{\text{AM}}}^{E_{\text{MFG}}^{\text{AM}}} + E_{\text{MFG}}^{\text{FM}} \\ &= (k \cdot m_P + m_A + m_S) \cdot U_E^{\text{AM}} + m_A \cdot U_E^{\text{CM}} \quad \left( \frac{\text{MJ}}{\text{part}} \right) \end{aligned}$$

### Transportation

The approximate transportation energy ( $E_{\text{TRN}}$ ) and carbon footprint ( $\text{CO}_2_{\text{TRN}}$ ) can be computed for each  $i$ -th transport of the life cycle. The energy ( $E_T$ , in MJ/kg\*km) or the  $\text{CO}_2$  ( $\text{CO}_2_T$ , in kg/kg\*km) penalty per unit weight and distance of the specific transportation type/fuel should be multiplied by the  $i$ -th moved mass and the  $i$ -th travelled distance. Fuel-vehicle coefficients are available in literature for this purpose (see, for example, Ashby, 2013).

$$E_{\text{TRN}} = \sum_{i=1}^n E_T \cdot m_i \cdot d_i \quad \left( \frac{\text{MJ}}{\text{part}} \right)$$

Only the main transportations listed in Table 38 have been considered for the approaches schematized in Figure 43. The additive manufacturing and the conventional machining equipment are assumed to work alongside each other, in the same production plant. Two different material suppliers are supposed for the provision of the workpiece and metal powder.



Transport	From	To	Moved mass		Distance	
			CM	AM + FM	CM	AM + FM
1	Material supplier	Production plant	$m_P + m_C$	$k \cdot m_P + m_A + m_S$	$d_1$	$d'_1$
2	Production plant	Point of sale	$m_P$	$k \cdot m_P$	$d_2$	
3	Production plant	Recycling plant	$m_C$	$m_A + m_S$	$d_3$	
4	Disposal site	Recycling plant	$m_P$	$k \cdot m_P$	$d_4$	

Table 38: Moved masses and travelled distances for each i-th(main) transportation in the life cycle (Ingarao et al., 2017).

### Use

The assessment of the energy demand and carbon emissions during the use phase deserves particular attention. According to Ashby (2013), two different classes of contributions can be identified. The contribution of the static products to the use phase is related to the power that is consumed by (in the case of powered apparatus), or on behalf of the product itself. For the products that are part of, or are carried by a transportation system, the masses directly affect energy consumption and the CO<sub>2</sub> burden. It is worth pointing out that, as far as different manufacturing approaches are concerned, the use phase could be neglected if the achievable product specifications are the same, and therefore if the in-use performance is expected to remain unchanged. This criterion has already been applied by the authors in a previous research (Ingarao et al., 2016). A potential weight reduction has been hypothesized in the present paper for the components produced via the AM + FM approach, and a k factor (lower or equal to 1) has been introduced into the previously presented equations. As a result, the in-use performance might differ, particularly for parts belonging to a transportation system (such as for aerospace or automotive components).

### Empirical models for the CM and AM + FM manufacturing approaches

The above mentioned considerations lead to the following two equations, which describe the energy demand throughout the whole life cycle for components produced by the CM approach and AM + FM approach, respectively (to be planned as in Figure 43). As mentioned above, CO<sub>2</sub> emissions can be assessed in a similar way.

$$E^{CM} = \underbrace{(m_P + m_C) \cdot (E_E + E_F)}_{E_{MAT}^{CM}} + \underbrace{m_C \cdot U_E^{CM}}_{E_{MFG}^{CM}} + \underbrace{E_T \cdot [(m_P + m_C) \cdot d_1 + m_P \cdot d_2 + m_C \cdot d_3 + m_P \cdot d_4]}_{E_{TRN}^{CM}} + E_{USE}^{CM} \left( \frac{MJ}{part} \right)$$

$$E^{AM+FM} = \underbrace{(k \cdot m_P + m_A + m_S) \cdot (E_E + E_A)}_{E_{MAT}^{AM+FM}} + \underbrace{(k \cdot m_P + m_A + m_S) \cdot U_E^{AM} + m_A \cdot U_E^{CM}}_{E_{MFG}^{AM+FM}} + \underbrace{E_T \cdot [(k \cdot m_P + m_A + m_S) \cdot d'_1 + k \cdot m_P \cdot d_2 + (m_A + m_S) \cdot d_3 + k \cdot m_P \cdot d_4]}_{E_{TRN}^{AM+FM}} + E_{USE}^{AM+FM} \left( \frac{MJ}{part} \right)$$

### Application of the tool to process selection

A possible application of the proposed process selection criterion could be the production of components made of either Ti-6Al-4V or stainless steel can be considered. Such materials have different ecological properties, and usually require different additive manufacturing techniques. The eco-properties pertaining to material production are listed in Table 39.

Eco-property	Ti-6Al-4V	Stainless steel
Energy for primary material production, $E_V$ (MJ/kg)	685.0	84.5
Energy for material recycling, $E_R$ (MJ/kg)	87.0	12.0
CO <sub>2</sub> emissions for primary material production, $CO_{2V}$ (kg/kg)	46.5	5.0
CO <sub>2</sub> emissions for material recycling, $CO_{2R}$ (kg/kg)	5.2	0.7
Material recyclability, $r$	0.8	0.9
Embodied energy for material production, $E_E$ (MJ/kg)	206.6	19.3
CO <sub>2</sub> emissions for material production, $CO_{2E}$ (kg/kg)	13.5	1.1
Energy for material deformation (such as rolling/forging), $E_F$ (MJ/kg)	14.5	8.2
CO <sub>2</sub> emissions for material deformation, $CO_{2F}$ (kg/kg)	1.2	0.6
Energy for atomization, $E_A$ (MJ/kg)	70.0	2.9
CO <sub>2</sub> emissions for atomization, $CO_{2A}$ (kg/kg)	3.8	0.2

Table 39: Eco-properties of the workpiece and powder production (Ingarao et al., 2017).

The average energy demand and CO<sub>2</sub> emission values for the primary and secondary material production can be obtained from Ashby (2013). Data taken from Mayyas et al. (2012) can be assumed for the recycling rates of both the new and old process scraps. The primary energy and CO<sub>2</sub> emissions ( $E_F$  and  $CO_{2F}$ ) for forming the workpiece that has to be machined are also listed in Table 39 (see Ashby, 2013). Electric energy consumption values of 23.8 MJ/kg for Ti-6Al-4V (computed from the 6.6 kWh/kg value proposed by Paris et al., 2016) and of 1.0 MJ/kg for stainless steel (according to Morrow et al., 2007) can be assumed for the powder atomization. The electric energy consumption can be converted into the primary energy source consumption ( $E_A$ , in Table 39) by considering an average efficiency of  $\eta = 0.34$  to account for energy generation and transmission losses. Moreover, the CO<sub>2</sub> emissions ( $CO_{2A}$ ) due to electric energy consumption can be computed using the CES method proposed by Jeswiet and Kara (2008), applying data for the Italian energy mix (CES = 0.16 kg/MJ). As regards component production, Baumers et al. (2011) presented an overview of electricity consumption for several major AM technology variants, and reported a value of 61 MJ/kg for the Electron Beam Melting (EBM) of Ti-6Al-4V (by monitoring an Arcam AB A1 machine), and of 83 MJ/kg for the Selective Laser Melting (SLM) of stainless steel (by monitoring an SLM250 machine produced by the MTT Group). In both cases, productive and nonproductive modes could be considered, and the machine was operating at full capacity. The primary energy demand ( $U_{EAM}$ ) and the corresponding CO<sub>2</sub> emissions ( $U_{CO_2AM}$ ) can be computed from these values and are shown in Table 40, for  $\eta = 0.34$  and CES = 0.16 kg/MJ. The specific energy demand for machining has proved to be dependent above all on the machine tool architecture and equipment, since the material removal operation has only a limited impact on the total energy consumption, as highlighted by Behrendt et al. (2012). Kara and Li (2011) modelled the unit process energy consumption for material removal processes and for different machine tools, and they found a relationship between the Specific Energy Consumption (SEC) and the Material Removal Rate (MRR).

Eco-property	Ti-6Al-4V	Stainless steel
Specific (primary) energy demand for AM, $U_E^{AM}$ (MJ/kg)	179.4 (EBM)	244.1 (SLM)
Specific CO <sub>2</sub> emissions for AM, $U_{CO_2}^{AM}$ (kg/kg)	9.8 (EBM)	13.3 (SLM)
Specific (primary) energy demand for CM, $U_E^{CM}$ (MJ/kg)	80.1	8.9
Specific CO <sub>2</sub> emissions for CM, $U_{CO_2}^{CM}$ (kg/kg)	4.4	0.5
Energy for transportation, $E_T$ (MJ/kg·km)	$0.71 \cdot 10^{-3}$	
CO <sub>2</sub> emissions for transportation, $CO_{2T}$ (kg/kg·km)	$0.05 \cdot 10^{-3}$	
Travelled distances, $d_1 = d'_1 = d_2 = d_3 = d_4$ (km)	200	

Table 40: Energy demands and CO2 emissions for component production and transportation (Ingarao et al., 2017).

The specific energy consumption could be computed for both materials using the model proposed for

wet cutting with a DMU 60P 5-axis milling machine, and hypothesizing finishing process parameters for a 16-mm diameter, 4-tooth, solid carbide end mill (for Ti-6Al-4V: cutting speed = 70 m/min, feed = 0.1 mm/tooth, axial depth of cut = 0.5 mm, radial depth of cut = 12 mm, MRR = 3.3 cm<sup>3</sup>/min; for stainless steel: cutting speed = 130 m/min, feed = 0.3 mm/tooth, axial depth of cut = 0.5 mm, radial depth of cut = 12 mm, MRR = 18.6 cm<sup>3</sup>/min). Table 40 shows the primary energy demand ( $U_{E\text{ CM}}$ ) and the CO<sub>2</sub> emissions for machining ( $U_{\text{CO}_2\text{ CM}}$ ) for  $\eta = 0.34$  and CES = 0.16 kg/MJ. Finally, the energy ( $E_T$ ) and the CO<sub>2</sub> penalty ( $\text{CO}_2\text{ T}$ ) per unit weight, considering a 55-t truck, can be extracted from Ashby (2013) for the material transportation. All the travelled distances could be fixed at 200 km, according to Frischknecht and Jungbluth (2007).

In Priarone et al. (2016c), the authors also build a similar model used to assess the life-cycle impact of metal-based components produced via 1) conventional subtractive manufacturing (CM hereafter), and 2) additive manufacturing plus finish machining (AM + FM hereafter). The goal and scope of their study have been to analyze the impact of both additive and subtractive manufacturing strategies in terms of energy demand, CO<sub>2</sub> emissions, and resource depletion. The production of components made of Ti-6Al-4V has been considered. In addition, given that the environmental performance of a manufacturing approach is affected by the type and the amount of the involved materials, an analysis has been designed, in which the component shape has been varied and different solid-to-cavity ratios have been considered. The solid-to-cavity ratio has been defined, according to Morrow and colleagues (2007), as the mass of the final part divided by the mass that would be contained within the bounding volumetric envelope of the part. As shown in Figure 44, three different shapes (namely, ID 1, ID 2, and ID 3) were taken into account. The part volume,  $V_p$  ( $\times 10^3$  mm<sup>3</sup>), is respectively: 62.5 for ID 1; 46.8 for ID 2; 15.3 for ID 3. The part weight,  $m_p$  (g), is respectively: 275 for ID 1; 206 for ID 2; 67 for ID 3.

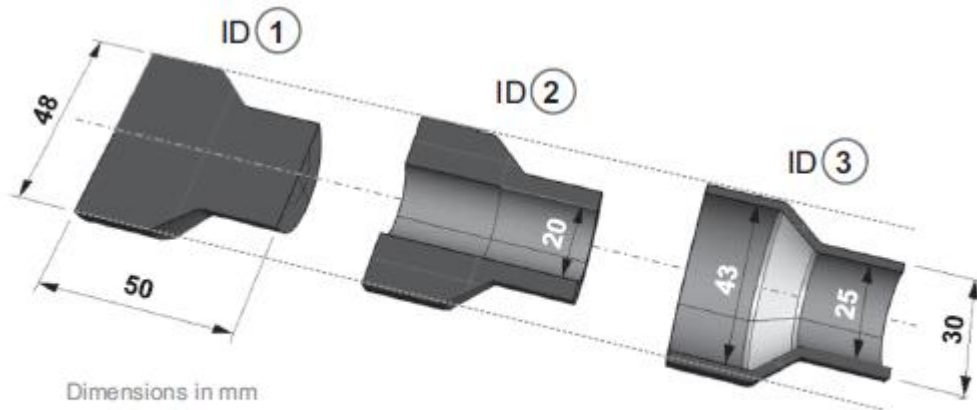


Figure 44: The three product shapes to be manufactured by additive and subtractive processes (Priarone et al., 2016c).

The life cycle results for the primary energy demand and CO<sub>2</sub> emissions are presented in Figures 45 and 46. The contribution of each considered factor as well as the shares of those of most influence are highlighted. Overall, it is possible to note that the material-related impact always plays a significant role. In fact, it accounts for more than 80% in all the considered scenarios for CM, whereas it is lower for the AM approach. For the ID 1 part geometry, CM results in substantial energy and CO<sub>2</sub> emission savings, even though the process scraps for AM ( $m_s$ ) are nullified, as shown in Figure 45. Vice versa, for the ID 3 part geometry (which exemplifies a thin-walled component), AM appears to be the best solution for both the considered metrics, even when a certain amount of process scraps is included. Figure 46 plots the results as a function of  $m_s$  (computed as a percentage value of  $m_p + m_a$ ,

where  $m_a$  is the weight of the machining allowance for postprocessing finishing operations) with reference to this claim.

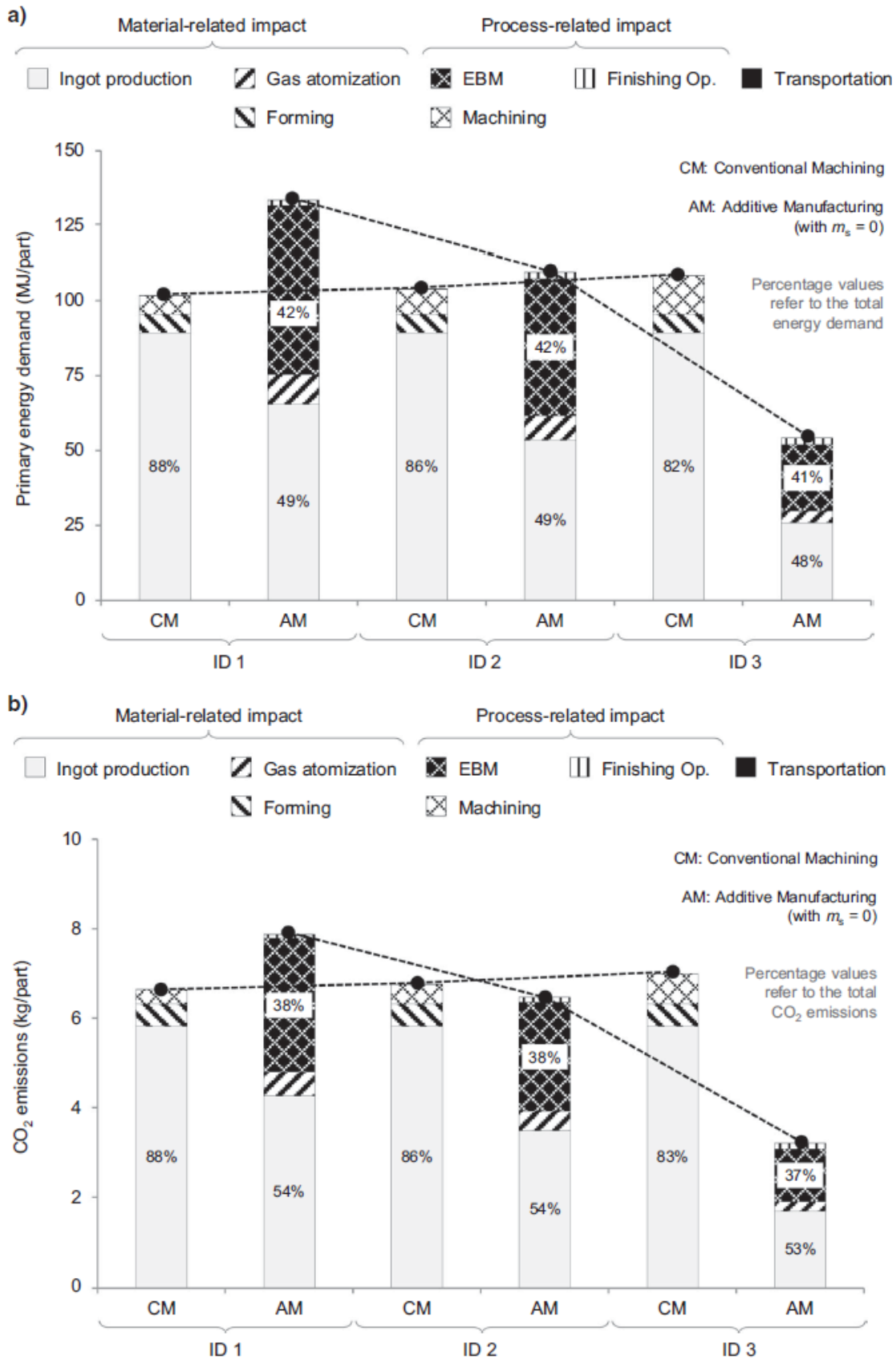


Figure 45: Shares of the energy demand (a) and CO<sub>2</sub> emissions (b). Note: The impact of transportation is negligible. CO<sub>2</sub> = carbon dioxide; EBM = electron beam melting; kg = kilograms; MJ = megajoules (Priarone et al., 2016c).

Specifically, the  $m_s$  value has been varied from 0% to 40%. The material-related impact as well as the process-related impact have been estimated, together with the impact of transportation. When  $m_s$  increases, the energy demand and the CO<sub>2</sub> emissions consequently increase. However, under the chosen hypothesis, the impacts of AM are always lower than those of CM. Higher  $m_s$  values than 105% and 124% would be necessary for the energy demand and CO<sub>2</sub> emissions, respectively, to make the CM process preferable over the AM one. The impact of transportation appears to be negligible (Figures 45 and 46) under the assumptions outlined in Transportation. Therefore, volumetric and handling differences related to workpiece and powder shipment were not analyzed in detail. Overall, it can be observed that the outcomes are mainly affected by the different amounts of used material and by the different SEC values of the two manufacturing approaches. When moving from ID 1 to ID 3, the machined-off material increases for the CM approach. As a result, the gap in material usage between the two approaches increases.

On the other hand, the manufacturing step is energy intensive for AM, especially when a large amount of material has to be deposited layer by layer (ID 1). In fact, the energy demand and the CO<sub>2</sub> emissions for ID 1 attributed to AM largely surpass the savings attributed to the reduction in material usage. On the contrary, when the solid-to-cavity ratio decreases, the performance of the CM approach is affected negatively by the larger amount of used material, and, as a result, the AM approach appears to be the best strategy.

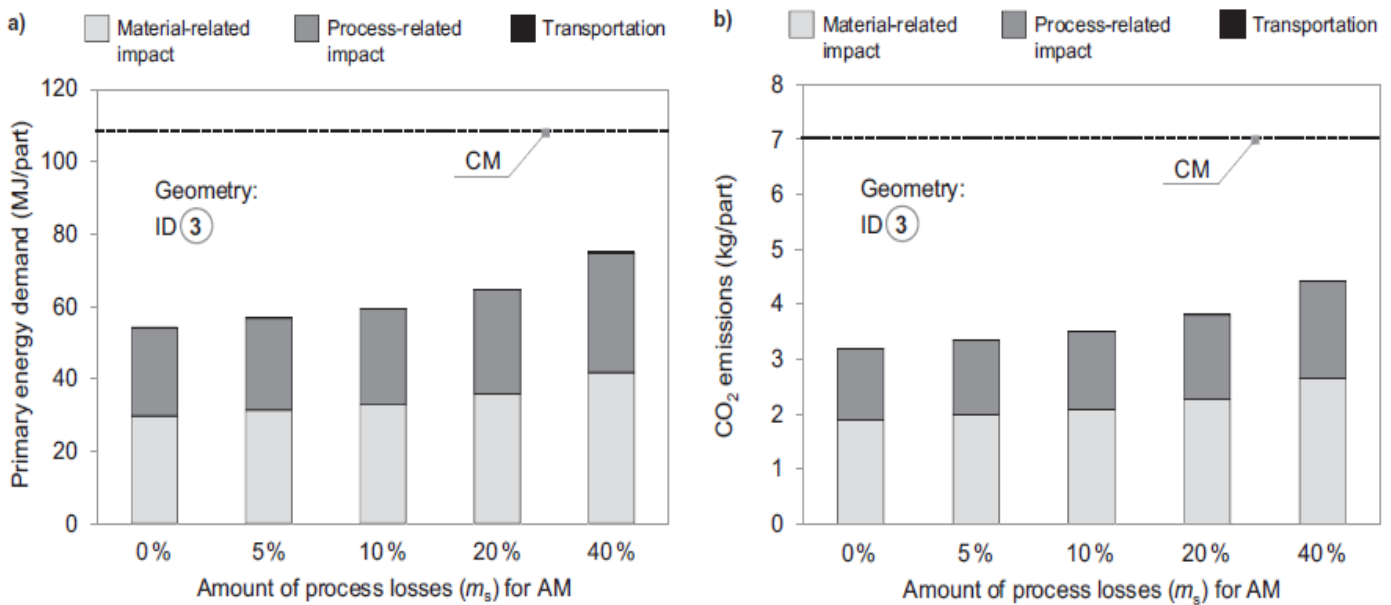


Figure 46: Variations in the energy demand (a) and CO<sub>2</sub> emissions (b) as functions of  $m_s$  for AM. Note: The impact of transportation is negligible.

### 3.3 Safety indexes

Human health impacts of toxic emissions have been an important concern in design for environment and life cycle assessment. A wide range of approaches has been used to address this problem. At the same time, the desire of environmentally-conscious consumers and manufacturers to choose more environmentally benign products and processes has led to the development of Life Cycle Assessment (LCA) and Design For Environment (DFE). In both of these areas, attention has focused initially on the development of inventories of emissions and raw materials consumption for particular products and processes. While LCA has been effective in creating inventories of waste production from cradle-to-grave for a product, there is no direct link from LCA to specific decision-making within process planning and product design. Instead, LCA has mainly functioned largely as an eco-audit mechanism

to assess current state. DFE research has to date concentrated on systems level design issues, such as disassembly, service or modular remanufacturing. In actuality, a significant amount of waste generation occurs during the pre-assembly stages of production. Therefore, a major concern is the analysis of environmental impact of unit-level manufacturing processes, especially influences of operational, setup, and process selection decisions. With these factors, environmental impact analysis at the unit process level depends largely on the ability to evaluate the effects of one waste stream versus a dissimilar waste stream in order to make a decision which is more benign to the environment within the process control volume. A number of methods for the comparison and evaluation of an inventory's dissimilar pollution loads and resource demands have been proposed. The aim of the next pages is to compare the structure and properties of different methods for the evaluation of these risks. Despite their use for the same purposes, often these methods differ in what they try to achieve, in the effects they consider, in the depth of analysis, in the way values influence the final score, and in use of ordinal or cardinal measures of impact. Moreover, the relative toxicity scores produced by these methods can also vary by 3 orders of magnitude when the same compounds are analyzed; thus method selection is critical.

In Hertwich et al. (1997), the authors discuss the Human Toxicity Potential method (HTP). HTP is a measure of mass releases normalized by toxicity and potential exposure. It is based on Paracelus' recognition that "the dose makes the poison" -- a basic principle of toxicology. HTP is an index that accounts for differences in exposure and toxicity and expresses the human health risk of a substance in terms of toxic equivalents. The basic measure of human health impact in HTP is the ratio of an exposure factor  $K$  to a Toxicity Measure (TM).

$$K = \frac{\text{exposure}}{1 \text{ kg/day release}}$$

The exposure factor expresses the exposure that results from a steady-state release to a specific environmental compartment. The toxicity measure gives the dose of a chemical that causes some common level of effect, such as the unit dose factor for carcinogens and the no-effect level for non-carcinogens. The total HTP score of a process is determined using following equation:

$$HTP = \sum_i \frac{\sum_{route} K_{route,i,comp} / TM_{route,i}}{\sum_{route} K_{route,ref,refcomp} / TM_{route,ref}}$$

The exposure of an individual to a pollutant  $i$  through a specific exposure *route* resulting from a steady state release of the pollutant into compartment *comp* is represented by  $K_{route,i,comp}$ . The first sigma indicates a sum over all exposure routes, the second sigma a sum over all pollutants, so that the HTP value represents the total human health impact caused by a specific process or product.

The authors of this research have chosen EPA's reference dose values and cancer slope factors as TM in two categories, noncarcinogens and carcinogens. In the following we explain how  $K$  is determined. The exposure factor is calculated using a generic fate and exposure model such as USES or CalTOX. The model consists of a level III fugacity model that determines the environmental concentrations of a pollutant and an exposure model that uses these concentrations to determine the exposure of an average individual (Figure 47). CalTOX is the model used in this paper. It requires the specification of three sets of inputs: the chemical and physical properties of the substance evaluated, the general environment, and the diet and activity patterns of the individual exposed. The latter two are the same for all chemicals. 1) Chemical-physical properties: key properties such as vapor pressure, solubility,

and reaction lifetimes have to be measured; 2) Specification of the environment: size of the control volume, fraction of area covered by surface water or vegetation, precipitation rate, wind speed, size and composition of different environmental compartments, etc; 3) Specification of exposure pathways: CalTOX includes 27 exposure pathways ranging from the inhalation of gaseous pollutants to the ingestion of milk produced by cows that eat fodder polluted by dry and wet deposition. The exposure scenarios are specified by activity patterns (air volume inhaled during outdoor activities) and diets (milk ingested).

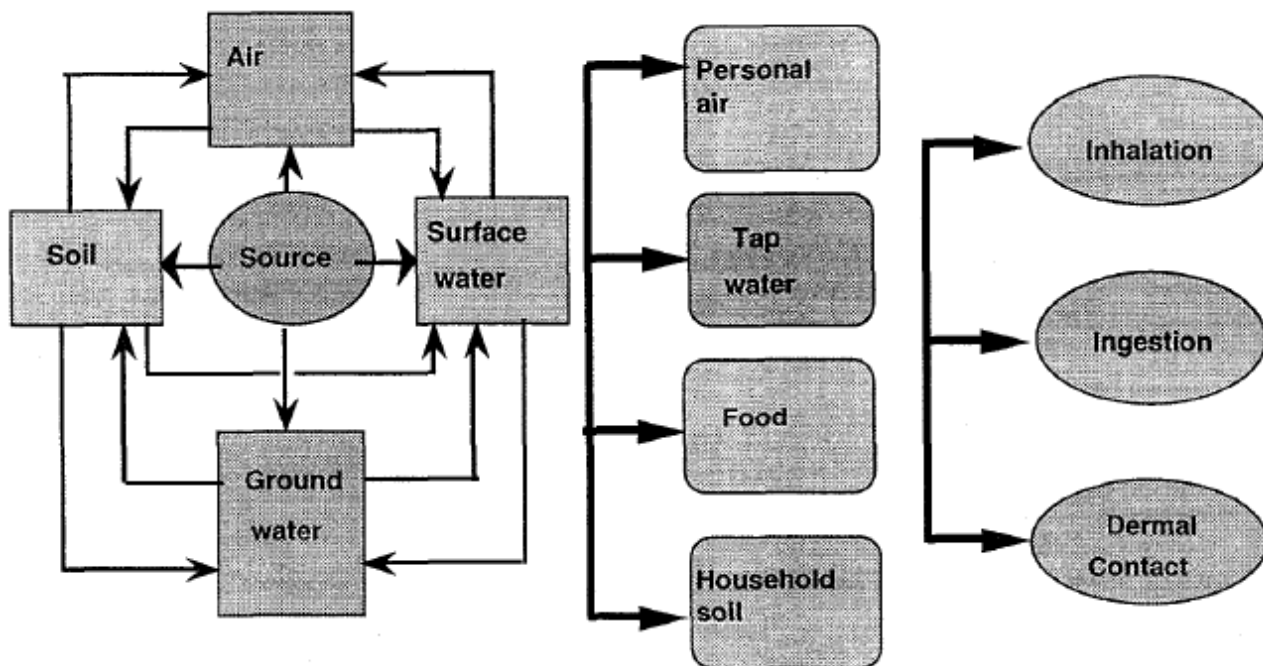


Figure 47: Fugacity model (left) and exposure model (right), part of CalTOX (Hertwich et al., 1997).

### *The Fugacity Model*

The fugacity model was developed by Mackay (Mackay et al., 1991; Mackay et al., 1993). Key concepts in fugacity modeling are partitioning, mass transfer between different environmental compartments, and removal through decay or advection. The CalTOX model describes seven environmental compartments: air, surface water, sediments, plants, ground-surface soil, root-zone soil, and vadose-zone soil. Each of these compartments consists of several different phases. Air consists of a gas phase and particulates, sediment consists of water and organic material, and a lipid phase. Figure 48 displays the seven phases and indicates the potential transfer of the pollutant between the phases.

**Partitioning:** When two phases are in chemical equilibrium with each other the ratio of their concentrations is given by a partitioning constant. Box 1 -displays important partitioning equations. The concept of fugacity or chemical potential reflects this partitioning: chemical concentrations in different phases are in equilibrium when they have the same fugacity, just as different bodies are in thermal equilibrium when they have the same temperature. The capacity of a certain phase to hold a chemical is the fugacity capacity  $Z$ . The concentration is the product of fugacity and fugacity capacity. A partitioning constant is the ratio of the two fugacity capacities; e.g., the bioconcentration factor BCF is the ratio of  $Z_{\text{fish}}$  or  $Z_{\text{water}}$ .

Intermedia transport: The model takes into account many different mechanisms of pollution transport between different environmental compartments. Diffusive processes such as volatilization and absorption, and one-way processes such as deposition.

Removal: Pollutants can be removed from the control volume either through a reaction (the chemical is transformed to a different chemical) or through advection out of the control volume. The authors have argued that advection should not be allowed as a removal mechanism when CalTOX is used for life cycle impact evaluation, because this does not adequately reflect the hazard posed by highly persistent substances. Organic chemicals can be removed through mechanisms such as oxidation, hydrolysis, and biodegradation.

Balancing gains and losses: The possible mechanisms that determine the concentration of a pollutant in the given compartment are listed in the following. Gains: 1) Sources; 2) Transformation and decay; 3) Flow from other compartments. Losses: 1) Transformation and decay; 2) Flow to other compartments; 3) transport out of the landscape. The level 111 fugacity model assumes steady-state conditions: the concentration in the compartment does not change, hence gains have to balance losses. The concentration in each compartment can be calculated by simultaneously solving all the mass balance equations.

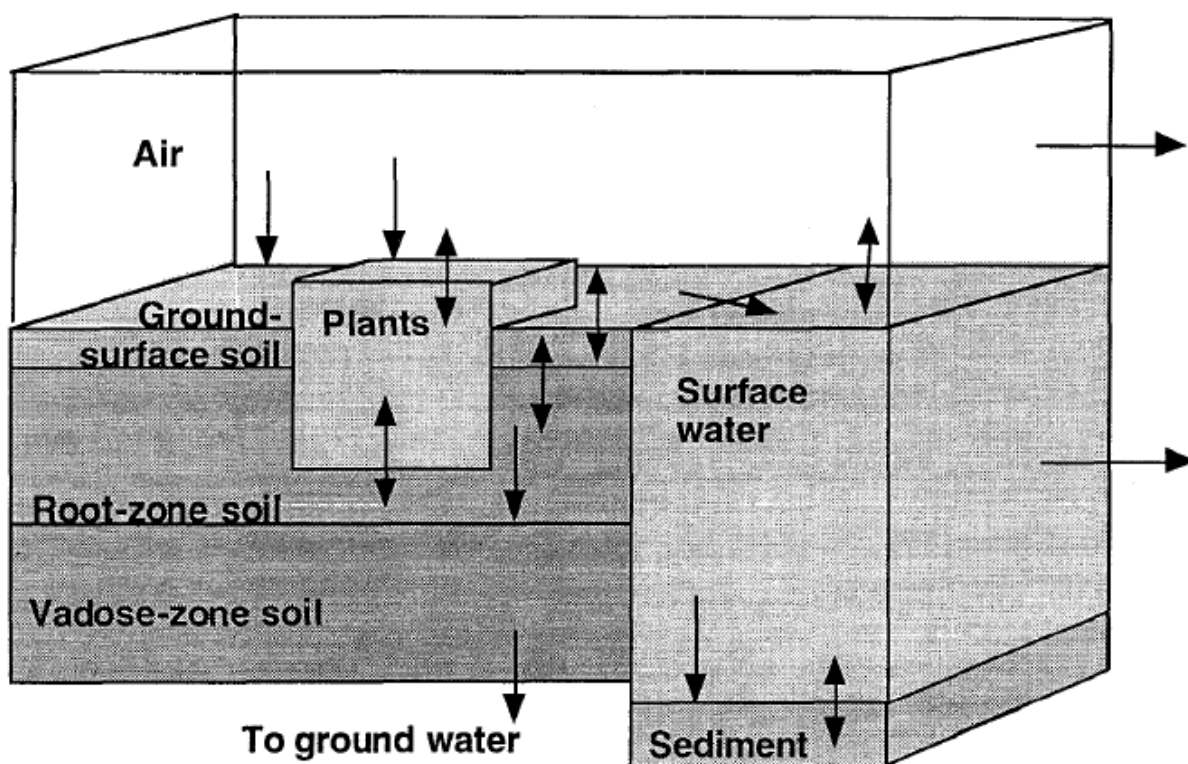


Figure 48: An illustration of mass-exchange processes modeled in the seven-compartment environmental transport and transformation model. (Ground water is not explicitly modeled in the system of equations but is used in the exposure calculations.) (Hertwich et al., 1997).

### *The Exposure Model*

The exposure model is also based on the concepts of partitioning and intermedia transport. The concentration in different exposure media is determined using partitioning functions, e.g., the bioaccumulation in fish, or the partitioning onto particles that are subsequently deposited onto produce. Calculations of potential exposure require additional input specifying exposure pathways and rates of mass exchange with the environment, as well as some additional partitioning constants.



Most partitioning constants used in the exposure modeling can be estimated from the octanol-water partition coefficient and Henry's Law constant.

*Illustration of CalTOX*

In the following the authors exhibit how CalTOX determines the hazard ratio of toluene. Table 41 displays the environmental concentrations that result from the steadystate emissions of 1 mole of toluene per day into an environment that they call "LCA new". Based on these concentrations, the dominant exposure mechanisms for toluene are calculated (Table 42). Toluene is a volatile chemical, hence inhalation exposure is important.

Concentration	Surface water discharge	Atmospheric emissions	
Air	2.1 E-08	4.5 E-08	mg/m3
Plants	4.1 E-10	8.8 E-10	mg/kg(FM)
Grnd-surface soil	1.6 E-10	3.3 E-10	mg/kg(total)
Root-zone soil	6.0 E-13	1.3 E-12	mg/kg(total)
Vadose-zone soil	6.7 E-16	1.4 E-15	mg/kg(total)
Ground water	3.2 E-17	6.9 E-17	mg/L(water)
Surface water	2.2 E-06	8.8 E-11	mg/L(water)
Sediment	5.5 E-06	2.2 E-10	mg/kg

Table 41: Compartment concentrations resulting from a release of 1mol/d of toluene (Hertwich et al., 1997).

For surface water discharges, two exposure mechanisms not included in simpler models turn out to be important: the volatilization of toluene contained in the shower water and subsequent inhalation in bathroom air, and the bioaccumulation of toluene in fish. Because of these two exposure mechanisms, surface water discharges present a higher risk.

	Surface water discharge	Atmospheric emissions
Inhalation		
air	14%	100%
surface water	36%	
Ingestion		
surface water	18%	
produce	2%	
fish	19%	
Dermal uptake		
surface water	11%	

Table 42: Distribution of exposure to toluene acc. to exposure routes (Hertwich et al., 1997).

*HTP calculations in case study*

The authors calculate the risk of carcinogens in benzene equivalents, the risk of non-carcinogens in toluene equivalents, where each refers to air emissions. The equivalency values in Table 43 indicate a significant range of HTP scores: lead and hexachlorobenzene are about 100,000 times as toxic as toluene, and dioxin is more than 1 billion times as effective in causing cancer as benzene.

equivalents	Atomspheric emissions		Surface water discharge	
	Benzene	Toluene	Benzene	Toluene
Benzene	1	0	1.6	0
Diethyl ether	0	2.4	0	3.3
Hexachloro-benzene	5.5 E3	1 E5	3.6 E4	6.3 E5
Lead	0	3.7 E5	0	1.1 E5
Methanol	0	1.3	0	8.2
2,3,7,8-TCDD	2.8 E9	0	2.1 E9	0

Table 43: Toxicity equivalents of the chemicals in the case study (Hertwich et al., 1997).

The scores listed in Table 44 show that the low volume discharges determine the final toxicity: Only dioxin emissions matter for the final cancer score, only hexachlorobenzene and lead matter for the non-cancer score. Process 2 has higher benzene and toluene equivalents, even though its total mass emissions and the Emissions Inventory Module (EIM) scores of Process 1 are higher, because Process 2 emits more of the highly toxic chemicals.

equivalents	Process 1		Process 2	
	Benzene	Toluene	Benzene	Toluene
Benzene	1.8 E+4	0.0 E+0	5.9 E+2	0
Diethyl ether	0	5.1 E+4	0	1.6 E+3
Hexachloro-benzene	3.5 E+5	6.2 E+6	1.1 E+6	1.7 E+7
Lead	0	1.9 E+6	0	1.9 E+5
Methanol	0	8.3 E+4	0	2.5 E+4
2,3,7,8-TCDD	1.3 E+7	0	4.3 E+7	0
Total	1.4 E+7	8.2 E+6	4.4 E+7	2.4 E+7

Table 44: HTP scores of the processes (Hertwich et al., 1997).

In Sheng and Hertwich (1998), the challenge in creating environmental metrics for unit processes is the integration of data at different levels of aggregation, abstraction and certainty into a hierarchical structure. This structure of metrics would then correspond to a hierarchy of process and product-levels decisions to be made, including process parameter selection, fixturing and catalyst selection, process selection, part specification and material selection. In this work is presented methodologies for assessing unit-process wastes at several hierarchical levels, including process, facility, and ecological levels. In general, the evaluations criteria can be either based on human effects, environmental load (sustainability of the process), or mass-flow based. The objective of the paper is to introduce the methodologies, data requirements, and uncertainties involved in the valuation of manufacturing process waste streams in order to gain an appreciation of how the integration of environmental assessment with manufacturing process mechanics might occur at an analytical level. The environmental analyses are influenced to a large degree by transport mechanisms, size of the control volume considered, and site-specific factors.

#### *Process-Level Metrics*

At the process level, the different forms of product and catalytic waste streams will have different environmental impacts, depending on the chemical species and physical phase. Within the process-level control volume, the acute factors of concern include oral toxicity, inhalation toxicity,

carcinogenesis, dermal irritation, eye irritation, reactivity and flammability. A problem in applying a multivariable evaluation is the different levels of data certainty and aggregation along these seven factors. For example, while flammability risk can be inferred through highly quantifiable parameters such as flashpoint, upper explosion limit and lower explosion limit, other factors, such as carcinogenic potential, can only be inferred through the degree of positive correlation found in catalogued experimental studies. Factors such as dermal and eye irritation show results only for animal studies, so human effects must be indirectly extrapolated. Toxicity factors are usually defined by a single data point (median lethal dose or concentration), with little understanding of the effects of exposure time. In order to address this range of data, a categorical scale can be implemented to create a 7 x 1 row vector of chemical subscores, where each element represents a dose x effect evaluation along each of the seven factors (Table 45). Each element may have a range from 0 to 9 in intensity. To introduce phase effects into the chemical hazard subscores, a phase matrix is constructed which partitions each factor among the different physical phases. For example, for oral toxicity, the overall hazard score of 1 can be partitioned into the following:

Solid: 0.3; Liquid: 0.4; Aerosol: 0; Vapor: 0; Particulates: 0.3.

### I. Oral Toxicity (O)

Effect		Dose	
3	lethal	3	<50 mg/kg
2	moderately serious (lost work time)	2	50 to 500 mg/kg
1	mild effect (nausea, unpleasant)	1	>500 mg/kg
0	no observed effect		

O = Effect x Dose,  $\in [0, \dots, 9]$ .

### II. Inhalation Toxicity (I)

(time-weighted average Threshold Limit Value)

Effect		Dose	
3	lethal	3	<50 mg/m <sup>3</sup>
2	moderately serious (lost work time)	2	50 to 500 mg/m <sup>3</sup>
1	mild effect (nausea, unpleasant)	1	>500 mg/m <sup>3</sup>
0	no observed effect		

I = Effect x Dose,  $\in [0, \dots, 9]$ .

### III. Eye Irritation (E) (rabbit) [3]

Effect		Dose	
3	severe	3	<50 mg
2	moderately	2	50 to 500 mg
1	mild	1	>500 mg
0	no observed effect		

E = Effect x Dose,  $\in [0, \dots, 9]$ .

### IV. Dermal Irritation (D) (rabbit) [3]

Effect		Dose	
3	severe	3	<200 mg
2	serious	2	200 to 500 mg
1	mild	1	>500 mg
0	no observed effect		

### V. Carcinogenesis (C) [3]

Score	Evidence
8-9	Evidence of oncogenicity from epidemiological studies or positive results in 2 or more mammalian species.
6-7	Evidence of oncogenicity in one or both sexes of a single mammalian species, with or without limited epidemiological data.
4-5	Suggestive evidence (not statistically significant) of oncogenic potential from epidemiological studies, mammalian bioassays (incl. preneoplastic change in vivo), cell transformation in vitro, or promoter/ cocarcinogenic activity.
3	Evidence of genotoxic potential.
1-2	Limited evidence of lack of oncogenic potential from epidemiological / in vivo / in vitro data.
0	No evidence of oncogenic potential from mammalian studies in two or more animal species.

### VI. Reactivity (R)

Score	Reacts with
9	metals, oxidizing agents, acids, bases, moist air, water, etc.
8	metals and moist air
7	metals
6	(moist) air
4-5	oxidizing agents
1-3	acids and/or bases
0	no known substance (inert)

### VII. Flammability (F)

Flashpoint (°F)		UEL-LEL (%)	
3	<100	3	>20
2	>100	2	10-19
1	>500	1	1-10
		0	0 (none)

F = flashpoint score x UEL-LEL score,  $\in [0, \dots, 9]$ .

Table 45: Formulation of HHS subscores (Sheng and Hertwich, 1998).

The aerosol and vapor phases have 0 partitions because a substance in one of these phases is inhaled rather than orally ingested. Using this approach, different phase vectors for solid, liquid, vapor, aerosol and particulate phases can be generated (Table 46). A substance which exhibits high oral toxicity, but is limited only to large solid blocks will have minimal risk of being ingested. This vector  $HP$  (where  $HP_i = Dose_i \times Effects_i \times Phase_i$ ) represents an effects-based multi-criteria measure of environmental effects released from a process. The data requirements for constructing the  $HP$  vector include information from sources such as Material Safety Data Sheet (MSDS), Registry of Toxic Effects of Chemical Substances (RTECS), ACGIH-TLV data, Centers for Disease Control (CDC) studies, and other public-domain information. This effects-based metric can be applied to evaluate the "quality" of waste stream emanating from a particular manufacturing process.

	Solid	Liquid	Aerosol	Vapor	Solid Particulate
Oral Toxicity	0.3	0.4	0	0	0.3
Inhaled Toxicity	0	0	0.5	0.3	0.2
Eye Irritation	0	0	0.4	0.4	0.2
Dermal Irritation	0.2	0.5	0	0	0.3
Carcinogenesis	0	0.3	0.3	0.3	0.1
Reactivity	0	0.5	0.2	0.2	0.1
Flammability	0.1	0.6	0.1	0.1	0.1

Table 46: Phase matrix (Sheng and Hertwich, 1998).

#### Facility-Level Metrics

At the production planning level, the  $HP$  vector metric described above is incomplete in so far as it does not account for site-specific factors which may influence fate and transport of specific waste streams. One method for accounting for site-specific factors is to establish a facility prioritization matrix  $[F]$ , in which a pairwise assessment of the seven health hazards factors can be made through the use of the Analytical Hierarchy Process (AHP) (Saaty et al., 1980). This matrix would incorporate issues such as workplace practices, protective gear, auxiliary equipment and post-processing, equipment and machinery selection, and facilities design. Two approaches for constructing  $[F]$  are presented in Gune et al., (1995): single respondent survey and group decision theory. In the single respondent knowledgeable about the facility. For each option, linkages are developed to the seven health hazard factors through (1) strong positive, (2) weak positive, (3) no effect, (4) weak negative, or (5) strong negative relations. Each of these linkages receives a comparative score which, when multiplied by a weighting factor corresponding to the question category (facility, machine, auxiliary equipment, protective gear or workplace practice), derives a comparative score which can modify  $[F]$ . After the prioritization matrix is finalized, a normalized  $F$  vector ( $1 \times 7$ ) can be constructed using **AHP**. In the group decision theory approach, multiple respondents rank order the seven factors. A composite importance value is derived from the degree of rank order agreement between all respondents. The seven importance values would comprise the  $F$  vector. Once the  $F$  vector has been determined, a composite score, termed Health Hazard Score (HHS), can be calculated as (Figure 49):

$$HHS = HP * F$$

The HHS score can either be used as an indicator of "in-situ" effect of a waste stream or as a weighting factor for mass flow through a process through:

$$\dot{m}_w = \dot{m}(HHS)$$

where  $m_w$  is the environmental-weighted mass flow and  $m$  is the raw mass flow. To assess the quality of aggregate output mass flows from a facility, multiple HHS values can be calculated:

$$\dot{m}_{wf} = \sum_j \dot{m}_j(HHS_j)$$

where  $\dot{m}_{wf}$  is the weighted mass flow for the facility,  $\dot{m}_j$  is the raw mass flow for the  $j$ th chemical species analyzed, and  $HHS_j$  is the health hazard score for the  $j$ th species. Subsequently, a facility-level effects assessment can be made through a composite health hazard score for the facility ( $HHS_f$ ):

$$HHS_f = \frac{\sum_j \dot{m}_j(HHS_j)}{\sum_j \dot{m}_j}$$

Data collection at the facility level is often highly aggregated, with parameters such as disposed wastes, scrap and energy use often measured for the entire facility. In order to derive weighted mass flows or facility HHS, accurate estimation of mass flows at the process level is required. To accomplish this, a set of unit-based process models can be developed. Each model can incorporate process mechanics to estimate scrap generation and geometry, catalyst mass flow and phases, process energy use, and process time required.

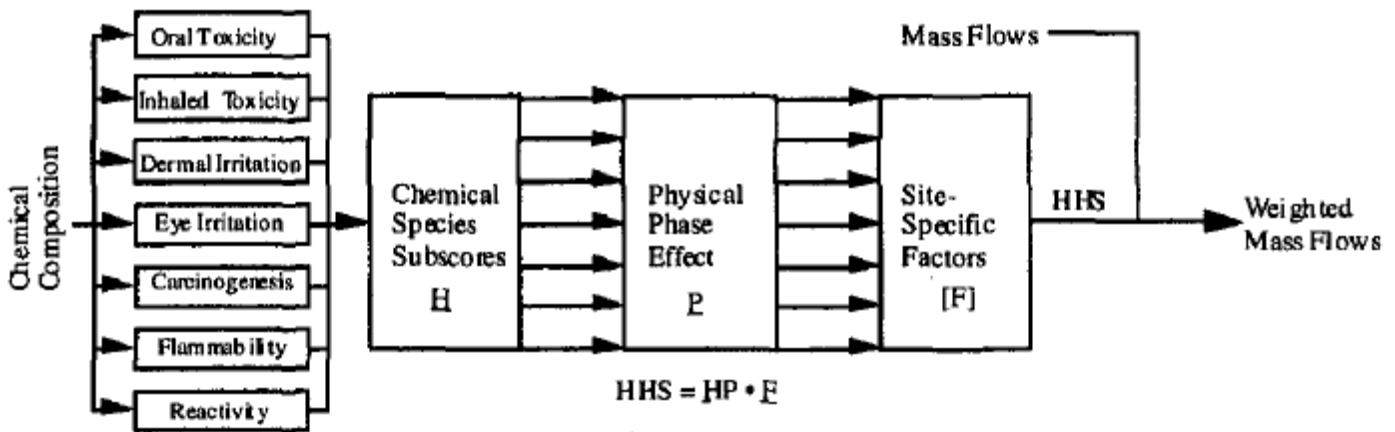


Figure 49: Site-influenced comparative waste assessment (Sheng and Hertwich, 1998).

### Ecological-Based Metrics

Once waste emissions reach outside the facility, ecological-based metrics must be provided to establish linkages to population-level effects such as reproductive hazards, chronic ecotoxicity, global warming, ozone depletion, etc. At this level, there is a trade-off in terms of a decrease in resolution versus incorporation of a larger number of evaluative dimensions. The ecological factors considered must also be tailored towards the population on which exposure control is required. Possible scenarios include occupational exposure affecting the workforce in a facility, community exposures affecting human populations in close proximity to a facility discharging effluents, ecological exposure such as short and long range exposures to plant and animal populations which stem from any effluent discharge from the facility, consumer exposures resulting from use of a product, and long-term exposures to humans and to eco-systems stemming from disposal of the product, or by products or wastes from the original process. The various compounds which may be of concern during a manufacturing process or within a facility may be of insignificant concern to the community except in the case of catastrophic failure or raw material storage. Conversely, materials discharged from a facility or contained in a products may be the primary risk to the community or the surrounding eco-system. Under these conditions, it is critical that engineers understand the differences in the types of exposures that may occur, the range of environmental endpoints that may be meaningful, and the

nature of the population(s) that may be exposed. The evaluation techniques at this level are based on environmental "load", mass flows, or ecological effects.

*Load-Based Evaluation.* At the highest level of aggregation is environmental "load" valuation, which attempts to use a single-scale value to describe the total ecological burden imposed by a material stream. In the simplest case, single or multiple respondents assign relative weights to various categories (global warming, acute toxicology, noise, resource use, etc.) according to their perceived importance. An expert judges the impact in each category on a scale of 0 to 9. This score is multiplied to the respective weight and the weighted values are summed up. The advantage of this process is its flexibility, as quantitative and qualitative data can be incorporated in one model. The model can also accommodate a variety of impacts ranging from biodiversity to noise to energy use. The systems boundaries and geographical specificity can be arbitrarily assigned by the user. However, the score is an ordinal measure and depends on the choices of the particular analyst. Also, the information requirements are vague and the evaluation scale is limited (i.e. a score of 9 in one area can easily be compensated in other categories, and outcomes may be masked by linear weighting). A second aggregate measure based on environmental load is the Swiss Life-Cycle Analysis method, which looks at the environmental load of a single chemical emission (i.e. CO<sub>2</sub>). The emissions of a particular pollutant into a general environment can be described by a parameter known as an ecofactor:

$$Eco - Factor = \frac{E_{Total}}{E_{Acceptable}}$$

where E<sub>Total</sub> is the total emission of a chemical species from the life cycle of a product and E<sub>Acceptable</sub> is the maximum allowable limit according to regulatory guidelines or scientific studies. A non-dimensional point system (eco-points) is also used as a process indicator:

$$Eco - Points = \frac{(E_{Process} * E_{Global})}{E_{Acceptable} * E_{Acceptable}}$$

where E<sub>Process</sub> is the single process emission of a particular control volume and E<sub>Global</sub> is the total emission into the control volume from all processes. The method of eco-factors has also been applied to resource use, assuming certain 'sustainable' resource flow levels. Local ecosystem regulations are used in the evaluation of E<sub>Acceptable</sub>. The first ratio measures how important an emission is by comparing it to the acceptable level. The second ratio is a measure of scarcity. The acceptable load has a large influence on the final result, it appears twice in the denominator, and contains a value statement, an environmental quality goal.

*Mass-Based Evaluation.* The second type of ecological indicator is based on material and mass consumption. One such technique is called Total Material Consumption (MIPS), whereby the total mass of materials consumed per service-unit is aggregated. The material input includes any material that is moved by the production process, such as ores and overburdens in mining, cooling water and combustion air of thermal power plants, and even biomass harvested for food production for human labor. Each primary material stream for production has associated amounts of secondary materials required for its production (e.g. coal and cooling water used for steel production). The total mass is aggregated in kilograms over the life-cycle of a product and related to the service provided by the product. Schmidt-Bleek (1994) gives some examples for services and products: one kilogram of paper utilizes 65 kg of water, 30 kg of air, and 3 kg of wood and chemicals. Implementation examples usually show a dominance of water, air and metals. MIPS does not attempt to place environmental impact valuation on each mass stream; instead, MIPS relies on the assumption that less mass consumption inherently leads to a more environmentally-conscious product. Therefore, the impact of

a small amount of highly hazardous material cannot be evaluated. A second mass-based measure used is called the Sustainable Process Index (SPI). The SPI relates the land area that would be required for an ecologically sustainable operation of a process or production of a product to the per capita area available in the region where the facility is located. The control volume is composed of the area required for raw materials and energy production, the area of the installation, the living area for the process staff, and the dilution area for waste dissipation. Finally, a "product area" can be defined as the area required to dissipate the product mass and effluents into the environment. The mass flow of an effluent is divided by the rate of replenishment in the release compartment and the actual concentration of the component in that environmental compartment. This procedure is based on the assumption that all products and by-products eventually end up disbursed in the environment. SPI is a cardinal measure and is specific to the context and the location. It also has fairly good reproducibility, given a consistent set of assumptions on dispersion and energy. However, one disadvantage of SPI is its equal treatment of different effluent discharge media. In copper plating, the collection and disposal of copper sulfate has a higher SPI than the direct discharge into the nearest stream. Also, the use of ambient standards or natural geological concentrations for the calculation of discharge equivalent areas is as arbitrary as their use for the determination of eco-factors.

*Effects-Based Evaluation.* Effects-based evaluation represent a category of less subjective, but more data intensive, methods for analyzing environmental impact. A method called the Environmental Priority System (EPS) was developed by Volvo to evaluate material selection in product design, and is similar in implementation to eco-factor analysis. In EPS, each waste stream in a product's life-cycle is measured along different eco-factor scales (i.e. global warming, ozone depletion, eco-toxicity, etc.). Acceptable limits are stored in a database. The scores for all scales are added to form a composite score, called an Environmental Load Unit (ELU) (Ehrenfeld, 1994). One application of EPS was the evaluation of environmental load of an aluminum vs steel automobile hood based on ELU scores for production, product use and recycling (Steen et al., 1991). A set of chemical equivalency potential standards is currently under development by the Society of Environmental Toxicologists and Chemists (SETAC). This impact assessment is divided into three steps: classification, characterization, and valuation (Fava et al., 1993). The classification step entails a categorical listing of emissions and resource use and the identification of benchmark compounds and exposure paths to evaluate material streams along each category. The individual emissions are converted into chemical equivalency potentials, such as the Global Warming Potential (GWP) in terms of CO<sub>2</sub> equivalent and toxicity in terms of benzene equivalent. The evaluation categories developed thus far include ozone depletion, photochemical ozone creation, acidification, eutrophication, human toxicity, as well as terrestrial and aquatic ecosystem toxicity. The characterization step analyses and estimates the magnitudes of the impacts on ecological health, human health, or resource depletion. The valuation step compares the different categories and assigns weights in order to obtain a final aggregate score. An example of calculating chemical equivalency is the determination of toxicity potential to evaluate and compare the toxicity of chemical releases to humans. All releases are converted to equally toxic releases of a reference substance (such as benzene). The equivalent mass for a chemical species *i* has the form:

$$m_{eq} = \frac{K_i / NEL_i}{K_{ref} / NEL_{ref}} * m_i$$

where *K* is the modeling or fate constant, the No-Effect Level (NEL), and *ref* is the reference substance. The equivalent releases of the various effluents can be summed to give the total human

toxicity of a process. The no-effect level for a particular substance on humans can often be found in the materials safety data sheet or toxicological literature base; however, the data availability becomes poorer when attempting to establish chemical equivalency for other categories of effects. The modeling constants  $K$  relates the actual exposure of a person to the release of a substance into the environment and involves the development of a Level III Fugacity (or critical vapor pressure) Model, which calculates ambient environmental concentration of substances from data on emission, partitioning functions, and decay rates. This model not only incorporates generic pathway information, but also includes regional-specific inputs such as the water/land ratio, rainfall, soil properties, and wind speeds. Although the original intent of the chemical equivalency method is LCA, the system as it is used considers only pollution and resource use and can be adapted to evaluate specific manufacturing processes or systems. The system boundaries external to the facility for this analysis are arbitrarily defined, but generally are drawn as wide as possible while still preserving data integrity. The potentials have a physical meaning and give a cardinal measure of the impact, but the comparison between the different potentials depends on the weights assigned. The measure is not specific to a product; thus the environmental impacts of one product or process can be compared to those of a different type of product or process. The most serious disadvantage is the taxing information requirement, especially for toxicity evaluation. The requirement to measure a large number of toxic substances in a large number of production facilities involved in the manufacture of a product will require a substantial data collection effort. However, current analyses typically use estimated values for a "typical" facility. As more evaluations are performed, collected data can be used for other assessments. A second disadvantage is the high degree of uncertainty about toxic effects and other scientific issues require that a generally accepted method be used for conversion and equilibrium factors. Finally, regional geographical factors are often difficult to model, although for effects such as eutrophication and acidification there is at least some effort to include geographical factors.

From the literature review presented in Priarone et al., (in press), the authors found out that, when cutting titanium-based alloys, the available knowledge concerning the effects of various cooling/lubrication conditions (and especially those exploiting lubricoolant mists) is still inadequate to offer a holistic understanding of the process performance. The correlation between the type of lubricoolant, the supplied amount, and the delivery mode to the cutting area heavily affects the results in terms of machinability (meant in its broadest sense) and process sustainability. In this paper, the cutting performance when turning of Ti-6Al-4V alloy by using carbide inserts under various lubrication conditions is studied. In addition to the dry cutting, three other lubrication/cooling conditions were applied: 1) Wet cutting; 2) Minimum Quantity Lubrication (MQL); 3) Emulsion Mist Cooling/Lubrication (EMCL). The Cutting Fluid (CF) consumption, which is obviously nullified in dry cutting, changes while varying the applied lubrication/cooling system. For MQL or EMCL, the sprayed oil or oil-in-water emulsion cannot be recovered and reused, so the CF consumption ( $q_L$ , in mL/h) is equal to the flow rate guaranteed by each external system. By contrast, under wet cutting conditions, part of the oil-in-water emulsion is collected, filtered, and re-circulated through the lubricoolant system which equips the lathe. Therefore, the CF consumption has to be addressed to the wastes due to the vapour stream generated through cutting fluid diffusion into the surrounding environment, and to the liquid stream resulting from cutting fluid coating of chips, tools, and workpiece. The CF consumption could be indirectly estimated by dividing the yearly CF consumption of the machine tool (including the amount of CF that was refilled and the complete CF replacements) by the effective usage time of the machine itself. In addition to the resource consumption, the environmental impact of a cutting fluid should also be evaluated with respect to the hazards for the workers' health. This last evaluation can be actuated by companies for a sustainable selection of



processes and materials in compliance with the growing environmental legislations aimed at preventing humans and the environment from certain hazardous substances. The Health Hazard Score (HHS) proposed by Sheng and Hertwich (1998) has been applied in this research. Such composite indicator can be computed as the product between two vectors, namely **HP** and **F** ( $HHS = \mathbf{HP} * \mathbf{F}$ ). The vector **HP** represents an effects-based multi-criteria measure of the environmental effects released from a process. Oral toxicity, inhalation toxicity, carcinogenesis, dermal irritation, eye irritation, reactivity, and flammability are the risk factors taken into account. Each *i*-th HP factor can be calculated by multiplying the specific values of dose, effect, and phase ( $HP_i = Dose_i * Effect_i * Phase_i$ ). The three (liquid, aerosol, and vapour) phases have been considered, and the dose/effect data concerning each specific applied cutting fluid have been obtained from the Material Safety Data Sheets (MSDS). The vector **F** accounts for site-specific factors which may influence fate and transport of specific waste streams. The Analytic Hierarchy Process (AHP) was used for the calculation of **F**, that results to be equal to  $[0.075, 0.354, 0.169, 0.085, 0.257, 0.037, 0.023]^T$ , as suggested by Sheng and Hertwich (1998). The Health Hazard Score for liquid ( $HHS_{liq}$ ), aerosol ( $HHS_{aer}$ ), and vapour ( $HHS_{vap}$ ) phases were then computed per each lubrication/cooling condition. The results are summarized in Table 47. The choice of the cutting fluid type is crucial to reduce the HHS. For instance, the use of an ester-based oil for EMCL is aimed at getting a lower impact on human health, since the system creates a mist dispersed in the surrounding workplace.

Lubrication condition	$HHS_{liq}$	$HHS_{aer}$	$HHS_{vap}$
Wet	0.07	0.73	0.52
MQL	0.04	0.24	0.17
EMCL	0.03	0.01	0.01

Table 47: Health hazard score as a function of cutting condition (Priarone et al., 2017).

In Hertwich et al. (1997), the authors compare the structure and properties of six different methods. The health hazard scoring (HHS) system uses the Analytical Hierarchy Process (AHP) to weight workplace toxic effects and accident risks. The HHS score is an ordinal measure of hazard. The scoring of toxic potency by orders of magnitude indicates that the HP vector is not linear, and Saaty (1980) asserts that AHP is of a non-linear nature. Due to its ordinality, the system does not allow for the determination of a per-kilogram HHS score and a subsequent scaling of that score by mass flow. The HHS system is based on (potential) effects. The implicit goal is to minimize occupational health and accidents risks. The analysis is ‘narrow’: it is concerned only with effects at the site of the process, not with problems of process waste disposal or the environmental risks of the production of inputs. The analysis is ‘shallow’: no attempt is made to physically represent the actual exposure routes or numerically evaluate the exposure of a worker. The valuation is both implicit and explicit: the HP vector is constructed according to predefined rules, the F vector is based on human judgment. It is impossible to investigate the effects of valuation or separate the values of the analyst from those of the designer of the scoring system. The strength of HHS is its simplicity and the availability of the required data. Toxicity values can be obtained from material safety data sheets, which, in the US, have to be present in every company that uses a specific substance. Every design or safety engineer is capable of conducting an HHS scoring without having to go through extensive training. In our assessment, the most severe shortcomings of HHS are its ordinality, its limited scope, and its ambiguity in valuation. The Material Input Per Service-unit (MIPS) aggregates the mass of all the material input required to produce a product or service. Designed as a basis for LCA and eco-labeling, MIPS should promote long service-lives, remanufacturing and recycling, and a careful use of materials. It is concerned mainly with large-volume inputs. There is no explicit inclusion of effects

like toxicity, global warming, or stratospheric ozone loss; the analysis is extremely shallow, but it is broad in including inputs to the entire lifecycle. MIPS is the direct translation of the insight that the current level of material throughput is unsustainable into a yardstick. Its strengths are the simplicity of the conversion of the inventory to a final score and the strong image of an unsustainable mass flow. It is a good tool for illustration and education and has been used for that purpose. If MIPS is a measurement of environmental impact, it implicitly assumes that each mass throughput is equally undesirable, whether it is the natural gas that fuels a power plant or the river water that cools it. If used for design or management optimization, MIPS would invariably lead to perverse outcomes, such as the replacement of a non-toxic high-volume input with a highly-toxic low-volume input, thereby increasing the burden on the environment. The Swiss Eco-Point (SEP) method scores pollutant loadings based on a source's contribution to an acceptable total pollution load and an environmental scarcity factor. The acceptable load has a large influence on the final result, it appears twice in the denominator, and contains a value statement, an environmental quality goal (Sage, 1993). For CO<sub>2</sub> for example Ahbe et al. (1990) suggest using the Toronto target of a 20% emissions reduction by 2005 over the 1988 levels, which gives a scarcity factor of 1.25. Hofstetter (1991) discusses the difficulty of determining the acceptable loads and suggests using natural geophysical flows instead. This approach would raise significant problems for artificially created substances and imply the goal of eliminating all chemical invented by humans independent of costs or environmental risks. The concept of SEP is elegant and seems to suggest that valuation can be achieved automatically through the use of scarcity. The valuation, however, implies that we are equally concerned about each pollutant, independent of the effect it causes. Ecopoint analysis is shallow: actual effects are not considered. The method reflects its goal of achieving sustainable materials flows, so each flow is valued equally. The authors of this paper, consider the inclusion of scarcity in the evaluation to be the merit of the SEP. The normalization of the emissions by an ill-defined critical resource flow, however, is questionable. The equal valuation of different pollutant flows is not justified by their actual impacts. The Sustainable Process Index (SPI) determines the area that would be required to operate a process sustainably, based on renewable resource generation and toxic degradation; an extension of the dilution volume approach. A case study of ethanol synthesis from sugar beet (Krotscheck, 1993) is used here to illustrate the method of evaluation. The annual production of 10 000 ton of ethanol requires 151 000 ton of sugar beet per year. With a yield of 4.9 kg/m<sup>2</sup> per year, 31 km<sup>2</sup> are required to grow the beets. The processing plant requires 14 GWh of steam and 50 MWh of electricity per year, is run by a staff of 12, and produces effluents with a Chemical Oxygen Demand (COD) of 694 ton/year. The renewable energy generation (biomass for steam and PV for electricity) requires 3.8 km<sup>2</sup>, and the staff requires 0.2 km<sup>2</sup> to be clothed, fed, and housed. The evaluation of the COD is based on the annual precipitation rate (1 m for central Europe) and the mean oxygen content. A single kilogram of COD requires 140 m<sup>2</sup>/year to be dissipated, so the effluent takes up an area of 96 km<sup>2</sup> or 62% of the total area demand of ethanol production. The production of 1 kg ethanol requires 15.5 m<sup>2</sup>/year. SPI is not based on effects, fish death from insufficient oxygen supply, but on environmental loads: how much area has to be set aside for the dissipation of the COD? The valuation is implicit in the goal of sustainability and the ambient concentrations used to estimate dilution areas. This causes problems when fossil fuels and minerals are considered: it takes millions of years to generate coal, petroleum, or natural gas via sedimentation and geophysical conversion processes. It is estimated that the generation of 1 kg(C) of fossils fuels requires on the order of 400.000 m<sup>2</sup>/year. The analysis of any process using fossil fuels would be dominated by these fuels, so Krotscheck (1995) arbitrarily picks a factor of 500 m<sup>2</sup>/kg(C) per year instead. Similarly, once dispersed, metals do not reconcentrate into ore deposits; following our interpretation of the SPI logic, a score of infinity would be required. Instead, an indirect method is invoked which sets the score to zero and only

accounts for other life-cycle impacts. This gross breach of its own logic shows the weakness of SPI and other systems that try to evade value questions using technical arguments and abstract criteria. In the authors' evaluation, the merit of SPI is to focus the attention on the concept of sustainability and to yield a measurement that can directly be related to the life-support capacity (area) available for the satisfaction of our needs. The copper-plating of 1 m<sup>2</sup> of printed circuit board, for example, requires between 6 (recycling of copper sludge) and 30 m<sup>2</sup>/ year (primary copper, dispersion of effluent), enough to grow 4-20 kg of wheat (Krotscheck, 1995). It is made clear that industrial activities compete with the satisfaction of basic needs. SPI calculations are based on a life-cycle view and are therefore broad. They have medium depth because they rely on ambient environmental quality standards instead of going back and determining the acceptable concentrations from experimental data. As a result, SPI is simpler and more tolerant of data gaps than SETAC. On the other hand, it lacks the consistency of SETAC, because ambient standards are based not only on environmental risk but also on economic and technical feasibility as well as political compromise. The Society of Environmental Toxicology and Chemistry's life-cycle impact assessment (SETAC LCA) impact assessment method aggregates pollutants with similar impacts to equivalency potentials (measured in kg CO<sub>2</sub> equivalent, kg benzene equivalent etc.) and uses decision analysis to assign weights to different adverse impacts. SETAC LCA is a "broad" analysis: pollution streams from every step of production, transport, use, and end-of-life are considered. At the same time, the analysis aims to be "deep": it considers not only pollution streams but also their relative contribution to a specific stress (e.g. acidification) or consequence (e.g. human toxic effect). This consideration, however, is only generic; the method's 'equivalency factors' are not based on a specific situation. Stress and consequences do not have to be analyzed for each individual situation and are therefore depicted as "indirect consideration" in Table 48. The equivalency potentials are cardinal measures of environmental impact. Depending on the method of valuation, the final score can be ordinal or cardinal. Traditional methods of decision analysis have been suggested for valuation, such as multi-attribute utility theory and the analytical hierarchy process (Fava et al., 1993). These are process-oriented methods which help to clarify the issues and exclude inconsistent preferences. They rely on explicit choices made by subjects in interviews and usually produce ordinal rankings (Saaty, 1980). LCA practitioners still debate whether to take specific local characteristics of the actual production, use, and disposal processes into account, or whether generic processes situated in a generic environment suffice to represent environmental impact. Linked to this debate is the issue of potential versus actual damage (Heijungs et al., 1995): should acidic effluent released into the ocean receive the same weight as if released into a sensitive lake-ecosystem? Location-independent impact analysis and the use of potential damage is not only simpler, it is intended to yield a result that is applicable to a broader range of cases and to avoid the shift of pollution to pristine areas or those with a large tolerance for pollutants. The SETAC LCA is extremely information-intensive and therefore expensive. It requires a host of data relating to resource depletion, human and ecosystem toxicity, substance lifetimes and partition functions, as well as dominant atmospheric reactions. No accepted procedures exist to deal with data gaps and it is unclear how to use proximate information, such as toxicity estimates derived from structure-activity relationships. Undesired outcomes could result from poor data quality and not keeping track of uncertainty. The environmental priority system (EPS) characterizes the environmental damage caused by equivalency potentials and expresses it in monetary terms, derived from environmental economics. EPS is even "deeper" than the LCA discussed in the previous section, because it requires a quantification of damage. It is an explicit valuation method, but it relieves the analyst or decision maker of the burden of assigning values or relative weights and instead tries to "scientifically" measure prices and social preferences that exist independent of the process of analysis. No justification is given why a valuation based on

environmental economics is superior to a social choice based on extensive discussion and group decision making. The valuation is based on a generic assessment and not on local conditions, but local susceptibilities are taken into account by using actual and not potential damage. Field et al. (1993) criticize EPS as difficult to implement and for using “costs” instead of worth, thereby neglecting that environmental absorption capacity and resources become more valuable as they become scarce. They assert that the reduction of unit effects to monetary values implies a linear additive preference structure and that this is a poor representation of actual preferences displayed by humans. In the authors’ assessment, EPS is flawed not because of its definition of social welfare, but because it is based on the prices and preferences that characterize our current unsustainable situation. The price of wood, for example, might be artificially low due to unsustainable harvest practices, so that the replacement value for a tree in EPS would be too low. The strength of EPS is its use of a comprehensible, indeed universal, currency. Social costs of production and consumption are displayed just as that. It remains questionable the prospect environmental science and economics being able to supply the data required for this extensive valuation.

The depth of analysis assesses how many of the elements in the chain of effects are analyzed and to what degree of quantification. This important issue is explored in Table 48. Ordinal measures give only relative rankings, whereas cardinal measures allow a statement that one process has twice the impact of another process. Cardinal measures are interesting because they allow a better comparison between the results of different analyses and provide information on whether the difference in impacts is really large enough to matter. Ordinal measures, however, may better represent the characteristics of human preferences; the utility functions of microeconomics are a most prominent example of ordinal preference measures. The depth of analysis of the various methods is illustrated in Table 48, which is based on the classification of the steps in the causal chain from emissions to damage: emissions result in environmental insults, such as the increase of certain material flows in the environment (e.g. sulfur), which cause a stress (e.g. exposure). The stress has the potential to cause a harmful consequence, such as fish death in response to the acidification of lakes or respiratory disease in response to exposure to sulfates (Holdren, 1980). This classification is not unambiguous and analytical depth may be hard to measure. The determination of the CO<sub>2</sub> equivalent of greenhouse gases, for example, is based on extensive research on the relative radiative forcing (heat-trapping capacity) of the gases, but also on a value judgment as to what time scale is relevant for the analysis. (The atmospheric lifetime of greenhouse gases varies by two orders of magnitude). This kind of mixing of value judgment and scientific data is unavoidable. The choice and design of a method is value-laden. Once the interested parties have agreed on general principles of a method, however, there remain many more apparent value judgments. The algorithm used within a method to produce an index is termed ‘analysis’, the assignment of importance weights to analytical results is termed ‘valuation’. Table 48 displays analytical depth and degree of quantification graphically. The shading ‘quantitative analysis’ indicates where the quantities calculated correspond to something measurable, at least in principle, such as ambient environmental concentrations (insults), or deaths as consequences. HHS exemplifies a system in which consequences are evaluated qualitatively: a subjective consideration of the situation at hand determines whether a specific pollutant could cause harm and hence how it should be valued. SEP and SPI do not consider stress or consequences explicitly, but presume that ambient environmental quality standards are set at a level at which insults do not result in any detrimental consequences. Legal standards are the product of a political process that depends on political conditions and includes technical and economic feasibility in addition to scientific considerations, hence they are a very indirect way of considering stress and consequences and are labeled as such in Table 48.

Steps	HHS	MIPS	SEP	SPI	SETAC	EPS	Example
Inventory	Quantitative Analysis	Quantitative Analysis	Quantitative Analysis	Quantitative Analysis	Quantitative Analysis	Quantitative Analysis	SO2 emissions
Insult	Quantitative Analysis	Indirect Consideration	Quantitative Analysis	Quantitative Analysis	Quantitative Analysis	Quantitative Analysis	sulfate in air
Stress	Quantitative Analysis	Indirect Consideration	Indirect Consideration	Indirect Consideration	Quantitative Analysis	Quantitative Analysis	sulfate dose to lung
Consequence	Quantitative Analysis	Indirect Consideration	Indirect Consideration	Indirect Consideration	Indirect Consideration	Quantitative Analysis	respiratory disease
Valuation	Quantitative Analysis	Indirect Consideration	Indirect Consideration	Indirect Consideration	Quantitative Analysis	Quantitative Analysis	treatment costs, lost work-days

Table 48: Depth of analysis and degree of quantification of the different indices (Hertwich et al., 1997).

In some categories in the SETAC analysis, stress is used to determine equivalency potentials, e.g. the absorption of IR radiation is used to determine the global warming potential of the various greenhouse gases. In other categories, such as acidification, stress is not considered at all. The stresses are weighted against each other, but not referred to some external value. The authors call this semi-quantitative analysis. For EPS, stress and consequences have to be quantified in order to be assigned a monetary value.

## Chapter 4: Case study

With new advances in AM, there is an opportunity for old design geometry to be optimized for weight and strength. AM allows for the creation of complicated but desired geometries that were once unable to be fabricated via conventional methods. The bearing bracket is a common component on control surfaces of various aircraft that provides a great platform for applying AM. As a dynamic component that interfaces with moving parts, the bearing bracket has to conform to a certain geometrical envelope as well as being able to sustain large loading forces in various directions. Redesigning the bracket for AM could provide significant weight savings and help reduce fuel consumption of airplanes. The objective of this section is to redesign a common old design of a bearing bracket in such a way that its topology and shape is optimized for minimizing weight while fitting in the target envelope and meeting the technical requirements. The new bracket is then fabricated via Selective Laser Melting. The new designs will be compared with the original one and their sustainability analysis is carried out.

### 4.1 Topology optimization study

The original object is shown in Figure 50 and 51. For the analysis and the experiment a reduction factor of 0.3 has been chosen in relation to the normal dimensions. The analyzed part fits in a target envelope of  $40 \times 26 \times 12 \text{ mm}^3$ .

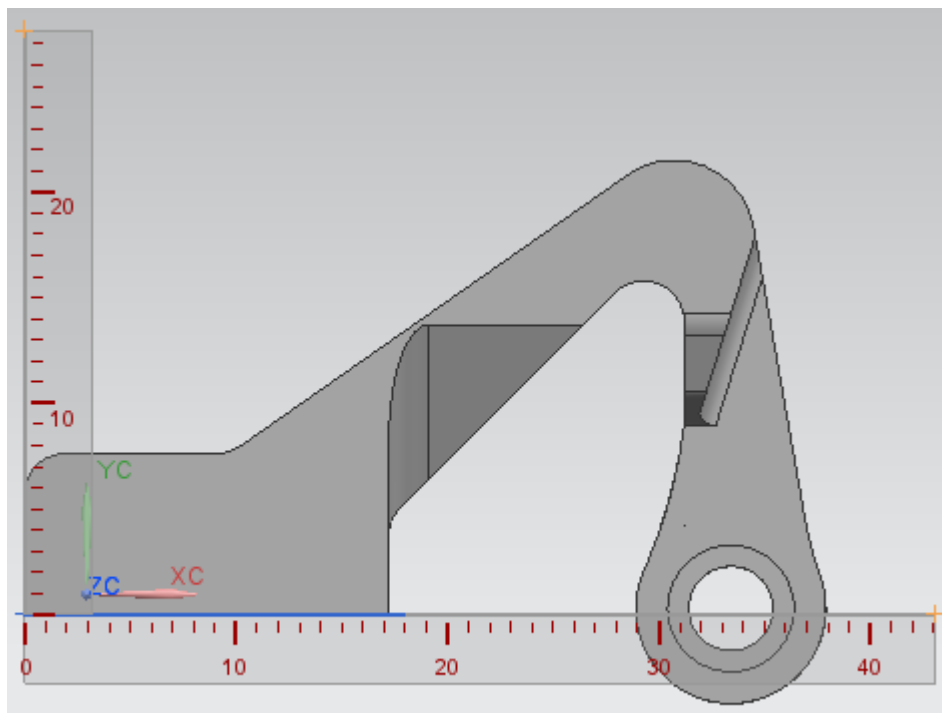


Figure 50: Analyzed object first view.

For the CAD design, the FEM static analysis and for the topology optimization the NX program (version 11) has been chosen. In Figure 52 it is possible to see the set of parameters for the meshing phase of the selected part. The dimension of 0.58 mm has been chosen as characteristic dimension of the elements. The studied material is Stainless Steel 316L, with a nominal density of  $7.93 \times 10^{-3} \text{ g/mm}^3$ , a modulus of elasticity of 200000 MPa in tension, 0.2% YS of 470 MPa and UTS of 570 MPa (these properties are taken from the data sheet of the powder material used for the experimental study and provided from CONCEPTLASER). In Figure 53 it is possible to observe a section of the original object that shows the constrained internal cylindrical surfaces. For all these nodes all degree of

freedom have been locked, in order to simulate bolt tightening constraints. Three different load conditions have been studied. The loads of 220 N, 135 N and 100N are used respectively for the direction of the resulting force along the y axis, 45 degrees from the y direction and the x axis.

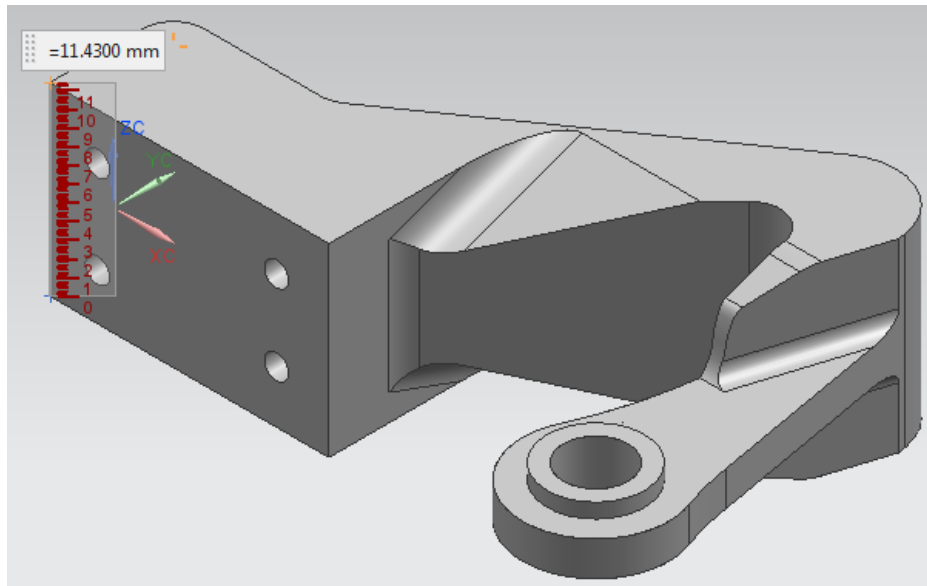


Figure 51: Analyzed object second view.

Proprietà elemento	
Tipo	CTETRA(10)
Parametri mesh	
Dimensioni elemento	0.58 mm
<input checked="" type="checkbox"/> Tentativo di mesh a mappatura libera	
<input type="checkbox"/> Tenta blocco multiplo dei cilindri	
Opzioni qualità mesh	
Metodo nodo centrale	Misto
<input type="checkbox"/> Tolleranza geometria	
Jacobiano	10
Impostazioni mesh	
Variatione dimensioni in base alla curvatura superficie	50.0000
Coefficiente di crescita elemento attraverso il volume	50.2000
<input type="checkbox"/> Spessore attraverso due elementi min	
<input type="checkbox"/> Elementi con errori di correzione automatica	
Opzioni di pulitura modello	
Tolleranza piccole feature (% di dimensione elemento)	10.2000
Lunghezza minima dell'elemento (di sola lettura)	0.05916
Agente di raccolta destinazioni	
<input checked="" type="checkbox"/> Creazione automatica	

Figure 52: Setting parameters for meshing phase.

In the following pages these different load conditions will be called respectively as first, second and third load condition. These three different load values have been chosen in order to have for each of the three situation the same minimum security factor on the yield strength of the material. These factors are 3.08, 2.97, 3.21 respectively for the first, second, third load condition. For each situation the total load is spread with a parabolic distribution in the inner cylindrical surface of the bearing bracket's arm along an arc of 180 grades.

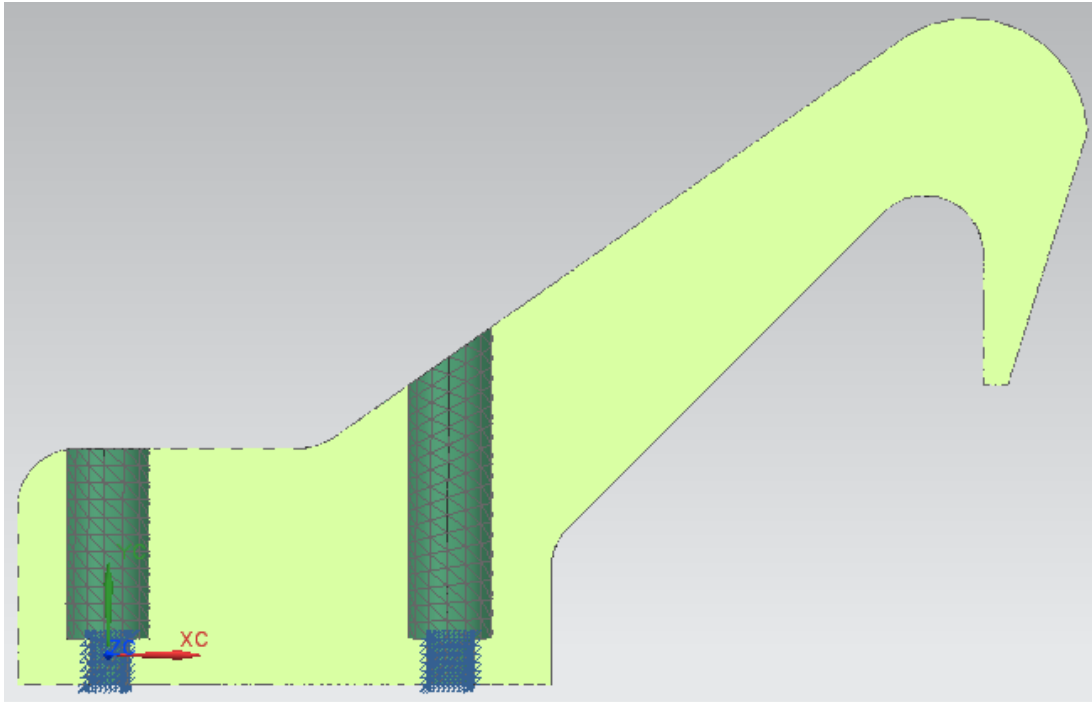


Figure 53: Constrained internal cylindrical surfaces, first view.

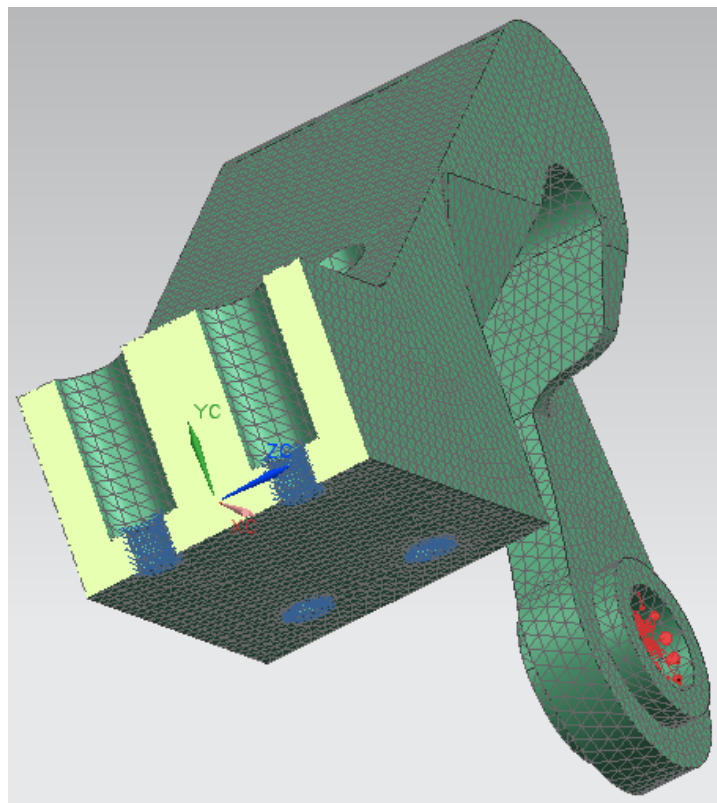


Figure 54: Constrained internal cylindrical surfaces, second view.



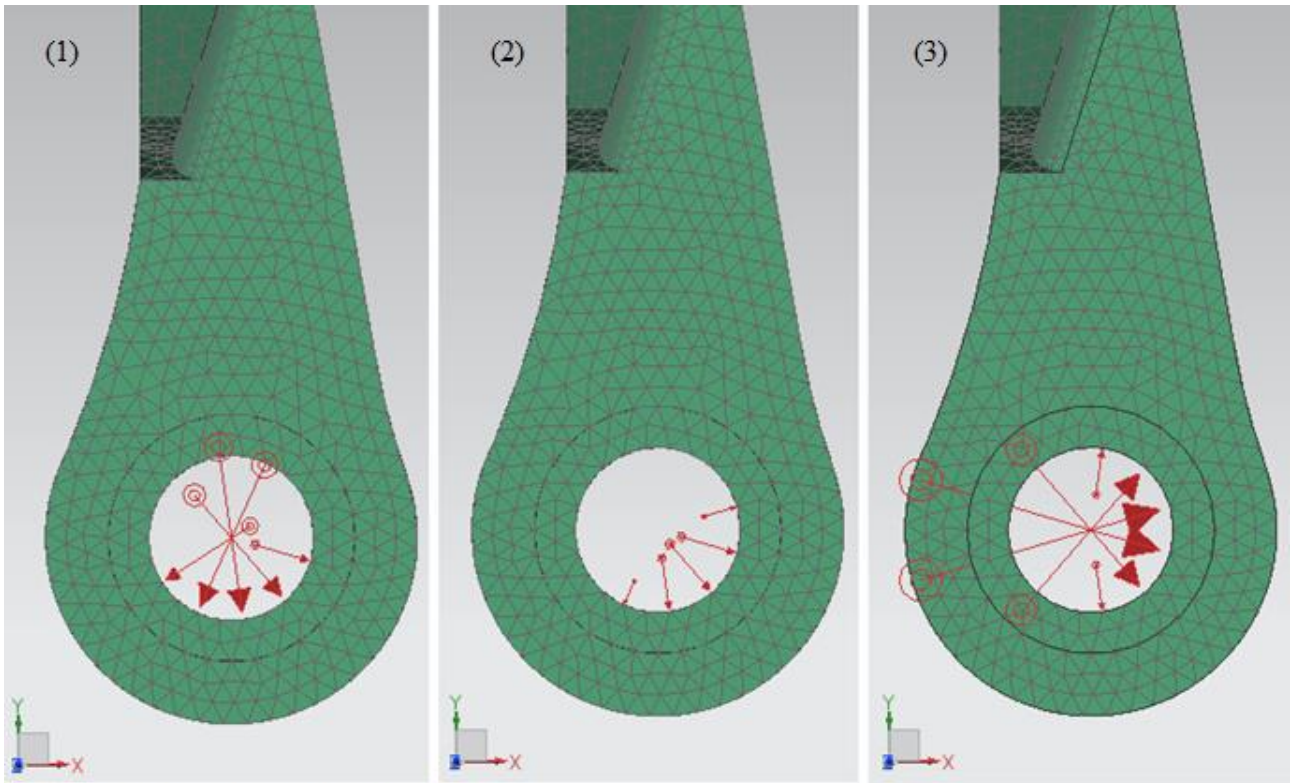


Figure 55: Three different load conditions.

From the Figure 56 to Figure 62 is possible to observe the equivalent Von Mises stress in the original object.

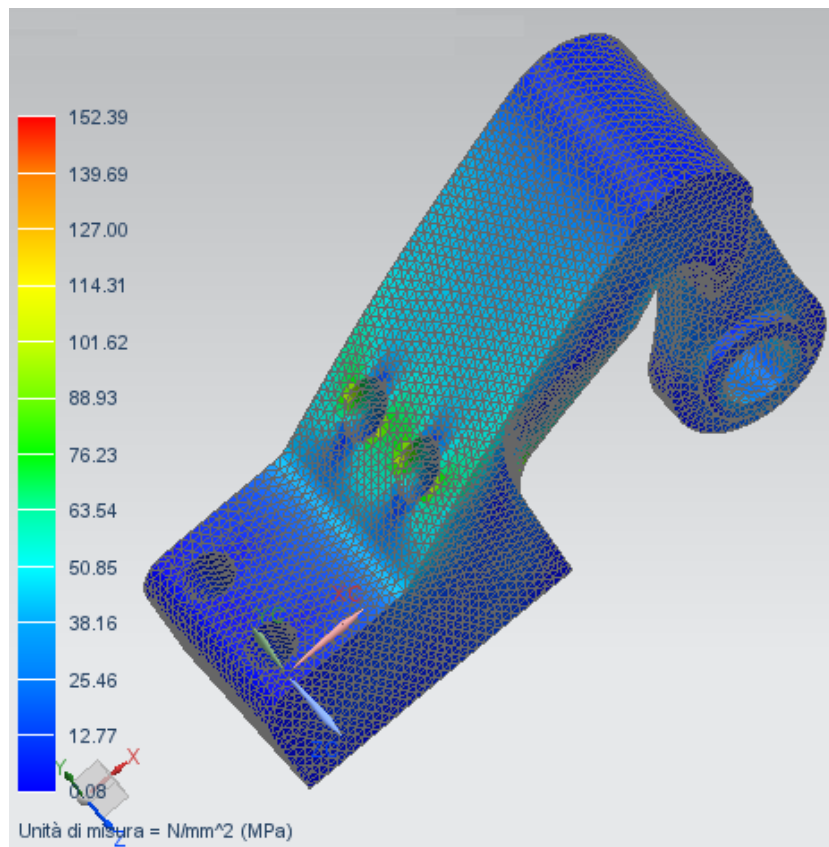


Figure 56: First view of equivalent Von Mises stress for load condition along y direction.

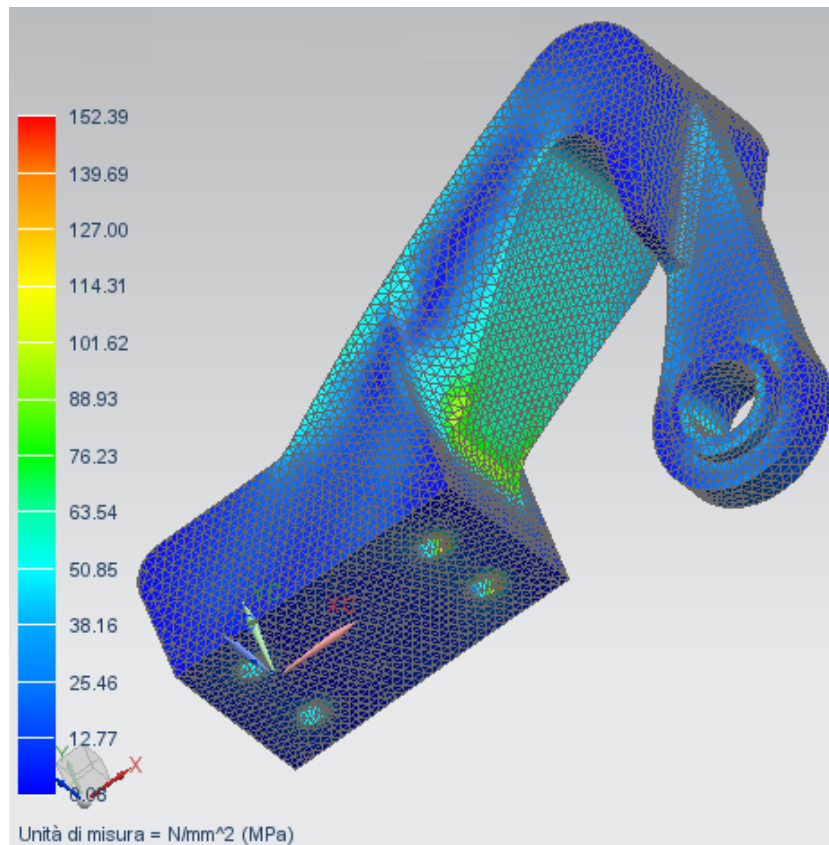


Figure 57: Second view of equivalent Von Mises stress for load condition along y direction.

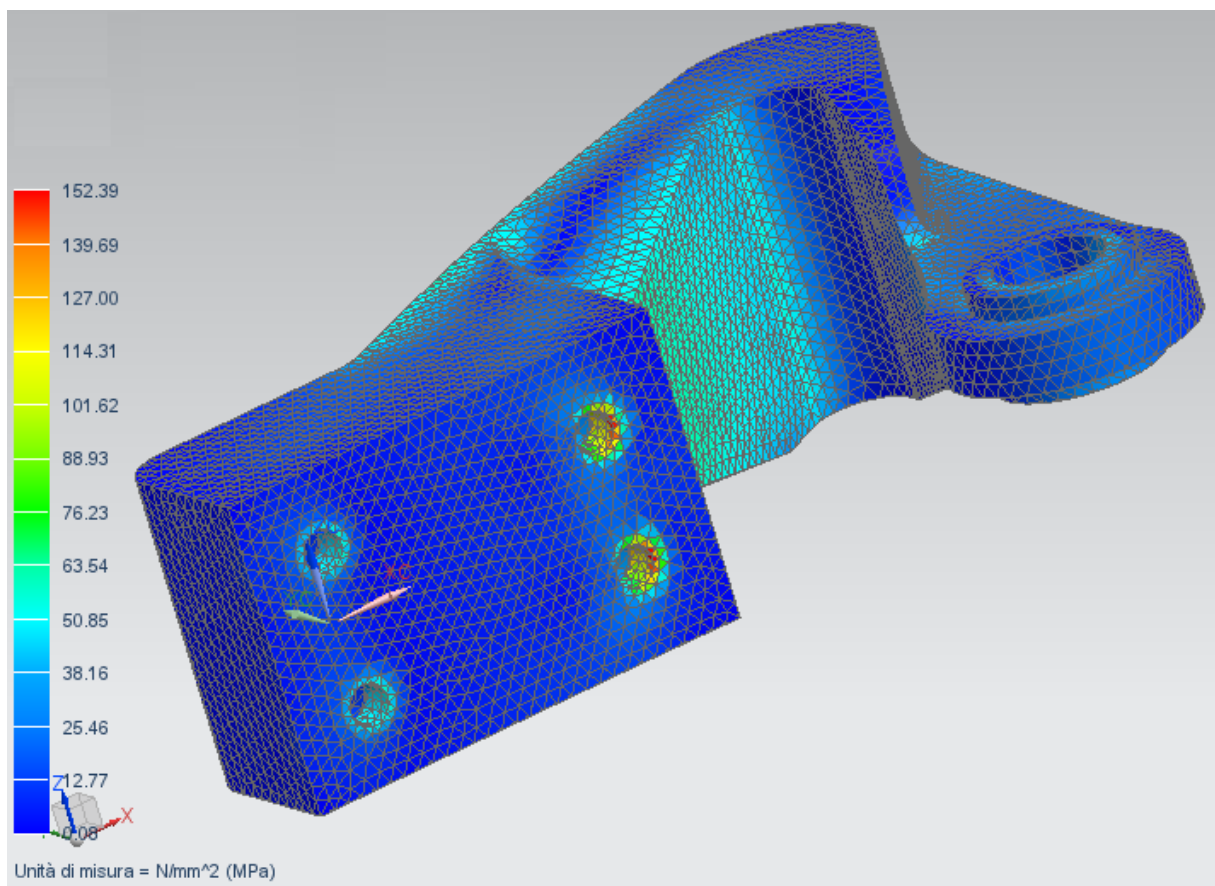


Figure 58: Third view of equivalent Von Mises stress for load condition along y direction.

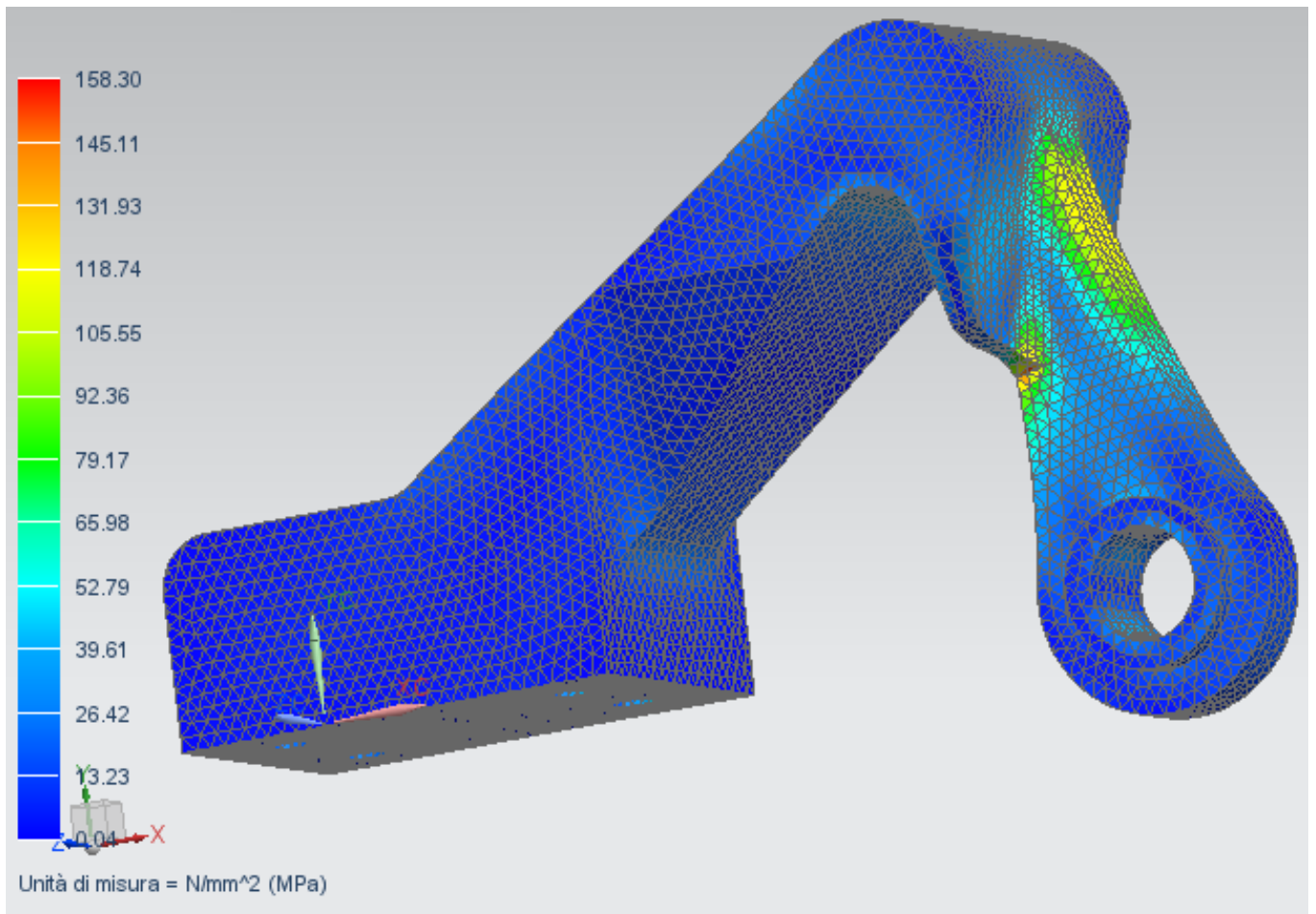


Figure 59: First view of equivalent Von Mises stress for load condition along the bisector of xy plane.

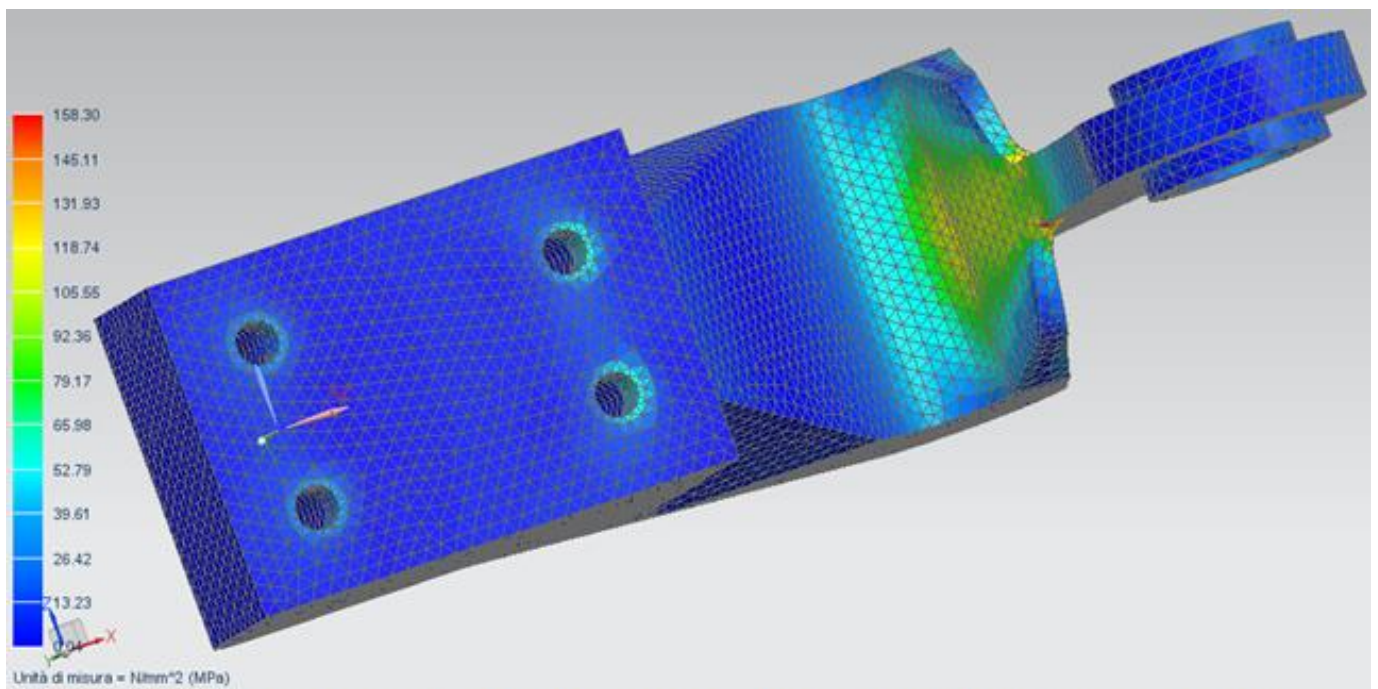


Figure 60: Second view of equivalent Von Mises stress for load condition along the bisector of xy plane.

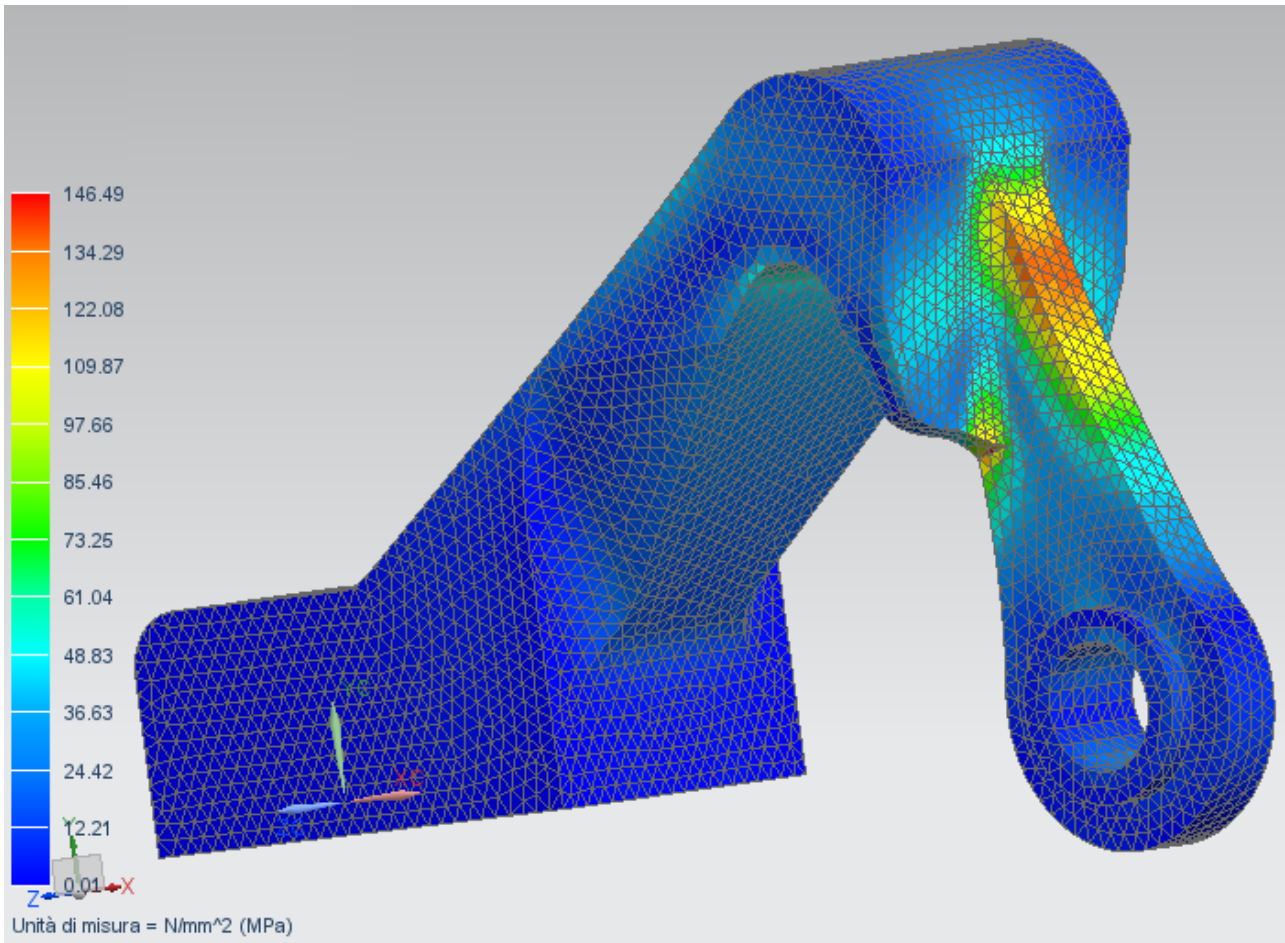


Figure 61: First view of equivalent Von Mises stress for load condition along x direction.

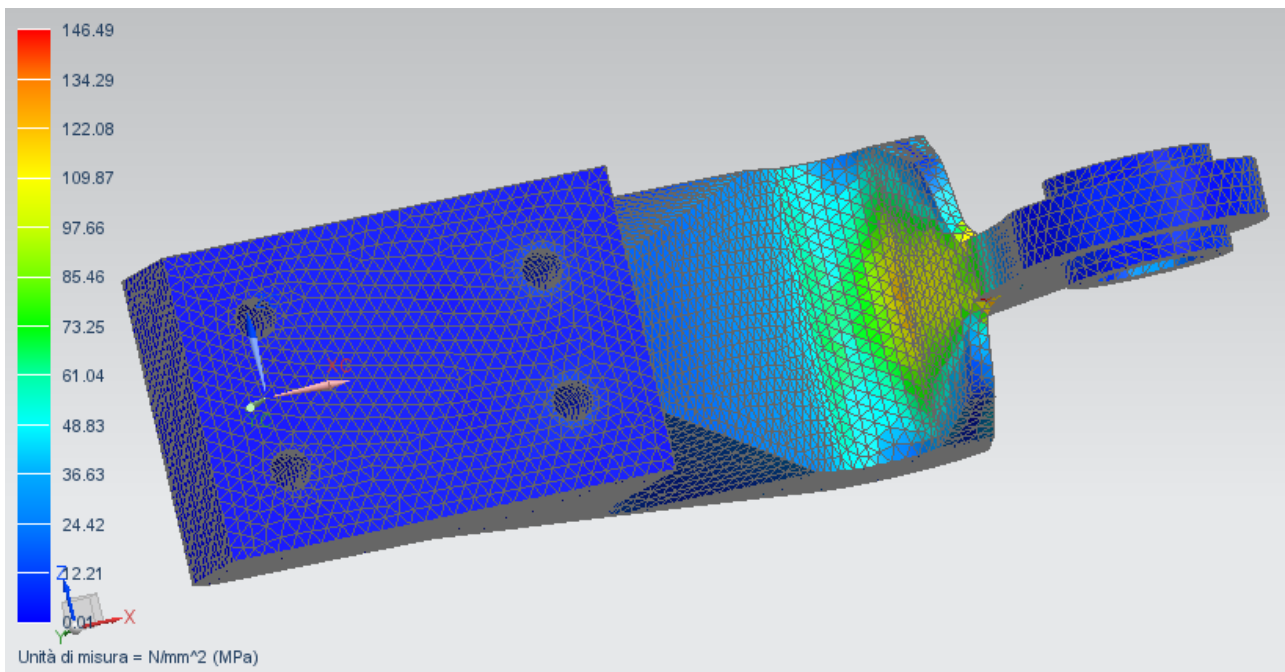


Figure 62: Second view of equivalent Von Mises stress for load condition along x direction.

From the Figure 63 to Figure 68 is possible to observe the displacement fields in the original object along the x and y direction.

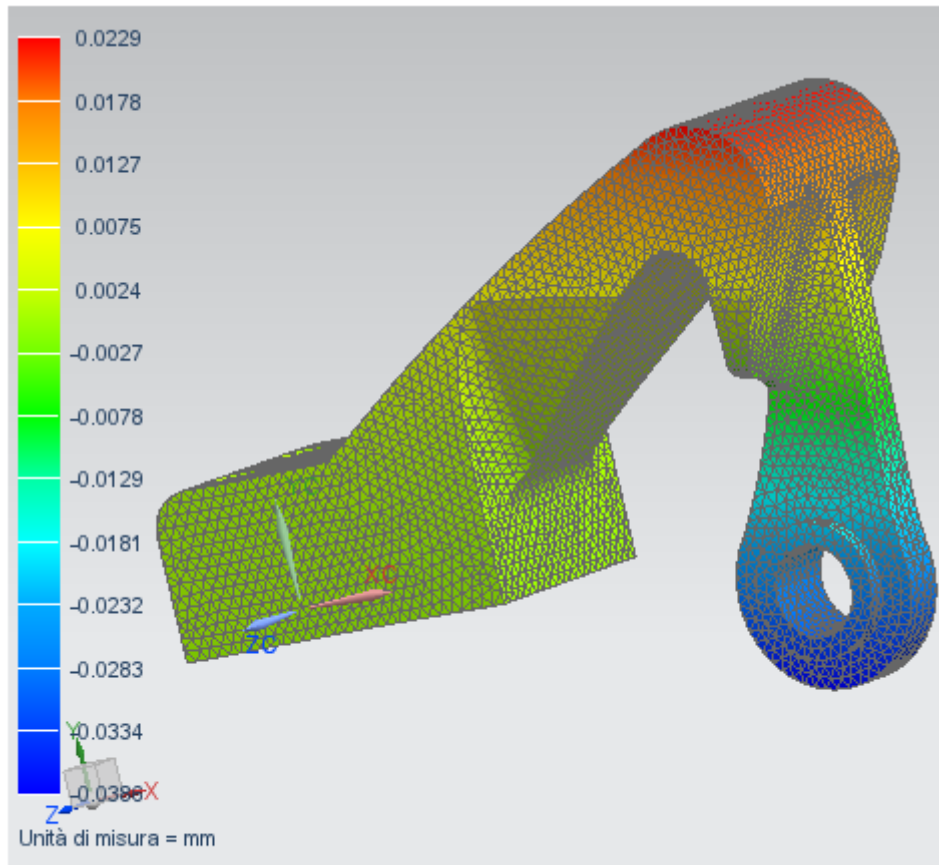


Figure 63: Displacement field for the first load condition along the x direction.

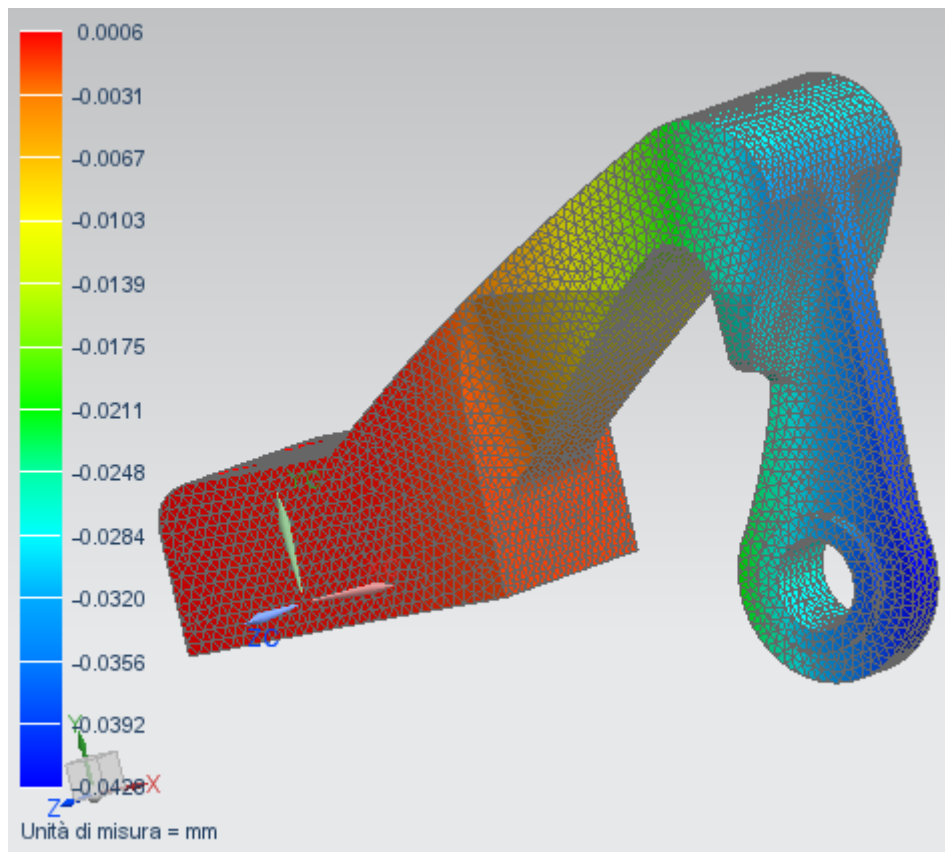


Figure 64: Displacement field for the first load condition along the y direction.

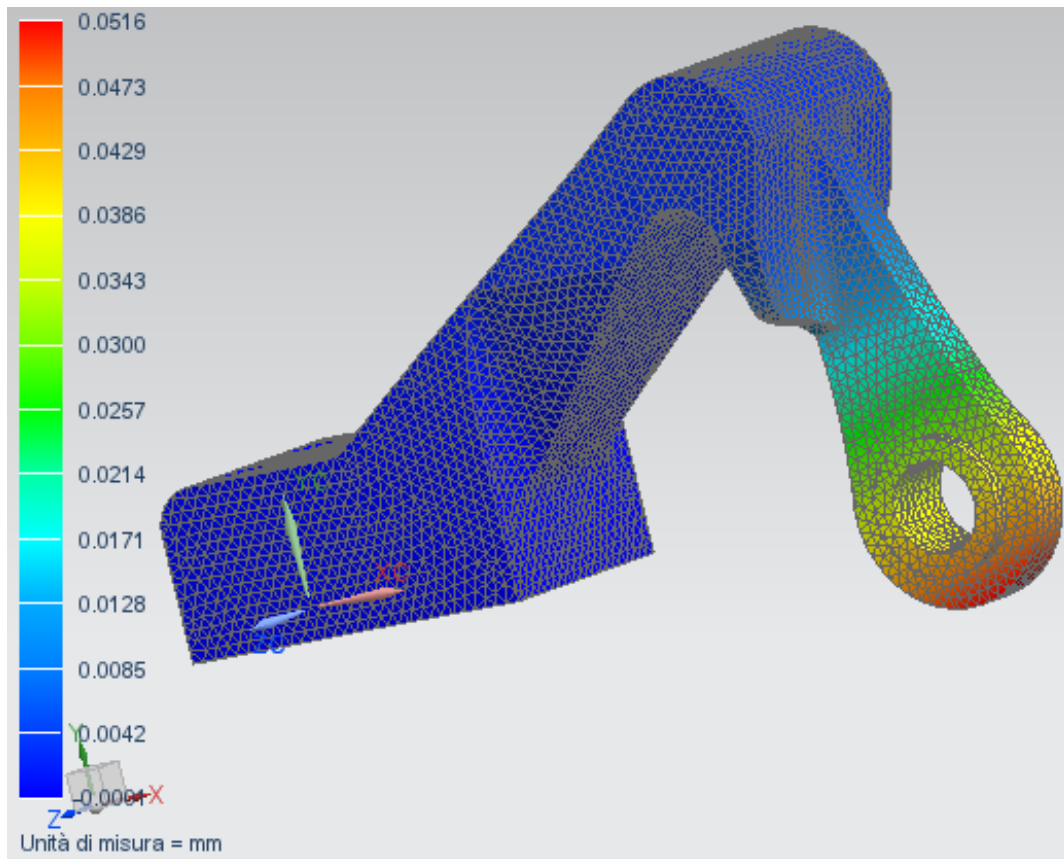
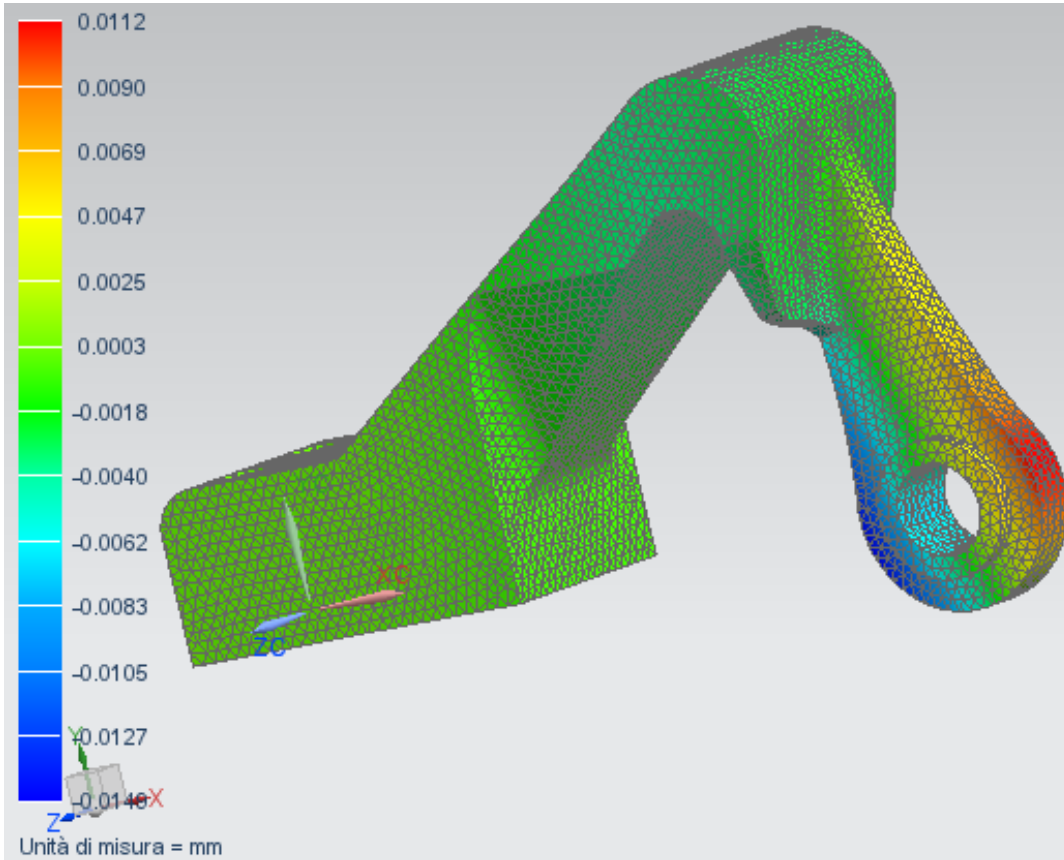


Figure 65: Displacement field for the second load condition along the x direction.



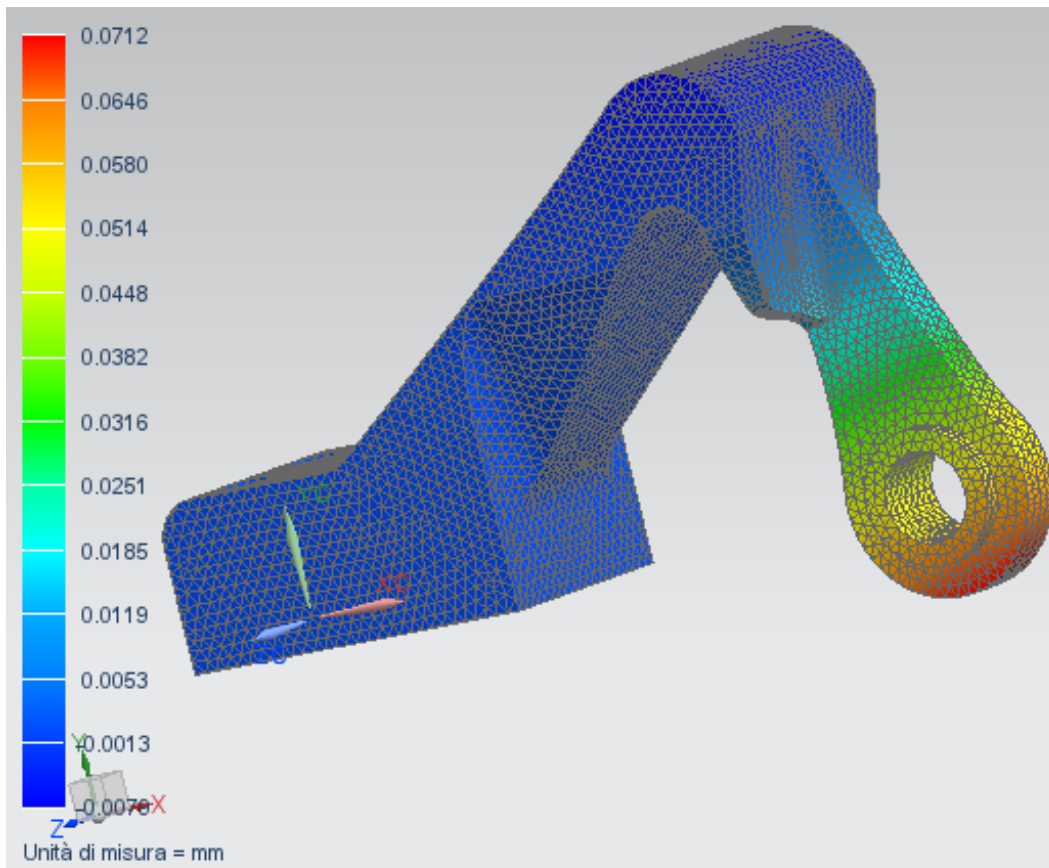


Figure 67: Displacement field for the third load condition along the x direction.

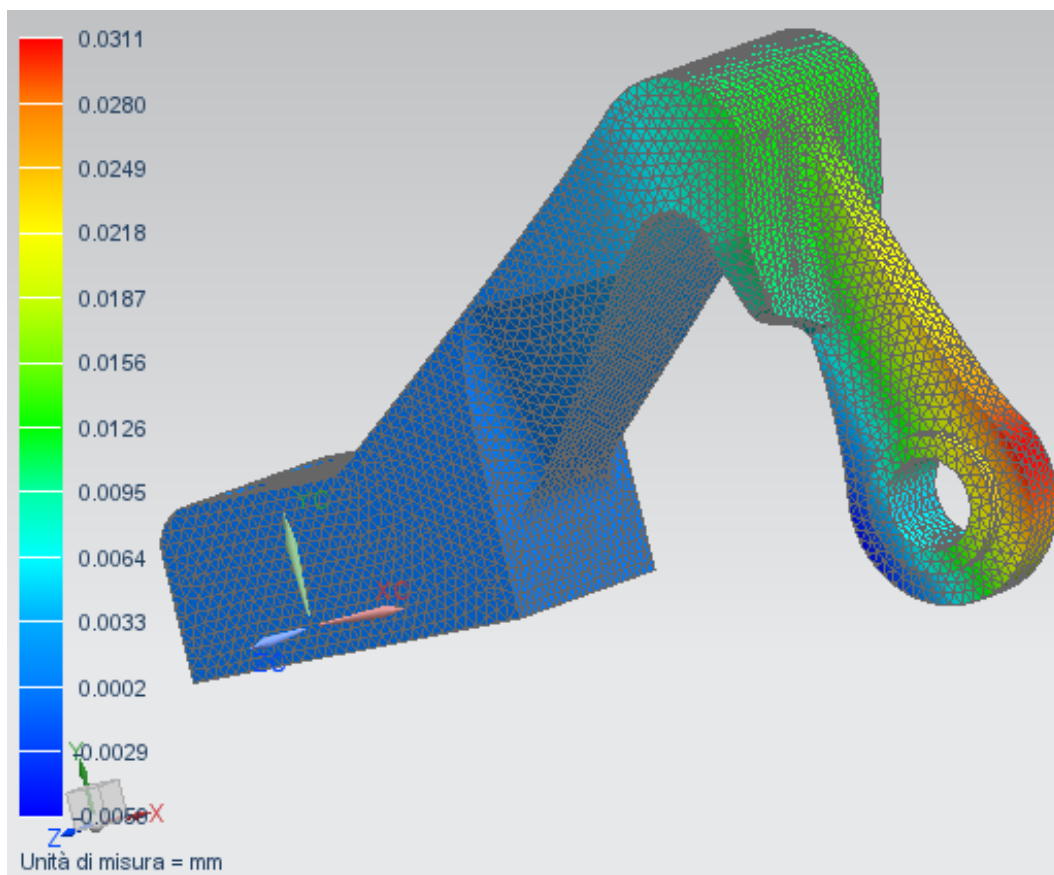


Figure 68: Displacement field for the third load condition along the y direction.

From the first load condition it is possible to see how the arm of the bearing bracket immediately connected to the constrained part of the object is subjected to bending, in fact the higher stresses are present on the external upper and lower surfaces. A concentration of stress is also present along the cylindrical constrained surfaces. For the second and the third load conditions, thanks to the force in the x direction, the external arm is subjected to bending. Moreover for the third load condition the constrained part of the object doesn't present important stress. From these results it is already possible to expect that for each load condition the low stress areas will be eliminated or reduced after the topology optimization analysis.

After these computations the topology optimization analysis was started. In Figure 69 it is possible to see the area restrict condition that has been imposed. In this way these parts of the object are excluded from the design volume, in order to realize a proper bolt tightening constraint and to have a proper cylindrical surface for applying the different loads. In these analyses two different project responses are requested. Volume information from all the meshed elements. Deformation energy from all the meshed elements (Group operator set on SUM). The minimization of the Deformation energy has been set as objective of the analysis and the Volume reduction to a fixed target has been imposed as constraint. After several analyses this number has been set to the relative value respect the original volume of 0.55. The topology optimization algorithm present on NX11 works with a continuous density logic from zero to the nominal value of the chosen material. This means that the output of the analysis is not a series of meshed elements with properties identical to the nominal material, instead it presents a series of meshed elements with a distribution of density and of all the other mechanical properties.



Figure 69: Restrict condition area imposed.

From the Figure 70 to Figure 76 it is possible to observe the equivalent Von Mises stress in the optimized objects, for each load condition.



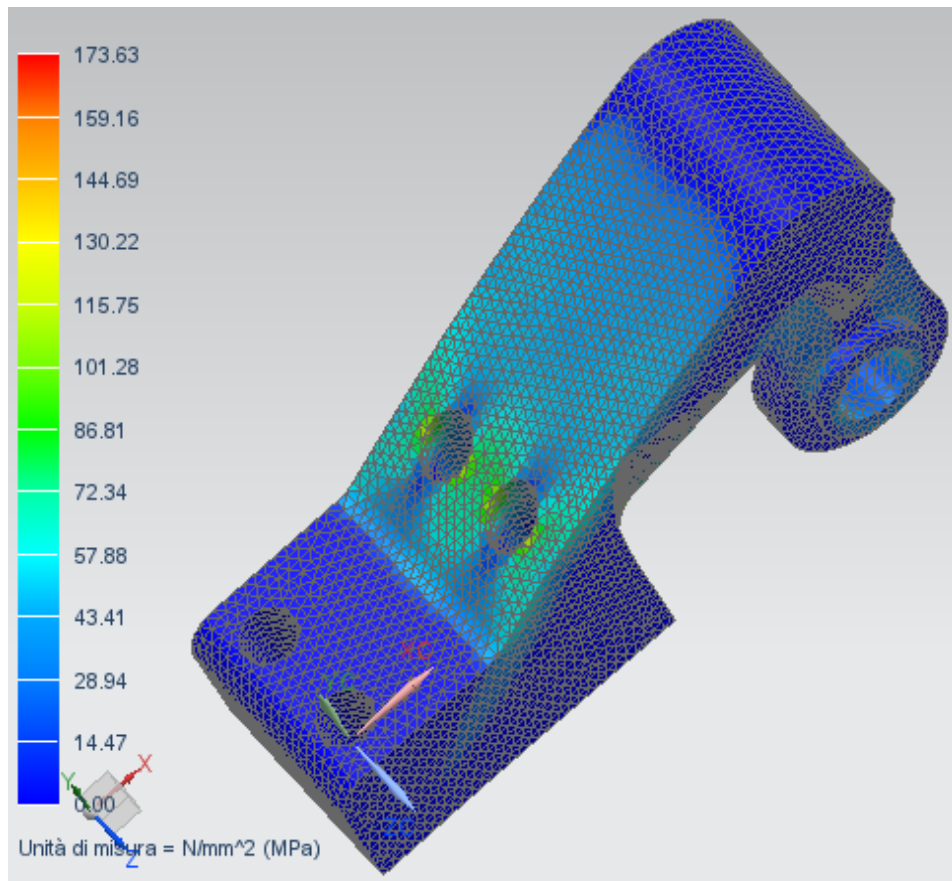


Figure 70: First view of equivalent Von Mises stress for load condition along y direction; optimized object.

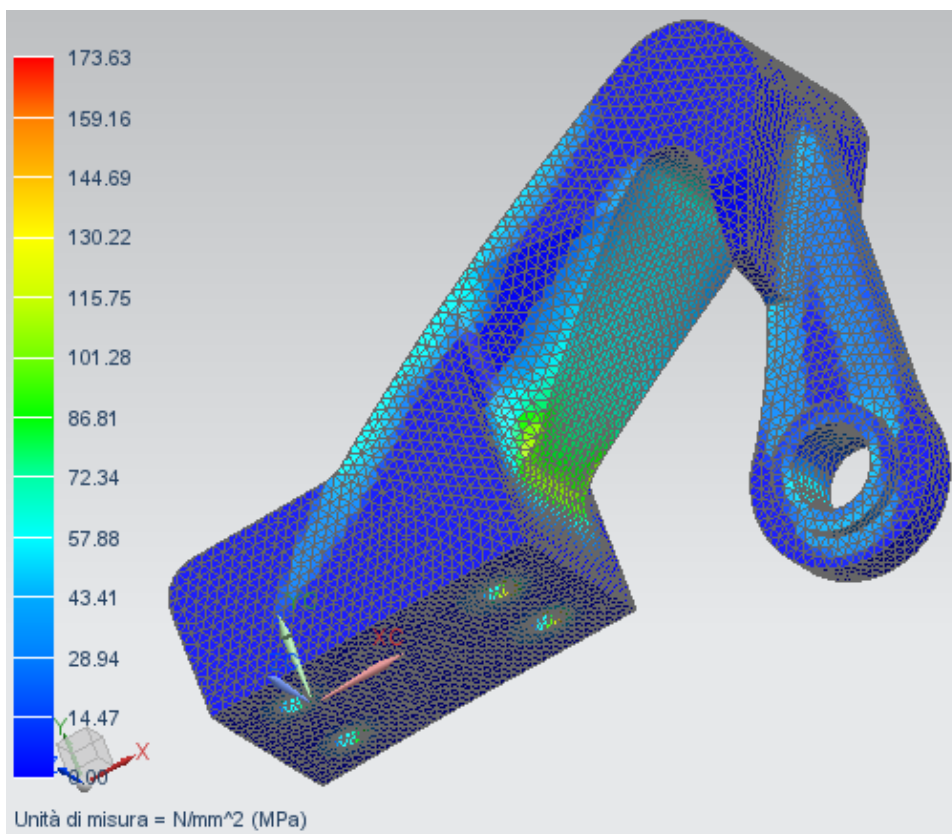


Figure 71: Second view of equivalent Von Mises stress for load condition along y direction; optimized object.

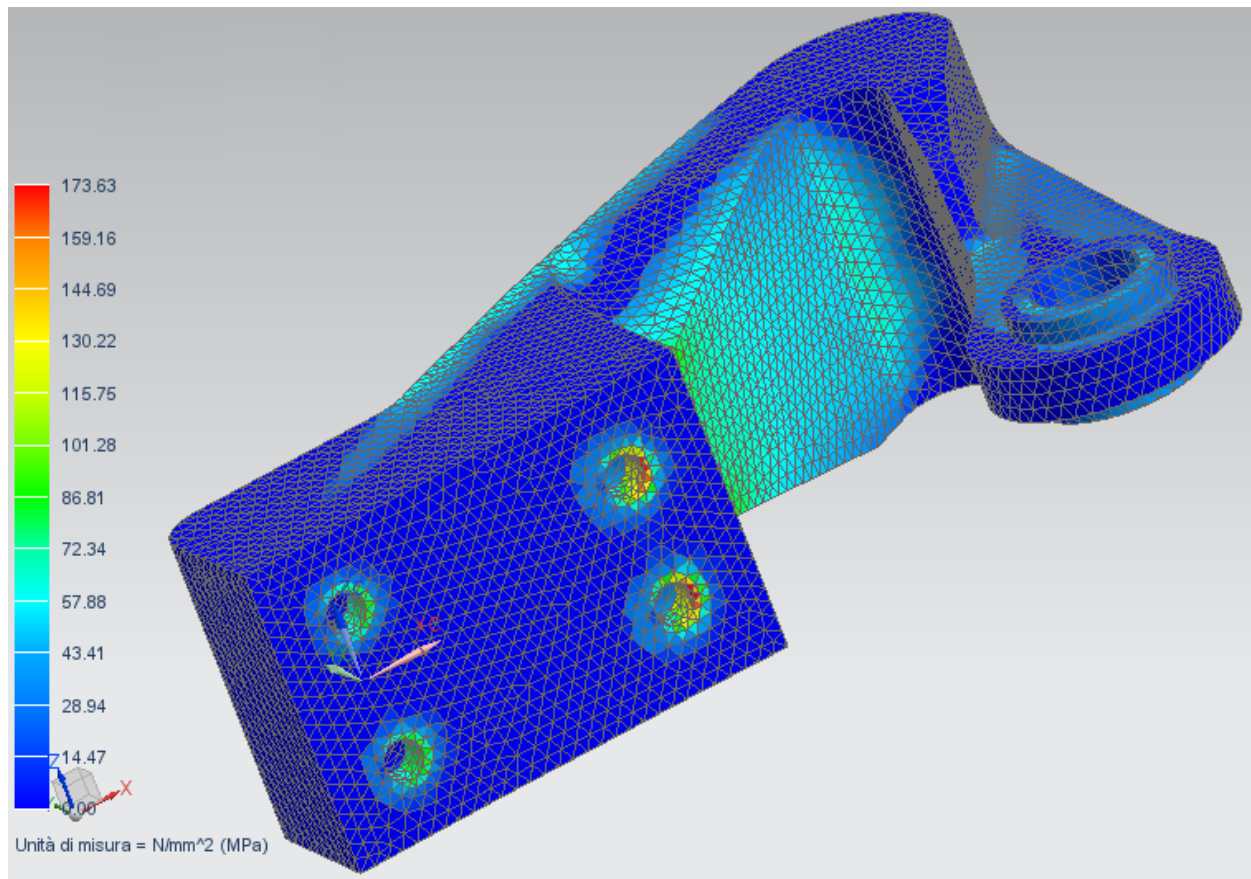


Figure 72: Third view of equivalent Von Mises stress for load condition along y direction; optimized object.

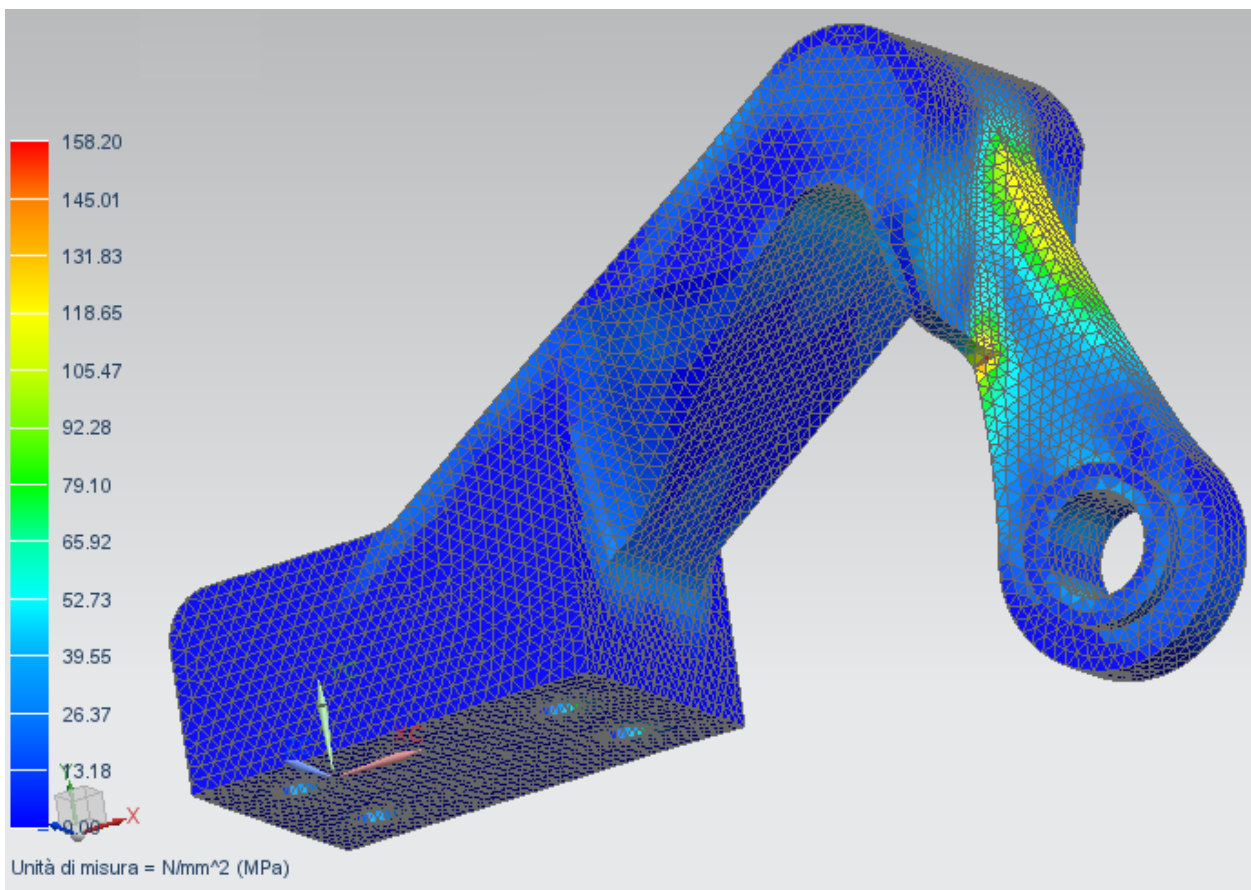


Figure 73: First view of equivalent Von Mises stress for the second load condition; optimized object.

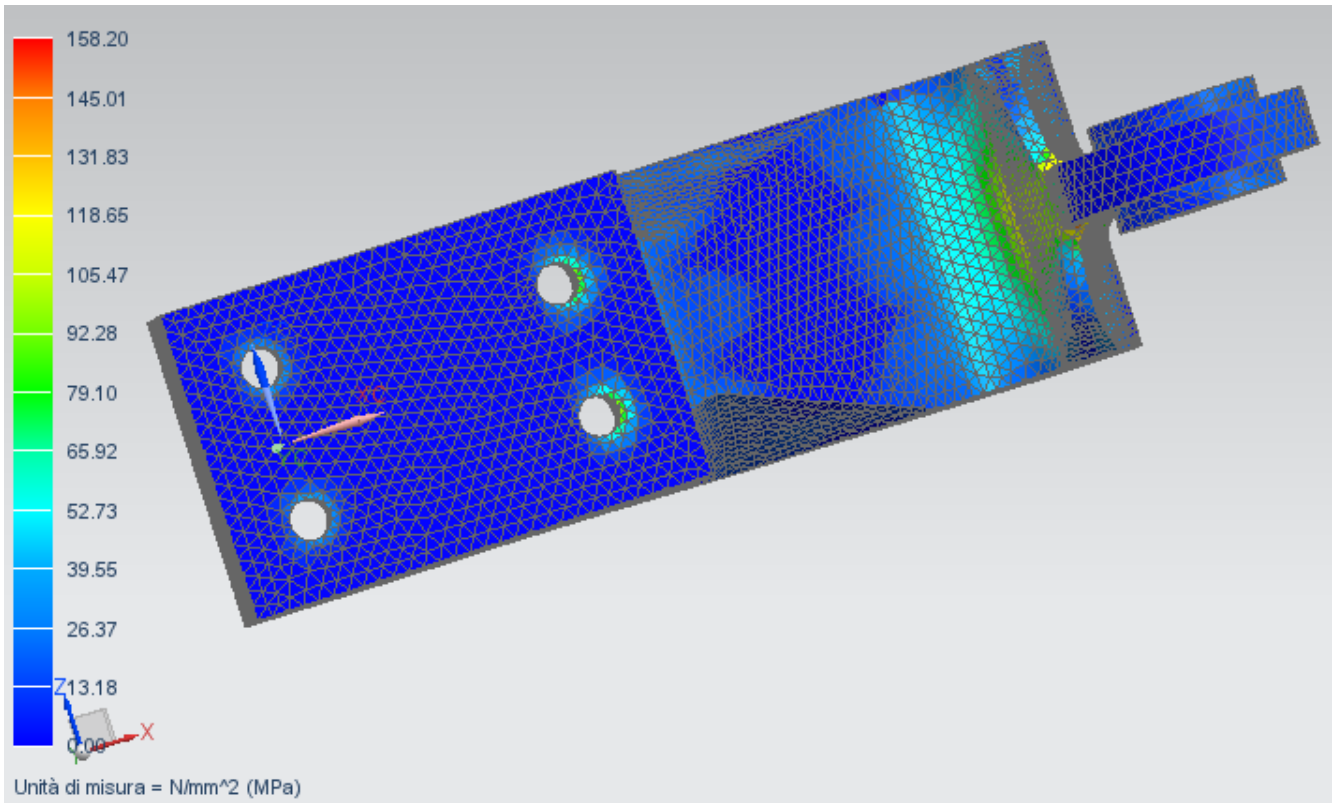


Figure 74: Second view of equivalent Von Mises stress for the second load condition; optimized object.

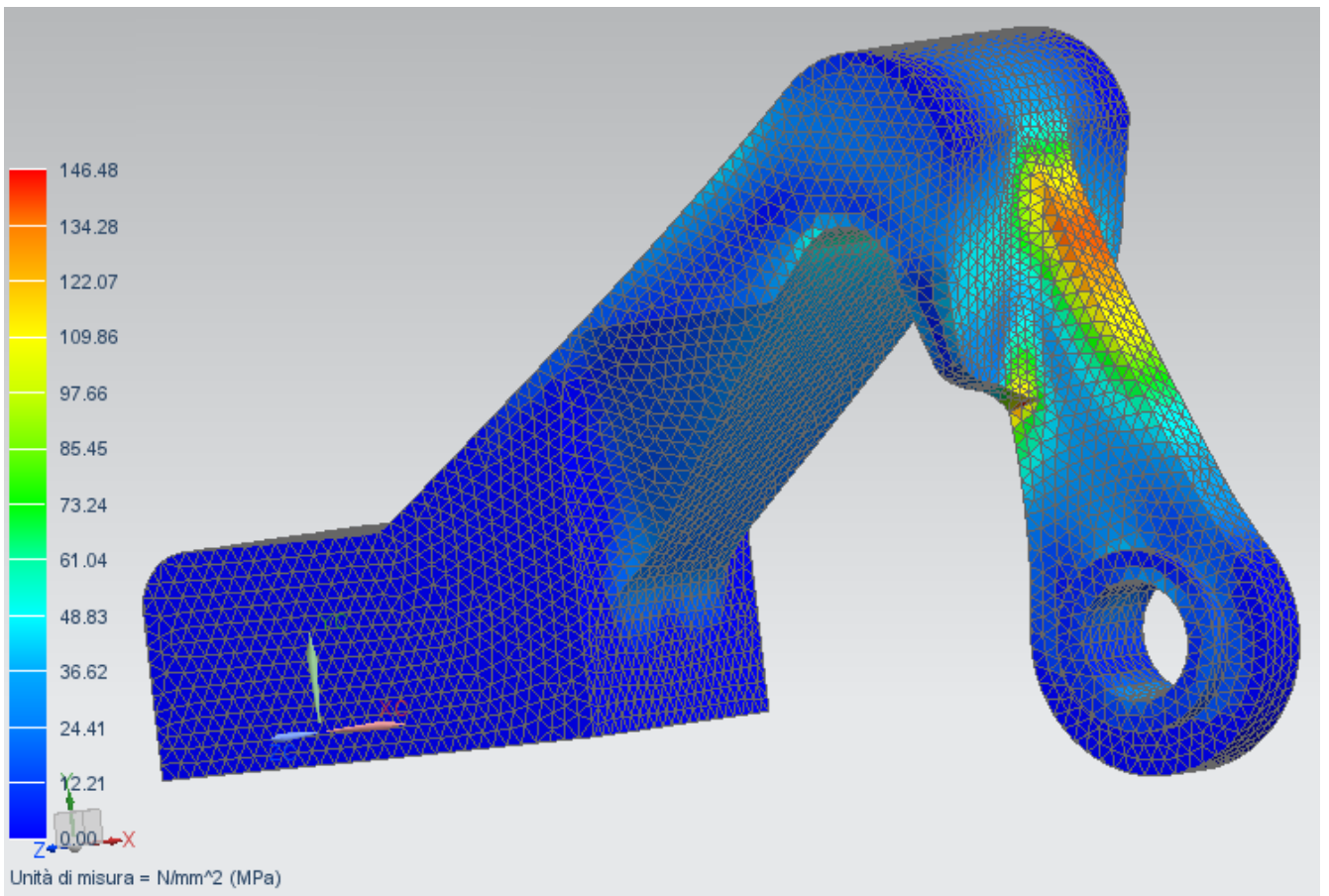


Figure 75: First view of equivalent Von Mises stress for load condition along x direction; optimized object.

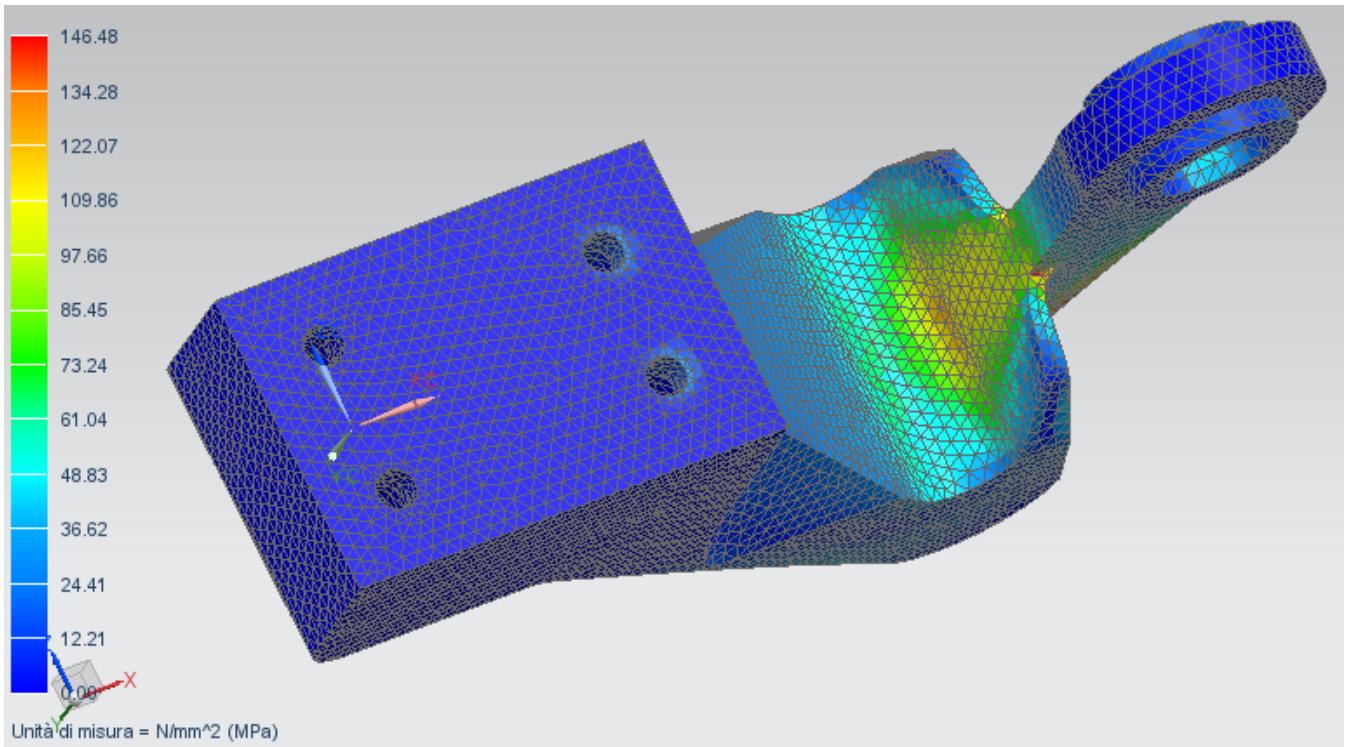


Figure 76: Second view of equivalent Von Mises stress for load condition along x direction; optimized object.

From the Figure 77 to Figure 82 is possible to observe the displacement fields in the original object along the x and y direction.

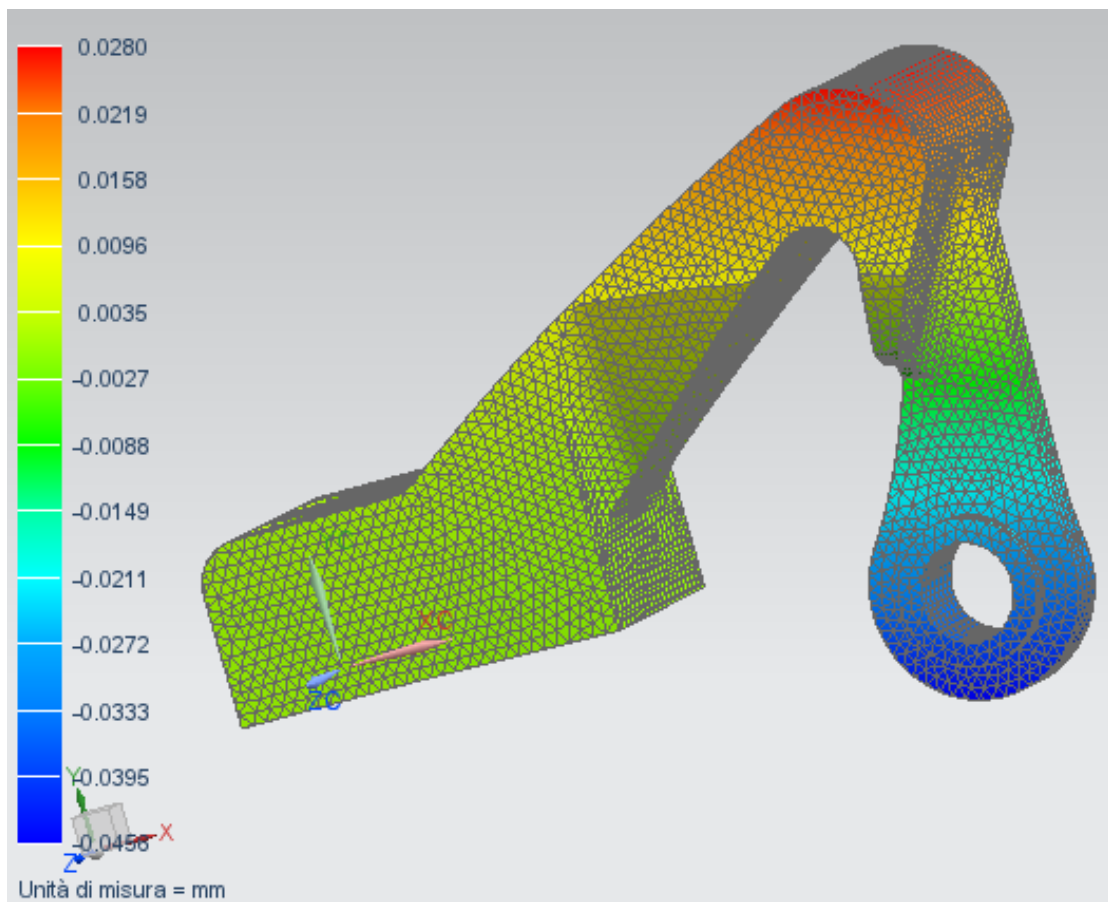


Figure 77: Displacement field for the first load condition along the x direction.

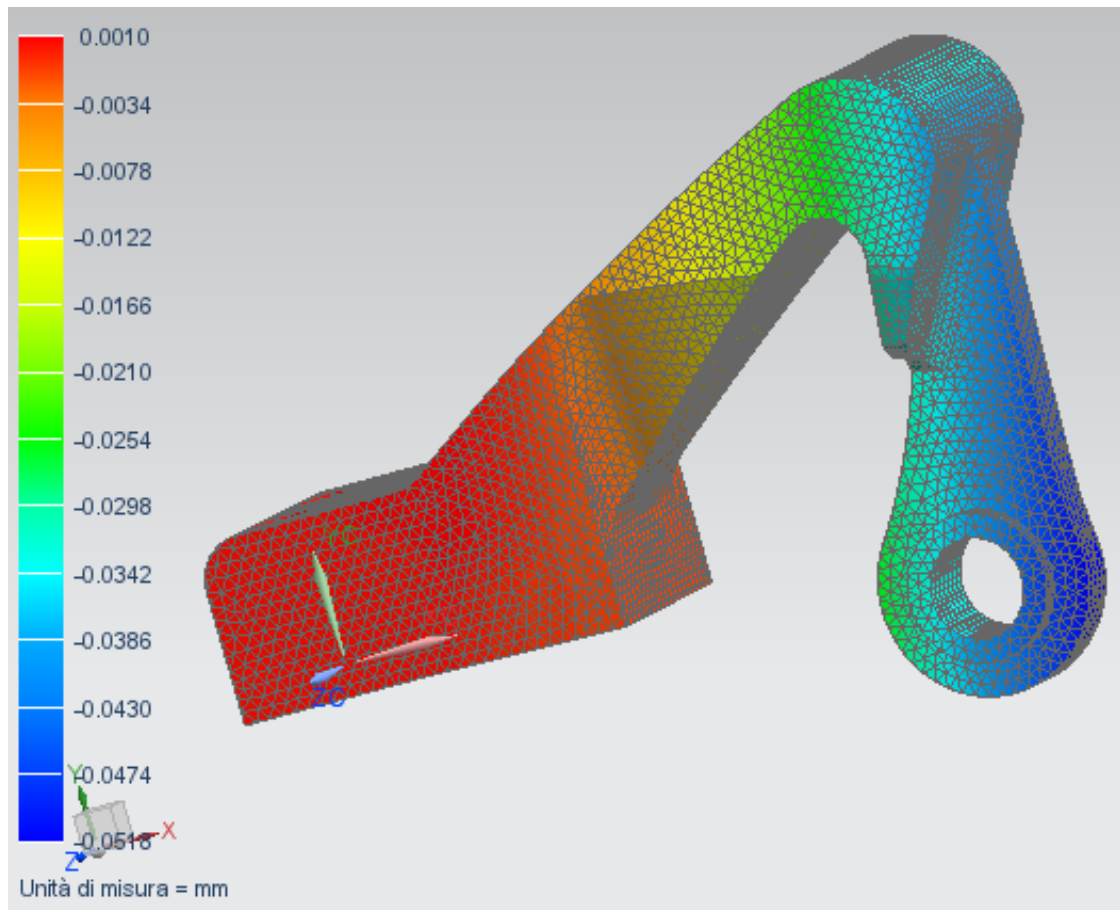


Figure 78: Displacement field for the first load condition along the y direction.

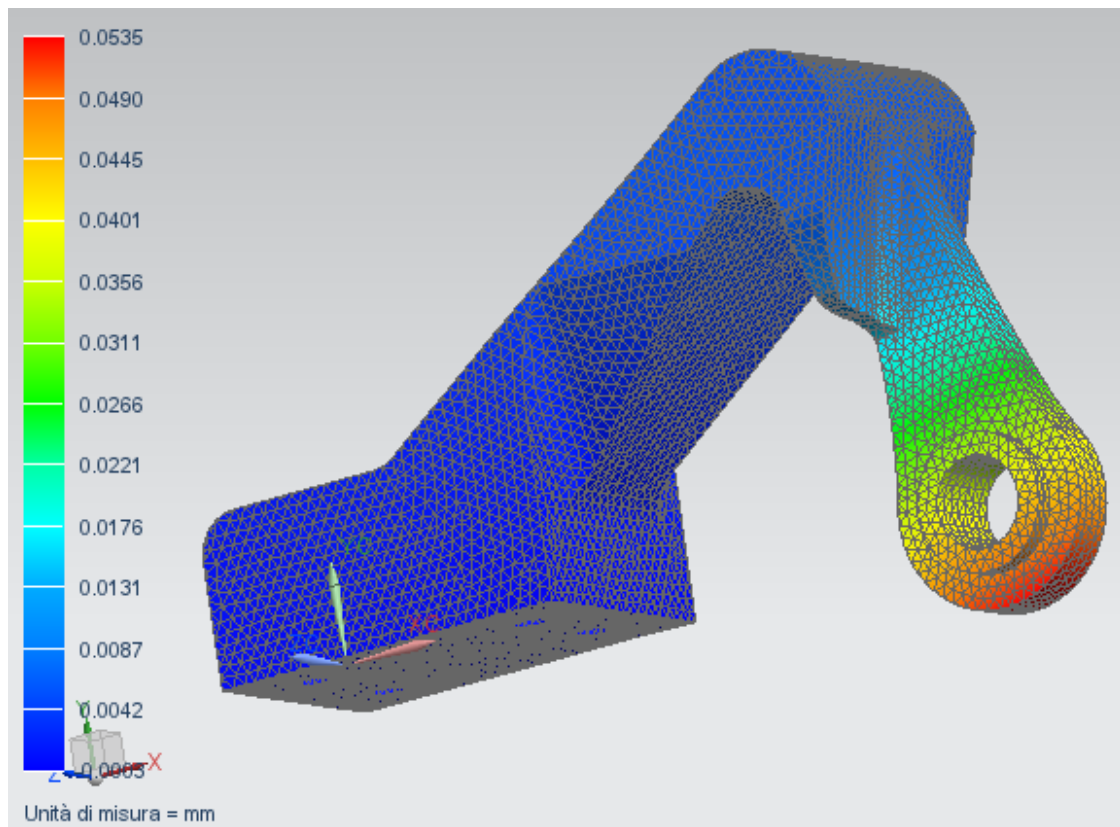


Figure 79: Displacement field for the second load condition along the x direction.

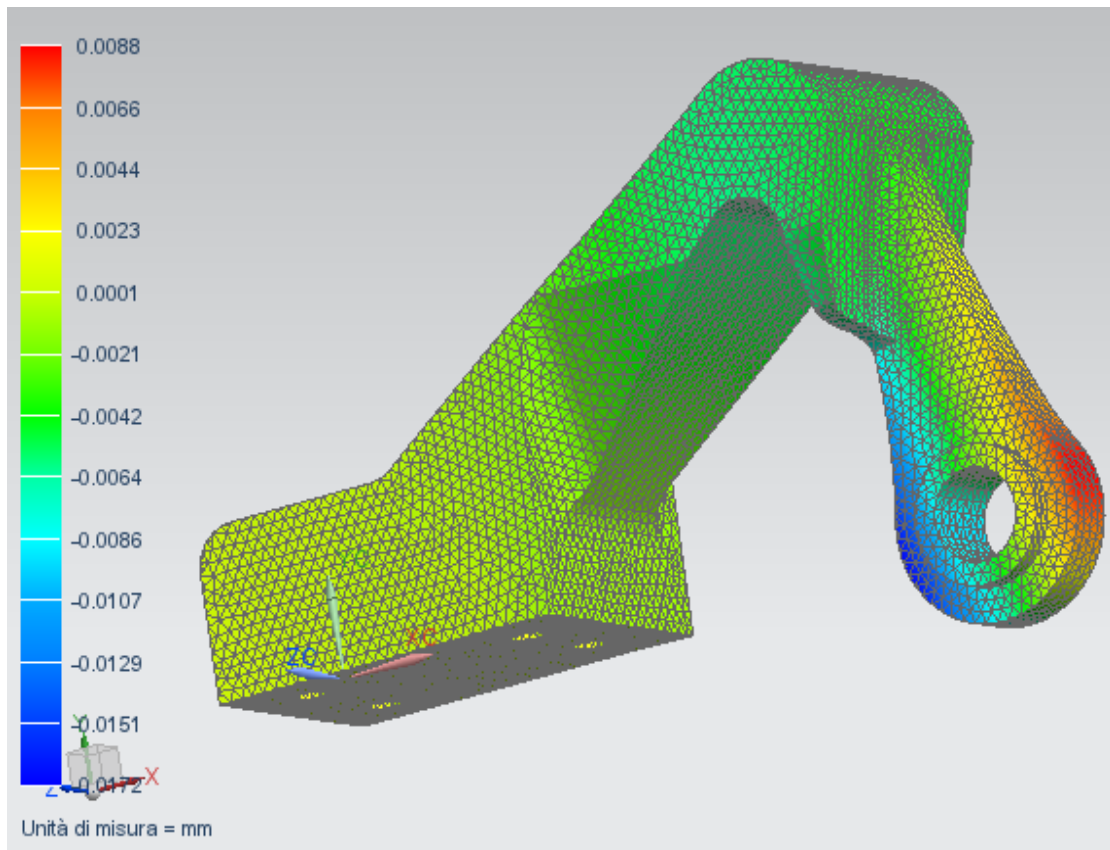


Figure 80: Displacement field for the second load condition along the y direction.

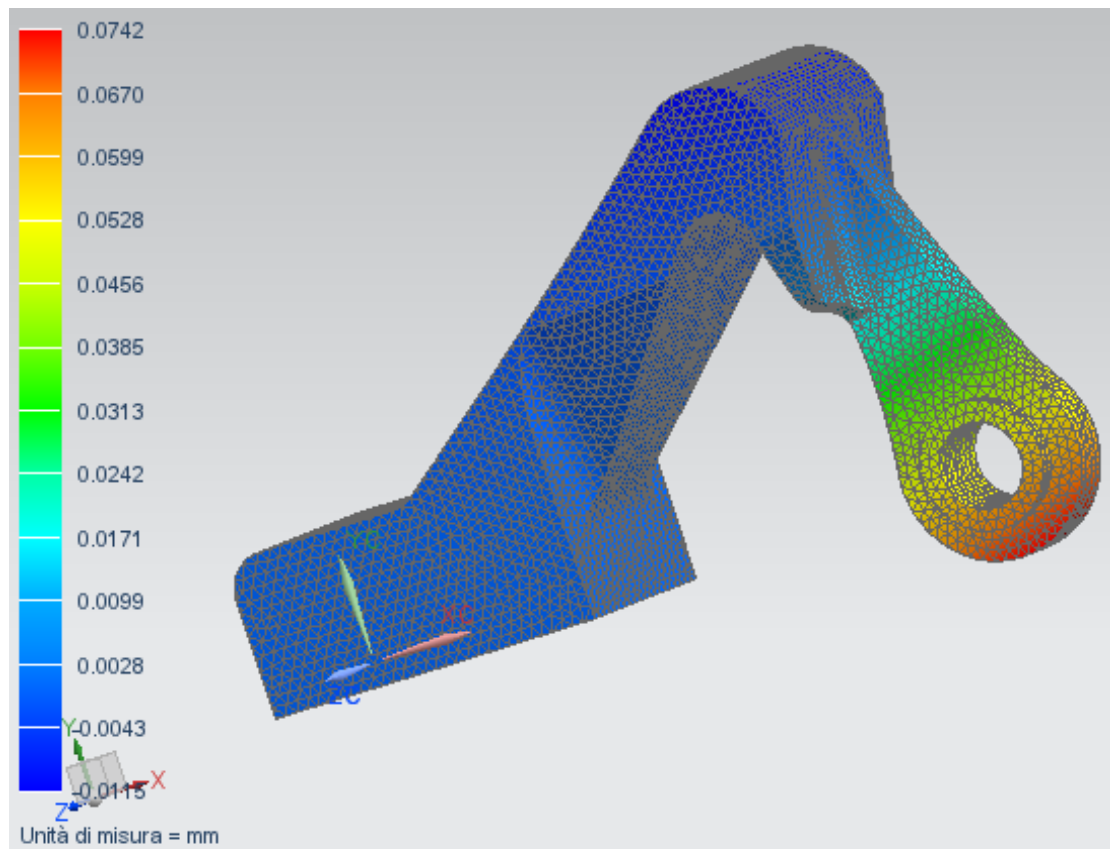


Figure 81: Displacement field for the third load condition along the x direction.

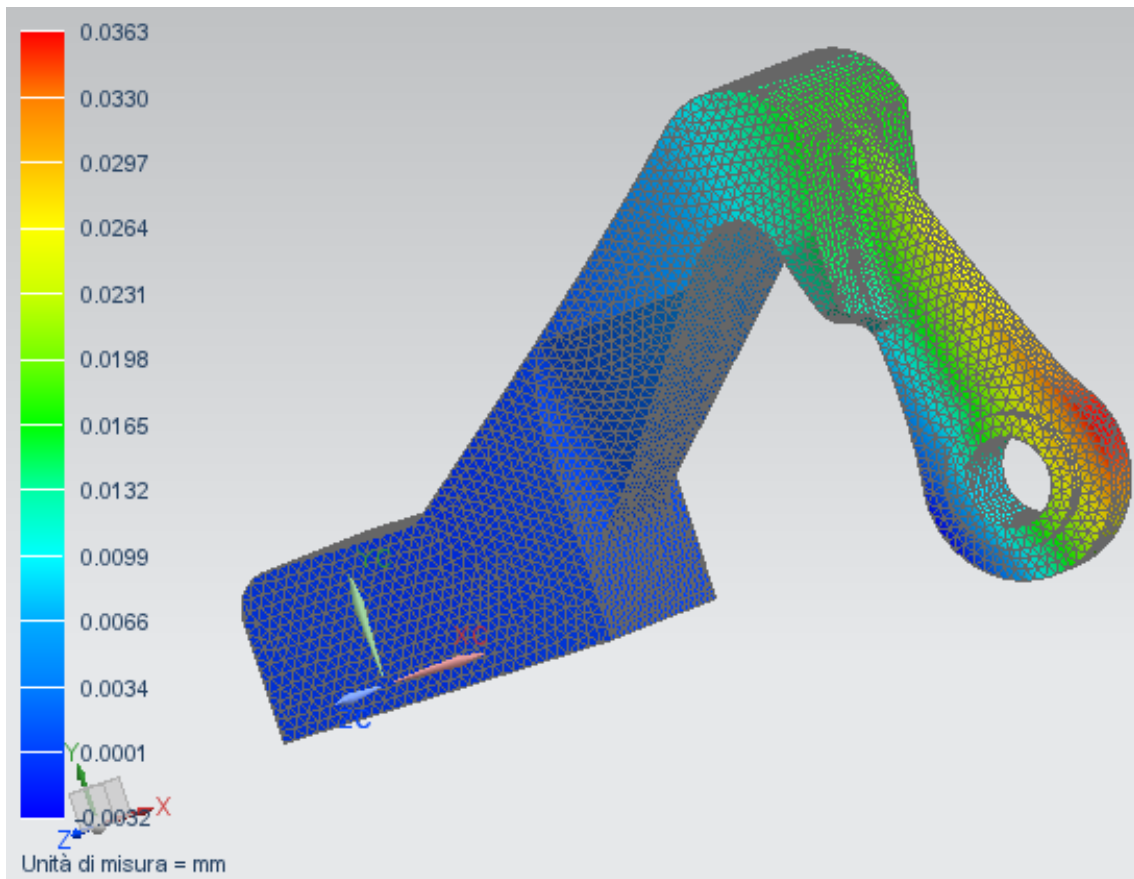


Figure 81: Displacement field for the second load condition along the y direction.

Is important to understand that the FEM static analysis results, presented in these figures, are output responses from analysis carried out on objects filled with meshed elements with a distribution of the mechanical properties. This can explain why apparently the shape and the volume on the previous and the present objects are identical, but the results are different. Comparing the pictures from Figure 56 to Figure 68 with the pictures from Figure 70 to Figure 81, it is possible to see that both the stress fields and the displacements are quite similar. About the stress field, the security factors for the three load conditions are respectively in order 2.71, 2.97 and 3.21.

In order to elaborate the CAD models of the optimize parts different STL files has been requested from these analysis. Is possible to set a cut off on the density of the meshed elements in relation to the nominal density (of relative value set to 1), in this way only the elements that have density greater than this number are considered. Three different files with density cut off set to 0.3, 0.5 and 0.7 have been requested for each load conditions. After the topology optimization analysis the STL files with a density cut off of 0.3 and 0.5 have been considered too massive and then rejected. For each of the three load conditions the STL files with a cut off set to 0.7 have been chosen. At the beginning it has been tried to use the CAD functions present in NX11 but by this way the process was too long. In fact the procedure should have been to recreate a part model using sketches of as more as possible different sections of the STL file, connect each other the neighbors sketches first with different lines and then with volume elements. The program Materialise 3-matic has been used to accelerate this phase. This program accepts STL files in input and can exports STL files. It has good tools for repairing the STL files from the topology optimization phase, infact usually these files have problems of intersections, holes and overlays between the triangles. It has some good tool for the reconstruction

of some particular zones of the object and some tool for the procedure of smoothing of the different edges. The different final optimized parts have been obtained in this way.

From Figure 83 to Figure 85 is possible to see the final optimized geometries for the three different load conditions. With a tool present in NX11, the nominal volume of these new parts have been calculated. The original object has a volum of 2694.15 mm<sup>3</sup>. For the first load condiction the nominal volume is 1452.83 mm<sup>3</sup> with a volume reduction of 46.07%. For the second load condiction the nominal volume is 1595.58 mm<sup>3</sup> with a volume reduction of 40.78%. . For the third load condiction the nominal volume is 1553.74 mm<sup>3</sup> with a volume reduction of 42.33%.

It is evident that these new parts could have a geometry slightly different from the original STL output files, but more over the mass will be different because these optimized volumes will be from now considered filled with a material that has the nomial properties of the chosen one. On the contrary, as written in the previous pages, the output of the topology optimization tool, present in NX11, is a volume filled with meshed element of different mechanical properties.

As explained, the FEM static analysis results, presented from Figure 69 to Figure 81, are output responces from analysis carried out on objects filled with meshed elements with a distribution of the mechanical properties. These results can also be trusted for the final optimized geometries, since in this second case they have directly less mesh elements but all of them characterized of the nominal properties of the chosen material.

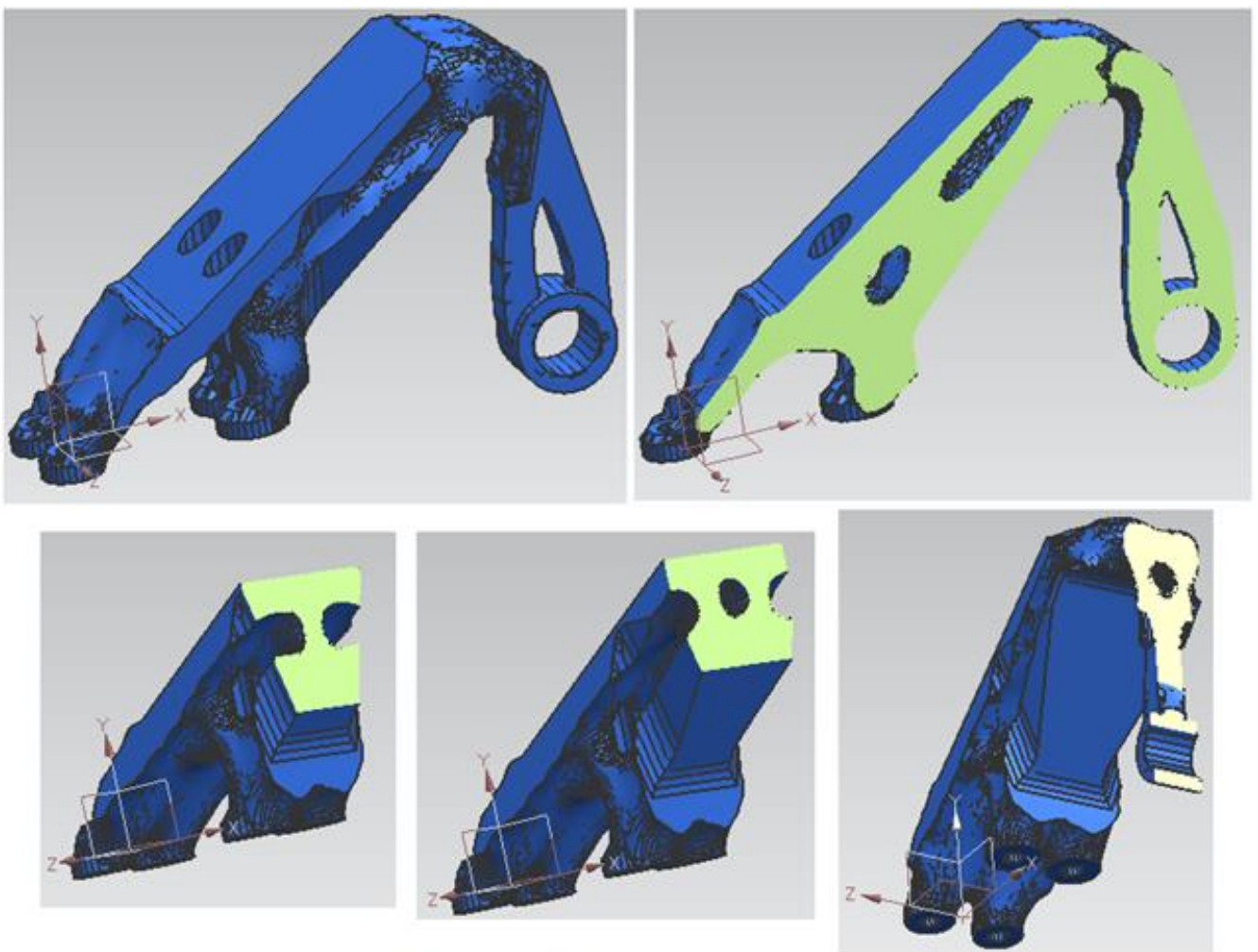


Figure 83: Optimized part for the first load condiction.



In according to the different optimized geometries has been considered an object with a stronger mass reduction and that can takes into account the three different load conditions. Its volume is 898.02 mm<sup>3</sup> with a volume reduction of 66.67%.

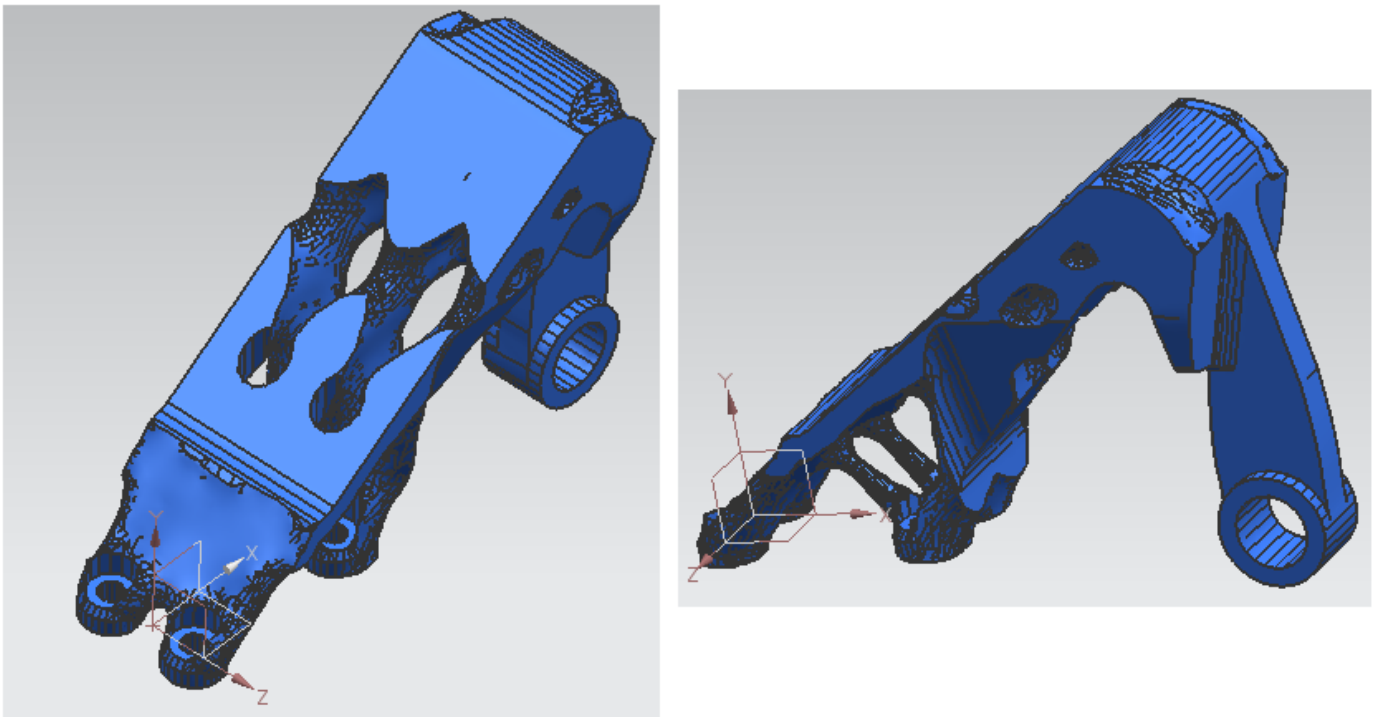


Figure 84: Optimized part for second load condition.

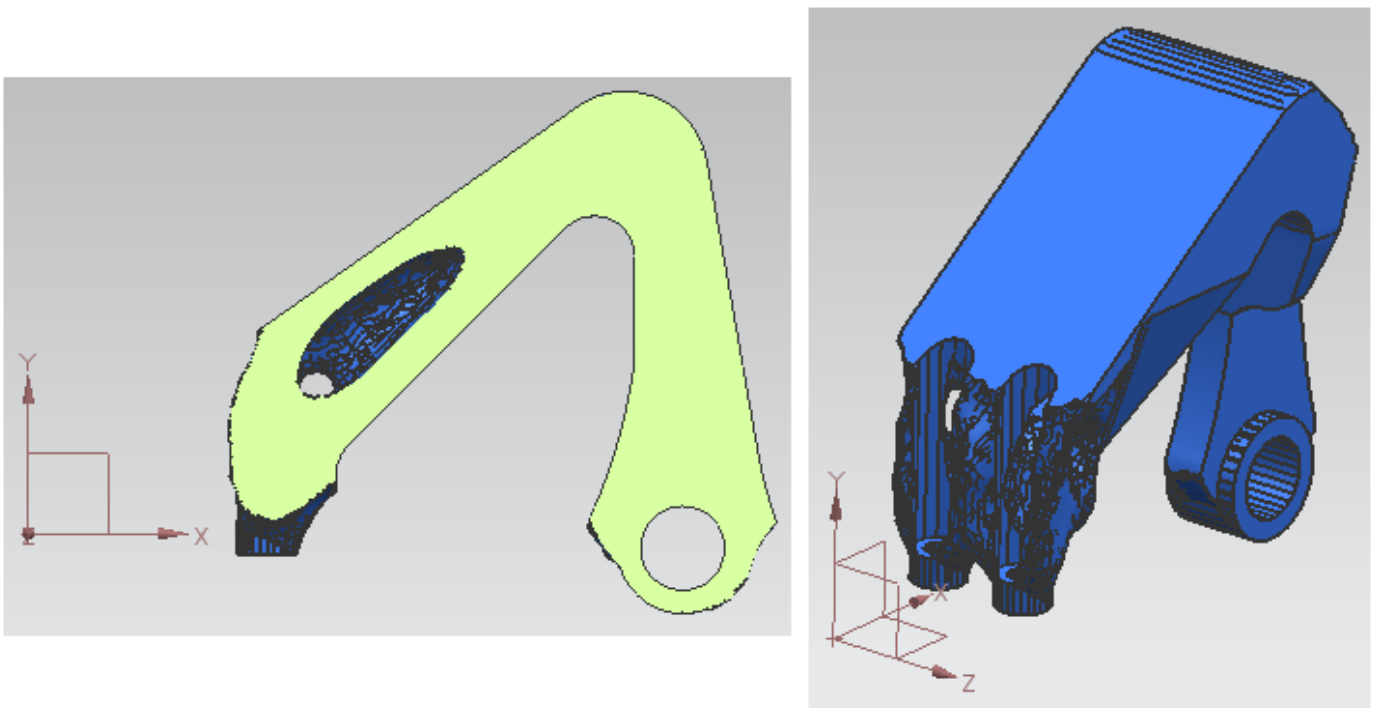


Figure 85: Optimized part for third load condition.

From the Figure 86 to Figure 91 is possible to observe the equivalent Von Mises stress in the optimized final object.

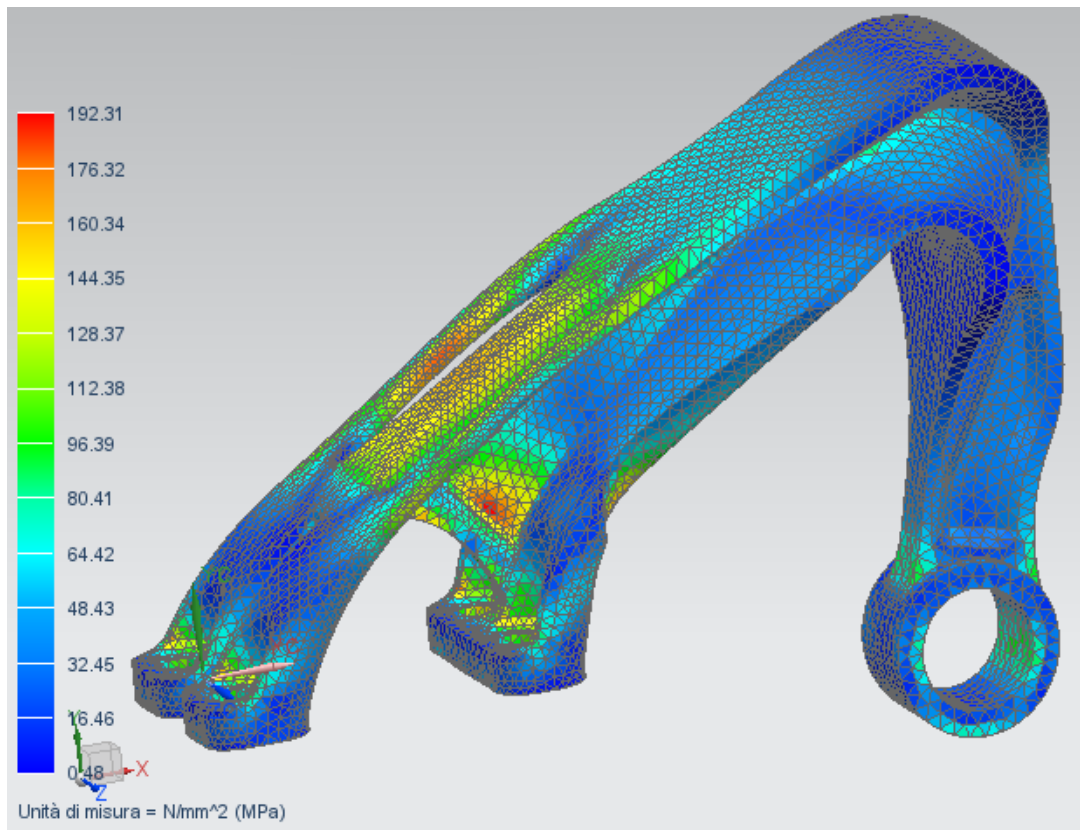


Figure 86: First view of equivalent Von Mises stress for the first load condition.

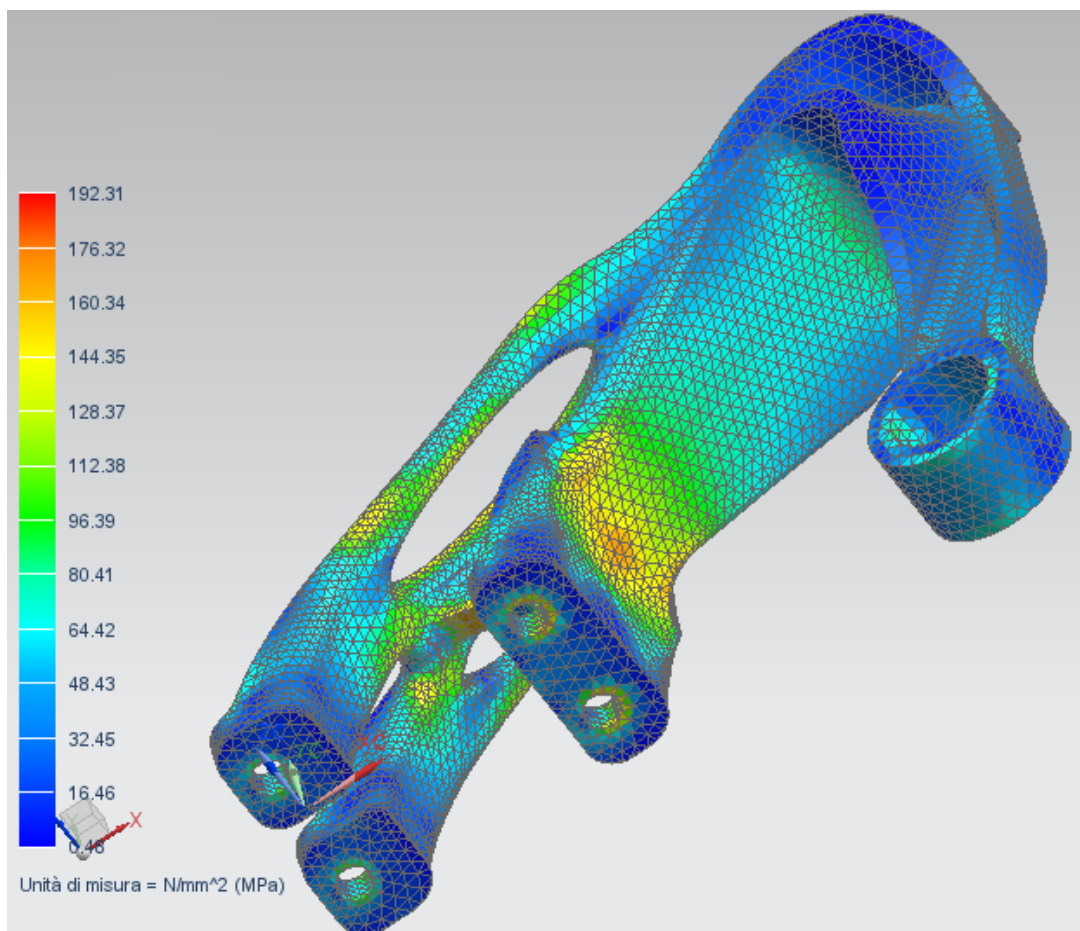


Figure 87: Second view of equivalent Von Mises stress for the first load condition.

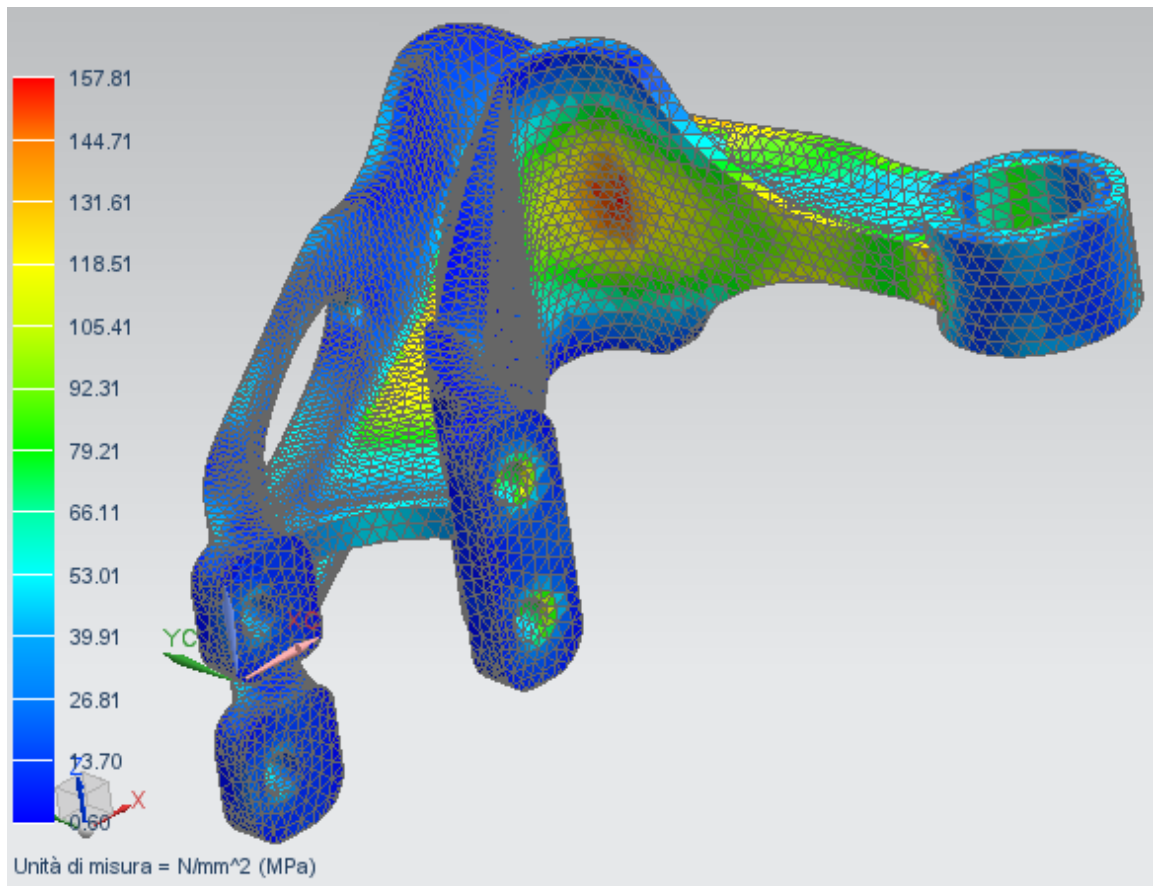


Figure 88: First view of equivalent Von Mises stress for the second load condition.

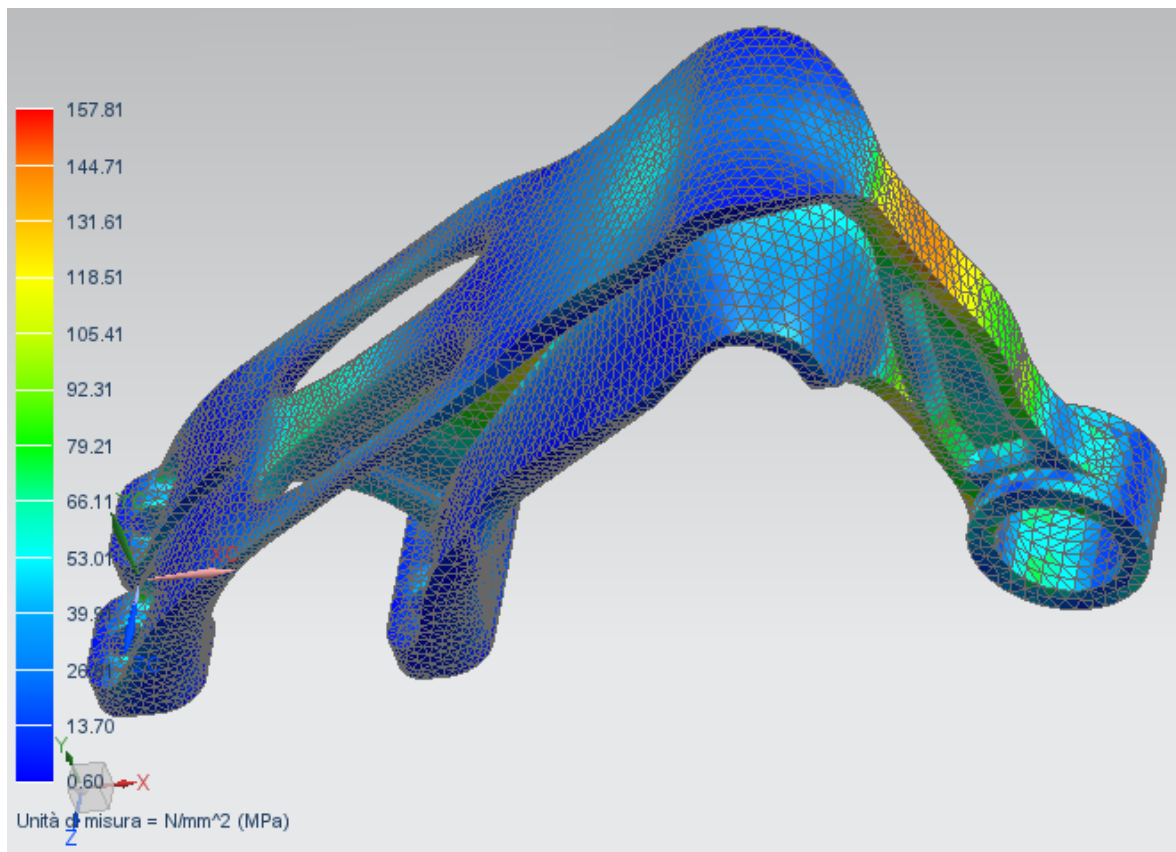


Figure 89: Second view of equivalent Von Mises stress for the second load condition.

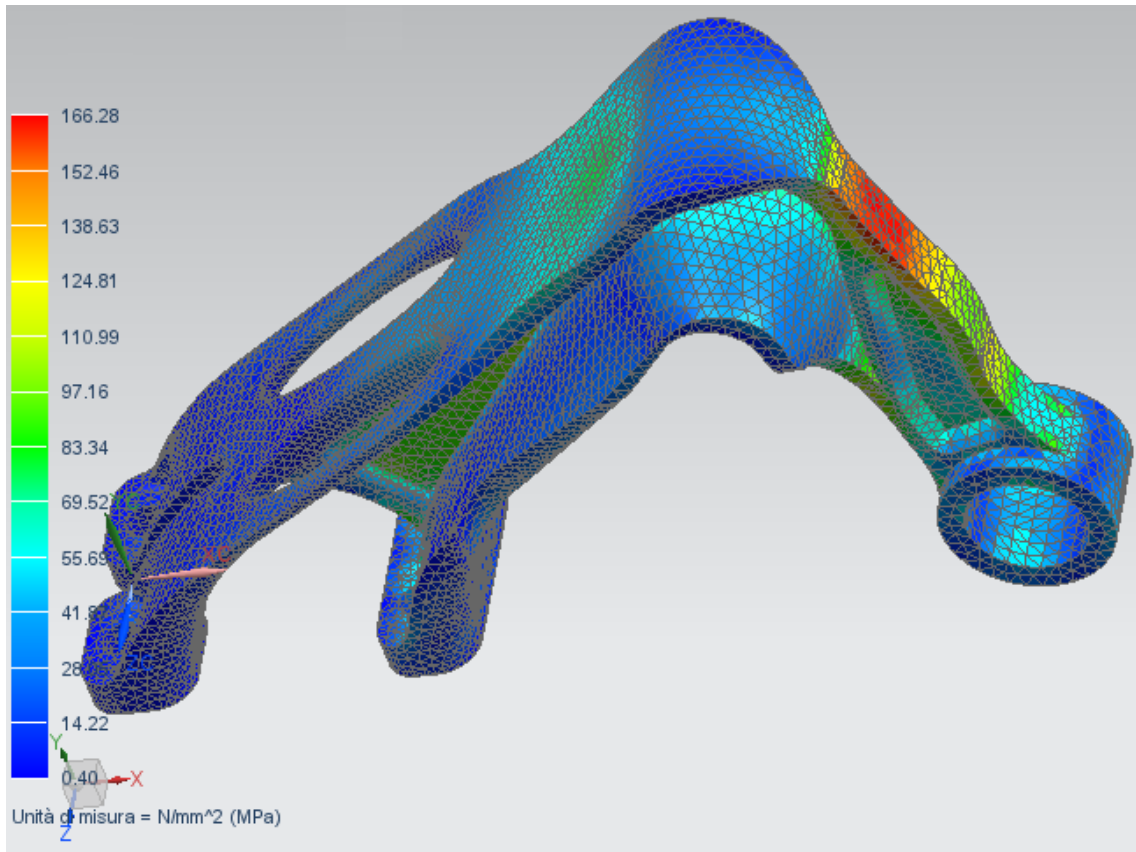


Figure 90: First view of equivalent Von Mises stress for the third load condition.

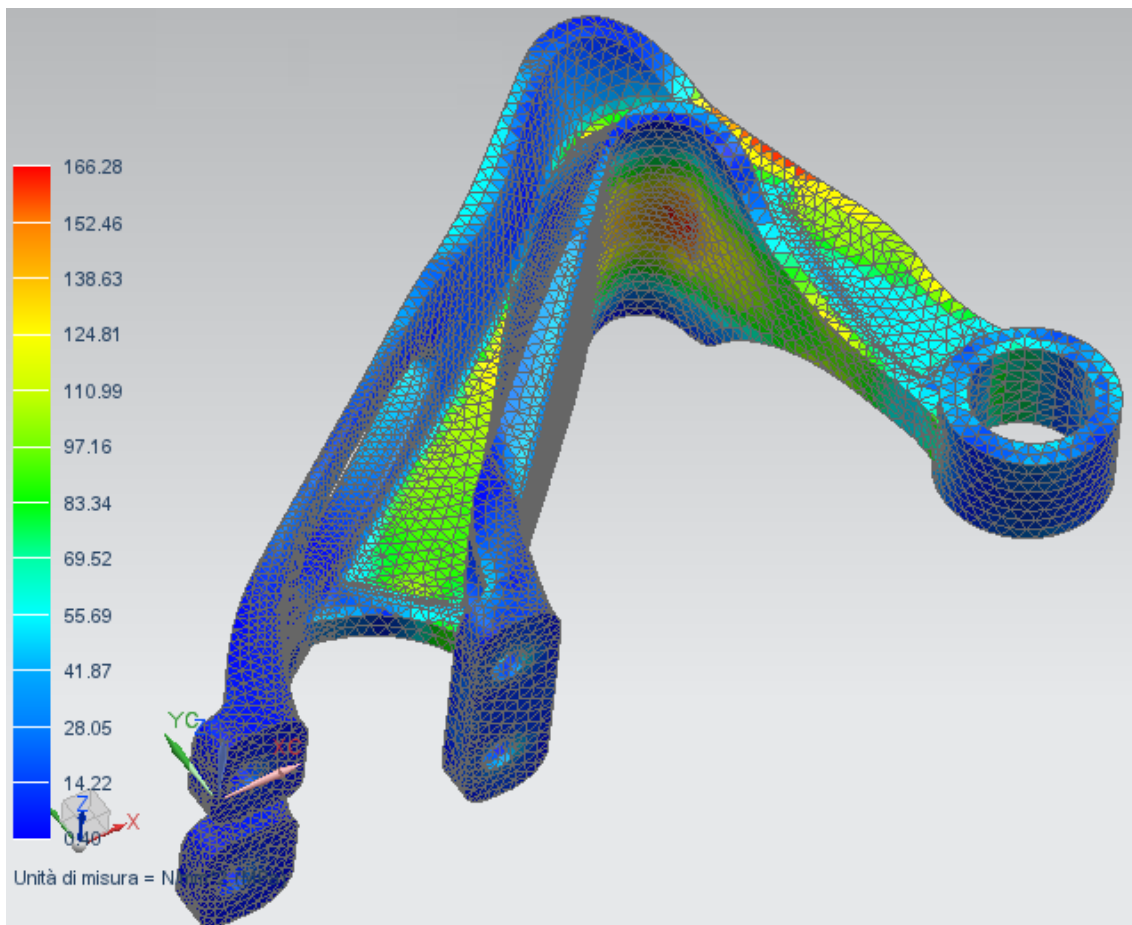


Figure 91: Second view of equivalent Von Mises stress for the third load condition.

From the Figure 92 to Figure 97 is possible to observe the displacement fields in the optimized final object along the x and y direction.

From these pictures is possible to observe that also for this final geometry all the load conditions are verified. Also the security factor calculated on the maximum stress for each load condition remains unchanged, although slightly decreasing.

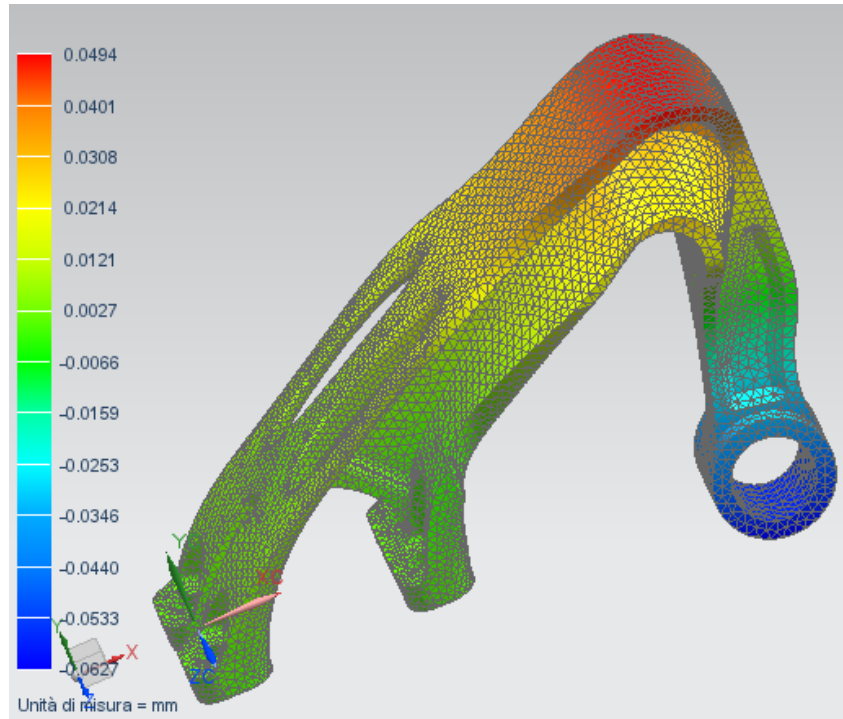


Figure 92: Displacement field for the first load condition along the x direction.

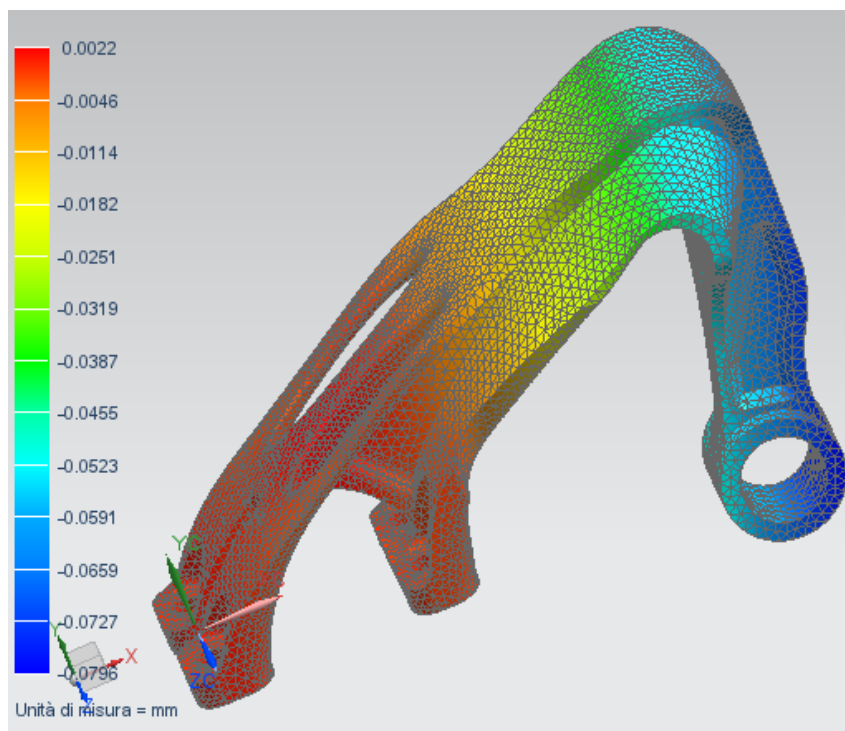


Figure 93: Displacement field for the first load condition along the y direction.

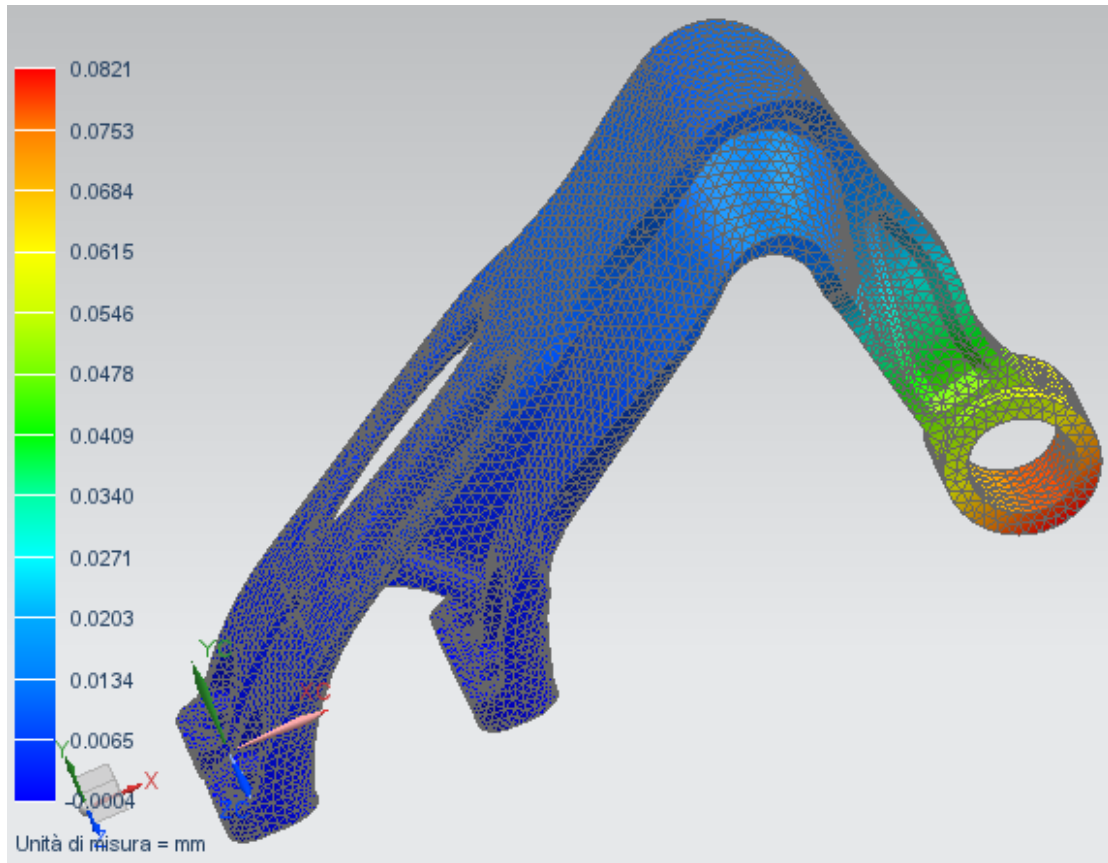


Figure 94: Displacement field for the second load condition along the x direction.

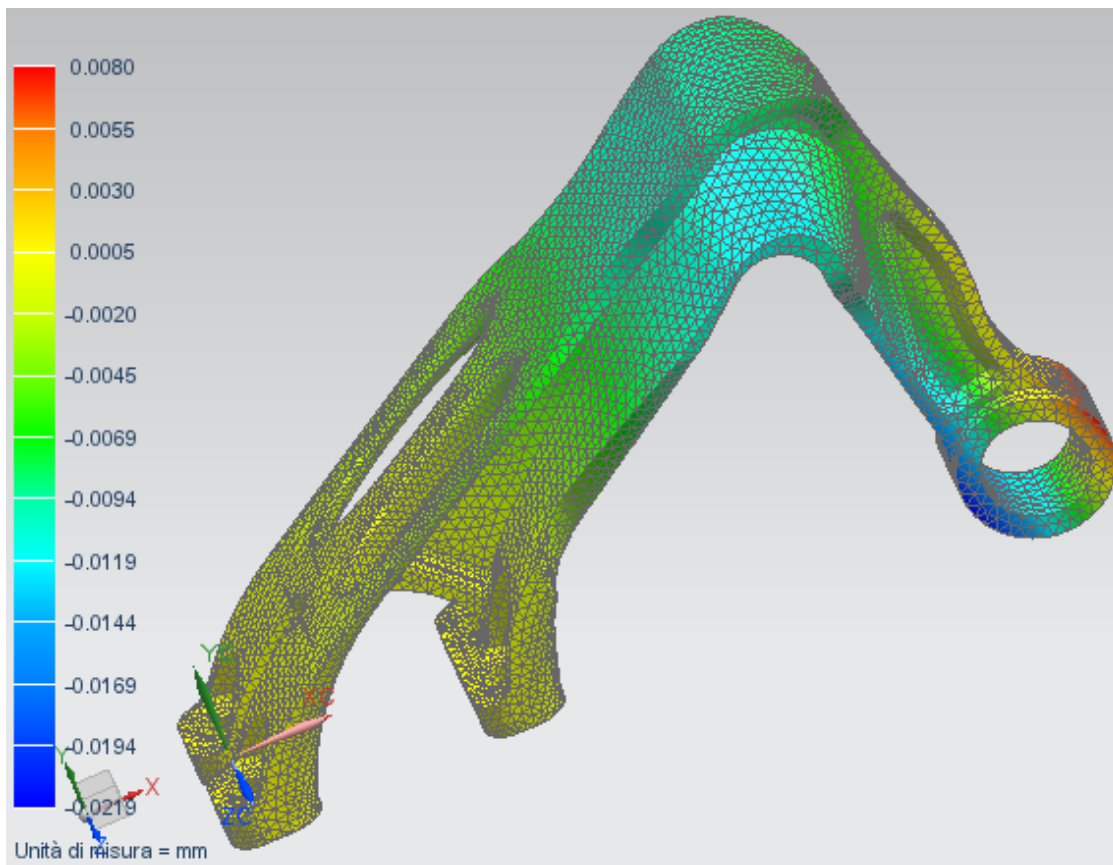


Figure 95: Displacement field for the second load condition along the y direction.

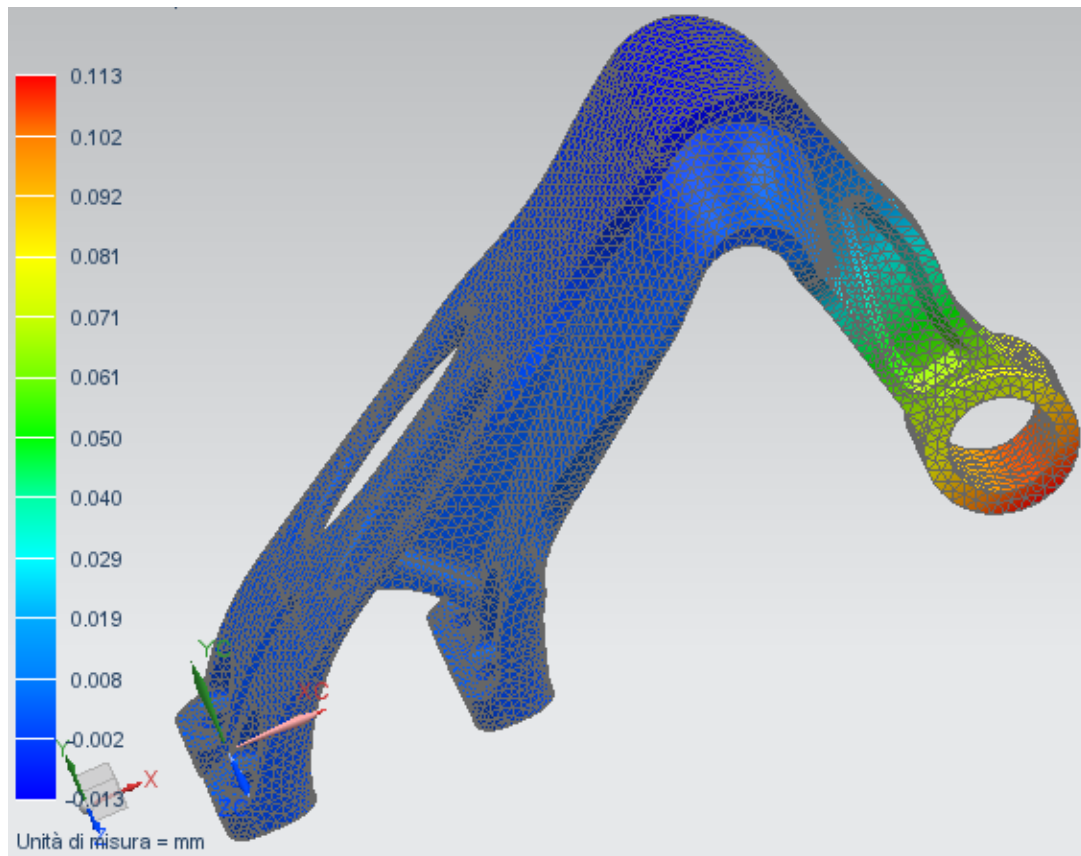


Figure 96: Displacement field for the third load condition along the x direction.

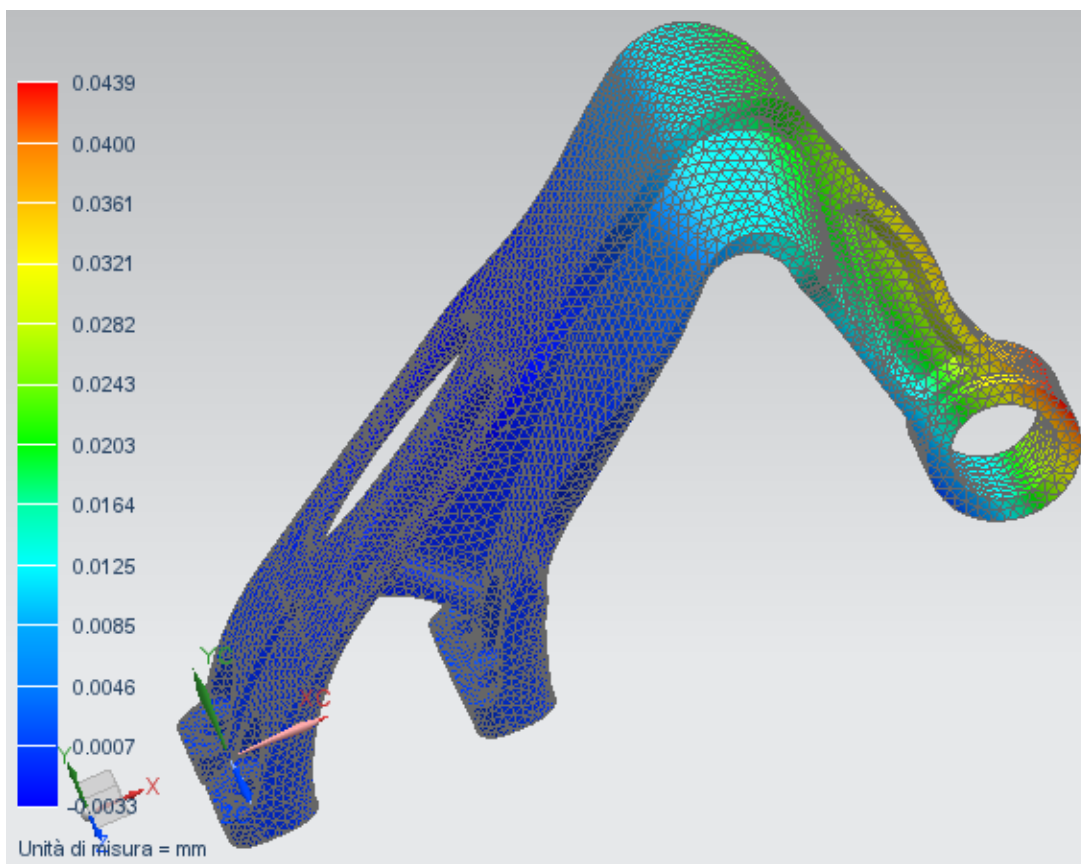


Figure 97: Displacement field for the first load condition along the y direction.

## 4.2 Experimental study

The original object, the three optimized geometries and the final optimized part have been realized via SLM on the machine M2 Cusing of CONCEPTLASER, in the additive manufacturing laboratory of the Institutt for produksjons og kvalitetsteknikk, NTNU. In the Figure 98 is possible to see the support structures for each parts.

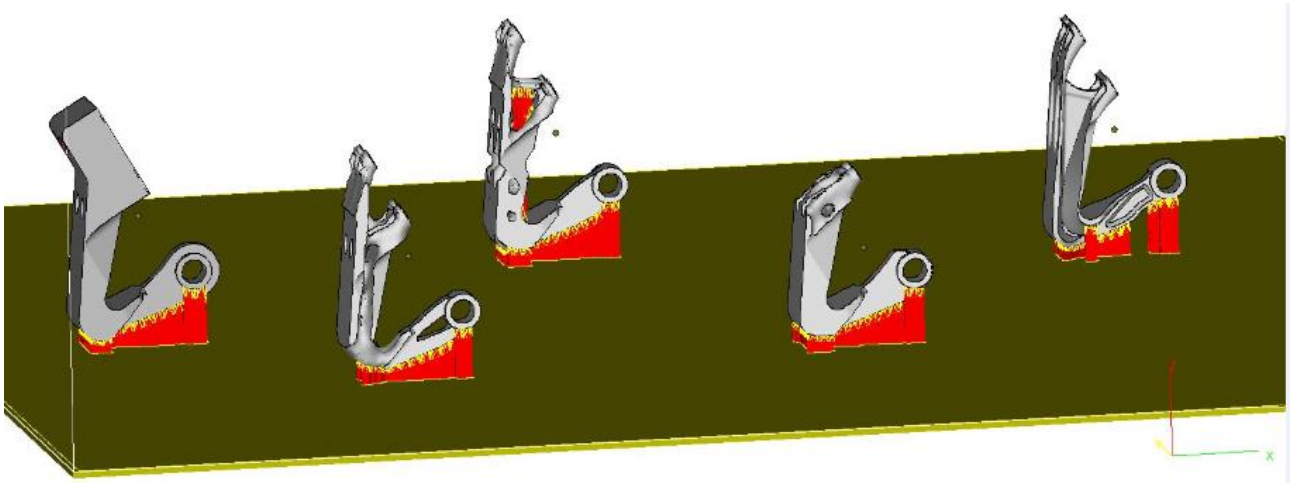


Figure 98: Input file to the AD machine and support structures.

The build chamber has the following dimensions:

250\*250\*280 (X\*Y\*Z) mm<sup>3</sup>.

The layer thickness has been imposed to 0,03 mm.

The process parameters for the laser beam have been set in the following way:

-skin:

Power laser 177 W; Speed 800 mm/s; focus diameter 0.15 mm.

-contures:

Power laser 140 W; Speed 800 mm/s; focus diameter 0.15 mm.

-support:

Power laser 120 W; Speed 1000 mm/s; focus diameter 0.15 mm.

The chosen supplied gas is Nitrogen, and the imposed flow is equal to 1 m<sup>3</sup>/h.

## 4.3 Application of the models

After the critical analysis of the models related to cost estimation, energy demand, footprints emission and safety indexes of parts made via metal AM processes, in this paragraph is proposed the life-cycle impact of the case study presented in this work. From the previous shown literature only the main model will be chosen and if necessary they will be integrated with more considerations. According to Ashby (2013), the environmental impacts of material production, part manufacturing, transportation, use, and disposal should be included when considering a cradle-to-grave system boundary. In according to the case study of this master thesis, the models are applied to each of the part presented in the first paragraph of this chapter. The different contributions to the primary energy



demand and CO<sub>2</sub> emissions in according to Ingarao et al. (2017), are presented and discussed in the following pages. The cost model used in Priarone et al. (2017) is used in this section.

In Priarone et al. (2017) are proposed models used to assess the life-cycle impact of metal-based components produced via conventional subtractive manufacturing, and additive manufacturing plus finish machining. Cost and energy models are both proposed, but only the cost model is reported in the following pages. A cradle-to-gate system boundary has been assumed, as shown in Figure 99. The material, energy, and resource flows have to be assessed for the material production and the part manufacturing stages of the life cycle. The impact of transportation from the raw material production plant to the manufacturing plant has been included ( $C_T$ ). As concerns AM, the mass of the required metal powder ( $m_{pvd}$ ) should comprise the masses of the finished part ( $m_{part}$ ), the process scraps ( $m_s$ ), and the allowance ( $m_a$ ) for the post-processing finish machining (FM) operation. The costs for the powder purchase ( $C_{mat}$  AM+FM) and for the part manufacturing ( $C_{mfg}$  AM+FM) represent the main cost drivers. In addition, the cost of transportation have to be accounted using the parameter  $d_i$  (travelled distance).

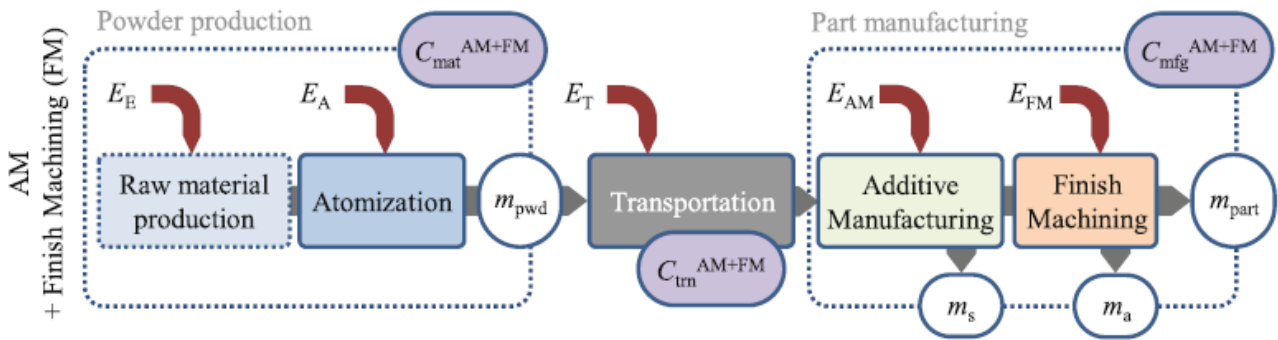


Figure 99: Cradle-to-gate system boundaries for AM + FM approach (Priarone et al., 2017).

In this paper the CM and AM+FM routes are compared in the case that all the manufactured parts comply with the same product specifications, guaranteeing the same in-use performance. This hypothesis is supported by the literature, EBM processes (proposed as case study in this paper) have proved to produce fully-dense parts, whose mechanical properties could be matched with those of traditionally manufactured. The system boundaries for the cost assessment have to include the main indirect costs (as listed in Table 49), that typically dominate the overall picture.

Production overhead	Rent, building area costs
Administration overhead	Amortization of hardware/software and consumables purchase
Production labor	Technician annual salary plus employer contributions
Machine costs	Amortization of machine and equipment purchase; Maintenance

Table 49: Typical data required for the indirect cost assessment (Priarone et al., 2017).

Handling the equation proposed in Priarone et al. (2017), the used relation for the cost estimation is:

$$\begin{aligned}
 C_{tot}^{AM+FM} = & (m_{pvd} * C_{pvd})^{Powder\ purchase} \\
 & + (C_T * (m_{pvd} * d_1 + m_{part} * d_2 + m_{part} * d_3))^{Transportation} \\
 & + ((m_{pvd} * S_C^{AM}) + (C_{Indirect}^{AM} * T_{Build}^{AM})) \\
 & + (Price_{Energy} * P_{Post}^{FM} * T_{Post}^{FM}) + (C_{Indirect}^{FM} * T_{Post}^{FM})^{Manufacturing} \\
 & + C_{Use} * m_{part} - (C_{scrap} * m_{part})^{Recycle}
 \end{aligned}$$

Where:

$S_C^{AM}$  is the specific cost per kg of deposited material for AM, expressed in €/kg;

All the mass factors are expressed on kg;

The distance factor is expressed on km;

$C_{pwd}$  is expressed in €/kg;

$C_T$  is expressed in €/(kg\*km);

$P_{Post}^{FM}$  is the used power from the finishing grinding machine;

$Price_{Energy}$  is the cost of the electricity, expressed in €/MJ;

$C^{AM}_{Indirect}$  and  $C^{FM}_{Indirect}$  take into account all the indirect costs. They are expressed in €/h.

$T^{AM}_{Build}$  considers the presetting operations, build phase, post cleaning machine and the removal of the supports.  $T^{FM}_{Post}$  considers the finishing operations for the part. They are expressed in h.

$C_{Use}$  is the cost per transported kg ;

$C_{scrap}$  represents the price of the scrap used material. In this way is possible to estimate the recycle of the objects at the end of their life. In this model in not considered the recycle of the factors  $m_a$  and  $m_s$  because these masses are totally lost.

As realized in this paper, in this work all the cost factors are divided into two main categories: direct and indirect cost. The only considered direct cost is the cost of the powder material.

Rearranging the equation proposed in Baumers et al. (2013), the  $S_C^{AM}$  factor is expressed by following equation:

$$S_C^{AM} = (E^{AM}_{Build} * Price_{Energy})$$

Where:

$E^{AM}_{Build}$  is the SEC factor (specific energy consumption) of the used machine, according to the used material. It is expressed in MJ/kg.

The use phase could be neglected if the product specifications are the same, and therefore if the in-use performance is expected to remain unchanged. Since the FEM analysis show that the mechinacal behaviors of the original object and the optimized one are quite similar, it is also possible to assume this hypothesis in this case study. However, a potential weight reduction has the effect that the in-use performance might differ, particularly for parts belonging to a transportation system (as in this case study) thank to a fuel saving. For this reasons, in this model only the fuel cost is considered for each part, but not all the other costs concerning the using phase, since they are considered be similar. The same consideration is applied for the energy and the CO<sub>2</sub> emission models.

In the following, all the factors presented in the previous equations are expressed numerically for the experiment carried out in the AM laboratory at Institutt for produksjons og kvalitetsteknikk, NTNU.

$m_{pwd}$ : The  $m_{part}$  for the original object is 21.36 g (in the following pages this value is called  $m_{original}$ ); for the optimized object from the first load condiction to the third is respectively 11.52 g, 12.65 g and 12.32 g; for the final optimized object the  $m_{part}$  is 7.12 g. For each parts the value of 0.1 g for the

factor  $m_a$  has been calculated. These values are calculated by applying the nominal density to the nominal volumes, calculated with NX11. A total of 35 g is lost on the cavities of the machine or is composed by grains of powders too big that are present at the end of the work normally. A total of 7 g is the calculated mass of the supports. These two last numbers are splitted between the five objects in equal rapports;

$C_{pwd}$ : SS316L powders, provided from ConceptLaser, with a price of 95 €/kg;

The shipping of the powders is done in normal parcel shipping from ConceptLaser, Germany which is not really expensive. However as reported in Priarone et al. (2017), a  $C_T$  factor of  $0.025 \cdot 10^{-3}$  €/(kg\*km) is here used. The traveled distance  $d_1$  is about 2000 km. The factor  $d_2$  and  $d_3$  are chosed equal to 200 km, in according with Priarone et al. (2017). They represent respectively the distance from the production plant to the point of sale and the distance from the disposal site to recycling plant;

$E^{AM}_{Build}$ : 588 MJ/kg in according to Baumers et al. (2011). This factor should be misured for each experimental condiction. However it wasn't possible to evaluate it on the AM laboratory in NTNU. In Baumers et al. (2011) a review of SEC parameters is presented for different AM machines and different materials. An experiment carried out on a M3 cusing machine with SS316L is present on this review. The M3 machine is quite similar to the M2 machine used at the AD laboratory of NTNU, and the used material is nominally the same. For this reason the empirical imformations about the case study present in Baumers et al. (2011) are used in this work. Moreover, during the experiment carried out at the AD laboratory of NTNU the construction chamber of the machine wasn't totally filled. For this reason, in a conservative manner, the value for building a single part is chosen from Baumers et al. (2011);

$Price_{Energy}$ : 0.08 €/kW in according with the Norwegian electricity price. This values is converted in €/MJ in the equation of the model;

$T^{AM}_{Build}$ : 13.40 h, composed of 11.40 h for the build phase, 1 h for the presetting of the machine (atmosphere generation, build chamber preparation and generation of the STL file for the machine) and 1 h for the post-cleaning of the machine. All these factors are divided in equal way for each part;

$C^{AM}_{Indirect}$ : 195 €/h. In this factor is considered the labor of the machine engineer (70 €/h). Since the machine can work stand alone, this cost/time is evaluated only for the pre/post-processing. Is also present the machine cost (70 €/h). It is considered only for the build phase. The factor 40 €/h is chosen for the administration and production overhead. In this last factor the cost/time unit of the laboratory building and the consumables purchase, like the electricity for the lighting the work area, the flow of nitrogen and the nitrogen machine generator, are considered. This factor is considered for the whole AM process. The cost of 15 €/h considers the amortization of the used softwares. It is considered only for the pre-setting phase;

$P_{Post}^{FM}$ : The value of 100 W has been estimated.

$C^{FM}_{Indirect}$ : In this factor is considered the labor of the machine engineer (70 €/h). Is also present the machine cost, the administration and production overhead (40 €/h). In this last factor the amortization of cost/time unit of the laboratory building and the consumables purchase, like the electricity for the for lighting the work area, are considered;

$T^{FM}_{Post}$ : 2 h, in total, for finishing activies carried out in two grinding machines. The first one used to finish the surface where the supports were present; the secondo one, for little dimensions, was used

to finish the surfaces that are used for the connections of the parts and the application of the loads. This time is divided on the five parts in equal way;

$C_{Use}$ : It is equal to 360 €/kg as proposed in Ashby (2013). In this paper the value is reported in \$/kg, then the factor has been converted to €/kg in according to the currency exchange of the same year of the paper;

$C_{scrap}$ : It is stimated to be equal to 1.5 €/kg.

In order to analyze the life-cycle impact of these metal-based components, the work of Ingarao et al. (2017) is here used. This model has been already reported in the chapter 3. The full model presented in this paper is here adapted to this case study:

$$E^{AM+FM} = ((m_{part} + m_a + m_s) * (E_E + E_A))^{Material} + (E_T * (m_{pwd} * d_1 + m_{part} * d_2 + m_{part} * d_3))^{Transportation} + ((m_{part} + m_a + m_s) * E^{AM}_{Build} + E^{FM}_{Post} + Q_{Gas} * E^{AM}_{Gas} * T^{AM}_{Gas})^{Manufacturing} + E_{Use} * m_{part}$$

The same equation can be arranged for having a CO<sub>2</sub> extimation model. The full model presented in Ingarao et al. (2017) is here adapted to this case study:

$$CO_2^{AM+FM} = ((m_{part} + m_a + m_s) * (CO_{2E} + CO_{2A}))^{Material} + (CO_{2T} * (m_{pwd} * d_1 + m_{part} * d_2 + m_{part} * d_3))^{Transportation} + ((m_{part} + m_a + m_s) * CO_2^{AM}_{Build} + CO_2^{FM}_{Post} + Q_{Gas} * CO_2^{AM}_{Gas})^{Manufacturing} + CO_{2Use} * m_{part}$$

Table 39 shows the eco-properties for the used material; it is reported here again. The factors E<sub>E</sub> and CO<sub>2E</sub>, as shown in chapter 3, take into account the recyclability of the material.

Eco-property	Stainless steel
Energy for primary material production, $E_V$ (MJ/kg)	84.5
Energy for material recycling, $E_R$ (MJ/kg)	12.0
CO <sub>2</sub> emissions for primary material production, $CO_{2V}$ (kg/kg)	5.0
CO <sub>2</sub> emissions for material recycling, $CO_{2R}$ (kg/kg)	0.7
Material recyclability, $r$	0.9
Embodied energy for material production, $E_E$ (MJ/kg)	19.3
CO <sub>2</sub> emissions for material production, $CO_{2E}$ (kg/kg)	1.1
Energy for atomization, $E_A$ (MJ/kg)	2.9

Table 39: Eco-properties of the workpiece and powder production (Ingarao et al., 2017).

$E^{FM}_{Post}$  is the primary energy used in the post processing phase. Its values is calculated dividing the electrical consumption for the conversion factor for the primary energy, in according with Jeswiet and Kara (2008). This value is equal to 0.42 MJ for each part;

$Q_{Gas}$  is the imposed flow. Its value is equal to 1000 l/h;

$E^{AM}_{Gas}$  is the primary energy for the gas production. As exposed in Froehlich (2013), for the nitrogen generator used for the experiment, 1976 kJ of electricity are necessary to produce 1 kg of nitrogen gas. By some conversions, using the conversion factor of 0.34 for the primary energy, as expressed in Jeswiet and Kara (2008), the value of 7.26 kJ/l is used in this work. This value is used for each part;

$T_{Gas}^{AM}$  is the period of time in which the gas is used. It has been set equal to 11.40 h. In the model this values is divided in equal way for each part.

The factor  $CO_{2A}$ , misured in kg/kg, in according with Jeswiet and Kara (2008), should be calculated applying data for the German energy mix (<https://www.energy-charts.de/energy.htm?source=all-sources&period=annual&year=2016>). Since the 43.21% of the electricity production is archieved with coal, and the 8.55% of the electricity production is archieved with natural gas, the CES factor is equal to 1.78 kg/MJ. A conversion efficiency of  $\eta = 0.34$  is used in this work, as proposed in Jeswiet and Kara (2008). The  $E_A$  factor, proposed in Ingarao et al. (2017), has been utilized for the calculation. The term  $CO_{2A}$  is equal to 5.18 kg/kg;

The factors  $CO_2^{AM}_{Build}$ ,  $CO_2^{FM}_{Post}$  and the factor  $CO_2^{AM}_{Gas}$  in according with Jeswiet and Kara (2008), should be calculated applying data for the Norwegian energy mix. Since the 98% on the electricity generation in Norway is made with renewables resources, this factor is largely negligible;

The energy  $E_T$  and the  $CO_{2T}$ , considering a 14 metric ton truck, have been extracted from Ashby (2013) for the material transportation. Their values are respectively 1.5 MJ/(metric ton\*km) and 0.11 kg/(metric ton\*km).

In order to take into account the use phase, the value for a Short-distance aircraft, reported in Table 50 from Ingarao et al. (2017), have been used.

Vehicle type	Fuel	Use phase	Use phase energy savings per 1 kg of reduced weight	Use phase CO <sub>2</sub> savings per 1 kg of reduced weight <sup>a</sup>
Passenger car	Gasoline	0.2·10 <sup>6</sup> km	230 MJ	15.0 kg
Passenger car	Diesel	0.2·10 <sup>6</sup> km	210 MJ	14.9 kg
Articulated truck	Diesel	1.2·10 <sup>6</sup> km	260 MJ	18.5 kg
Short-distance aircraft	Kerosene	30 y	150·10 <sup>3</sup> MJ	10.2·10 <sup>3</sup> kg
Long-distance aircraft	Kerosene	30 y	200·10 <sup>3</sup> MJ	13.6·10 <sup>3</sup> kg

Table 50: Assumed average values for end energy and CO<sub>2</sub> savings in trasportation systems achieved by light-weighting (Ingarao et al., 2017).

The energy  $E_{Use}$  and the  $CO_{2Use}$  have respectively the values 150·10<sup>3</sup> MJ/kg and 10.2·10<sup>3</sup> kg/kg.

### 4.3 Considerations on the obtained results

From Figure 100 to Figure 102 is possible to observe the results of the three models applied to all the object of this case study. The results have been organized such that it is possible to understand each contributing factor to the total amount. About the cost model results, the AM building phase dominates on all the other factors. There is this result because the indirect cost, such as the cost of the labor of the machine engineer (70 €/h), the AM machine cost (70 €/h), the administration and production overhead cost (40 €/h) and the cost of the used softwares (15 €/h) have all a high value comparing with all the other cost factors. However, it is interesting to note that the cost for the AM building phase are related to objects that had been redacted with a factor of 0.3 respect to the common dimensions. But in any case maintaining unchanged the AM building phase cost and dividing the  $m_{part}$  and  $m_s$  for the factor 0.3, the situation remains largely unchanged.

From Figure 101, it is possible to see that, also for this model, the most energy consuming phase is the AM building phase. But this is an easily expected outcome for these processes. About the CO<sub>2</sub> model results, shown in Figure 102, it is possible to observe that the worse phase is the material production one. The building phase or the finishing one, don't produce CO<sub>2</sub> only because they are carried out in Norway, where the electric energy is produced with renewable resources. If these phase would be carried out in other contries these phases could become much more important than the

others. It is possible to estimate this, just examining the energy consumption for each phase, shown in Figure 101.

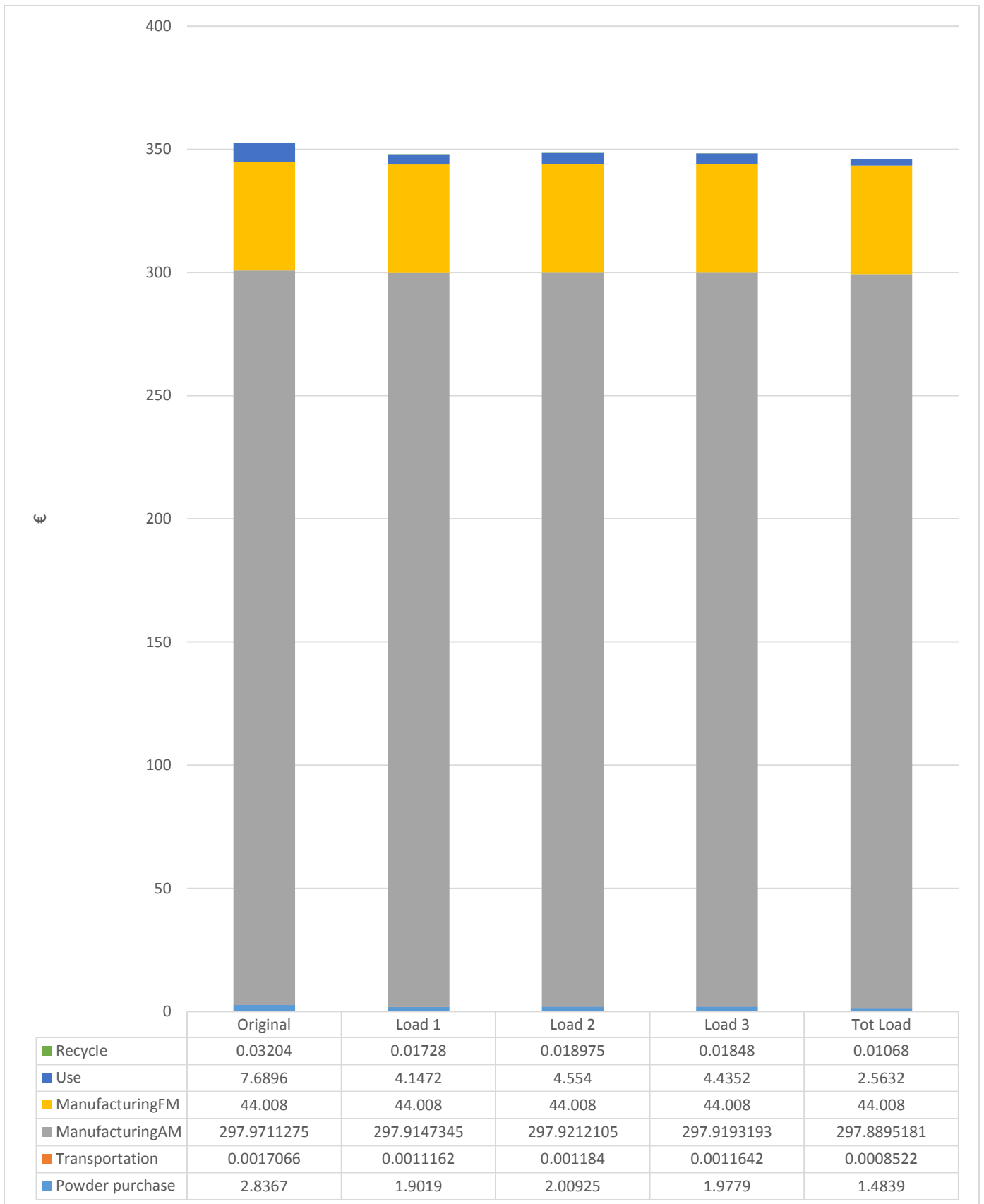


Figure 100: Cost comparison for each object with all the contributing factors.

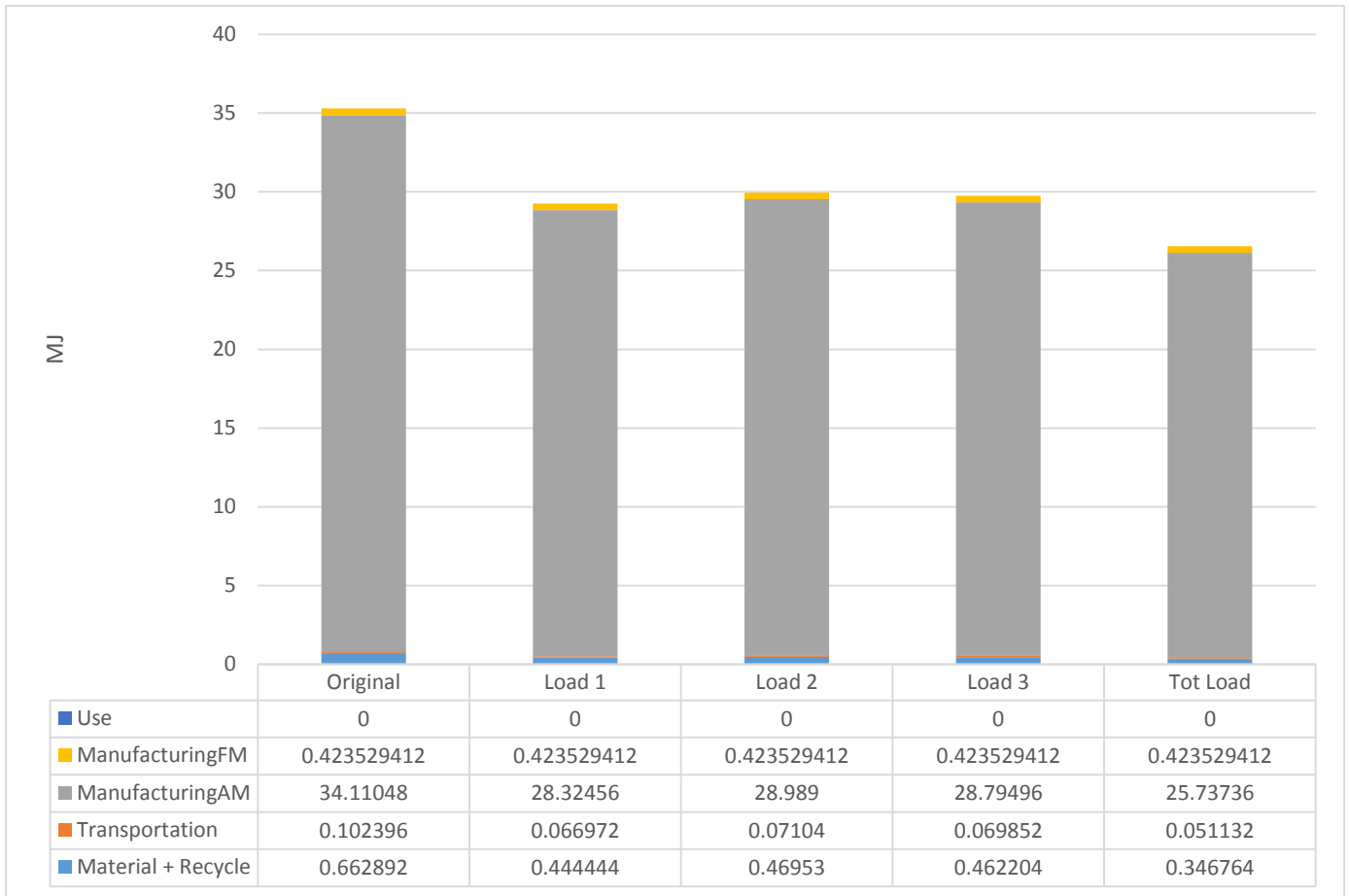


Figure 101: Energy comparison for each object with all the contributing factors.

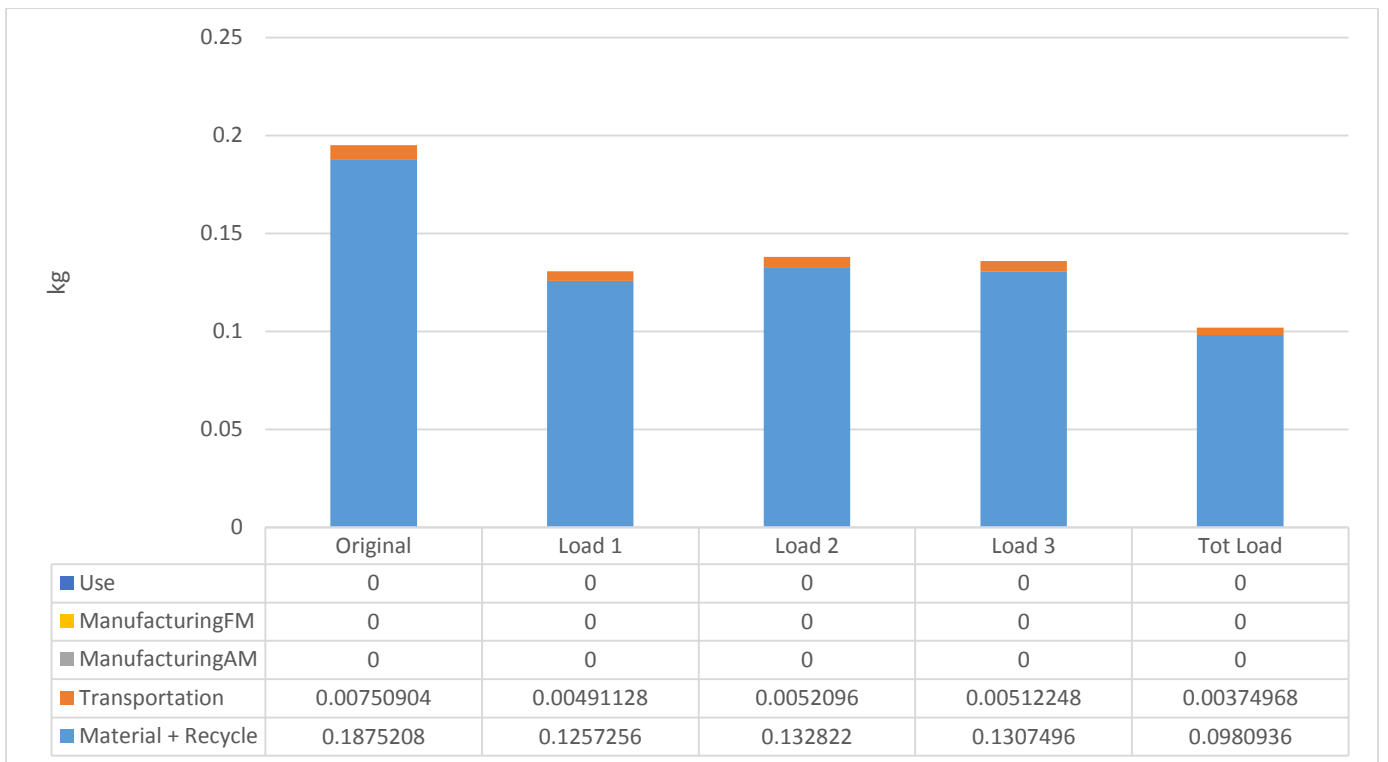


Figure 102: CO2 comparison for each object with all the contributing factors.

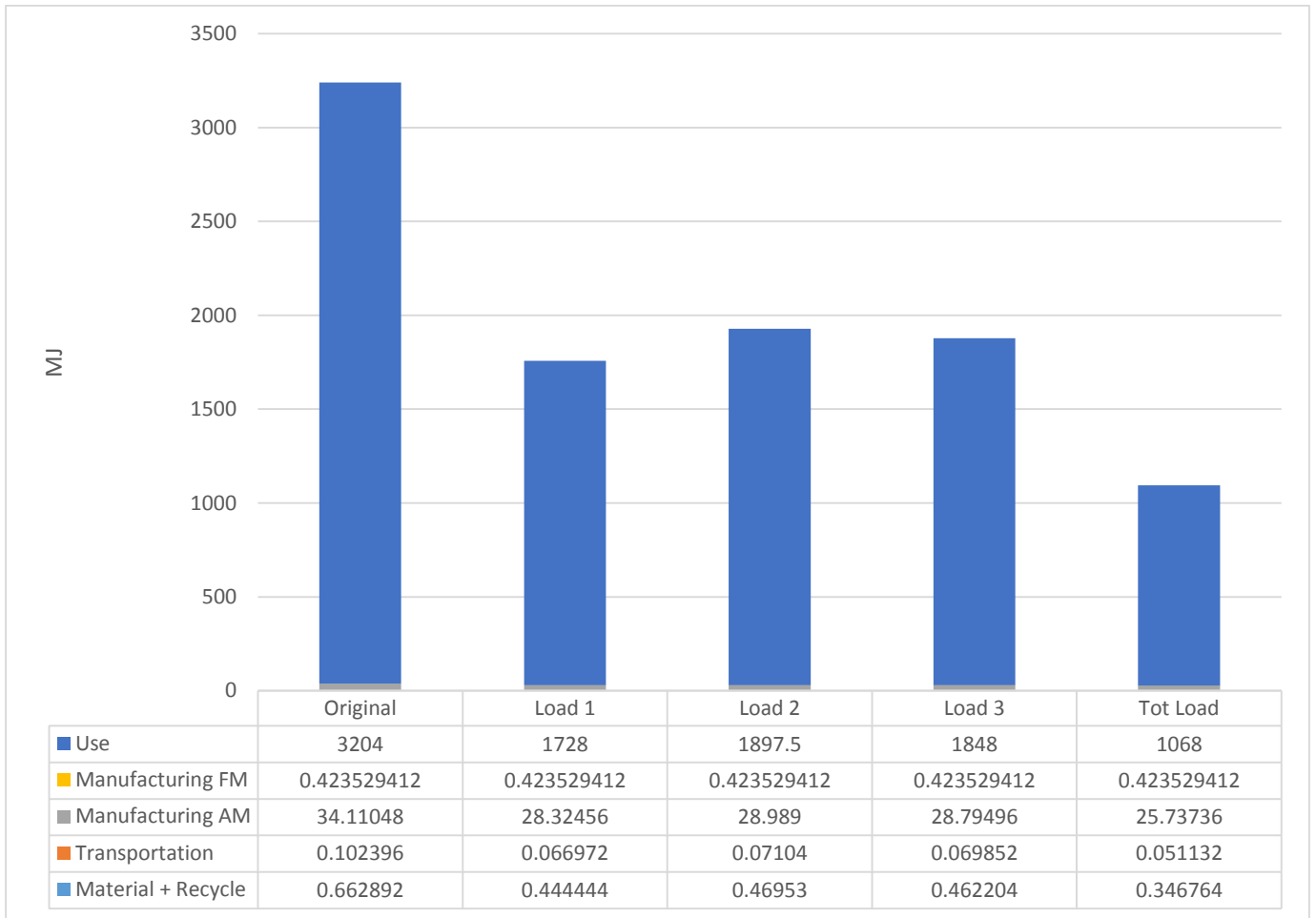


Figure 103: Energy comparison for each object considering also the use contributing factor.

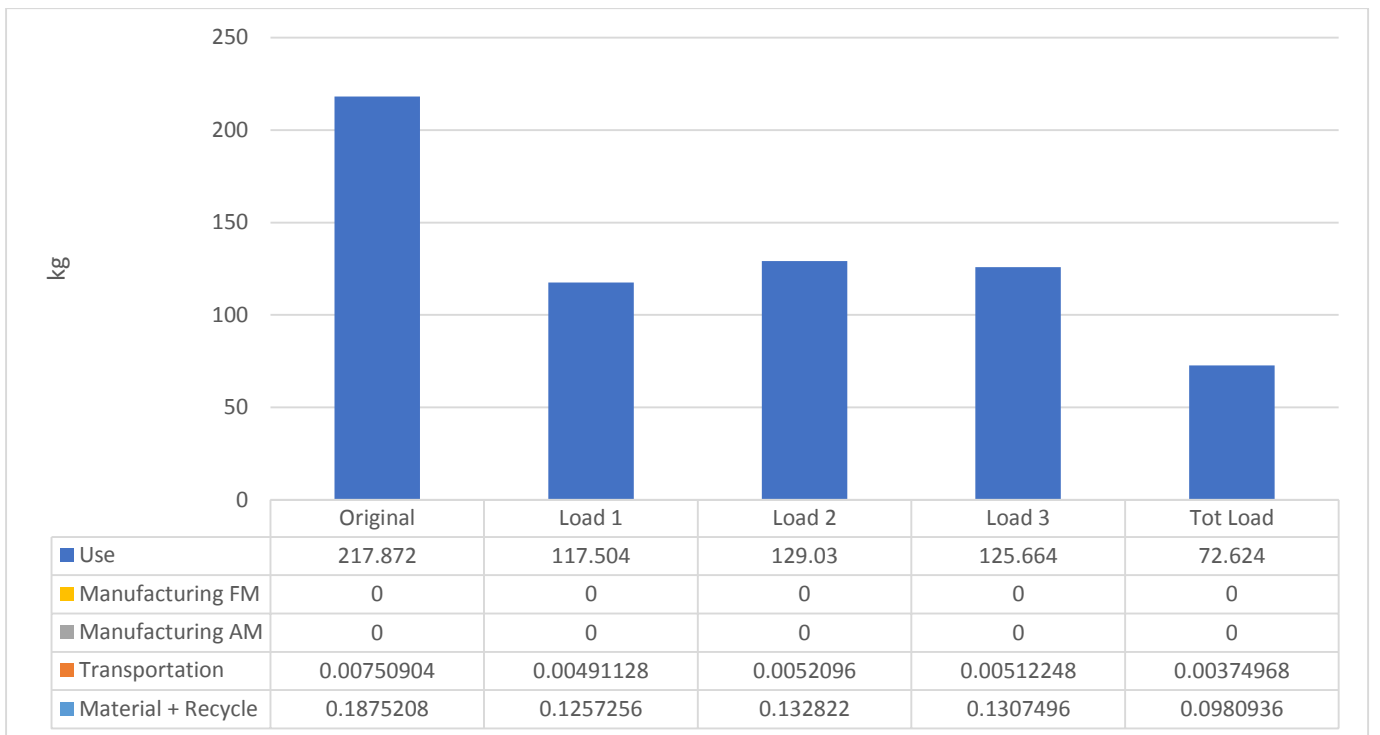


Figure 104: CO2 comparison for each object considering also the use contributing factor.



In Figure 100 the using phase effect is already considered. Though this number is higher than the transportation, material purchase and recycle factors, it is much smaller than the contribution of the AM building and FM finishing phases.

From Figure 103 and Figure 104 the effects of the using phase are considered for the energy and CO<sub>2</sub> emission models. It is possible to see that now the situation is totally changed. In fact the using phase, considering an aeronautical application for the objects, needs much more energy and produces more CO<sub>2</sub> than the other phases.

The AM building phase is so expensive that it is difficult to understand in Figure 100 the differences of cost related to the mass reduction effect. Instead from Figure 101 and Figure 102, it is possible to see that the mass reduction has a higher effect on the energy and CO<sub>2</sub> models. Moreover if the using phase is considered the effect of the weight reduction is much more important than in the previous cases. From Figure 103 and Figure 104, it is possible to observe the numerical difference.

## Appendix B

Respiratory protection for some metal substances exposed on Chapter 2

### **RESPIRATORY PROTECTION FOR CHROMIUM METAL AND INSOLUBLE CHROMIUM SALTS (AS CHROMIUM)**

<b>Condition</b>	<b>Minimum Respiratory Protection* Required Above 1 mg/m<sup>3</sup></b>
<b>Particulate Concentration</b>	
<b>5 mg/m<sup>3</sup> or less</b>	Any dust and mist respirator.
<b>10 mg/m<sup>3</sup> or less</b>	Any dust and mist respirator, except single-use or quarter-mask respirator. Any fume respirator or high efficiency particulate respirator. Any supplied-air respirator. Any self-contained breathing apparatus.
<b>50 mg/m<sup>3</sup> or less</b>	A high efficiency particulate filter respirator with a full facepiece. Any supplied-air respirator with a full facepiece, helmet, or hood. Any self-contained breathing apparatus with a full facepiece.
<b>500 mg/m<sup>3</sup> or less</b>	A powered air-purifying respirator with a high efficiency particulate filter. A Type C supplied-air respirator operated in pressure-demand or other positive pressure or continuous-flow mode.
<b>Greater than 500 mg/m<sup>3</sup> or entry and escape from unknown concentrations</b>	Self-contained breathing apparatus with a full facepiece operated in pressure-demand or other positive pressure mode.  A combination respirator which includes a Type C supplied-air respirator with a full facepiece operated in pressure-demand or other positive pressure or continuous-flow mode and an auxiliary self-contained breathing apparatus operated in pressure-demand or other positive pressure mode.
<b>Fire Fighting</b>	Self-contained breathing apparatus with a full facepiece operated in pressure-demand or other positive pressure mode.

\*Only NIOSH-approved or MSHA-approved equipment should be used.

OSHA, (1978). Occupational guideline for Chromium Metal and insoluble Chromium Salts.

## RESPIRATORY PROTECTION FOR CHROMIC ACID AND CHROMATES

<b>Condition</b>	<b>Minimum Respiratory Protection* Required Above 0.1 mg/m<sup>3</sup></b>
<b>Particulate Concentration</b>	
<b>5 mg/m<sup>3</sup> or less</b>	A high efficiency particulate filter respirator with a full facepiece. Any supplied-air respirator with a full facepiece, helmet, or hood. Any self-contained breathing apparatus with a full facepiece.
<b>30 mg/m<sup>3</sup> or less</b>	A powered air-purifying respirator with a full facepiece and a high efficiency particulate filter. A Type C supplied-air respirator with a full facepiece operated in pressure-demand or other positive pressure mode or with a full facepiece, helmet, or hood operated in continuous-flow mode.
<b>Greater than 30 mg/m<sup>3</sup> or entry and escape from unknown concentrations</b>	Self-contained breathing apparatus with a full facepiece operated in pressure-demand or other positive pressure mode. A combination respirator which includes a Type C supplied-air respirator with a full facepiece operated in pressure-demand or other positive pressure or continuous-flow mode and an auxiliary self-contained breathing apparatus operated in pressure-demand or other positive pressure mode.
<b>Fire Fighting</b>	Self-contained breathing apparatus with a full facepiece operated in pressure-demand or other positive pressure mode.
<b>Escape</b>	A high efficiency particulate filter respirator. Any escape self-contained breathing apparatus.

\*Only NIOSH-approved or MSHA-approved equipment should be used.

OSHA, (1978). Occupational health guideline for Chromic Acid and Chromates.

## RESPIRATORY PROTECTION FOR COBALT METAL FUME AND DUST

<b>Condition</b>	<b>Minimum Respiratory Protection* Required Above 0.1 mg/m<sup>3</sup></b>
<b>Particulate Concentration</b>	
<b>0.5 mg/m<sup>3</sup> or less</b>	Any dust and mist respirator, except single-use.
<b>1.0 mg/m<sup>3</sup> or less</b>	Any dust and mist respirator, except single-use or quarter-mask respirator. Any fume respirator or high efficiency particulate filter respirator.
<b>5 mg/m<sup>3</sup> or less</b>	A high efficiency particulate filter respirator with a full facepiece. Any supplied-air respirator with a full facepiece, helmet, or hood. Any self-contained breathing apparatus with a full facepiece.
<b>20 mg/m<sup>3</sup> or less</b>	A powered air-purifying respirator with a full facepiece and a high efficiency particulate filter. A Type C supplied-air respirator with a full facepiece operated in pressure-demand or other positive pressure mode or with a full facepiece, helmet, or hood operated in continuous-flow mode.
<b>Greater than 20 mg/m<sup>3</sup> or entry and escape from unknown concentrations</b>	Self-contained breathing apparatus with a full facepiece operated in pressure-demand or other positive pressure mode. A combination respirator which includes a Type C supplied-air respirator with a full facepiece operated in pressure-demand or other positive pressure or continuous-flow mode and an auxiliary self-contained breathing apparatus operated in pressure-demand or other positive pressure mode.
<b>Fire Fighting</b>	Self-contained breathing apparatus with a full facepiece operated in pressure-demand or other positive pressure mode.
<b>Escape</b>	A high efficiency particulate filter respirator with a full facepiece. Any escape self-contained breathing apparatus.

\*Only NIOSH-approved or MSHA-approved equipment should be used.

OSHA, (1978). Occupational health guideline for Cobalt Metal Fume and Dust.

## RESPIRATORY PROTECTION FOR NICKEL METAL AND SOLUBLE COMPOUNDS

<b>Condition</b>	<b>Minimum Respiratory Protection* Required Above 1 mg/m<sup>3</sup></b>
<b>Dust, Mist, or Fume Concentration</b>	
10 mg/m <sup>3</sup> or less	Any fume respirator or high efficiency particulate respirator. Any supplied-air respirator. Any self-contained breathing apparatus.
50 mg/m <sup>3</sup> or less	A high efficiency particulate filter respirator with a full facepiece. Any supplied-air respirator with a full facepiece, helmet, or hood. Any self-contained breathing apparatus with a full facepiece.
1000 mg/m <sup>3</sup> or less	A powered air-purifying respirator with a high efficiency particulate filter. A Type C supplied-air respirator operated in pressure-demand or other positive pressure or continuous-flow mode.
2000 mg/m <sup>3</sup> or less	A Type C supplied-air respirator with a full facepiece operated in pressure-demand or other positive pressure mode or with a full facepiece, helmet, or hood operated in continuous-flow mode.
Greater than 2000 mg/m <sup>3</sup> or entry and escape from unknown concentrations	Self-contained breathing apparatus with a full facepiece operated in pressure-demand or other positive pressure mode.  A combination respirator which includes a Type C supplied-air respirator with a full facepiece operated in pressure-demand or other positive pressure or continuous-flow mode and an auxiliary self-contained breathing apparatus operated in pressure-demand or other positive pressure mode.
<b>Fire Fighting</b>	Self-contained breathing apparatus with a full facepiece operated in pressure-demand or other positive pressure mode.

\*Only NIOSH-approved or MSHA-approved equipment should be used.

OSHA, (1978). Occupational health guideline for Nickel Metal and Soluble Nickel Compounds.

## RESPIRATORY PROTECTION FOR TITANIUM DIOXIDE

Condition	Minimum Respiratory Protection* Required Above 15 mg/m <sup>3</sup>
Dust or Mist Concentration	
75 mg/m <sup>3</sup> or less	Any dust and mist respirator.
150 mg/m <sup>3</sup> or less	Any dust and mist respirator, except single-use or quarter-mask respirator.
Dust, Mist, or Fume Concentration	
150 mg/m <sup>3</sup> or less	Any fume respirator or high efficiency particulate filter respirator. Any supplied-air respirator. Any self-contained breathing apparatus.
750 mg/m <sup>3</sup> or less	A high efficiency particulate filter respirator with a full facepiece. Any supplied-air respirator with a full facepiece, helmet, or hood. Any self-contained breathing apparatus with a full facepiece.
7,500 mg/m <sup>3</sup> or less	A powered air-purifying respirator with a high efficiency particulate filter. A Type C supplied-air respirator operated in pressure-demand or other positive pressure or continuous-flow mode.
Greater than 7,500 mg/m <sup>3</sup> or entry and escape from unknown concentrations	Self-contained breathing apparatus with a full facepiece operated in pressure-demand or other positive pressure mode.  A combination respirator which includes a Type C supplied-air respirator with a full facepiece operated in pressure-demand or other positive pressure or continuous-flow mode and an auxiliary self-contained breathing apparatus operated in pressure-demand or other positive pressure mode.
Fire Fighting	Self-contained breathing apparatus with a full facepiece operated in pressure-demand or other positive pressure mode.

\*Only NIOSH-approved or MSHA-approved equipment should be used.

OSHA, (1978). Occupational health guideline for Titanium Dioxide.

## Reference list:

- Abd El-Rahman SS (2003). Neuropathology of aluminum toxicity in rats (glutamate and GABA impairment). *Pharmacol Res* 47(3):189-194.
- Adriana R. Oller, Daniel T. Kirkpatrick, Ann Radovsky, Hudson K. Bates (2008). Inhalation carcinogenicity study with nickel metal powder in Wistar rats.
- Agarwal SK, Ayyash L, Gourley CS, et al. (1996). Evaluation of the developmental neuroendocrine and reproductive toxicology of aluminum. *Food Chem Toxicol* 34(1):49-53.
- Akila R, Stollery BT, Riihimaki V. 1999. Decrements in cognitive performance in metal inert gas welders exposed to aluminum. *Occup Environ Med* 56(9):632-639.
- Alexander CS. (1972). Cobalt-beer cardiomyopathy: A clinical and pathological study of twenty-eight cases. *Am J Med* 53:395-417.
- Alexander CS. (1969). Cobalt and the heart. *Ann Intern Med* 70:411-413.
- Alomar A, Conde-Salazar L, Romaguera C. (1985). Occupational dermatosis from cutting oils. *Contact Dermatitis* 12:129-138.
- Ambrose AM, Larson PS, Borzelleca JF, et al. (1976). Long term toxicologic assessment of nickel in rats and dogs. *J Food Sci Technol* 13:181-187.
- American Biogenics Corporation. (1988). Ninety day gavage study in albino rats using nickel. Final report submitted to U.S. Environmental Protection Agency, Office of Solid Waste. Submitted by Research Triangle Institute and American Biogenics Corporation.
- Anderson RA. (1998b). Effects of chromium on body composition and weight loss. *Nutr Rev* 56(9):266-270.
- Anderson RA, Bryden NA, Polansky MM. (1997b). Lack of toxicity of chromium chloride and chromium picolinate in rats. *J Am Coll Nutr* 16(3):273-279.
- Anttila A, Pukkala E, Aitio A, et al. (1998). Update of cancer incidence among workers at a copper/nickel smelter and nickel refinery. *Int Arch Occup Environ Health* 71(4):245-250.
- Antilla S, Sutinen S, Paananen M, et al. (1986). Hard metal lung disease: A clinical, histological, ultra structural and x-ray micro analytical study. *Eur J Respir Dis* 69:83-94.
- Arena VC, Sussman NB, Redmond CK, et al. (1998). Using alternative comparison populations to assess occupation-related mortality risk. Results for the high nickel alloys workers cohort. *J Occup Environ Med* 40(10):907-916.
- Ashby, M.F. (2013). *Materials and the Environment: Eco-informed Material Choice*. ISBN: 978-0-12-385971-6, second ed. Butterworth Heinemann/Elsevier, Waltham, MA, USA and Kidlington, Oxford, UK.
- Atzeni, E., Salmi, A. (2012). Economics of additive manufacturing for end-useable metal parts. *Int. J. Adv. Manuf. Technol.* 62 (9), 1147–1155.
- Baetjer AM, Lowney JF, Steffee H, et al. (1959b). Effect of chromium on incidence of lung tumors in mice and rats. *Arch Ind Health* 20:124-135.
- Bajželj B., J. M. Allwood, and J. M. Cullen (2013). Designing Climate Change Mitigation Plans That Add Up. *Environmental Science & Technology* 47, 8062 – 8069. doi: 10.1021/es400399h, ISSN: 0013-936X.
- Barborik M, Dusek J. (1972). Cardiomyopathy accompanying industrial cobalt exposure. *Br Heart J* 34:113-116.

- Bataineh H, Al-Hamood MH, Elbetieha A, et al. (1997). Effect of long-term ingestion of chromium compounds on aggression, sex behavior and fertility in adult male rat. *Drug Chem Toxicol* 20(3):133-149.
- Bourell, D.L., Leu, M.C., Rosen, D.W. (Eds.), (2009). Roadmap for additive manufacturing, identifying the future of freeform processing. *The University of Texas at Austin, Austin*.
- Bast-Pettersen R, Skaug V, Ellingsen D, et al. (2000). Neurobehavioral performance in aluminum welders. *Am J Ind Med* 37(2):184-192.
- Bast-Pettersen R, Drablos PA, Goffeng LO, et al. (1994). Neuropsychological deficit among elderly workers in aluminum production. *Am J Ind Med* 25(5):649-662.
- Baumers, M., Tuck, C., Wildman, R., Ashcroft, I., Rosamond, E., Hague, R. (2016). Shape complexity and process energy consumption in electron beam melting. A case of something for nothing in additive manufacturing? *J. Ind. Ecol.* [http:// dx.doi.org/10.1111/jiec.12397](http://dx.doi.org/10.1111/jiec.12397) (in press).
- Baumers Martin, Phill Dickens, Chris Tuck, Richard Hague (2015). The cost of additive manufacturing: machine productivity, economies of scale and technology-push. 0040-1625/© 2015 Elsevier Inc. *Technological Forecasting & Social Change* 102 (2016) 193–201.
- Baumers Martin, Chris Tuck, Ricky Wildman, Ian Ashcroft, Emma Rosamond, and Richard Hague. Transparency Built-in Energy Consumption and Cost Estimation for Additive Manufacturing (2013). *Volume 17, Number 3, Journal of Industrial Ecology*.
- Baumers, M., Tuck, C., Wildman, R., Ashcroft, I., Hague, R. (2011). Energy Inputs to Additive Manufacturing: Does Capacity Utilization Matter? *SOLID FREEFORM FABRICATION PROCEEDINGS; 30-40; Solid freeform fabrication; an additive manufacturing conference by University of Texas, Austin*.
- Baumers, M., C. Tuck, R. Hague, I. Ashcroft and R.Wildman. (2010). A comparative study of metallic additive manufacturing power consumption. *Paper presented at the 2010 Solid Freeform Fabrication Symposium, 9–11 August, Austin, TX, USA*.
- Beaumont JJ, Sedman RM, Reynolds SD, et al. (2008). Cancer mortality in a Chinese population exposed to hexavalent chromium in drinking water. (*Comment in: Epidemiology* 19(1):1-2, *Epidemiology* 19(1):24-26). *Epidemiology* 19(1):12-23.
- Bedello PG, Goitre M, Alovise V, et al. (1984). Contact dermatitis caused by cobalt naphthenate. *Contact Dermatitis* 11:247-264.
- Bednar CM, Kies C. (1991). Inorganic contaminants in drinking water correlated with disease occurrence in Nebraska. *Water Resour Bull* 27(4):631-635.
- Behrendt, T., Zein, A., Min, S., (2012). Development of an energy consumption monitoring procedure for machine tools. *CIRP Ann. - Manuf. Technol.* 61 (1), 43-46.
- Benson JM, Chang I-Y, Cheng YS. (1995a). Particle clearance and histopathology in lungs of F344/N rats and B6C3F1 mice inhaling nickel oxide or nickel sulfate. *Fundam Appl Toxicol* 28:232-244.
- Berge SR, Skyberg K. (2003). Radiographic evidence of pulmonary fibrosis and possible etiologic factors at a nickel refinery in Norway. *J Environ Monit* 5(4):681-688.
- Beyersmann D. (2002). Effects of carcinogenic metals on gene expression. *Toxicol Lett* 127(1-3): 63-68.
- Beyersmann D, Hartwig A. (1992). The genetic toxicology of cobalt. *Toxicol Appl Pharmacol* 115(1): 137-145.
- Bingham E, Barkley W, Zerwas M, et al. (1972). Responses of alveolar macrophages to metals. I. Inhalation of lead and nickel. *Arch Environ Health* 25:406-414.



- Bonenfant JL, Auger C, Miller G, et al. (1969). Quebec beer-drinkers' myocardiosis: pathological aspects. *Ann N Y Acad Sci* 156(1):577-582.
- Borneff I, Engelhardt K, Griem W, et al. (1968). Carcinogenic substances in water and soil. XXII. Mouse drinking study with 3,4-benzopyrene and potassium chromate. *Arch Hyg* 152:45-53.
- Bovet P, Lob M, Grandjean M. 1977. Spirometric alterations in workers in the chromium electroplating industry. *Int Arch Occup Environ Health* 40:25-32.
- Brem, A., Voigt, K.-I., (2009). Integration of market pull and technology push in the corporate front end and innovation management – Insights from the German software industry. *Technovation* 29 (5), 351–367.
- Brewer G. (1940). A statistical study of cobalt polycythemia in the dog. *Am J Physiol* 128:345-348.
- Brieger H. (1920). The symptoms of acute chromate poisoning. *Z Exper Path Therap* 21:393-408.
- Brinke, E. A cost estimation tool applied in the sheet metal domain, (2002). *Ipskamp, Enschede, The Netherlands*.
- Bucher JR, Hailey JR, Roycroft JR, et al. (1999). Inhalation toxicity and carcinogenicity studies of cobalt sulfate. *Toxicol Sci* 49:56-67.
- Bucher JR, Elwell MR, Thomson MB, et al. (1990). Inhalation toxicity studies of cobalt sulfate in F344/N rats and B6C3F1 mice. *Fundam Appl Toxicol* 15:357-372.
- Buchta M, Kiesswetter E, Schaper M, et al. (2005). Neurotoxicity of exposures to aluminium welding fumes in the truck trailer construction industry. *Environ Toxicol Pharmacol* 19(3):677-685.
- Burrows D, Creswell S, Merrett JD. (1981). Nickel, hands, and hip prosthesis. *Br J Dermatol* 105:437-444.
- Cai HR, Cao M, Meng FQ, et al. (2007). Pulmonary sarcooid-like granulomatosis induced by aluminum dust: Report of a case and literature review. *Chin Med J* 120(17):1556-1560.
- Cavalieri, S., Maccarone, P., and Pinto, R. Parametric vs. neural network models for the estimation of production costs: a case study in the automotive industry. *Int. J. Prod. Econ.*, 2004, 91, 165–167.
- Chashschin VP, Artunina GP, Norseth T. (1994). Congenital defects, abortion and other health effects in nickel refinery workers. *Sci Total Environ*, 148:287-291.
- Chen W-J, Monnat RJJ, Chen M, et al. (1978). Aluminum induced pulmonary granulomatosis. *Hum Pathol* 9(6):705-711.
- Chiappino G, Alois D, Wagner GR. (2011). Hard metal disease. *10 RESPIRATORY SYSTEM Ed. Encyclopedia of Occupational Health and Safety (Stellman J M, Editor-in-Chief). International Labor Organization, Geneva. © 2011. <http://www.ilo.org/oshenc/>.*
- Choi JW, Lee KS, Chung MP et al. (2005). GIANT CELL INTERSTITIAL PNEUMONIA: HIGH-RESOLUTION CT AND PATHOLOGIC FINDINGS IN FOUR ADULT PATIENTS. *AJR Am J Roentgenol.* 2005;1 84 (1 ): 268-72.
- Chopra JS, Kalra OP, Malik VS, et al. (1986). Aluminum phosphide poisoning: A prospective study of 16 cases in one year. *Postgrad Med J* 62:1113-1116.
- Chovil A, Sutherland RB, Halliday M. (1981). Respiratory cancer in a cohort of nickel sinter plant workers. *Br J Ind Med* 38:327-333.
- Chowdhury AR, Mitra C. (1995). Spermatogenic and steroidogenic impairment after chromium treatment in rats. *Indian J Exp Biol* 33:480-484.

- Christensen OB, Moller H. (1975). External and internal exposure to the antigen in the hand eczema of nickel allergy. *Contact Dermatitis* 1:136-141.
- Clochesy JM. (1984). Chromium ingestion: A case report. *J Emerg Nurs* 10:281-282.
- Clyne N, Lins L-E, Pehrsson SK, et al. (1988). Distribution of cobalt in myocardium, skeletal muscle and serum in exposed and unexposed rats. *Trace Elem Med* 5(2):52-54.
- Commissaris RL, Cordon JJ, Sprague S, et al. (1982). Behavioral changes in rats after chronic aluminum and parathyroid hormone administration. *Neurobehav Toxicol Teratol* 4(3):403-410.
- Cornell RG. (1984). Mortality patterns around stainless-steel workers. In: Sunderman FW Jr, Aitio A, Berlin A, eds. *Nickel in the human environment. IARC scientific publication no. 53. Lyon, France: International Agency for Research on Cancer, 65-71.*
- Cox JE, Doll R, Scott WA, et al. (1981). Mortality of nickel workers: Experience of men working with metallic nickel. *Br J Ind Med* 38:235-239.
- Cragle DL, Hollis DR, Newport TH, et al. (1984). A retrospective cohort study among workers occupationally exposed to metallic nickel powder at the Oak Ridge Gaseous Diffusion Plant. In: Sunderman FW Jr, Aitio A, Berlin A, eds. *Nickel in the human environment. IARC scientific publication no. 53. Lyon, France: International Agency for Research on Cancer, 57-64.*
- Crombie DW, Blaisdell JL, MacPherson G. (1944). The treatment of silicosis by aluminum powder. *Can Med Assoc J* 50:318-328.
- Cronin E, DiMichiel AD, Brown SS. (1980). Oral challenge in nickel-sensitive women with hand eczema. In: Brown SS, Sunderman FW Jr, eds. *Nickel toxicology. New York, NY: Academic Press, 149-152.*
- Davis JE. (1937). Cobalt polycythemia in the dog. *Proc Soc Exp Biol Med* 37:96-99.
- Davison AG, Haslam PL, Corrin B, et al. (1983). Interstitial lung disease and asthma in hard-metal workers: bronchoalveolar lavage, ultrastructural, and analytical findings and results of bronchial provocation tests. *Thorax* 38:119-128.
- De Flora S, Iltcheva M, Balansky RM. (2006). Oral chromium(VI) does not affect the frequency of micronuclei in hematopoietic cells of adult mice and of transplacentally exposed fetuses. *Mutat Res* 610:38-47.
- De Vuyst P, Dumortier P, Schandenè L, et al. (1987). Sarcoidlike lung granulomatosis induced by aluminum dusts. *Am Rev Respir Dis* 135(2):493-497.
- Demedts M, Gheysens B, Lauweryns J, et al. (1984a). "Hard-metal" lung disease due to cobalt in diamond polishers. *Am Rev Respir Dis* 129:A155.
- Demedts M, Gheysens B, Nagels J, et al. (1984b). Cobalt lung in diamond polishers. *Am Rev Respir Dis* 130:130-135.
- Deng JF, Sinks T, Elliott L, et al. (1991). Characterization of respiratory health and exposures are a sintered permanent magnet manufacturer. *Br J Ind Med* 48:609-615.
- Derelanko NJ, Rinehart WE, Hilaski RJ, et al. (1999). Thirteen-week subchronic rat inhalation toxicity study with a recovery phase of trivalent chromium compounds, chronic oxide, and basic chromium sulfate. *Toxicol Sci* 52(2):278-288.
- De Vuyst P, Dumortier P, Rickaert F, et al. (1986). Occupational lung fibrosis in an aluminum polisher. *Eur J Respir Dis* 68(2):131-140.

- Di Angelo, L. and P. Di Stefano. (2011). A neural network-based build time estimator for layer manufactured objects. *International Journal of Advanced Manufacturing Technology* 57(1): 215–224.
- Dick RB, Krieg EFJ, Sim MA, et al. (1997). Evaluation of tremor in aluminum production workers. *Neurotoxicol Teratol* 19(6):447-453.
- Dieter MP, Jameson CW, Tucker AN, et al. (1988). Evaluation of tissue disposition, myelopoietic, and immunologic responses in mice after long-term exposure to nickel sulfate in the drinking water. *J Toxicol Environ Health* 24:356-372.
- Dietrich, D. (2010). Emerging Technology Supply Chain Model for additive manufacturing. *Dissertation presented at the Missouri University of Science and Technology in 2010.*
- Doll R, Mathews JD, Morgan LG. (1977). Cancers of the lung and nasal sinuses in nickel workers. A reassessment of the period of risk. *Br J Ind Med* 34:102-105.
- Domingo JL, Llobet JM, Gomez M, et al. (1987b). Nutritional and toxicological effects of short-term ingestion of aluminum by the rat. *Res Commun Chem Pathol Pharmacol* 56(3):409-419.
- Domingo JL, Llobet JM. (1984). Treatment of acute cobalt intoxication in rats with L-methionine. *Rev Esp Fisiol* 40:443-448.
- Domingo JL, Llobet JM, Bernat R. (1984). A study of the effects of cobalt administered orally to rats. *Arch Farmacol Toxicol* 10:13-20.
- Dooms-Goossens A, Ceuterick A, Vanmalaele N, et al. (1980). Follow-up study of patients with contact dermatitis caused by chromates, nickel, and cobalt. *Dermatologica* 160:249-260.
- Drew RT, Gupta BN, Bend JR, et al. (1974). Inhalation studies with a glycol complex of aluminumchloride-hydroxide. *Arch Environ Health* 28(6):321-326.
- Edel J, Sabbioni E, Pietra R, Rossi A, Torre M, Rizzato G, Fraioli P. (1990). Trace metal lung disease: In vitro interaction of hard metals with human lung and plasma components. *Sci Total Environ* 95: 107-117.
- Edenhofer, O., R. Pichs-Madruga, Y. Sokona, E. Farahani, S. Kadner, K. Seyboth, A. Adler, I. Baum, S. Brunner, P. Eickemeier, B. Kriemann, J. Savolainen, S. Schlömer, C. von Stechow, T. Zwickel and J.C. Minx (eds.). Climate Change. Contribution of Working Group III to the Fifth Assessment Report of the Intergovernmental Panel on Climate Change. *Cambridge University Press, Cambridge, United Kingdom and New York, NY, USA.*
- Edgar G. Hertwich, William S. Pease, Catherine P. Koshland (1997). Evaluating the environmental impact of products and production processes: a comparison of six methods. *The Science of the Total Environment* 196 13-19.
- Egedahl R, Carpenter M, Lundell D. (2001). Mortality experience among employees at a hydrometallurgical nickel refinery and fertiliser complex in Fort Saskatchewan, Alberta (1954-95). *Occup Environ Med* 58(11):711-715.
- Ehrenfeld, J., (1994). Industrial Ecology: A Strategic Framework for Product Policy and Other Sustainable Practices. *The Second International Conference and Workshop on Product Oriented Policy, Stockholm, Sweden.*
- Elbetieha A, Al-Hamood MH. (1997). Long-term exposure of male and female mice to trivalent and hexavalent chromium compounds: Effect on fertility. *Toxicology* 116:39-47.
- Ellis H, Scurr JH. (1979). Axillary hyperhidrosis - topical treatment with aluminium chloride hexahydrate. *Postgrad Med J* 55:868-869.

- Enterline PE, Marsh GM. (1982). Mortality among workers in a nickel refinery and alloy plant in West Virginia. *J Natl Cancer Inst* 68:925-933.
- Fabrication Symposium, 23 (2012), 177-188; *SFF Symposium, International Solid Freeform Fabrication Symposium*, 23.
- Fava, J., Consoli, F., Denison, R., Dickson, K., Mohin, T., and Vigon, B., eds., (1993). Conceptual Framework for Life-Cycle Impact Assessment. *Society of Environmental Toxicology and Chemistry, Pensacola, Florida*.
- Fellone, L. (2013) Metalli duri: produzione, impieghi, rischi e prevenzione. Updating medicina del lavoro 1(3), 4-17. <http://dx.doi.org/10.5281/zenodo.12433>.
- Fischer T, Rystedt I. (1983). Cobalt allergy in hard metal workers. *Contact Dermatitis* 9:115-121.
- Fischedick M., J. Roy, A. Abdel-Aziz, A. Acquaye, J. M. Allwood, J.-P. Ceron, Y. Geng, H. Kheshgi, A. Lanza, D. Perczyk, L. Price, E. Santalla, C. Sheinbaum, and K. Tanaka (2014). *Industry. In: Climate Change 2014*.
- Flaten TP, Odegard M. (1988). Tea, aluminium and Alzheimer's disease. *Food Chem Toxicol* 26(1112): 959-960.
- Frischknecht, R., Jungbluth, N. (2007). Overview and Methodology. *EcoInvent, Swiss Centre for Life Cycle Inventories, Dübendorf, Switzerland*.
- Fristedt B, Lindqvist B, Schutz A, et al. (1965). Survival in a case of acute oral chromic acid poisoning with acute renal failure treated by haemodialysis. *Acta Med Scand* 177:153-159.
- Gad SC, Powers WJ, Dunn BJ, et al. (1986). Acute toxicity of four chromate salts. *In: Serrone DM, ed. Chromium symposium 1986: An update. Pittsburgh, PA: Industrial Health Foundation Inc., 43-58*.
- Gaffuri E, Donna A, Pietra R, et al. (1985). Pulmonary changes and aluminum levels following inhalation of alumina dust: A study on four exposed workers. *Med Lav* 76(3):222-227.
- Gallego H, Lewis EJ, Crutchfield CE. (1999). Crystal deodorant dermatitis: Irritant dermatitis to alum-containing deodorant. *Cutis* 64(1):65-66.
- Gallorini M, Edel J, Pietra R, Sabbioni E, Mosconi G. (1994). Cobalt speciation in urine of hard metal workers— a study carried out by nuclear and radioanalytical techniques. *Sci Total Environ* 150(1-3): 153-160.
- Gawkrodger DJ, Cook SW, Fell GS, et al. (1986). Nickel dermatitis: The reaction to oral nickel challenge. *Br J Dermatol* 115:33-38.
- Gell-Mann, M. (1995). What is complexity?. *Complexity* 1(1): 16–19.
- Gennart J, Lauwerys R. (1990). Ventilatory function of workers exposed to cobalt and diamond containing dust. *Int Arch Occup Environ Health* 62:333-336.
- Gesamtverband der Aluminiumindustrie (GDA), (2007). Safety instructions for handling and processing aluminium powder.
- Gheysens B, Auwerx J, Van den Eeckhout A, et al. (1985). Cobalt-induced bronchial asthma in diamond polishers. *Chest* 88:740-744.
- Gibb HJ, Lees PSJ, Pinsky PF, et al. (2000a). Clinical findings of irritation among chromium chemical production workers. *Am J Ind Med* 38:127-131.

- Gibson, I.; Rosen, D. W.; Stucker, B. (2010): Additive manufacturing technologies. Rapid prototyping to direct digital manufacturing. *New York ; London: Springer*.
- Gilks B, Churg A. (1987). Aluminum-induced pulmonary fibrosis: Do fibers play a role?. *Am Rev Respir Dis* 136(1):176-179.
- Glaser U, Hochrainer D, Kloppel H, et al. (1985). Low level chromium(VI) inhalation effects on alveolar macrophages and immune functions in Wistar rats. *Arch Toxicol* 57:250-256.
- Glaser U, Hochrainer D, Kloppel H, et al. (1986). Carcinogenicity of sodium dichromate and chromium(VI/III) oxide aerosols inhaled by male Wistar rats. *Toxicology* 42:219-232.
- Glaser U, Hochrainer D, Oldiges H. (1988). Investigations of the lung carcinogenic potentials of sodium dichromate and Cr VI/III oxide aerosols in Wistar rats. *Environ Hyg* 1:111-116.
- Glaser U, Hochrainer D, Steinhoff D. (1990). Investigation of irritating properties of inhaled CrVI with possible influence on its carcinogenic action. *Environ Hyg* 2:235-245.
- Godbold JH, Tompkins EA. (1979). A long-term mortality study of workers occupationally exposed to metallic nickel at the Oak Ridge Gaseous Diffusion Plant. *J Occup Med* 21:799-806.
- Goh CL. (1990). Aluminum chloride hexahydrate versus palmar hyperhidrosis. Evaporimeter assessment. *Int J Dermatol* 29(5):368-370.
- Goldoni M, Catalani S, De Palma G, Manini P, Acampa O, Corradi M, Bergonzi R, Apostoli P, Mutti A. (2004). Exhaled breath condensate as a suitable matrix to assess lung dose and effects in workers. *Environ Health Perspect* 112(13): 1293-1298.
- Golub MS, Germann SL, Han B, et al. (2000). Lifelong feeding of a high aluminum diet to mice. *Toxicology* 150(1-3):107-117.
- Golub MS, Han B, Keen CL, et al. (1992b). Effects of dietary aluminum excess and manganese deficiency on neurobehavioral endpoints in adult mice. *Toxicol Appl Pharmacol* 112(1):154-160.
- Gomez M, Domingo JL, Llobet JM, et al. (1986). Short-term oral toxicity study of aluminum in rats. *Arch Farmacol Toxicol* 12(2-3):145-151.
- Goossens A, Bedert R, Zimerson E. (2001). Allergic contact dermatitis caused by nickel and cobalt in green plastic shoes. *Contact Dermatitis* 45(3):172.
- Grimm, T. (2004). User's guide to rapid prototyping. *Rapid Prototyping Association of SME, Dearborn, Michigan*.
- Grimsrud TK, Berge SR, Martinsen JI, et al. (2003). Lung cancer incidence among Norwegian nickel-refinery workers 1953-2000. *J Environ Monit* 5(2):190-197.
- Gross P, Harley RA Jr, deTreville RTP. (1973). Pulmonary reaction to metallic aluminum powders. *Arch Environ Health* 26:227-236.
- Guha Manogharan, Richard A Wusk & Ola L.A. Harrysson (2016) Additive manufacturing–integrated hybrid manufacturing and subtractive processes: economic model and analysis. *International Journal of Computer Integrated Manufacturing*, 29:5, 473-488, DOI: 10.1080/0951192X.2015.1067920.
- Guo, Y., Duflou, J.R., Qian, J., Tang, H., Lauwers, B., (2015). An operation-mode based simulation approach to enhance the energy conservation of machine tools. *J. Clean. Prod.* 101, 348-359.
- Gutowski, T.G., Branham, M.S., Dahmus, J.B., Jones, A.J., Thiriez, A., Sekulic, D.P. (2009). Thermodynamic analysis of resources used in manufacturing processes. *Environ. Sci. Technol.* 43 (5), 1584–1590.

- Froehlich (2013). A Sustainable Approach to the Supply of Nitrogen. Copyright Parker Hannifin Corporation 2013
- Hänninen H, Matikainen E, Kovala T, et al. (1994). Internal load of aluminum and the central nervous system function of aluminum welders. *Scand J Work Environ Health* 20(4):279-285.
- Hartung M, Schaller K-H, Brand E. (1982). On the question of the pathogenetic importance of cobalt for hard metal fibrosis of the lung. *Int Arch Occup Environ Health* 50:53-57.
- Hartwig A. (2000). Recent advances in metal carcinogenicity. *Pure Appl Chem* 72(6): 1007-1014.
- Hartwig A, Asmuss M, Ehleben I, Herzer U, Kostelac D, Pelzer A, Schwerdtle T, Bürkle A. (2002). Interference by toxic metal ions with DNA repair processes and cell cycle control: molecular mechanisms. *Environ Health Perspect* 110(Suppl 5): 797-799.
- Hazard and risk-based approaches to comparing toxic emissions. Edgar G. Hertwich, Thomas E. McKone, and William S. Pease. 0-7803-3808-1 / 97\$10.00 O1997 IEEE.
- He SC, Qiao N, Sheng W. (2003). Neurobehavioral, autonomic nervous function and lymphocyte subsets among aluminum electrolytic workers. *Int J Immunopathol Pharmacol* 16(2):139-144.
- Herbert A, Sterling G, Abraham J, et al. (1982). Desquamative interstitial pneumonia in an aluminum welder. *Hum Pathol* 13(8):694-699.
- Hindsen M, Bruze M, Christensen OB. (2001). Flare-up reactions after oral challenge with nickel in relation to challenge doses and intensity and time of previous patch test reactions. *J Am Acad Dermatol* 44(4):616-623.
- Hogstedt C, Alexandersson R. (1990). Dödsorsaker hos Hardmetallarbetare. *Arbete och Hälsa* 21: 1-26.
- Holly RG. (1955). Studies on iron and cobalt metabolism. *JAMA* 158:1349-1352.
- Horie A, Tanaka I, Haratake J, et al. (1985). Electron microscopy of pulmonary lesions including carcinoma, induced by inhalation exposure of rats to nickel oxide aerosol. In: Brown SS, Sunderman FW Jr, eds. *Progress in nickel toxicology. Proceedings of the 3rd International Congress on Nickel Metabolism and Toxicology. Oxford, UK: Blackwell, 41-44.*
- Hopkinson N. and Dickens P.M, (2003). Analysis of rapid manufacturing-using layer manufacturing processes for production. Proceed-ings of the Institute of Mechanical Engineers, Part C: Journal of Mechanical Engineering Science, 217 (C1), pp. 31-39.
- Horowitz SF, Fischbein A, Matza D, et al. (1988). Evaluation of right and left ventricle function in hard metal workers. *Brit J Ind Med* 45:742-746.
- Hosovski E, Mastelica Z, Sunderic D, et al. (1990). Mental abilities of workers exposed to aluminum. *Med Lav* 81(2):119-123.
- Huang, R., Riddle, M., Graziano, D., Warren, J., Das, S., Nimbalkar, S., Cresko, J., Masanet, E., (2016). Energy and emissions saving potential of additive manufacturing: the case of lightweight aircraft components. *J. Clean. Prod.* 135, 1559-1570.
- Huax F, Lasfargues G, Lauwerys R, Lison D. (1995). Lung toxicity of hard metal particles and production of interleukin-1, tumor necrosis factor-alpha, fibronectin, and cystatin-c by lung phagocytes. *Toxicol Appl Pharmacol* 132(1): 53-62.
- Hughson G. W., K. S. Galea and K. E. Heim (2010). Characterization and Assessment of Dermal and Inhalable Nickel Exposures in Nickel Production and Primary User Industries. *Ann. Occup. Hyg., Vol. 54, No. 1, pp. 23–30.*

- Hull, C. (2012). On stereolithography. *Virtual Phys. Prototyp.* 7 (3), 177.
- Hull MJ, Abraham JL. (2002). Aluminum welding fume-induced pneumoconiosis. *Hum Pathol* 33(8):819-825.
- IARC. (1984). Polynuclear aromatic compounds. Part 3: Industrial exposures in aluminum production, coal gasification, coke production, and iron and steel founding. *Vol. 34. Lyon, France: World Health Organization, International Agency for Research on Cancer*, 37-64.
- Ingarao Giuseppe, Priarone Paolo C. (2017). Towards criteria for sustainable process selection: On the modelling of pure subtractive versus additive/subtractive integrated manufacturing approaches. *Journal of Cleaner Production* 144 57-68.
- Ingarao, G., Priarone Paolo C., Di Lorenzo, R., Settineri, L. (2016). A methodology for evaluating the influence of batch size and part geometry on the environmental performance of machining and forming processes. *J. Clean. Prod.* 135, 1611-1622.
- International Committee on Nickel Carcinogenesis in Man. (1990). Report of the International Committee on Nickel Carcinogenesis in Man. *Scand J Work Environ Health* 16(1):1-82.
- Iseron KV, Banner W, Froede RC, et al. (1983). Failure of dialysis therapy in potassium dichromate poisoning. *J Emerg Med* 1:143-149.
- Ivankovic S, Preussmann R. (1975). Absence of toxic and carcinogenic effects after administration of high doses of chromic oxide pigment in subacute and long-term feeding experiments in rats. *Food Cosmet Toxicol* 13:347-351.
- Jarvis JQ, Hammond E, Meier R, et al. (1992). Cobalt cardiomyopathy: A report of two cases from mineral assay laboratories and a review of the literature. *J Occup Med* 34(6):620-626.
- Jederlinic PJ, Abraham JL, Churg A, et al. (1990). Pulmonary fibrosis in aluminum oxide workers. Investigation of nine workers with pathologic examination and microanalysis in three of them. *Am Rev Respir Dis* 142:1179-1184.
- Jensen CS, Menne T, Lisby S, et al. (2003). Experimental systemic contact dermatitis from nickel: A dose-response study. *Contact Dermatitis* 49(3):124-132.
- Jephcott CM. (1948). Fume exposure in the manufacture of alumina abrasives. *Occup Med* 5:701-709.
- Jeswiet, J., Kara, S. (2008). Carbon emissions and CESTM in manufacturing. *CIRP Ann. - Manuf. Technol.* 57 (1), 17-20.
- Johansson A, Curstedt T, Camner P. (1991). Lung lesions after combined inhalation of cobalt and nickel. *Environ Res* 54:24-38.
- Jordan WP, King SE. (1979). Nickel feeding in nickel-sensitive patients with hand eczema. *J Am Acad Dermatol* 1:506-508.
- Jordan C, Whitman RD, Harbut M, et al. (1990). Memory deficits in workers suffering from hard metal disease. *Toxicol Lett* 54:241-243.
- Johansson A, Curstedt T, Rasool O, et al. (1992). Rabbit lung after combined exposure to soluble cobalt and trivalent chromium. *Environ Res* 58:80-96.
- Johansson A, Curstedt T, Robertson B, et al. (1984). Lung morphology and phospholipids after experimental inhalation of soluble cadmium, copper, and cobalt. *Environ Res* 34:295-309.
- Johansson A, Robertson B, Camner P. (1987). Nodular accumulation of type II cells and inflammatory lesions caused by inhalation of low cobalt concentrations. *Environ Res* 43:227-243.

- Junaid M, Murthy RC, Saxena DK. (1996b). Embryotoxicity of orally administered chromium in mice: Exposure during the period of organogenesis. *Toxicol Lett* 84:143-148.
- Kaaber K, Veinen NK, Tjell JC. (1978). Low nickel diet in the treatment of patients with chronic nickel dermatitis. *Br J Dermatol* 98:197-201.
- Kanerva L, Estlander T, Jolanki R. (1988). Occupational skin disease in Finland. *Int Arch Occup Environ Health* 60:89-94.
- Kanerva L, Estlander T, Jolanki R. (1998). Bank clerk's occupational allergic nickel and cobalt contact dermatitis from coins. *Contact Dermatitis* 38:217-218.
- Kara, S., Li, W. (2011). Unit process energy consumption models for material removal processes. *CIRP Ann. - Manuf. Technol.* 60 (1), 37-40.
- Karjalainen S, Kerttula R, Pukkala E. (1992). Cancer risk among workers at a copper/nickel smelter and nickel refinery in Finland. *Int Arch Occup Environ Health* 63:547-551.
- Kellens, K., E. Yasa, W. Dewulf, and J. R. Duflou. (2010). Environmental assessment of selective laser melting and selective laser sintering. *Paper presented at Going Green – CARE INNOVATION 2010: From Legal Compliance to Energy-efficient Products and Services, 8–11 November, Vienna, Austria.*
- Kesteloot H, Roelandt J, Willems J, et al. (1968). An enquiry into the role of cobalt in the heart disease of chronic beer drinkers. *Circulation* 37:854-864.
- Kerfoot EJ. (1975). Semi-chronic inhalation study on cobalt. *Diss Abstr Int B* 35:6054-6055.
- Keskinen H, Kalliomaki P, Alanko K. (1980). Occupational asthma due to stainless steel welding fumes. *Clin Allergy* 10:151-159.
- Khosla SN, Nand N, Khosla P. (1988). Aluminum phosphide poisoning. *J Trop Med Hyg* 91:196-198.
- Kiec-Swierczynska M, Krecisz B. (2002). Allergic contact dermatitis in dentists and dental nurses. *Exog Dermatol* 1(1):27-31.
- Kiec-Swierczynska M, Krecisz B. (2000). Occupational skin diseases among the nurses in the region of Lodz. *Int J Occup Med Environ Health* 13(3):179-184.
- Kim HY, Lee SB, Jang BS. (2004). Subchronic inhalation toxicity of soluble hexavalent chromium trioxide in rats. *Arch Toxicol* 78:363-368.
- Kitamura F, Yokoyama K, Araki S, et al. (2003). Increase of olfactory threshold in plating factory workers exposed to chromium in Korea. *Ind Health* 41(3):279-285.
- Korallus U, Ehrlicher H, Wustefeld E, et al. (1974a). Trivalent chromium compounds - results of a study in occupational medicine. *Arb Soz Prev* 9:51-54.
- Kornhauser C, Wrobel K, Wrobel K, et al. (2002). Possible adverse effect of chromium in occupational exposure of tannery workers. *Ind Health* 40(2):207-213.
- Korogiannos C, Babatsikou F, Tzimas S, et al. (1998). Aluminum compounds and occupational lung disease. *Eur Respir J* 12(Suppl 28):139S.
- Krasovskii GN, Vasukovich LY, Chariev OG. (1979). Experimental study of biological effects of lead and aluminum following oral administration. *Environ Health Perspect* 30:47-51.
- Krasovskii GN, Fridlyand SA. (1971). Experimental data for the validation of the maximum permissible concentration of cobalt in water bodies. *Hyg Sanit* 26:277-279.



- Kraus T, Schaller KH, Angerer J, et al. (2000). Aluminum dust-induced lung disease in the pyro-powderproducing industry: Detection by high-resolution computed tomography. *Int Arch Occup Environ Health* 73(1):61-64.
- Kumar A, Rana SVS. (1982). Lipid accumulation in chromium-poisoned rats. *Int J Tissue React* 4(4):291-295.
- Kusaka Y, Ichikawa Y, Shirakawa T, et al. (1986a). Effect of hard metal dust in ventilatory function. *Brit J Ind Med* 43:486-489.
- Kusaka Y, Iki M, Kumagai S, et al. (1996a). Decreased ventilatory function in hard metal workers. *Occup Environ Med* 53:194-199.
- Kusaka Y, Iki M, Kumagai S, et al. (1996b). Epidemiological study of hard metal asthma. *Occup Environ Med* 53:188-193.
- Kusaka Y, Iki M, Kumagai S, et al. (1996b). Epidemiological study of hard metal asthma. *Occup Environ Med* 53:188-193.
- Kyono H, Kusaka Y, Homma K, et al. (1992). Reversible lung lesions in rats due to short-term exposure to ultrafine cobalt particles. *Ind Health* 30:103-118.
- Kumar S, Sathwara NG, Gautam AK, et al. (2005). Semen quality of industrial workers occupationally exposed to chromium. *J Occup Health* 47(5):424-430.
- Kusaka Y, Nakano Y, Shirakawa T, Morimoto K. LYMPHOCYTE TRANSFORMATION WITH COBALT IN HARD METAL ASTHMA. *Ind Health* 1989; 27:1 55-1 63.
- Lasfargues G, Wild P, Moulin JJ, Hammon B, Rosmorduc B, Rondeau du Noyer C, Lavandier M, Moline J. (1994). Lung cancer mortality in a French cohort of hard-metal workers. *Am J Ind Med* 26(5): 585-595.
- Lansdown AB. (1973). Production of epidermal damage in mammalian skins by some simple aluminum compounds. *Br J Dermatol* 89:67-76.
- Lee KP, Ulrich CE, Geil RG, et al. (1989). Inhalation toxicity of chromium dioxide dust to rats after two years exposure. *Sci Total Environ* 86:83-108.
- Liebow AA, Carrington CB. ALVEOLAR DISEASES: THE INTERSTITIAL PNEUMONIAS. *Simon M, Potchen EJ, Le May M, editors. FRONTIERS OF PULMONARY RADIOLOGY. New York: Grune and Stratton; 1969. pp. 1 02-1 41.*
- Lieberman H. (1941). Chrome ulcerations of the nose and throat. *New Engl J Med* 225:132-133.
- Lindemann, C., Jahnke, U., Moi, M., Koch, R. Analyzing Product Lifecycle Costs for a Better Understanding of Cost Drivers in Additive Manufacturing. *SOLID FREEFORM FABRICATION PROCEEDINGS; 177-188; Annual international solid freeform fabrication symposium von University of Texas, Austin; 2012.*
- Linos A, Petralias A, Christophi CA, et al. (2011). Oral ingestion of hexavalent chromium through drinking water and cancer mortality in an industrial area of Greece--an ecological study. *Environ Health* 10:50.
- Linnainmaa M, Kiilunen M. (1997). Urinary cobalt as a measure of exposure in the wet sharpening of hard metal and stellite blades. *Int Arch Occup Environ Health* 69(3): 193-200.
- Lison D. (1996). Human toxicity of cobalt-containing dust and experimental studies on the mechanism of interstitial lung disease (hard metal disease). *Crit Rev Toxicol* 26(6): 585-616.
- Littorin M, Hogstedt B, Stromback B, et al. (1983). No cytogenetic effects in lymphocytes of stainless steel welders. *Scand J Work Environ Health* 9:259-264.

- Lloyd DR, Carmichael PL, Phillips DH. (1998). Comparison of the formation of 8-hydroxy-2'-deoxyguanosine and single- and double-strand breaks in DNA mediated by Fenton reactions. *Chem Res Toxicol* 11(5): 420-427.
- Lombaert N, De Boeck M, Ecordier I, Undari E, Lison D, Irsch-Volders M. (2004). Evaluation of the apoptogenic potential of hard metal dust (WC-Co), tungsten carbide, and metallic cobalt. *Toxicol Lett* 154: 23-34.
- Loubieres Y, de Lassence A, Bernier M, et al. (1999). Acute, fatal, oral chromic acid poisoning. *J Toxicol Clin Toxicol* 37(3):333-336.
- Lucas JB, Kramkowski RS. (1975). Health hazard evaluation determination report number 74-87-221. Cincinnati, OH: U.S. Department of Health, Education, and Welfare, Center for Disease Control, National Institute for Occupational Safety and Health.
- Mackay, Donald and Sally Patterson (1991), Evaluating the Multimedia Fate of Organic Chemicals: A Level III Fugacity Model. *Environmental Science & Technology* 25:427-436.
- Mackay, D., W. Shiu, and K. Ma (1993). *Illustrated Handbook of Physical-Chemical Properties and Environmental Fate for Organic Chemicals*, Lewis Publishers, Boca Raton.
- MacKenzie RD, Byerrum RU, Decker CF, et al. (1958). Chronic toxicity studies: II. Hexavalent and trivalent chromium administered in drinking water to rats. *Arch Ind Health* 18:232-234.
- Magnus K, Andersen A, Hogetveit AC. (1982). Cancer of respiratory organs among workers at a nickel refinery in Norway. *Int J Cancer* 30:681-685.
- Mancuso TF. (1951). Occupational cancer and other health hazards in a chromate plant: A medical appraisal: II. *Clinical and toxicologic aspects*. *Ind Med Surg* 20:393-407.
- Manfredi D., F. Calignano, E. P. Ambrosio, M. Krishnan, R. Canali, S. Biamino, M. Pavese, E. Atzeni, L. Iuliano, P. Fino, C. Badini. Direct Metal Laser Sintering: an additive manufacturing technology ready to produce lightweight structural parts for robotic applications. *La Metallurgia Italiana* · October 2013.
- Marcussen PV. (1963). Cobalt dermatitis. Clinical picture. *Acta Derm Venereol (Stockh)* 43:231-234.
- Martin, M.J.C. (1994). Managing innovation and entrepreneurship in technology based firms. *Wiley, New York*.
- Mathur AK. (2005). Effects of dermal application of chromium and linear alkylbenzene sulphonate alone and in combination in guinea pigs. *Toxicol Int* 12(1):9-12.
- Mathur AK, Gupta BN. (1994). Dermal toxicity of nickel and chromium in guinea pigs. *Vet Hum Toxicol* 36(2):131-132.
- Mathur AK, Agarwal C, Singh A, et al. (1988). Effect of sodium lauryl sulphate and nickel alone and in combination on the skin of guinea pigs. *Toxicol Lett* 42:249-256.
- Mathur AK, Gupta BN, Singh S, et al. (1992). Cutaneous toxicity of sodium lauryl sulphate, nickel, and their combination in guinea pigs: Biochemical and histopathological observations. *Bull Environ Contam Toxicol* 49:871-878.
- Mayyas, T.A., Qattawi, A., Mayyas, A.R., Omar, M.A. (2012). Life cycle assessment based selection for a sustainable lightweight body-in-white design. *Energy* 39, 412-425.
- McLaughlin AIG, Kazantzis G, King E, et al. (1962). Pulmonary fibrosis and encephalopathy associated with the inhalation of aluminum dust. *Br J Ind Med* 19:253-263.

- Meecham HM, Humphrey P. (1991). Industrial exposure to cobalt causing optic atrophy and nerve deafness: A case report. *J Neurol Neurosurg Psychiatry* 54(4):374-375.
- Meiklejohn A, Posner E. (1957). The effect of the use of calcined alumina in china biscuit placing on the health of the workman. *Br J Ind Med* 14:229-231.
- Meyers JB. (1950). Acute pulmonary complications following inhalation of chromic acid mist. *Ann Ind Hyg Occup Med* 2:742-747.
- Miller RR, Churg AM, Hutcheon M, et al. (1984b). Pulmonary alveolar proteinosis and aluminum dust exposure. *Am Rev Respir Dis* 130(2):312-315.
- Minamoto K, Nagano M, Inaoka T, et al. (2002). Occupational dermatoses among fibreglass-reinforced plastics factory workers. *Contact Dermatitis* 46:339-347.
- Mitchell J, Manning GB, Molyneux M, et al. (1961). Pulmonary fibrosis in workers exposed to finely powdered aluminum. *Br J Ind Med* 18:10-20.
- Mohiuddin SM, Taskar PK, Rheault M, et al. (1970). Experimental cobalt cardiomyopathy. *Am Heart J* 80(4):532-543.
- Mognol, P., D. Lopicart, and N. Perry. (2006). Rapid prototyping: Energy and environment in the spotlight. *Rapid Prototyping Journal* 12(1): 26–34.
- Morin Y, Daniel P. (1967). Quebec beer-drinkers' cardiomyopathy: etiological considerations. *Can Med Assoc J* 97:926-928.
- Morin Y, Tetu A, Mercier G. (1971). Cobalt cardiomyopathy: Clinical Aspects. *Br Heart J* 33:175-178.
- Moulin JJ, Clavel T, Roy D, et al. (2000). Risk of lung cancer in workers producing stainless steel and metallic alloys. *Int Arch Occup Environ Health* 73(3):171-80.
- Moulin JJ, Wild P, Romazini S, Lasfargues G, Peltier A, Bozec C, Deguerry P, Pellet F, Perdrix A. (1998). Lung cancer risk in hard-metal workers. *Am J Epidemiol* 148(3): 241-248.
- Muir DCF, Jadon N, Julian JA, et al. (1994). Cancer of the respiratory tract in nickel sinter plant workers: Effect of removal from sinter plant exposure. *Occup Environ Med* 51(1):19-22.
- Munguia, F. J. (2009). RMADS: Development of a concurrent rapid manufacturing advice system. *Ph.D. thesis, Universitat Politecnica de Catalunya, Barcelona, Spain.*
- Munoz DG. (1998). Is exposure to aluminum a risk factor for the development of Alzheimer disease? *No. Arch Neurol* 55(5):737-739.
- Mur JM, Moulin JJ, Charruyer-Seinerra MP, et al. (1987). A cohort mortality study among cobalt and sodium workers in an electrochemical plant. *Am J Ind Med* 11:75-81.
- Murdock HR. (1959). Studies on the pharmacology of cobalt chloride. *J Am Pharm Assoc Sci Ed* 48:140-142.
- Musk AW, Greeville HW, Tribe AE. (1980). Pulmonary disease from occupational exposure to an artificial aluminum silicate used for cat litter. *Br J Ind Med* 37(4):367-372.
- Mussi I, Calzaferrri G, Buratti M, et al. (1984). Behaviour of plasma and urinary aluminum levels in occupationally exposed subjects. *Int Arch Occup Environ Health* 54(2):155-161.
- Mutafova-Yambolieva V, Staneva-Stoytcheva D, Lasova L, et al. (1994). Effects of cobalt or nickel on the sympathetically mediated contractile responses in rat-isolated vas deferens. *Pharmacology* 48:100110.

- Nackerdien Z, Kasprzak KS, Rao G, Halliwell B, Dizdaroglu M. (1991). Nickel(II)- and cobalt(II)-dependent damage by hydrogen peroxide to the DNA bases in isolated human chromatin. *Cancer Res* 51(21): 5837-5842.
- Nandwana, P., Peter, W.H., Dehoff, R.R., Lowe, L.E., Kirka, M.M., Medina, F., Babu, S.S., (2016). Recyclability study on Inconel 718 and Ti-6Al-4V powders for use in electron beam melting. *Metall. Mater. Trans. B* 47 (1), 754-762.
- Nemery B, Verbeken EK, Demedts M. GIANT CELL INTERSTITIAL PNEUMONIA (HARD METAL LUNG DISEASE, COBALT LUNG). *Semin Respir Crit Care Med*. 2001 Aug; 22(4):435-48. Murata M, Gong P, Suzuki K, Koizumi S. 1999. Differential metal response and regulation of human heavy metal-inducible genes. *J Cell Physiol* 180(1): 105-113.
- Nemery B, Casier P, Roosels D, et al. (1992). Survey of cobalt exposure and respiratory health in diamond polishers. *Am Rev Respir Dis* 145:610-616.
- Nettesheim P, Szakal AK. (1972). Morphogenesis of alveolar bronchiolization. *Lab Invest* 26(2):210-219.
- Nettesheim P, Hanna MG, Doherty DG, et al. (1971). Effect of calcium chromate dust, influenza virus, and 100 R whole-body X-radiation on lung tumor incidence in mice. *J Natl Cancer Inst* 47(5):1129-1144.
- Nicolaou G, Pietra R, Sabbioni E, Mosconi G, Cassina G, Seghizzi P. (1987). Multielement determination of metals in biological specimens of hard metal workers: a study carried out by neutron activation analysis. *J Trace Elem Electrolytes Health Dis* 1(2): 73-77.
- Nielsen GD, Jepson LV, Jorgensen PJ, et al. (1990). Nickel-sensitive patients with vesicular hand eczema: Oral challenge with a diet naturally high in nickel. *Br J Dermatol* 122:299-308.
- NTP. (2009). Report on Carcinogens Background Document for Cobalt-Tungsten Carbide Powders and Hard Metals. *National Toxicology Program*.  
[http://ntp.niehs.nih.gov/ntp/roc/twelfth/2010/finalbds/hardmetalsbd20100408\\_508.pdf](http://ntp.niehs.nih.gov/ntp/roc/twelfth/2010/finalbds/hardmetalsbd20100408_508.pdf).
- NTP. (2008a). NTP technical report on the toxicology and carcinogenesis studies of sodium dichromate dihydrate (CAS No. 7789-12-0) in F344/N rats and B6C3F1 mice (drinking water studies). *Washington, DC: National Toxicology Program. NTP TR 546*. [http://ntp.niehs.nih.gov/files/546\\_web\\_FINAL.pdf](http://ntp.niehs.nih.gov/files/546_web_FINAL.pdf). August 13, 2008.
- NTP. (2008b). NTP technical report on the toxicology and carcinogenesis studies of chromium picolinate monohydrate (CAS No. 27882-76-4) in F344/N rats and B6C3F1 mice (feed studies). *Scheduled peer review date: February 27-28, 2008. Washington, DC: National Toxicology Program. NTP TR 556*. [http://ntp.niehs.nih.gov/files/TR556board\\_webRev.pdf](http://ntp.niehs.nih.gov/files/TR556board_webRev.pdf). May 21, 2008.
- NTP. (2007). NTP technical report on the toxicity studies of sodium dichromate dihydrate (CAS No. 7789-12-0) administered in drinking water to male and female F344/N rats and B6C3F1 mice and male BALB/c and am3-C57BL/6 mice. *Washington, DC: National Toxicology Program. Toxicity Report Series Number 72*. [http://ntp.niehs.nih.gov/ntp/htdocs/ST\\_rpts/TOX72.pdf](http://ntp.niehs.nih.gov/ntp/htdocs/ST_rpts/TOX72.pdf). October 7, 2008.
- NTP. (1998). NTP report on the toxicity studies of cobalt sulfate heptahydrate in F344/N rats and B6C3F1 mice (inhalation studies). *National Institutes of Health, National Toxicology Program. NIH Publication No. 471*.
- NTP. (1996a). Final report on the reproductive toxicity of potassium dichromate (hexavalent) (CAS No. 7778-50-9) administered in diet to SD rats. *National Institute of Environmental Health Sciences, National Toxicology Program. PB97125355*.
- NTP. (1996a). NTP technical report on the toxicology and carcinogenesis studies of nickel oxide (CAS No. 1313-99-1) in F344/N rats and B6C3F1 mice (inhalation studies). *Research Triangle Park, NC: U.S.*

Department of Health and Human Services, Public Health Service, National Institutes of Health. NTPTRS No. 451.

NTP. (1996b). Final report on the reproductive toxicity of potassium dichromate (hexavalent) (CAS No. 7778-50-9) administered in diet to BALB/c mice. *National Institute of Environmental Health Sciences, National Toxicology Program. PB97125363.*

NTP. (1996b). NTP technical report on the toxicology and carcinogenesis studies of nickel subsulfide (CAS No. 12035-72-2) in F344/N rats and B6C3F1 mice (inhalation studies). *Research Triangle Park, NC: U.S. Department of Health and Human Services, Public Health Service, National Institutes of Health. NTP-TRS No. 453.*

NTP. (1996c). NTP technical report on the toxicology and carcinogenesis studies of nickel sulfate hexahydrate (CAS No. 10101-97-0) in F344/N rats and B6C3F1 mice (inhalation studies). *Research Triangle Park, NC: U.S. Department of Health and Human Services, Public Health Service, National Institutes of Health. NTP-TRS No. 454.*

NTP. (1991). NTP report on the toxicity studies of cobalt sulfate heptahydrate in F344/N rats and B6C3F1 mice (inhalation studies). *National Institutes of Health, National Toxicology Program. NIH Publication No. 91-3124.*

Obone E, Chakrabarti SK, Bai C, et al. (1999). Toxicity and bioaccumulation of nickel sulfate in Sprague-Dawley rats following 13 weeks of subchronic exposure. *J Toxicol Environ Health A 57:379401.*

OSHA, (1978). Occupational health guideline for Chromium Metal and insoluble Chromium Salts.

OSHA, (1978). Occupational health guideline for Chromic Acid and Chromates.

OSHA, (1978). Occupational health guideline for Cobalt Metal Fume and Dust.

OSHA, (1978). Occupational health guideline for Nickel Metal and Soluble Nickel Compounds.

OSHA, (1978). Occupational health guideline for Titanium Dioxide.

Oteiza PI, Keen CL, Han B, et al. (1993). Aluminum accumulation and neurotoxicity in Swiss-Webster mice after long-term dietary exposure to aluminum and citrate. *Metabolism 42(10):1296-1300.*

Ottolenghi AD, Haseman JK, Payne WW, et al. (1974). Inhalation studies of nickel sulfide in pulmonary carcinogenesis of rats. *JNCI 54:1165-1172.*

Palmes ED, Nelson N, Laskin S, et al. (1959). Inhalation toxicity of cobalt hydrocarbonyl. *Am Ind Hyg Assoc J 20:453-468.*

Pascale LR, Waldstein SS, Engbring G, et al. (1952). Chromium intoxication with special reference to hepatic injury. *J Am Med Assoc 149:1385-1389.*

Pandey R, Srivastava SP. (2000). Spermatotoxic effects of nickel in mice. *Bull Environ Contam Toxicol 64(2):161-167.*

Pang D, Burges DC, Sorhan T. (1996). Mortality studies of nickel platers with special reference to cancers of the stomach and lung. *Occup Environ Med 53(10):714-717.*

Paternain JL, Domingo JL, Llobet JM, et al. (1988). Embryotoxic and teratogenic effects of aluminum nitrate in rats upon oral administration. *Teratology 38:253-257.*

Pedersen E, Hogetveit AC, Andersen A. (1973). Cancer of respiratory organs among workers at a nickel refinery in Norway. *Int J Cancer 12:32-41.*

- Peto R, Cuckle H, Doll R, et al. (1984). Respiratory cancer mortality of Welsh nickel refinery workers. *In: Sunderman FW Jr, Aitio A, Berlin A, eds. Nickel in the human environment. IARC scientific publication no. 53. Lyon, France: International Agency for Research on Cancer, 37-46.*
- Petrovic, V., Ninerola, R. (2015). Powder recyclability in electron beam melting for aeronautical use. *Aircr. Eng. Aerosp. Technol. Int. J.* 87 (2), 147-155.
- PHS. (1953). Health of workers in chromate producing industry: A study. *Washington, DC: U.S. Public Health Service. Publication no. 192.*
- Pigott GH, Gaskell BA, Ishmael J. (1981). Effects of long term inhalation of alumina fibres in rats. *Br J Exp Pathol* 62(3):323-331.
- Polednak AP. (1981). Mortality among welders, including a group exposed to nickel oxides. *Arch Environ Health* 36:235-242.
- Polizzi S, Pira E, Ferrara M, et al. (2001). Neurotoxic effects of aluminum among foundry workers. *Neurotoxicology* 22(4):540.
- Posner E, Kennedy MCS. (1967). A further study of china biscuit placers in Stoke-on-Trent. *Br J Ind Med* 24:133-142.
- Prescott E, Netterstrom B, Faber J, et al. (1992). Effect of occupational exposure to cobalt blue dyes on the thyroid volume and function of female plate painters. *Scand J Work Environ Health* 18:101-104.
- Preventing explosions: How to safely clean up combustible dusts. (2010). [www.powderbulk.com](http://www.powderbulk.com).
- Pryce DW, King CM. (1990). Orofacial granulomatosis associated with delayed hypersensitivity to cobalt. *Clin Exp Dermatol* 15:384-386.
- Psarra, S. and T. Grajewski. (2001). Describing shape and shape complexity using local properties. *In Proceedings of the 3rd International Space Syntax Symposium, 7-11 May, Atlanta, GA, USA.*
- Priarone Paolo C., Maria G. Faga, Matteo Robiglio, Luca Settineri and Vincenzo Tebaldo. Technological and sustainability implication of dry, near-dry, and wet turning of Ti-6Al-4V alloy. *INTERNATIONAL JOURNAL OF PRECISION ENGINEERING AND MANUFACTURING-GREEN TECHNOLOGY (in press).*
- Paolo C. Priarone, Matteo Robiglio, Giuseppe Ingarao, and Luca Settineri (2017). Assessment of Cost and Energy Requirements of Electron Beam Melting (EBM) and Machining Processes. *Sustainable Design and Manufacturing 2017 pp 723-735.*
- Priarone, P.C., Ingarao, G., Settineri, L., Di Lorenzo, R., (2016a). On the impact of recycling strategies on energy demand and CO<sub>2</sub> emissions when manufacturing Al-based components. *Procedia CIRP* 48, 194e199.
- Priarone Paolo C., Robiglio, M., Settineri, L., Tebaldo, V. (2016b). Modelling of specific energy requirements in machining as a function of tool and lubricoolant usage. *CIRP Ann. - Manuf. Technol.* 65 (1), 25-28.
- Priarone Paolo C., Giuseppe Ingarao, Rosa di Lorenzo, and Luca Settineri (2016c). Influence of Material-Related Aspects of Additive and Subtractive Ti-6Al-4V Manufacturing on Energy Demand and Carbon Dioxide Emissions. *Journal of Industrial Ecology.*
- Priarone Paolo C., Stefania Rizzuti, Luca Settineri and Guido Vergnano (2012). Effects of cutting angle, edge preparation, and nanostructured coating on milling performance of a gamma titanium aluminide. *Journal of Materials Processing Technology.*
- Quinteros FA, Poliandri AHB, Machiavelli LI, et al. (2007). In vivo and in vitro effects of chromium VI on anterior pituitary hormone release and cell viability. *Toxicol Appl Pharmacol* 218:79-87.

- Raffn E, Mikkelsen S, Altman DG, et al. (1988). Health effects due to occupational exposure to cobalt blue dye among plate painters in a porcelain factory in Denmark. *Scand J Work Environ Health* 14:378-384.
- Rastogi SK, Gupta BN, Husain T, et al. (1991). A cross-sectional study of pulmonary function among workers exposed to multimetals in the glass bangle industry. *Am J Ind Med* 20:391-399.
- Redmond CK. (1984). Site-specific cancer mortality among workers involved in the production of high nickel alloys. In: Sunderman FW Jr, Aitio A, Berlin A, eds. *Nickel in the human environment. IARC scientific publication no. 53. Lyon, France: International Agency for Research on Cancer, 73-86.*
- Rendall REG, Phillips JI, Renton KA. (1994). Death following exposure to fine particulate nickel from a metal arc process. *Ann Occup Hyg* 38(6):921-930.
- Rickenbacher L., A. Spierings K. Wegener, (2013). An integrated cost-model for selective laser melting (SLM). *Rapid Prototyping Journal, Vol. 19 Iss 3 pp. 208 – 214.*
- Rhodes MC, Hebert CD, Herbert RA, et al. (2005). Absence of toxic effects in F344/N rats and B6C3F1 mice following subchronic administration of chromium picolinate monohydrate. *Food Chem Toxicol* 43(1):21-29.
- Riddell AR. (1948). Pulmonary changes encountered in employees engaged in the manufacture of alumina abrasives. *Occup Med* 5:710-717.
- Rifat SL, Eastwood MR, Crapper-McLachlan DR, et al. (1990). Effect of exposure of miners to aluminum powder. *Lancet* 336(8724):1162-1165.
- Riihimäki V, Hanninen H, Akila R. (2000). Body burden of aluminum in relation to central nervous system function among metal inert-gas welders. *Scand J Work Environ Health* 26(2):118-130.
- Rizzato G, Lo Cicero S, Barberis M, Torre M, Pietra R, Sabbioni E. (1986). Trace of metal exposure in hard metal lung disease. *Chest* 90(1): 101-106.
- Roberts RS, Julian JA, Muir DCF, et al. (1989a). A study of mortality in workers engaged in the mining, smelting, and refining of nickel. II: Mortality from cancer of the respiratory tract and kidney. *Toxicol Ind Health* 5(6):975-993.
- Roig JL, Fuentes S, Teresa CM, et al. (2006). Aluminum, restraint stress and aging: Behavioral effects in rats after 1 and 2 years of aluminum exposure. *Toxicology* 218(2-3):112-124.
- Roberts RS, Julian JA, Swezey D, et al. (1989b). A study of mortality in workers engaged in the mining, smelting, and refining of nickel. I: Methodology and mortality by major cause groups. *Toxicol Ind Health* 5(6):957-974.
- Romaguera C, Lecha M, Grimalt F, et al. (1982). Photocontact dermatitis to cobalt salts. *Contact Dermatitis* 8:383-388.
- Rosenman KD, Stanbury M. (1996). Risk of lung cancer among former chromium smelter workers. *Am J Ind Med* 29:491-500.
- Roy PE, Bonenfant JT, Turcot L. (1968). Thyroid changes in cases of Quebec beer drinkers myocardiosis. *Am J Clin Pathol* 50:234-239.
- Royle H. (1975a). Toxicity of chromic acid in the chromium plating industry. *Environ Res* 10:39-53.
- Ruffo M., R Hague. Cost estimation for rapid manufacturing—simultaneous production of mixed components using laser sintering. *Proc. IMechE Vol. 221 Part B: J. Engineering Manufacture 2007.*
- Ruffo M., C Tuck, and R Hague (2006). Cost estimation for rapid manufacturing – laser sintering production for low to medium volumes. *Proc. IMechE Vol. 220 Part B: J. Engineering Manufacture.*

- RTI. (1988a). Two-generation reproduction and fertility study of nickel chloride administered to CD rats in the drinking water: Fertility and reproductive performance of the Po generation. Final study report (II of III). *Research Triangle Park, NC: Office of Solid Waste Management, U.S. Environmental Protection Agency.*
- RTI. (1988b). Two-generation reproduction and fertility study of nickel chloride administered to CD rats in the drinking water: Fertility and reproductive performance of the F1 generation. Final study report (III of III). *Research Triangle Park, NC: Office of Solid Waste Management, U.S. Environmental Protection Agency.*
- Rudgley, M. (2001). Rapid manufacturing – the revolution is beginning. *Proceedings of the uRapid*, pp. 441–444 (2001, May, Amsterdam).
- Ruffo, M., Tuck, C., and Hague, R. (2006). An empirical laser sintering time estimator for Duraform PA. *Int. J. Prod. Res.*, accepted for publication.
- Ruokonen E-L, Linnainmaa M, Seuri M, et al. (1996). A fatal case of hard-metal disease. *Scand J Work Environ Health* 22:62-65.
- Santucci B, Manna F, Cannistraci C, et al. (1994). Serum and urine concentrations in nickel-sensitive patients after prolonged oral administration. *Contact Dermatitis* 30:97-101.
- Sabbioni E, Mosconi G, Minoia C, Seghizzi P. (1994b). The European Congress on cobalt and hard metal disease. Conclusions, highlights and need of future studies. *Sci Total Environ* 150(1-3): 263-270.
- Sassi C. (1956). Occupational pathology in a chromate plant. *Med Lav* 47(5):314-327.
- Scansetti G, Botta GC, Spinelli P, Reviglione L, Ponzetti C. (1994). Absorption and excretion of cobalt in the hard metal industry. *Sci Total Environ* 150(1-3): 141-144.
- Scansetti G, Maina G, Botta GC, Bambace P, Spinelli P. (1998). Exposure to cobalt and nickel in the hard-metal production industry. *Int Arch Occup Environ Health* 71(1): 60-63.
- Schmidt-Bleek, F. (1994). *Wieviel Umwelt braucht der Mensch? mips -Das Mass für Ökologisches Wirtschaften*, Birkhauser Verlag GmbH, Berlin.
- Schroeder HA, Mitchener M, Nason AP. (1974). Life-term effects of nickel in rats: Survival, tumors, interactions with trace elements and tissue levels. *J Nutr* 104:239-243.
- Schroeder HA, Balassa JJ, Vintin WH Jr. (1964). Chromium, lead, cadmium, nickel and titanium in mice: Effect on mortality, tumors and tissue levels. *J Nutr* 83:239-250.
- Schroeder HA, Balassa JJ, Tipton IH. (1962). Abnormal trace metals in man: Chromium. *J Chron Dis* 15:941-964.
- Schuster B.E., L.E. Roszell, L.E. Murr, D.A. Ramirez, J.D. Demaree, B.R. Klotz, A.B. Rosencrance, W.E. Dennis, W. Bao, E.J. Perkins, J.F. Dillman, D.I. Bannon (2012). In vivo corrosion, tumor outcome, and microarray gene expression for two types of muscle-implanted tungsten alloys. *Toxicology and Applied Pharmacology* 265 (2012) 128–138.
- Seilkop SK, Oller AR. (2003). Respiratory cancer risks associated with low-level nickel exposure: An integrated assessment based on animal, epidemiological, and mechanistic data. *Regul Toxicol Pharmacol* 37:173-190.
- Shannon HS, Julian JA, Roberts, RS. (1984b). A mortality study of 11,500 nickel workers. *J Natl Cancer Inst* 73(6):1251-1258.
- Shannon HS, Walsh C, Jadon N, et al. (1991). Mortality of 11,500 nickel workers -- extended follow up and relationship to environmental conditions. *Toxicol Ind Health* 7:277-294.



- Shara M, Kincaid AE, Limpach AL, et al. (2007). Long-term safety evaluation of a novel oxygen-coordinated niacin-bound chromium (III) complex. *J Inorg Biochem* 101(7):1059-1069.
- Shara M, Yasmin T, Kincaid AE, et al. (2005). Safety and toxicological evaluation of a novel niacin-bound chromium (III) complex. *J Inorg Biochem* 99(11):2161-2813.
- Shaver CG. (1948). Pulmonary changes encountered in employees engaged in the manufacture of alumina abrasives. *Occup Med* 5:718-728.
- Shaver CG, Riddell AR. (1947). Lung changes associated with the manufacture of alumina abrasives. *J Ind Hyg Toxicol* 29:145-157.
- Sheng, P. and Hertwich, E. (1998). Indices for Comparative Waste Assessment in Environmentally-Conscious Manufacturing. *J. Manuf. Sci. Eng., Vol. 120, No. 1, pp. 129-140.*
- Shirakawa T, Kusaka Y, Fujimura N, et al. (1989). Occupational asthma from cobalt sensitivity in workers exposed to hard metal dust. *Chest* 95(1):29-37.
- Shirakawa T, Kusaka Y, Fujimura N, et al. (1988). The existence of specific antibodies to cobalt in hard metal asthma. *Clin Allergy* 18:451-460.
- Shmitova LA. (1980). Content of hexavalent chromium in the biological substrates of pregnant women and women in the immediate post-natal period engaged in the manufacture of chromium compounds. *Gig Trud Prof Zabol* 2:33-35.
- Shrivastava VK, David CV, Khare N, et al. (1996). Cobalt chloride induced histopathological changes in thyroid gland of female mice. *Mus musculus (P.). Pollut Res* 15(3):307-309.
- Sim M, Dick R, Russo J, et al. (1997). Are aluminum potroom workers at increased risk of neurological disorders? *Occup Environ Med* 54(4):229-235.
- Simonsen LO, Harbak H, Bennekou P. (2012). COBALT METABOLISM AND TOXICOLOGY--A BRIEF UPDATE. *Sci Total Environ*; 432:21 0-5.
- Singh PP, Junnarkar AY. (1991). Behavioral and toxic profile of some essential trace metal salts in mice and rats. *Indian J Pharmacol* 23:153-159.
- Sjögren B, Ljunggren KG, Almkvist O, et al. (1996). A follow-up study of five cases of aluminosis. *Int Arch Occup Environ Health* 68(3):161-164.
- Sjögren B, Gustavsson P, Hogstedt C. (1990). Neuropsychiatric symptoms among welders exposed to neurotoxic metals. *Br J Ind Med* 47(10):704-707.
- Sjovall P, Christensen OB, Moller H. (1987). Oral hyposensitization in nickel allergy. *J Am Acad Dermatol* 17(1):774-778.
- Sorahan T, Burges DCL, Hamilton L, et al. (1998). Lung cancer mortality in nickel/chromium platers, 1946-95. *Occup Environ Med* 55:236-242.
- Sorenson JRJ, Campbell IR, Tepper LB, et al. (1974). Aluminum in the environment and human health. *Environ Health Perspect* 8:3-95.
- Speijers GJA, Krajnc EI, Berkvens JM, et al. (1982). Acute oral toxicity of inorganic cobalt compounds in rats. *Food Chem Toxicol* 20:311-314.
- Sprince NL, Oliver LC, Eisen EA, et al. (1988). Cobalt exposure and lung disease in tungsten carbide production: A cross-sectional study of current workers. *Am Rev Respir Dis* 138:1220-1226.

- Stanley AJ, Hopps HC, Shideler AM. 1947. Cobalt polycythemia. II. Relative effects of oral and subcutaneous administration of cobaltous chloride. *Proc Soc Exp Biol Med* 66:19-20.
- Steen, B., and Ryding, S. (1991). The EPS Environmental Accountin Method: An Application of Environmental Accounting Principles for Evaluation and Valuation of Environmental Impact on Product Design. *IVL Swedish Environmental Research Institute Publication*.
- Steffee CH, Baetjer AM. (1965). Histopathologic effects of chromate chemicals. *Arch Environ Health* 11:66-75.
- Steinhagen WH, Cavender FL, Cockrell BY. (1978). Six month inhalation exposures of rats and guinea pigs to aluminum chlorhydrate. *J Environ Pathol Toxicol* 1:267-277.
- Strutt, P. R. (1980). A comparative study of electron beam and laser melting of M2 tool steel. *Materials Science and Engineering* 44(1): 239–250.
- Stone CJ, McLaurin DA, Steinhagen WH, et al. (1979). Tissue deposition patterns after chronic inhalation exposures of rats and guinea pigs to aluminum chlorhydrate. *Toxicol Appl Pharmacol* 49:71-76.
- Sullivan JF, Egan JD, George RP. (1969). A distinctive myocardopathy occurring in Omaha, Nebraska: Clinical aspects. *Ann N Y Acad Sci* 156(1):526-543.
- Stockmann-Juvala H., Y Hedberg, NK Dhinsa, DR Griffiths, PN Brooks, A Zitting, I Odnevall Wallinder and T Santonen (2013). Inhalation toxicity of 316L stainless steel powder in relation to bioaccessibility. *Human and Experimental Toxicology* 32(11) 1137–1154.
- Stopford W, Turner J, Cappellini D, Brock T. (2003). Bioaccessibility testing of cobalt compounds. *J Environ Monit* 5(4): 675-680.
- Sundaram P, Agrawal K, Mandke JV, et al. (2001). Giant cell pneumonitis induced by cobalt. *Indian J Chest Dis Allied Sci* 43 (1):47-49.
- Sunderman FW Jr. (1993). Biological monitoring of nickel in humans. *Scand J Work Environ Health* 19(Suppl 1):34-38.
- Sunderman FW Jr, Horak E. (1981). Biochemical indices of nephrotoxicity, exemplified by studies of nickel nephropathy. In: *Brown SS, Davies DS, eds. Organ-directed toxicity: Chemical indices and mechanisms. London, UK: Pergamon Press, 52-64.*
- Sunderman FW Jr. (1993). Biological monitoring of nickel in humans. *Scand J Work Environ Health* 19(Suppl 1):34-38.
- Sunderman FW Jr. (1989a). Carcinogenicity of metal alloys in orthopedic prostheses: Clinical and experimental studies. *Fundam Appl Toxicol* 13:205-216.
- Swennen B, Buchet J-P, Stanescu D, et al. (1993). Epidemiological survey of workers exposed to cobalt oxides, cobalt salts, and cobalt metal. *Br J Ind Med* 50:835-842.
- Tabatowski K, Roggli VL, Fulkerson WJ, et al. (1988). Giant cell interstitial pneumonia in a hard-metal worker: Cytologic, histologic and analytical electron microscopic investigation. *Acta Cytol* 32(2):240-246.
- Tanaka I, Horie A, Haratake J, et al. (1988). Lung burden of green nickel oxide aerosol and histopathological findings in rats after continuous inhalation. *Biol Trace Elem Res* 16:19-26.
- Telenko, C., and Seepersad, C. C. (2010). Assessing Energy Requirements and Material Flows of Selective Laser Sintering of Nylon Parts. *Proceedings of the Solid Freeform Fabrication Symposium 2010, Austin, USA, 8 – 10.08.2010, pp. 289-297.*

Toxicological inhalation profile for cobalt (2014). *U.S. DEPARTMENT OF HEALTH AND HUMAN SERVICES*.

Toxicological profile for aluminum (2008). *U.S. DEPARTMENT OF HEALTH AND HUMAN SERVICES, Public Health Service Agency for Toxic Substances and Disease Registry*.

Toxicological profile for aluminum (2008). *U.S. DEPARTMENT OF HEALTH AND HUMAN SERVICES, Public Health Service Agency for Toxic Substances and Disease Registry*.

Toxicological profile for nickel (2005). *U.S. DEPARTMENT OF HEALTH AND HUMAN SERVICES, Public Health Service Agency for Toxic Substances and Disease Registry*.

Toxicological profile for cobalt (2004). *U.S. DEPARTMENT OF HEALTH AND HUMAN SERVICES, Public Health Service Agency for Toxic Substances and Disease Registry*.

Toxicological profile for chrome (2002). *U.S. DEPARTMENT OF HEALTH AND HUMAN SERVICES, Public Health Service Agency for Toxic Substances and Disease Registry*.

Valer M, Somogyi Z, Racz I. (1967). Studies concerning the sensitizing effect of cobalt. *Dermatologica* 134:36-50.

Van Cutsem EJ, Ceuppens JL, Lacquet LM, et al. (1987). Combined asthma and alveolitis induced by cobalt in a diamond polisher. *Eur J Respir Dis* 70:54-61.

Vassilev PP, Venkova K, Pencheva N, et al. (1993). Changes in the contractile responses to carbachol and in the inhibitory effects of verapamil and nitrendipine on isolated smooth muscle preparations from rats subchronically exposed to Co<sup>2+</sup> and Ni<sup>2+</sup>. *Arch Toxicol* 67:330-337.

Veien NK, Hattel T, Justesen O, et al. (1987). Oral challenge with nickel and cobalt in patients with positive patch tests to nickel and/or cobalt. *Acta Derm Venereol* 67:321-325.

Ward NI. (1989). Environmental contamination of aluminum and other elements in North Cornwall as a result of the Lowermoor water treatment works incident. In: *Vernet J-P, ed. Heavy metals in the environment. Edinburgh: CEP Consultants, 118-121*.

Warheit D. B., W. J. Brock, K. P. Lee, T. R. Webb, and K. L. Reed. Comparative Pulmonary Toxicity Inhalation and Instillation Studies with Different TiO<sub>2</sub> Particle Formulations: Impact of Surface Treatments on Particle Toxicity. *TOXICOLOGICAL SCIENCES* 88(2), 514–524 (2005) doi:10.1093/toxsci/kfi331.

Wehner AP, Busch RH, Olson RJ, et al. (1977). Chronic inhalation of cobalt oxide and cigarette smoke by hamsters. *Am Ind Hyg Assoc J* 38:338-346.

Weischer CH, Kordel W, Hochrainer D. (1980). Effects of NiCl<sub>2</sub> and NiO in Wistar rats after oral uptake and inhalation exposure, respectively. *Zent Bakteriolog Mikrobiol Hyg (B)* 171:336-351.

White DM, Longstreth WTJ, Rosenstock L, et al. (1992). Neurologic syndrome in 25 workers from an aluminum smelting plant. *Arch Intern Med* 152:1443-1448.

Wild P, Perdrix A, Romazini S, Moulin JJ, Pellet F. (2000). Lung cancer mortality in a site producing hard metals. *Occup Environ Med* 57(8): 568-573.

Zanelli R, Barbic F, Migliori M, et al. (1994). Uncommon evolution of fibrosing alveolitis in a hard metal grinder exposed to cobalt dusts. *Sci Total Environ* 150:225-229.

Zhang J, Li X. (1987). Chromium pollution of soil and water in Jinzhou. *J Chinese Prev Med* 21:262-264.